ELECTRICAL IMPEDANCE SPECTROSCOPY AND 3D CELL CULTURES AS EMERGING TECHNOLOGIES FOR STUDYING SIGNAL TRANSDUCTION PATHWAYS: THE CURIOUS CASE OF CATHELICIDINS.

Eddy-Tim Verjans

Supervisor

Prof. L. Schoofs, KU Leuven

Co-supervisors

Prof. W. Luyten, KU Leuven

Dr. ir. B. Landuyt, KU Leuven

Members of the Examination Committee:

Prof. L. Temmerman, KU Leuven
Prof. L. Moons, KU Leuven
Dr. B. Van Hiel, KU Leuven
Dr. S. Zels, KU Leuven
Prof. S. Husson , U Antwerpen
Dr. T. Wahle, Leibniz Research Institute for Environmental Medicine

Dissertation presented in partial fulfilment of the requirements for the degree of Doctor in Science

December 2017

Doctoraatsproefschrift aan de faculteit Wetenschappen van de KU Leuven

Uitgegeven in eigen beheer, Eddy-Tim Verjans, Zoölogisch Instituut, Naamsestraat 59, B-3000 Leuven, België.

“GPCR function is more like Nature's Bach symphony than a set of independent notes where it’s combinations of interactions rather than the binding of a single molecule that result in a complex physiological response.” – ***Ashutosh Jogalekar***

Dankwoord

Graag zou ik iedereen willen bedanken die mij de voorbije jaren heeft geholpen om mijn doctoraatsproefschrift tot een goed einde te brengen. Hoewel verschillende collega's mij met raad en/of praktische hulp hebben bijgestaan doorheen dit project, verdienen sommigen een bijzondere vermelding. Zonder hen was dit doctoraat simpelweg niet mogelijk geweest.

Ik vind het gepast om te beginnen met de personen die er vrijwel elke dag waren om het dagelijkse werk op te fleuren: Zjef, Valérie, Chetan, en Lentel. Ik weet zeker dat ik later met nostalgische gevoelens ga terugdenken aan ons bureautje *achter den walvis*. Ik heb veel van jullie geleerd de voorbije jaren, gaande van praktische tips in het labo tot praktische grappen erbuiten. Later kwamen ook de *manne van de Kempen* Jordi en Jurgen ons team vervoegen. Vooral met Jordi heb ik in een periode nauw samengewerkt omtrent 3D celculturen en impedantiemetingen. Aan deze periode hou ik goede herinneringen over en ben van mening dat we een mooi eindresultaat kunnen voorleggen. Hopelijk kunnen we deze lijn in de toekomst doortrekken binnen de start-up CellSine.

Mijn promotor Liliane Schoofs wil ik natuurlijk ook bedanken, omwille van de kans die ze me gaf en de financiële ondersteuning van dit project. Ook wil ik haar bedanken om, ondanks haar drukke job als vicerector van onderzoeksbeleid, tijd vrij te maken om mijn papers en doctoraat na te lezen.

Verder wil ik mijn copromotoren Bart Landuyt en Walter Luyten bedanken. Jullie waren vaak een bron van inspiratie voor het opzetten van nieuwe experimenten. Ook ben ik dankbaar dat jullie me toelieten om op een zelfstandige basis aan onderzoek te doen, wat me ongetwijfeld heeft doen groeien als onderzoeker. Bart wil ik via deze weg nog eens extra bedanken voor de huidige kans die hij mij biedt in CellSine.

Vervolgens gaat mijn dank uit naar alle leden van de examencommissie voor het gedetailleerd nalezen van dit proefschrift (in het bijzonder Tina Wahle, die verschillende keren de tijd en moeite nam om vanuit Duitsland naar Leuven af te zakken), alsook alle leden van het HSTV-lab. Jullie zorgden voor een gezellige en behulpzame werksfeer. Ik denk met veel plezier terug aan de vele labactiveiten, zoals de memorabele laboweekends, kajaktochtjes, kerstfeestjes, 'PhD-kickoff-parties', en voetbalwedstrijdjes.

Last but absolutely not least wil ik mijn vriendin, ouders, en zussen bedanken voor hun engelengeduld en onvoorwaardelijke steun.

Allemaal erg bedankt!

Eddy-Tim

Table of contents

List of abbreviations

10-DEBC	10-[4'-(*N,N*-diethylamino)butyl]-2-chlorophenoxazine
2-APB	2-aminoethoxydiphenyl borate
2D	Two-dimensional
2DGE	Two-dimensional gel electrophoresis
3D	Three-dimensional
7TM	Seven-transmembrane
Aβ	Amyloid-beta
AB	Antibiofilm
AC	Anticancer
ACSS1	Acyl-coenzyme A synthetase family member 1
ACSS2	Acyl-coenzyme A synthetase family member 2
AD	Alzheimer's disease
ADAM	A disintegrin and metalloproteinase
ADH1C	Alcohol dehydrogenase 1C
AM	Antimicrobial
AMP	Antimicrobial peptide
ANOVA	Analysis of variance
ALDOA	Aldolase A
ALDOC	Aldolase C
APP	Amyloid precursor protein
APD	Antimicrobial peptide database
AQP5	Aquaporin 5
ASIP	Agouti-signaling peptide
ATP	Adenosine triphosphate
BAPTA-AM	1-2-bis(2-aminophenoxy)ethane-tetraacetic acid acetoxymethyl ester
BAR	Beta-adrenergic receptor
BKCa	Ca^{2+}-activated K^{+}-channel
Bp	Base pair
BSA	Bovine serum albumin
C. albicans	*Candida albicans*
C. elegans	*Caenorhabditis elegans*
Ca^{2+}	Calcium
cAMP	Cyclic adenosine monophosphate
CART	Cocaine and amphetamine regulated transcript protein
CDH1	Cadherin-1
cDNA	Complementary deoxyribonucleic acid
CHO	Chinese hamster ovary
Cl^{-}	Chloride
CRC	Colorectal cancer
Curc	Curcumin
CXCR2	CXC chemokine receptor type 2
CXCR4	CXC chemokine receptor type 4
Da	Dalton
DAG	Diacylglycerol
DAPI	Diamidino-2-phenylindole
DAPT	N-[N-(3,5-Difluorophenacetyl)-L-alanyl]-S-phenylglycine t-butyl ester
DC	Dendritic cell
DEG	Differentially expressed gene
DIDS	Diisothiocyanato-2,2'-stilbenedisulfonic acid

DME	Drug-metabolizing enzyme
DMEM	Dulbecco's modified eagle medium
DNA	Deoxyribonucleic acid
EC_{50}	Half maximal effective concentration
ECACC	European collection of authenticated cell cultures
ECL	Extracellular loop
EDTA	Ethylenediamine tetraacetic acid
EGFR	Epidermal growth factor receptor
eIF3A	Eukaryotic translation initiation factor 3 subunit A
EIPA	5-(N-ethyl-N-isopropyl)amiloride
EIS	Electrical impedance spectroscopy
ELISA	Enzyme-linked immunosorbent assay
EMEM	Eagle's minimal essential medium
ENO2	Enolase 2
ERK	Extracellular signal-regulated kinase
Erlo HCl	Erlotinib hydrochloride
FBS	Fetal bovine serum
FDR	False discovery rate
FMOC	Fluorenylmethyloxycarbonylchloride
FPR2	*N*-formyl peptide receptor 2
FoxO	Forkhead box O
FSK	Forskolin
G protein	Guanine nucleotide-binding protein
GALM	Galactose mutarotase
GAPDH	Glyceraldehyde-3-phosphate dehydrogenase
GDP	Guanosine diphosphate
Gen	Genistein
GFP	Green fluorescent protein
Glut1	Glucose transporter 1
GPant-2	G protein antagonist 2
GPCR	G protein-coupled receptor
GRK	G protein-coupled kinase
GS	Goat serum
GTP	Guanosine triphosphate
GO	Gene ontology
hβD	Human β-defensin
HBCD	2-hydroxypropyl-β-cyclodextrin
HB-EGF	Heparin-binding EGF-like growth factor
HBSS	Hanks' balanced salt solution
HCC	Hepatocellular carcinoma
HEK	Human embryonic kidney
Hep	Heparinase
Hept	Heparitinase
HGP	Human genome project
HIF-1	Hypoxia-inducible factor 1
HRP	Horseradish peroxidase
HS	Horse serum
HSPC	Human hematopoietic stem/progenitor cells
HTR1D	5-hydroxytryptamine receptor 1D
IAV	Influenza A virus
ICL	Intracellular loop
IFN	Interferon

IGF1R	Insulin-like growth factor 1 receptor
Il	Interleukin
IL1RN	Interleukin-1 receptor antagonist
Insl6	Insulin-like peptide 6
IOF	Industrieel onderzoeksfonds
IP3	Inositol 1,4,5-triphosphate
IP3R	Inositol 1,4,5-triphosphate receptor
K^+	Potassium
KEGG	Kyoto encyclopedia of genes and genomes
KRBG	Krebs-Ringer bicarbonate glucose buffer
LaCl3	Lanthanum (III) chloride
LDHA	Lactate dehydrogenase A
LGIC	Ligand-gated ion channel
LL-37	Leucine leucine-37
LPS	Lipopolysaccharide
LRC	Ligand-receptor-capture
LrECM	Laminin-rich extracellular matrix
LTB4	Leukotriene B4
MAPK	Mitogen-activated protein kinase
MBCD	Methyl-β-cyclodextrin
MC4R	Melanocortin 4 receptor
MCP1	Monocyte chemotactic protein-1
M-CSF	Macrophage colony-stimulating factor
MDC	Monodansylcadaverine
MMP7	Matrix metalloproteinase-7
MrgX2	Mas-related gene X2
mRNA	Messenger ribonucleic acid
mTOR	Molecular target of rapamycin
MS	Mass spectrometry
MS/MS	Tandem mass spectrometry
MSH	Melanocyte-stimulating hormone
Na^+	Sodium
NaN_3	Sodium azide
NANIVID	NANo IntraVital Imaging Device
NaP	Sodium pyruvate
NC	Negative control
NCBI	National Center for Biotechnology Information
ND	Not determined
NEAA	Non-essential amino acids
NET	Neutrophil extracellular trap
NGF	Nerve growth factor
NK-cells	Natural killer cells
NMR	Nuclear magnetic resonance
NO	Nitric oxide
NOA	Neurite outgrowth assay
$P2X_7$	Purinergic receptor 7
P2Y11	Purinoceptor 11
P318	Peptide 318
PAMP	Pathogen-associated molecular pattern
PAR1-AP	Protease-activated receptor 1- activating peptide
PBS	Phosphate buffered saline
PC1	First principal component

PCA	Principal component analysis
PDK1	Pyruvate dehydrogenase kinase 1
PFA	Paraformaldhyde
PFKL	ATP-dependent 6-phosphofructokinase
PGM1	Phosphoglucomutase-1
PHN	Primary hippocampal neuron
PIP2	Phosphatidylinositol 4,5-bisphosphate
PLA_2	Phospholipase A_2
PLC	Phospholipase C
PLD	Phospholipase D
PPADS	Pyridoxalphosphate-6-azophenyl-2'-4'-disulfonic acid
PRP	Pattern-recognition receptor
PTM	Post-translational modification
PTX	Pertussis toxin
qPCR	Quantitative polymerase chain reaction
RAFT	Real Architecture for 3D Tissue
RFU	Relative fluorescence units
RGS	Regulator of G protein signaling
RhoGEF	Rho-guanine nucleotide exchange factor
RNAi	RNA interference
RNA-seq	RNA-sequencing
ROS	Reactive oxygen species
RPMI	Roswell park memorial institute
rRNA	Ribosomal ribonucleic acid
RTK	Receptor tyrosine kinase
RyR	Ryanodine receptor
SAR	Structure-activity relation
SBO	Strategisch basisonderzoek
SCFFA	Short-chain fatty acid
Scg2	Secretogranin 2
Scg3	Secretogranin 3
SDF-1	Stromal-derived factor-1
SEM	Standard error of the mean
SFG	Sum frequency generation
SH2	SRC homology 2
SOC	Store-operated channel
SPR	Surface plasmon resonance
T/E	Trypsin/EDTA
TEA	Tetraethyl ammonium
TGF-α	Transforming growth factor-alpha
TLR	Toll-like receptor
TMB-8	8-(Diethylamino)octyl-3,4,5-trimethoxybenzoate
TNF-α	Tumor Necrosis factor-alpha
TRPV2	Transient receptor potential cation
Tyr AG-1478	Tyrphostin AG-1478
VEGF	Vascular endothelial growth factor
VIB	Vlaams instituut voor biotechnologie

List of peptides, antagonists, and toxins

Peptides	
LL-37	Only human member of the cathelicidin family of AMPs. LL-37 owes its nomenclature to its 37 amino acid overall length with two leucine residues on its NH_2 terminus.
KI-26	Truncated fragment of LL-37 which lacks eleven amino acids at the N-terminus of the full sequence of LL-37. In analogy of the nomenclature of LL-37, KI-26 is 26 amino acids long and starts with a lysine and isoleucine residue on its NH2 terminus. Shares 52% homology with P318.
P318	26-amino acid fragment of murine CRAMP identified in the islets of Langerhans of the murine pancreas.
CRAMP	34-amino acid cathelicidin-related AMP which plays a role in host defense and wound repair in mice.
P384	18-residue fragment derived from eIF3a.
P649	15-residue fragment derived from secretogranin 2.
PAR1-AP	Protease-activated receptor 1 agonist.
MMK 1	FPR2 agonist.
WKYMVm	FPR2 agonist.
SDF-1α	Also known as C-X-C motif chemokine 12 (CXCL12). CXCR4 agonist.
Broad-spectrum antagonists	
PTX	Bacterial toxin that catalyzes ADP-ribosylation of G proteins G_i, G_o and G_t. Impairs G protein heterotrimer interaction with receptors.
GPant2	Substance P-related peptide that inhibits binding of G proteins to their receptors. Competitively and reversibly inhibits M2 muscarinic receptor activation of G_i or G_o and inhibits G_s activation by β-adrenoceptors.
Gallein	Antagonist of Gβγ subunit-dependent signaling.
Genistein	Isoflavone compound. Inhibits various RTKs including EGFR.
Curcumin	Natural phenolic compound. Inhibitor of EGFR tyrosine kinase, cyclooxygenase, and IκB kinase. Accumulates in the cellular membrane and nuclear envelope.
BAPTA-AM	Cell permeant chelator with high selectivity for calcium over magnesium. Commonly used to control intracellular calcium levels.
Suramin	Inhibitor of P2X and P2Y purinergic receptors. Uncouples G proteins from receptors and interferes with growth factor signaling.

PPADS	Non-selective P2 purinergic antagonist.
GM6001	Broad spectrum matrix metalloproteinase (MMP) inhibitor.
Paclitaxel	Complex dipentene and antitumor agent. Acts as a promoter of tubulin polymerization and has an impact on cytosolic calcium signals by opening the mitochondrial permeability transition pore.
Brefeldin A	Fungal metabolite that inhibits intracellular protein transport and affects endocytic pathways.
Dynasore	Inhibits dynamin-dependent endocytosis.
MDC	Inhibits clathrin-mediated endocytosis.
Cytochalasin B	Fungal metabolite that inhibits cell division, cell migration, and glucose transport. Blocks monomer addition to actin filaments at the growing end of the polymer.
Z-VAD-fmk	Non-selective, cell permeable antagonist of caspase-1 as well as caspase-3-related proteases.
Cycloheximide	Protein synthesis inhibitor.
DAPT	γ-secretase inhibitor.
(Receptor-) selective antagonists	
WRW4	Selective antagonist of formyl peptide receptor 2 (FPR2) signaling. Inhibits WKYMVm binding to FPR2 (IC_{50} = 0.23 μM) and inhibits intracellular calcium release
SB225002	Potent and selective CXCR2 chemokine receptor antagonist (IC_{50} = 22 nM). Causes inhibition of IL-8 and GROα-mediated calcium mobilization in HL60 cells (IC_{50} values are 8 and 10 nM respectively).
SB265610	Potent CXCR2 antagonist (IC_{50} = 4 nM).
NF-157	Potent P2Y11R inhibitor (IC_{50} = 463 nM).
Erlotinib HCl	Potent and specific EGFR inhibitor with IC_{50} of 2 nM.
Tyr AG1478	Potent and specific EGFR tyrosine kinase inhibitor with IC_{50} of 3 nM.
CP-724714	Potent and selective ErbB2 inhibitor with IC_{50} of 10 nM.
AG-1024	Inhibits IFG1R autophosphorylation with IC_{50} of 7 μM.
Oxidized ATP	Slow but irreversible inhibitor of P2 purinoceptors.
U0126	MAPK/ERK kinase inhibitor.

10-DEBC	Selective inhibitor of Akt. Inhibits IGF-1-stimulated phosphorylation and activation of Akt (complete inhibition at 2.5 μM), suppressing downstream activation of mTOR, p70S6 kinase and S6 ribosomal protein. Shows no activity at PDK1, SGK1 or PI 3-kinase.
BAY 11-7082	Selective and irreversible inhibitor of NF-κB activation.
STA-21	A Stat3 transcription factor signaling antagonist.
U73122	Inhibits phospholipase C signaling.
LR disrupting agents	
MBCD	Cyclic oligosaccharide commonly used as LR disrupting agent by depleting cholesterol from the cell membrane
HBCD	Cyclic oligosaccharide commonly used as LR disrupting agent by depleting cholesterol. HBCD causes less damage to cells than MBCD.
AY9944	Inhibitor of hedgehog (Hh) signaling. Inhibits Δ7-dehydrocholesterol reductase (IC_{50} = 13 nM), thereby reducing cholesterol biosynthesis, and also inhibits cholesterol esterification.
Filipin III	Polyene macrolide antibiotic and antifungal. Alters membrane permeability by binding to membrane sterols.
Ion channel antagonists	
2-APB	A functional and membrane permeable IP_3 receptor antagonist (IC_{50} = 42 μM). Stimulates store-operated channel (SOC) calcium release at low concentrations (< 10 μM) and inhibits it at higher concentrations (up to 50 μM). Increases STIM-Orai channel conductance and limits ion selectivity.
TMB-8	TMB-8 is a protein kinase C (PKC) inhibitor which also serves as an intracellular calcium antagonist. TMB-8 possesses both Ca_{2+} channel- and Na+ channel-blocking properties and reduces the membrane K_+ conductance.
Dantrolene	Inhibits release of calcium from sarcoplasmic reticulum via inhibition of ryanodine receptor (RyR) channels.
Nifedipine	L-type calcium channel inhibitor.
$LaCl_3$	Inhibits activity of calcium channels.
EIPA	Inhibits Na^+/H^+ exchanger and TRPP3 channel inhibitor (IC_{50} = 10.5 μM).
TEA	Inhibits K^+-channels; blocks nicotinic acetylcholine neurotransmission by blocking receptor-mediated K^+ currents.
A-438079	Competitive $P2X_7$ receptor antagonist.
NF449	Purinergic receptor antagonist with high selectivity for $P2X_1$.

Samenvatting

Dit doctoraatsproefschrift bestaat uit twee grote delen. Het eerste deel beoogt de signaaltransductiewegen van recent geïdentificeerde potentiële bioactieve peptiden op te helderen. Het tweede deel introduceert 3D celcultuursystemen en vergelijkt verschillen in genexpressie tussen 2D en 3D celculturen.

Bioactieve peptiden vervullen belangrijke taken als inter- en intracellulaire signaalmoleculen, waardoor ze onmisbaar zijn voor het bestaan van meercellig leven. Peptiden worden doorgaans gevormd uit precursorproteïnen, waarna ze verscheidene fysiologische processen beïnvloeden zoals voedselopname, lichaamsgewicht, slaap, pijn, angst, en geheugen. Dankzij alsmaar betere peptidomicstechnieken kunnen peptiden tegenwoordig uit zeer complexe biologische mengsels geïdentificeerd worden zoals weefselextracten. De peptidensequentie vertelt echter niet altijd iets over de mogelijke functie van een peptide. De meerderheid van de peptiden verricht zijn functie door met een receptor te binden, waarna een intracellulaire signaaltransductieweg geactiveerd wordt. Kennis over de receptor en de signaaltransductiecascade vormen een uitstekend vertrekpunt om meer over de functie van een peptide te weten te komen en om eventueel later geneesmiddelen te onwikkelen.

Door gebruik te maken van een grensverleggende peptidomicsstrategie was de onderzoeksgroep van prof. Schoofs in staat om een peptidenbibliotheek te synthetiseren van meer dan 700 potentiële biologisch actieve peptiden. Om meer inzicht te krijgen in de eventuele functie van deze peptiden, werd er een interuniversitaire samenwerking opgezet, met expertise vanuit verschillende celbiologische vakgebieden. Onze onderzoeksgroep hield zich voornamelijk bezig met het testen van peptiden op celculturen die verschillende muizen- en humane celtypes vertegenwoordigen.

In een eerste fase werden experimenten uitgevoerd om te achterhalen of de peptiden enige activiteit vertoonden. Deze screeningexperimenten werden eerst verricht met onzuivere peptiden die op een kleine schaal geproduceerd werden. Zodra er een effect gedetecteerd werd met deze peptiden, werd hetzelfde peptide in een hogere zuiverheid getest met als doel de activiteit van het onzuivere peptide te bevestigen. Het bleek echter vaak een hele uitdaging om de oorspronkelijke effecten van onzuivere peptiden te reproduceren, wat leidde tot de conclusie dat de peptidekwaliteit van cruciaal belang is om resultaten op een correcte manier te interpreteren. Hoe dan ook vonden we verschillende zuivere peptiden die een activiteit vertoonden in één of meerdere onderzoeken. Deze peptiden werden geselecteerd voor verder onderzoek.

Misschien het meest beloftevolle peptide was een peptide genaamd P318, gezien zijn uiteenlopende effecten op diverse celtypes. P318 is een nieuw peptidefragment gevormd uit het cathelicidine-verwante antimicrobieel peptide (CRAMP). Cathelicidines vervullen een belangrijke functie in het

immuunsysteem omdat ze zowel immunomodulerende als rechtstreekse antimicrobiële activiteit bezitten. LL-37 (leucine leucine-37), het enige humane cathelicidine dat tot op heden geïdentificeerd is, is waarschijnlijk het meest bestudeerde lid van de familie van cathelicidines.

De meerderheid van de effecten van LL-37 op gastheercellen zijn een gevolg van de rechtstreekse of onrechtstreekse activatie van structureel onverwante celoppervlaktereceptoren of intracellulaire doelwitten. Het blijft tot op heden een raadsel hoe één enkel peptide in staat is om verschillende receptoren te activeren die niet tot dezelfde receptorklasse behoren, des te meer omdat de meeste 'ligand-receptor' interacties net op een zeer specifieke wijze gebeuren. Om meer inzicht in dit onderwerp te verkrijgen publiceerden we een overzichtsartikel omtrent de functie van LL-37 en brachten dit in verband met alle receptoren en ionenkanalen waarvan reeds gekend is dat ze geactiveerd worden door LL-37. Daarnaast onderzochten we ook het activiteitsprofiel van LL-37 op verschillende celculturen. Dit kan nuttig zijn om later de effecten van P318 beter te begrijpen, zoals b.v. de bepaling van de receptor en de opheldering van de signaaltransductiecascade.

Omdat LL-37 verschillende werkingsmechanismen gebruikt om de activiteit van gastheercellen te moduleren, hebben we een aspecifieke techniek nodig die toelaat om een cellulaire respons te detecteren ongeacht welke receptor of signaaltransductieweg geactiveerd wordt. Wij rapporteren dat elektrische impedantie spectroscopie (EIS) voldoet aan de vereisten om de effecten van LL-37 te bestuderen. Impedantiemetingen voorzien een integratieve meting van alle signaaltransductiewegen die geactiveerd worden na behandeling met LL-37. Op basis van deze impedantieresponsen kunnen hypothesen over het werkingsmechanisme van LL-37 geformuleerd worden die daarna met behulp van farmacologische agentia getoetst kunnen worden. Verschillen in het effect van LL-37 bezorgen ons een kijk op de receptor en de betrokken signaaltransductiecascade.

In aanvulling van het bevestigen van reeds gekende activiteit van LL-37 op enkele cellijnen werd er ook nieuwe activiteit van LL-37 ontdekt via impedantiemetingen. Zo werden er bijvoorbeeld effecten van LL-37 op HEK293T en U87 glioblastoomcellen gedetecteerd die tot op heden niet gerapporteerd zijn. In een volgende stap werden secundaire boodschapper onderzoeken uitgevoerd om na te gaan welke secundaire boodschapper het signaal doorgeeft in de cel. Uit deze onderzoeken bleek bijvoorbeeld dat LL-37 HEK293T cellen op een dosisafhankelijke manier activeert via de vrijlating van calcium vanuit intracellulaire opslagplaatsen. Sterke aanwijzingen werden ook gevonden dat LL-37 met de plasmamembraan interageert i.p.v. met specifieke ligandbindingsplaatsen. Naast calciumvrijzetting oefende LL-37 ook een cytotoxisch effect uit op HEK293T cellen via het creëren van membraanporiën. Het voorbehandelen van HEK293T cellen met suramine of suramine-analogen beschermde HEK293T cellen echter tegen de cellulaire schade aangericht door LL-37.Het gebruik van EIS kan ook helpen om een onderscheid te maken tussen de verschillende werkingsmechanismen van LL-37. Zo blijken A549 longcarcinoomcellen LL-37 op te nemen via endocytosepaden. In U87

glioblastoomcellen getransfecteerd met de humane chemokine receptor CXCR4 versterkte LL-37 de reactie op lage dosissen van SDF-1 via de opname van CXCR4 in lipide rafts.

Hoewel er verschillende parallelle effecten van LL-37 en P318 werden waargenomen, ontdekten we dat P318 B16 melanoomcellen activeert via een ander werkingsmechanisme dan LL-37. Blootstelling van B16 cellen aan P318 leidde bijvoorbeeld tot de snelle productie van cAMP als secundaire boodschapper, terwijl dit effect niet werd waargenomen na behandeling met LL-37. Bovendien veroorzaakte P318 ook een calciumrespons en hyperpolarisatie in B16 cellen, wat duidt op een complexe wisselwerking tussen verschillende signaaltransductiewegen. Het signaal werd vervolgens verdergezet via protein kinase B.

Onze pogingen om op een ondubbelzinnige wijze de identiteit van de receptor van LL-37 en P318 te achterhalen in één van deze celtypes gaven geen uitsluitsel. Het moet echter opgemerkt worden dat zowel LL-37 als P318 in staat zijn om een cellulaire respons te induceren in een breed scala aan celtypes, wat erop kan wijzen dat het amfipatische karakter van de peptiden hen toelaat om signaaltransductiewegen te activeren door eerst met de celmembraan te binden. In deze positie kunnen LL-37 en P318 allosterische veranderingen in receptoren teweegbrengen, receptoren herlokaliseren in lipide rafts, of de beweeglijkheid van componenten van receptorcomplexen beïnvloeden. Structuur-activiteitstudies op P318 wijzen ook meer in de richting van een rol voor P318 in de celmembraan. Dit aspecifiek mechanisme – dat in overeenstemming is met de doorgaans promiscue en lage-affiniteit type activering van LL-37 en P318 – duidt mogelijk op een meer algemene manier waarmee amfipatsiche peptiden signaaltransductiewegen kunnen activeren in gastheercellen.

In het tweede deel van dit proefschrift geven we een overzicht van verschillende 3D celcultuursystemen en bespreken de voor- en nadelen van het gebruik van 3D celculturen in vergelijking met de gebruikelijke 2D celculturen. Er is een toenemende belangstelling voor het gebruik van 3D celculturen in preklinisch onderzoek, omdat 3D celculturen de complexe 3D opbouw van *in vivo* cellen beter nabootsen dan 2D celculturen. Verschillende factoren verhinderen echter dat 3D celculturen routinematig worden gebruikt in onderzoeken ter ontdekking van nieuwe geneesmiddelen, zoals b.v. het gebrek aan een gedetailleerde biochemische typering van meercellige sferoïden. Daarom gebruikten we RNA-sequencing om differentiële genexpressie te meten tussen 2D en 3D celculturen van humane HT-29 colorectale carcinoomcellen. Verschillende GPCRs, RTKs en ionenkanalen werden geïdentificeerd die differentieel tot expressie kwamen, waarvan sommigen reeds in verband werden gebracht met de voortgang van colorectale kanker. Aangezien HT-29 3D celculturen beter de *in vivo* structuur van tumorcellen weergeven, zijn de receptoren die tot over- of onderexpressie komen mogelijke doelwitten in de zoektocht naar nieuwe colorectale kanker therapieën.

Summary

This doctoral dissertation consists of two main parts. The first part aims to elucidate the signal transduction pathways of recently discovered putative bioactive peptides. The second part introduces 3D cell culture systems and measures differential gene expression between 2D- and 3D-cultured cells.

Bioactive peptides perform important functions as inter- and intracellular signaling molecules, making them indispensable for the existence of multicellular life. Processed from larger precursors, they influence various physiological processes, including feeding and body weight regulation, sleep, pain, anxiety, and memory. Thanks to improved hyphenated peptidomics techniques, peptides can be identified in very complex mixtures like tissue extracts. However, the peptide sequence itself does not always provide information on the putative biological function of the peptide. The majority of peptides function by binding to their cognate receptor, initiating a cascade of reactions inside the cell. Determination of the receptor type and unraveling the signal transduction pathway provides a starting point for functional elucidation and, consequently, possible future drug development.

Previously, exploiting a state-of-the-art peptidomics strategy, the research group of prof. Schoofs was able to create a peptide library containing more than 700 potentially bioactive peptides. To gain more insight into the function of these candidate peptides, an inter-university consortium was set up, including experts in distinct fields of cell biology and animal experimentation. Our laboratory primarily focused on testing the candidate peptides on a panel of cultured cell lines representative for almost all cell types present in humans or mice. In a first stage, experiments were conducted to investigate whether the candidate peptides have any bioactivity. These screening experiments were conducted with peptide material from a small scale crude synthesis. Once activity was observed with crude peptide material, the same peptide was re-used at a higher purity level in order to reproduce the original observation. The effects induced by crude peptides were often difficult to reproduce, suggesting that peptide quality is a critical attribute for adequate interpretation of results. However, several purified peptides were found to be active in one or more assays and these were selected for follow-up analysis.

Arguably the most promising candidate peptide was a peptide codenamed P318, due to its pleiotropic effects on various cell types. P318 is a novel peptide fragment of the mouse cathelicidin-related antimicrobial peptide (CRAMP). Cathelicidin peptides form an essential part of the immune system as they exhibit both immunomodulatory and direct antimicrobial activities. Probably the most widely studied member of the cathelicidin family of antimicrobial peptides is LL-37 (leucine-leucine-37), the only human cathelicidin identified to date.

On host cells, the majority of LL-37-induced effects are mediated via direct or indirect activation of various structurally unrelated cell surface receptors or intracellular targets. It remains a conundrum how one peptide is able to activate putative receptors belonging to different receptor classes, particularly as most 'ligand-receptor' interactions occur in a very specific manner. To elucidate this matter, we published a review article about the function of LL-37 and put this in relation with all the receptors and ion channels presently known as activated by LL-37. In addition, we investigated the activity profile of LL-37 across a range of cultured cell lines. This proved helpful for further characterization of the effect of P318, *e.g.* determination of the receptor type and elucidation of the signal transduction pathway.

Because LL-37 modulates host cell activity by virtue of distinctly different mechanisms, a more aspecific technique is required to detect cell activation, regardless of the receptor or intracellular signaling pathway that is triggered. We report that electrical impedance spectroscopy meets the necessary requirements to monitor the activity of LL-37. Impedance responses provide a real-time, label-free, and integrative measure of the signaling repertoire engaged upon LL-37 treatment. Based on the impedance response of cultured cell lines to LL-37, hypotheses on the mode of action can be formulated and tested using a collection of pharmacological agents. Differences in the effect of LL-37 deliver important information regarding its cognate receptor and the implicated signaling transduction cascade.

In addition to confirming known activity on a number of cell lines, novel activity of LL-37 was discovered using EIS. For example, we were able to detect previously undocumented effects of LL-37 on HEK293T and U87 glioblastoma cells. Subsequently, second messenger assays were performed to obtain information about which second messenger propagates the signal inside the cell. This revealed that LL-37 dose-dependently activates HEK293T cells through calcium release from intracellular stores. Strong indications were found that LL-37 interacts with the plasma membrane rather than specific ligand-binding sites. Aside from calcium mobilization, LL-37 exerted a cytotoxic effect on HEK293T cells by creating transmembrane pores. Pretreatment with suramin or suramin analogues protected HEK293T cells from LL-37-induced cell injury.

We also report that the use of EIS can help discriminate between different modes of action of LL-37. Endocytic pathways appear to be involved in LL-37-internalization in A549 lung carcinoma cells. In U87 glioblastoma cells transfected with the human chemokine receptor CXCR4, LL-37 enhanced signaling in response to low doses of stromal cell-derived factor 1 by incorporating CXCR4 into lipid rafts (LRs).

Even though several parallel effects of P318 and LL-37 were discovered, P318 induced a response in B16 melanoma cells through a different molecular mechanism than LL-37. Administration of P318 to B16 cells led to the rapid production of cAMP as a second messenger, whereas this effect was not

observed when B16 cells were treated with LL-37. Furthermore, P318 evoked a calcium response and caused hyperpolarization in B16 cells, suggestive of a complex interplay between multiple signaling pathways. The signal was then transduced through a protein kinase B-dependent pathway.

Efforts to unambiguously obtain the identity of the cognate receptor for LL-37 or P318 on any of these cell lines were inconclusive. However, it must be noted that LL-37 and P318 evoked a response of various cell types, favoring the hypothesis that the amphipathic nature of the peptides enables them to induce cell signaling by first binding to the cell membrane. In this position, LL-37 and P318 can induce allosteric changes in receptors, relocalize them into LRs, or change the motility of receptor complex components. Structure-activity relationship studies of P318 also point more into the direction of a role in the cell membrane. This rather aspecific mechanism – which is consistent with the promiscuous and generally low-affinity type of activity of LL-37 and P318 – might have a more general effect to our understanding how amphipathic peptides such as LL-37 and P318 modify signal transduction in host cells.

In the second part of this dissertation, we provide the reader with an overview of various 3D cell culture model systems, and outline the (dis)advantages of using 3D cell culture models in comparison to conventional 2D cell cultures. 3D cell cultures have gained increasing interest in preclinical research as they provide a more accurate depiction of the complex 3D architecture observed *in vivo*. However, the routine use of 3D cell culture models in platforms for drug discovery has been hampered by several factors, including the lack of a detailed biochemical characterization of multicellular 3D spheroids. We used RNA-sequencing to measure differential gene expression in the human colon adenocarcinoma cell line HT-29 cultivated in 2D and 3D. We identified several differentially expressed GPCRs, RTKs, and ion channels of which some have been associated with colorectal cancer progression and/or metastasis. Because 3D cell cultures of HT-29 better recapitulate the *in vivo* structure of tumor cells, receptors that are up- or downregulated in spheroids can be promising targets for colorectal cancer therapy. In addition, pathway enrichment analysis on differentially expressed genes in 3D compared with 2D revealed changes to a number of pathways, including cell cycle and metabolic pathways.

Chapter I

A general introduction

1.1 Situating the research project

1.1.1 The bigger picture: peptidomics arrives on the scene.

"May you live in interesting times." This old saying would be well suited to describe the recent progress made in different fields of modern science. We are living in the midst of a technological revolution, which is fundamentally reshaping everything from industry to medicine. Technological advancements have made a profound impact on almost every aspect of our daily lives, including the way we communicate, learn, and work. Many of us have become (too?) dependent on technology and this trend is expected to continue. In our increasingly globalized and dynamic world, life without technology is meaningless.

From a biological perspective, present-day scientists are taking the fruits of this recent boom in technology. Envisioned concepts that seemed practically impossible just a few decades ago are now a reality. Few would have believed that one day we would be able to retrieve information from genomes of extinct species by means of a simple mouse-click. However, according to the National Center for Biotechnology Information (NCBI) website, DNA sequence data of more than a hundred extinct species are publicly available at GenBank [1]. Today, it is also no longer science-fiction to create synthetic cells, completely controlled by predetermined genetic instructions [2]. The result will be a coming era of digital biology, in which digitally transformed genomes may generate viable cells fitted for specific needs such as fuel, food, or therapeutics [3]. However, future work requires an unprecedented insight into epigenetics, RNA-editing and alternative splicing if we want to surpass the theoretical stage.

Technological progress also changes the way researchers design and conduct their experiments. As today's scientists have access to a large amount of publicly available gene expression data, they can pursue deep insights into genetic disorders without ever having to enter a laboratory. Not the manual lab work, but the ability to work with large-scale datasets is considered as one of the core competencies of a twenty-first century scientist. Therefore, data scientists are in high demand by various academic institutions and biotech companies.

In the early 2000s, improved dealing with large data sets along with increased performance of analytical techniques such as mass spectrometry (MS) shaped the background of this PhD project. At the time, a new promising field within the 'omics' family, named peptidomics, was launched into biology. Peptidomics can be defined as the branch of molecular biology that analyzes the complement of endogenous peptides in a cell, tissue, or organism [4]. Peptides are found in all living

organisms and regulate various physiological and pathological processes. Therefore, they receive considerable interest from the pharmaceutical industry [5].

In essence, peptidomics is a subfield of proteomics that targets physiologically active peptides [4]. For a long time, peptides were not studied to the same extent as their protein counterparts. This can partially be explained by the fact that most bioactive peptides are present at very low concentrations compared to major proteins in a cell. In addition, peptides have a short half-life and are quickly degraded by proteolytic enzymes, highlighting the need for efficient peptide extraction procedures that suspend proteolytic activity [5]. Furthermore, the primary workhorse of proteomics has been two-dimensional gel electrophoresis (2DGE), which separates a mixture of proteins according to their isoelectric point and molecular mass. 2DGE retains proteins with a molecular weight above a certain cut-off value, but releases lower molecular weight proteins such as bioactive peptides [6]. As a consequence, physiologically relevant peptides often slipped through the mazes of the net and were not investigated to the same extent as proteins.

Even though various gels are currently available that are specifically designed for separating peptides in the small to medium range (0.5-10 kDa), the field of peptidomics was mainly boosted by mass spectrometers excelling in sensitivity and dynamic range along with an improved control of proteolytic degradation [4,7,8]. In hindsight, the research group of prof. Schoofs can be considered as 'peptidomics-pioneers' as they were among the first to develop a complete peptidomics platform including hyphenated techniques and bioinformatics. This approach enabled them to identify more than thousand putative peptide sequences originating from various animal tissues and body fluids. After a well-considered selection step, a peptide library was constructed containing more than 700 candidate bioactive peptides from mouse and human. Each peptide with a certain biological activity offers the potential to develop new therapeutics and diagnostics, in case it is implicated in a certain physiological or disease process [5].

Identification of the amino acid sequence of a peptide leads to the question of its function and mechanism of action on cells. Even though many biotech companies offer a variety of functional cell-based assays, it remains a genuine challenge to assign functions to newly discovered peptides. Only through the combination of the right methods and techniques in a logical manner can increased insights into the mechanisms by which peptides regulate cellular activities be obtained. Unraveling the mode of action of a candidate peptide typically involves identifying its cognate receptor and elucidating the signal transduction pathway that it activates. We devised a strategy based on electrical impedance spectroscopy (EIS) and second messenger assays, along with a collection of pharmacological agents, to identify the cognate receptor of a putative bioactive peptide. Knowledge

about the receptor of a candidate peptide is of great value in advanced stages of the research, in case the candidate peptide is involved in a particular biological or disease process. A detailed overview of the methodology used in this thesis, as well as a brief introduction to EIS, will be provided later in this chapter.

We used conventional 2-dimensional (2D) cell cultures to identify the receptor and elucidate the signal transduction pathway of a candidate peptide. 2D cell cultures permit a simpler and more controlled analysis than *in vivo* models. However, one of the most important disadvantages of using 2D cell culture models is that they do not always generate predictive data for *in vivo* tests. This is often referred to as the '*in vitro*-*in vivo* gap'. Over the past few decades, scientists have been looking to bridge this gap by developing cell culture models that more accurately mimic *in vivo* cell behavior. This has led to the introduction of various types of 3D cell culture models, in which the 3D structure of a cell is preserved [9,10]. In the second part of this dissertation, we will introduce 3D cell culture systems and compare receptor transcription profiles between 2D- and 3D-cultured cells.

The goal of this introductory chapter is to provide the reader with the essential context needed to understand the research problem and its significance. In addition, the basic principles of signal transduction will be explained and a brief overview of the most common receptor families activated by peptides will be given. We also explain the relatively new concept of functional selectivity, as a single receptor can impinge upon multiple signaling cascades. For a detailed introduction to 3D cell culture systems, the reader is referred to chapter 6.

It must be noted that this thesis project builds upon previous work. Therefore, we start the following section by describing how the project started and evolved throughout the years.

1.1.2 The functional peptidomics initiative

In 1990, the world's largest collaborative biological project, called the Human Genome Project (HGP), was initiated with the objective of determining the entire DNA sequence of the human genome. Even though it took almost 15 years until the program was completed, HGP provided biologists with a wealth of information about the location, function, and organization of the complete set of human genes [11]. It also supported the characterization of genomes of other model organisms, including mice, fruit flies, and roundworms [12-14]. The next challenge faced by many researchers was to extract useful information encoded within these billions of nucleotides.

Analysis of the human and mouse genomes revealed the presence of many G protein-coupled receptors (GPCRs) whose endogenous ligand had not yet been identified. This observation aroused interest of many research groups, including the laboratory of prof. Schoofs. Because her research

group had a strong background in the field of invertebrate peptide discovery, she was particularly interested in peptide receptors.

In 2006, a so-called *Strategisch Basisonderzoek* (SBO) project funded by the Flemish government was initiated to identify and functionally characterize as many novel bioactive peptides as possible in various human and mouse tissues and body fluids. Their systematic discovery was made possible by exploiting a peptidomics strategy, using proprietary peptide extraction technologies in combination with multi-dimensional liquid chromatography, high-resolution MS, and bioinformatics (e.g. *in silico* prediction, advanced peptide identification software). This work resulted in the creation of a synthetic peptide library, harboring more than 700 candidate bioactive peptides. Due to a precise control of proteolysis, the peptide library should be largely devoid of proteolytic degradation products. All the candidate peptides contained several hallmarks of biologically active peptides and were not described in the scientific or patent literature.

The newly discovered putative bioactive peptides were then tested in different labs, employing various *in vitro*, *in vivo* and *ex vivo* assays. These tests were funded by an *Industrieel Onderzoeksfonds* (IOF) project granted in 2011, together with a second SBO project which examined interactions of peptides with various target proteins. Our laboratory primarily focused on testing the peptide library on a panel of more than 40 cultured cell lines of human and mouse origin.

With little more but knowledge of their amino acid sequence, the goal was set to elucidate the mechanism of action of candidate peptides on a variety of cultured cell lines. Early-stage screening for peptide activity was done employing a technique (EIS) that does not depend on the type of receptor or the signal transduction pathway that is activated. Once a cellular response was detected upon exposure to a purified candidate peptide, follow-up experiments were performed to investigate whether this cell type possesses a receptor for this peptide. A large collection of broad-spectrum and receptor-specific antagonists were then applied to cells to obtain information about the receptor type and the activated signaling cascade. Simultaneously, RNA-sequencing (RNA-Seq) experiments were conducted on cell lines observed to respond to a candidate peptide in order to gain insight into the endogenous receptor repertoire of this cell line. These messenger RNA (mRNA) expression data can help narrow down the list of possible molecular targets of a candidate peptide.

Note that each peptide-receptor pair represents a great starting point for peptide-based drug development. Bioactive peptides have an attractive pharmacological profile, as they are generally selective and efficacious signaling molecules [5]. In addition, they have good tolerability and safety profiles. Nevertheless, peptides often cannot be used directly as therapeutics or diagnostics, because they possess intrinsic weaknesses such as a relatively short half-life, poor oral bioavailability, and

suboptimal chemical and physical properties. To mitigate these weaknesses, peptidomimetic elements are often introduced into the sequences to facilitate the rational design of peptide therapeutics [5].

In the following section, we will briefly introduce some general aspects of bioactive peptides. In addition, we will discuss the most common classes of molecules that participate in signal transduction pathways.

1.2 Bioactive peptides

Bioactive peptides that function as extracellular signaling molecules play fundamental roles in intercellular communication mechanisms. More than 7000 naturally occurring peptides have been identified, and these regulate various essential physiological processes such as feeding and body weight regulation, sleep, pain, anxiety, learning, and memory [5]. In essence, they are a type of biological messengers that carry information for cells to thrive and survive.

Peptides are short chains of amino acid monomers linked by amide bonds between the amino group of one amino acid and the carboxyl group of the next amino acid. Peptides are subdivided into oligopeptides (2 to 20 amino acids) and polypeptides (20 to 50 amino acids). Proteins are essentially larger polypeptides consisting of more than 50 amino acids. However, the size boundaries that distinguish proteins from peptides are not absolute. Proteins can also be distinguished from peptides by their tendency to fold into higher-order 3D conformations [15].

One of the first discovered peptides was Substance P, a neuropeptide associated with inflammation and pain [16]. Other well-known peptides include glucagon, leptin, vasoactive intestinal peptide, angiotensin, and bradykinin. Many peptides are currently in use as therapeutics or diagnostics, and this trend is expected to continue. Fosgerau *et al*. estimate that the global peptide drug market will increase from €12.6 billion in 2011 to €22,7 billion in 2018 [5].

In general, biologically active peptides are produced from a larger precursor protein, called a prepropeptide. The prepropeptide contains a signal sequence as well as specific cleavage sites for several post-translational modification (PTM) enzymes such as prohormone convertases, carboxpeptidase E, and peptidyl-amidating monooxygenases. Upon arrival at the endoplasmic reticulum (ER), the initial signal peptide is removed by a signal peptidase. Cleavage of the signal sequence produces a propeptide, which is transferred to the Golgi complex where it undergoes additional post-translational processing. PTMs, including sulfation, amidation, acetylation, or pyroglutamate formation, often occur in the last steps of peptide biogenesis which turns the inactive propeptide into an active state [17]. The mature peptides are then packaged in intracellular secretory vesicles and are released in response to a specific environmental stimulus. Once secreted, the peptide acts as a regulatory compound on the same cell (autocrine signaling), neighboring cells (paracrine signaling) or more distant cells (endocrine signaling) [18]. The binding of a peptide to its cognate receptor initiates a process called signal transduction. In the following section, we will outline the general principles of signal transduction.

It must be noted that other ways exist by which bioactive peptides activate target cells. For example, cell-penetrating peptides (CPPs) cross the cellular membrane of eukaryotic cells in a receptor-independent fashion [19]. CPPs have an amphipathic, hydrophobic or polycationic nature and often serve as vehicles for the transport of molecular cargo into cells.

1.3 The process of signal transduction: basic principles

At least 3.8 billion years ago, the earliest living cells emerged from a sea of organic molecules [20]. How this exactly happened remains the subject of ongoing discussion, as only parts of this process can be reproduced experimentally. There is a consensus that the earliest living cells on earth were able to acquire energy directly from their environment, allowing them to perform basic life functions such as reproduction, growth, and movement. It appears any living cell possesses the intrinsic universal feature to be 'aware' of its surroundings and to respond to signals indicating environmental change [21]. Obtaining a better understanding of the underlying mechanisms by which cells perceive, transmit and respond to various physical and chemical stimuli has been one of the most active research areas in biology.

Signal transduction is the process of transferring extracellular information to a cell's interior via a series of molecular events (figure 1.1). Signal transduction pathways comprise a variety of players which often interact sequentially. Evolution enabled a structurally diverse set of chemical (*e.g.* peptides, ions, nucleotides, metabolites) or physical (*e.g*. temperature, light, pressure) components to pass on the message [20,21].

Chemical messengers, termed ligands, produce a signal by specifically binding to a target protein. Ligands are classified in different ways depending on their molecular mass, structure, or lipophilicity. Lipophilic signal molecules have the ability to cross the cell membrane and interact with intracellular targets in the cytoplasm or nucleus. Lipophobic ligands require specialized proteins on the cell surface to get their message across. These specialized proteins, called receptors, change conformation upon ligand binding and transduce the signal to various downstream intracellular effector proteins [20,21]. In the field of pharmacology, ligands are classified into different efficacy groups. A full agonist is a ligand that has the ability to evoke a maximal response, whereas partial agonists have only partial efficacy relative to a full agonist. Neutral antagonists prevent other ligands from interacting with the receptor protein, without activating a signaling cascade. Inverse agonists bind to constitutively active receptors and reduce their basal activity [22].

Ligand binding often induces conformational changes in specific cell surface proteins, which in turn generates a cascade of specific cellular responses. Once a cell has responded to a particular stimulus, the signal must be turned off. Without such cessation, cells lose their responsiveness to new environmental stimuli [21].

Signaling circuits are often represented as if they were linear chains, although this does not correspond to the complex *in vivo* situation. A more holistic view shows that molecular cross-talk

among signaling pathways enables cells to process and respond to multiple inputs [23]. Cross-talk can generate inter-dependent cyclic adenosine monophosphate (cAMP) and calcium oscillations, leading to synergistic or inhibitory effects on two or more signal transduction pathways. More recent phosphoproteomic studies point to a regulatory role for various phopsphorylation sites which serve as molecular switches for pathway cross-talk [22,24]. Progress in the fields of systems biology and mathematical modelling are expected to extend our knowledge on these important topics.

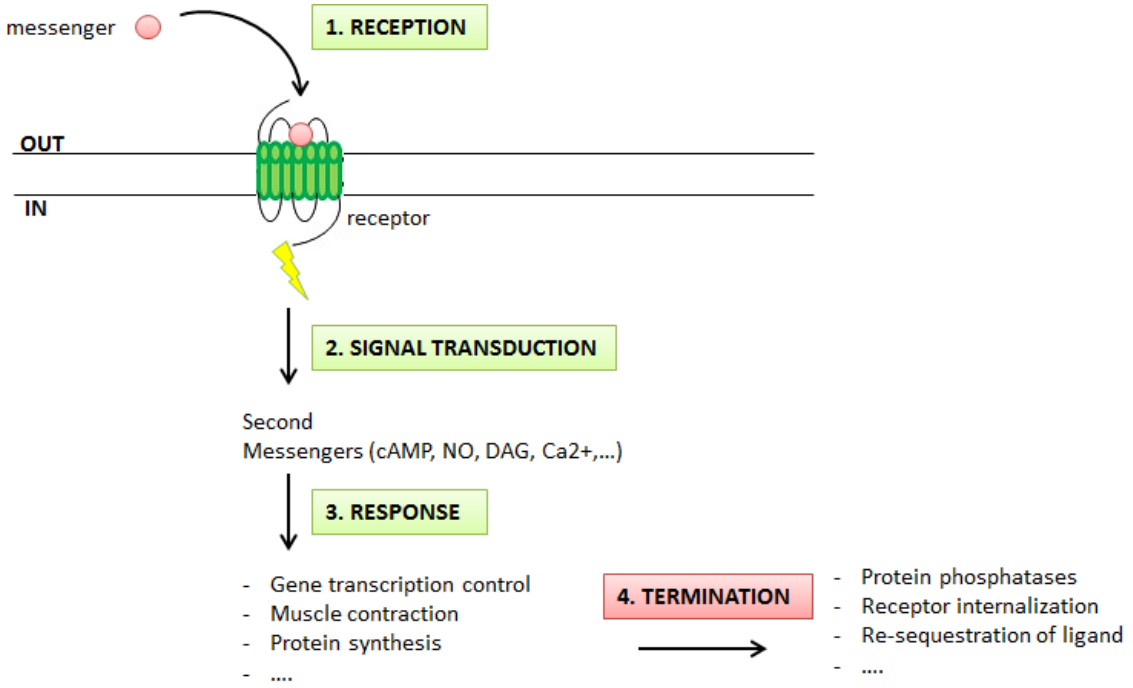

Fig.1.1. Basic principles of signal transduction. A chemical or physical message is perceived by dedicated proteins on the cell surface, after which the signal is converted into a variety of chemical forms. The signal is then amplified before it evokes a certain cellular response. Mechanisms that attenuate cell signaling eventually terminate the signal transduction cascade (NO: nitric oxide; DAG: diacylglycerol; cAMP: cyclic adenosine monophosphate; Ca^{2+}: calcium).

1.3.1 Reception of the signal by receptors

Receptors are highly specialized proteins which allow cells to communicate with the extracellular environment. They are embedded in the plasma membrane (cell surface receptor) or located in the cytoplasm (cytoplasmic receptor) or nucleus (nuclear receptor). Each cell type possesses different combinations of receptor proteins, which determines the cell's sensitivity to a particular stimulus. A 'lock-and-key' analogy is often used to describe a conventional ligand-receptor interaction.

Throughout this manuscript, the main focus will be on cell surface receptors, which typically consist of three domains: (i) an extracellular domain that recognizes a specific ligand, (ii) a transmembrane domain that either changes conformation or forms a pore upon interaction with a ligand, (iii) an intracellular domain that relays the signal [21]. Arguably the most important receptor classes are GPCRs, enzyme-linked receptors, and ion channel-linked receptors.

1.3.1.1 G protein-coupled receptors

GPCRs, also known as seven-transmembrane (7TM) domain receptors, comprise a large and versatile family of integral membrane proteins. The human genome encodes more than thousand different GPCRs [25]. Many vital physiological processes are regulated by GPCRs, including neurotransmission, blood pressure, cell growth, as well as the 'fight-or-flight' response. GPCRs are also responsible for vision, olfaction, and taste [26,27]. Dysfunction of GPCRs is associated with some of the most prevalent human diseases such as cancer, Alzheimer's disease (AD), Parkinson's disease, and cardiovascular disease [26-30]. Therefore, GPCRs are the subject of active drug discovery research. It is currently estimated that 30 to 50% of all marketed pharmaceutical drugs target GPCRs. However, only a small fraction (~10 %) of known GPCRs is targeted by these drugs, thereby fueling the continuous interest for future GPCR-based drug discovery efforts [25].

Various peptides target GPCRs, which makes them promising drug candidates [25]. One example thereof is probably the peptide hormone angiotensin II, which causes vasoconstriction by activating a GPCR. Angiotensin II receptor inhibitors are commonly used to treat conditions such as high blood pressure and heart failure [31].

Aside from peptides, GPCRs act as receptors for a variety of biomolecules such as photons, ions, odor molecules, pheromones, and neurotransmitters [29]. A single GPCR typically responds to a limited amount of biologically active molecules which possess unique structural motifs. The basic architecture of GPCRs comprises seven evolutionary conserved transmembrane α-helical domains, connected by three intracellular (ICL) and three extracellular loops (ECL). Depending on the GPCR family, one or more of the ECLs form the ligand-binding pocket, together with an extracellular N-terminal segment. Intracellularly, a carboxy-terminal tail along with one or more ICLs interact with monomeric or heterotrimeric guanine nucleotide-binding proteins (G proteins), which function as intracellular molecular switches [28,29].

G proteins are characterized by their ability to bind guanosine triphosphate (GTP) and guanosine diphosphate (GDP). Heterotrimeric G proteins are membrane-associated proteins composed of three subunits: Gα, Gβ, and Gγ. Gα-subunits are usually classified into four subfamilies ($G\alpha_s$, $G\alpha_{q/11}$, $G\alpha_{i/o}$, $G\alpha_{12/13}$) on the basis of their DNA sequence homologies [21,32]. Each Gα-subunit possesses a well-defined set of intracellular interaction partners, thereby enabling cells to respond appropriately to an extracellular stimulus. For example, the general function of $G\alpha_s$ is to produce cAMP from ATP by activating adenylyl cyclase, as opposed to $G\alpha_i$ which inhibits adenylyl cyclase from generating cAMP. $G\alpha_{q/11}$ activates phospholipase C (PLC) which in turn cleaves phosphatidylinositol 4,5-bisphosphate (PIP_2) into diacylglycerol (DAG) and inositol 1,4,5-triphosphate (IP_3). IP_3 diffuses to the ER and acts on

inositol 1,4,5-triphosphate receptors (IP_3R) to promote the release of calcium from intracellular stores [21,32]. $G\alpha_{12/13}$-subunits regulate a variety of physiological processes by specifically interacting with Rho-guanine nucleotide exchange factors (RhoGEFs) containing an N-terminal regulator of G protein signaling (RGS) homology domain [33].

G proteins undergo repeated cycles of activation and deactivation [21]. In the inactive state, GDP remains bound to the Gα-subunit. Upon binding of a ligand, the GPCR undergoes a conformational change which causes the Gα-subunit to exchange GDP for GTP. The active Gα-subunit dissociates from the Gβγ-dimer, enabling both subunits to activate distinct downstream effector proteins such as PLC or adenylyl cyclase (figure 1.2). Hydrolysis of the bound GTP to GDP by intrinsic GTPase activity of the Gα-subunit terminates the transduced signal and leads to the re-association of the heterotrimeric G protein. G protein-coupled kinases (GRKs) also play a role in turning off the signaling cascade by phosphorylating the cytosolic portion of the activated GPCR. Once phosphorylated, the GPCR binds with high affinity to β-arrestin, which inactivates signaling by preventing its interaction with G proteins. β-arrestins also guide the phosphorylated receptor to specific endocytic pathways where they are either degraded or recycled [26,27].

Recent ground-breaking work by Lefkowitz and Kobilka on the β-adrenergic receptor (BAR) led to a better understanding of how GPCRs function [34-36]. In these studies, crystallography was used to obtain a better understanding of the mechanisms underlying GPCR activation. GPCRs are notoriously difficult to crystallize and rapidly lose their integrity when taken out of the plasma membrane. Kobilka and Lefkowitz used combinations of detergents and antibodies, together with deletions of small segments of BAR, to stabilize BAR when lifted out of the cell membrane. Their technical tour-de-force eventually resulted in atomic-level crystal structures of BAR in both their active and inactive state. In 2011, they discovered their long-sought Holy Grail in the form of an image of BAR at the exact moment when it was activated by its ligand and transduces the signal into the cell [34]. As this image is truly a molecular masterpiece and can help improve structure-based drug design, they were awarded the 2012 Nobel Prize in Chemistry.

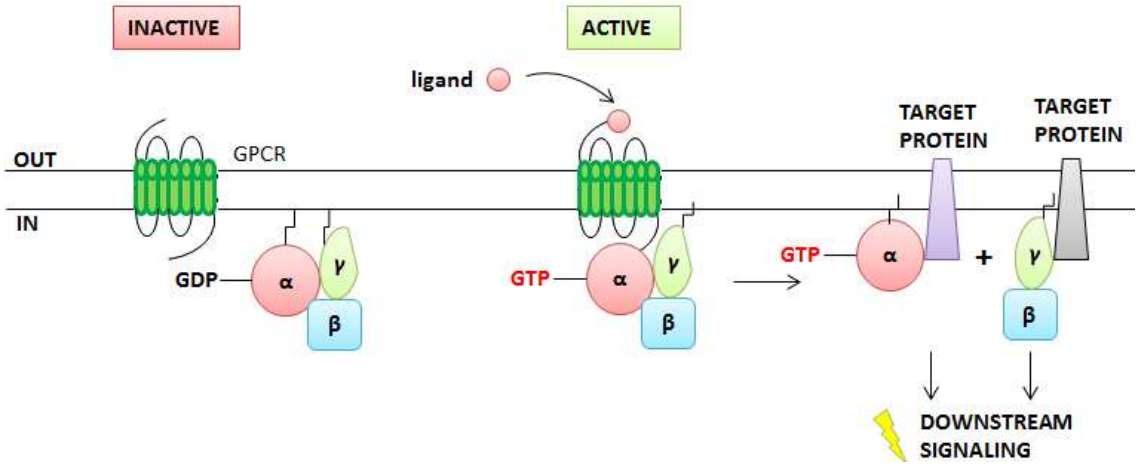

Fig.1.2. GPCR signaling pathway. In the absence of an extracellular ligand, GDP remains bound to the α-subunit of the G protein. Ligand binding induces a conformational change in the GPCR which causes the α-subunit to exchange its GDP for a GTP. The activated G protein then dissociates and interacts with specific effector proteins within the cell, before evoking a particular cellular response.

1.3.1.2 Enzyme-linked receptors

Enzyme-linked receptors constitute another major family of cell surface receptors. These receptors are characterized by an intracellular domain that has intrinsic enzymatic activity or associates directly with an enzyme. Binding of an extracellular ligand induces a conformational change which stimulates the cytoplasmic catalytic function. Many different types of enzymes have been reported to amplify and propagate the signal inside the cell, including cyclases, phosphatases, and kinases [37].

Receptor tyrosine kinases (RTKs) are probably the most widely studied enzyme-linked receptors. RTKs are activated by growth factor ligands and regulate many key cellular processes such as cell migration, proliferation, differentiation, and cell-cycle progression. To date, 58 human RKTs have been identified, which can be classified into 20 subfamilies [38]. Just like GPCRs, aberrant activation of RTKs has been linked to the pathogenesis of several human diseases, including cancer, diabetes, arteriosclerosis, and bone disorders [37-39].

In 1990, Ullrich and Schlessinger discovered that growth factor binding activates RTKs by forming a cross-linked dimer [39]. Cross-linking activates the intrinsic tyrosine kinase activity, and each RTK in the dimer phosphorylates the tyrosine residues on the other RTK. Once cross-phosphorylated, the phosphorylated tyrosines serve as docking platforms for various Src Homology 2 (SH2) domain-containing signaling proteins. The signal is then transduced into the cytosol and ultimately evokes a particular cellular response (figure 1.3).

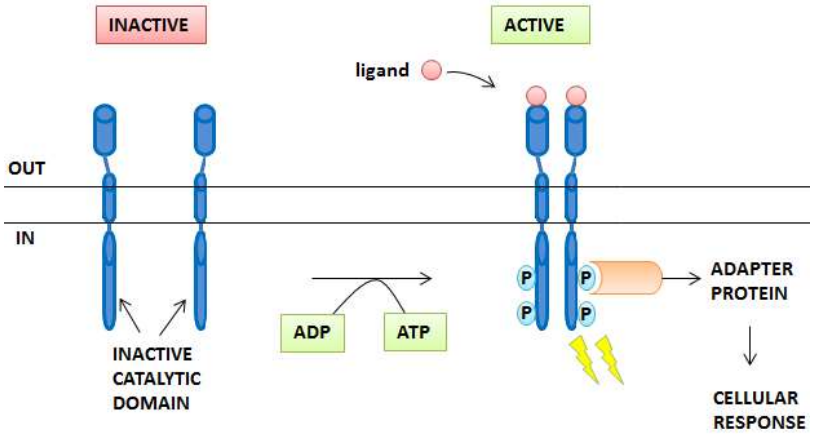

Fig.1.3. Enzyme-linked receptor signaling cascade. Binding of a ligand such as EGF induces a conformational change which activates the intrinsic enzymatic activity of the receptor. In the case of EGFR, ligand-binding causes autophosphorylation of the tyrosine residues of the receptor. This creates new binding sites for adapter proteins, thereby further transducing the signal.

1.3.1.3 Ion channel-linked receptors

Ion channel-linked receptors, more commonly known as ligand-gated ion channels (LGIC), are transmembrane ion channels that open and close upon binding of a ligand. They are abundantly expressed in both excitable and non-excitable cells and play a pivotal role in various physiological processes such as neurotransmission and inflammation [40]. Similar to GPCRs, ion channel-linked receptors are common drug targets. For instance, barbiturates are commonly prescribed to treat insomnia, anxiety, and sleep disorders [41]. In addition, peptide toxins that target ion channels are currently in clinical use [42].

A common feature of these types of receptors is their ability to convert an extracellular chemical message, *e.g.* peptide hormones or neurotransmitters, to an intracellular electrical signal (figure 1.4). Ligands typically bind to a defined binding site on the receptor, which causes a closed channel to open for the selective transport of ions such as potassium (K^+), chloride (Cl^-), calcium (Ca^{2+}), and sodium (Na^+). The influx or efflux of ions changes the electrical properties of the cell, which in turn activates a second family of ion channels, termed voltage-gated ion channels. Unlike ligand-gated ion channels, voltage-gated ion channels depend on differences in the membrane potential across the cell membrane to propagate the signal within or between cells [21,43].

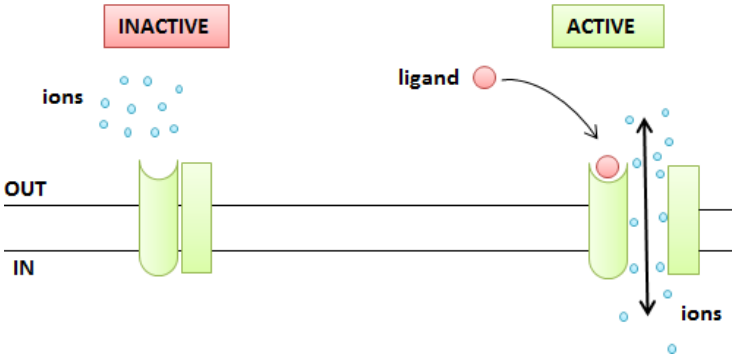

Fig.1.4. Schematic representation of LGIC activation. Activation of the receptor by its matching ligand induces a conformational change, which results in an opened or closed formation of the channel. Selective transport of ions across the plasma membrane changes the electrical properties of the cell, thereby further transducing the signal.

1.3.2 Passing on the message via second messengers and protein phosphorylation

Immediately after the perception and transmission of the signal by cell surface receptors, the message is amplified and passed on by a set of highly specialized signaling molecules, called second messengers. Calcium, cAMP, cyclic guanosine monophosphate (cGMP), arachidonic acid (AA), diacylglycerol (DAG), nitric oxide (NO) and IP_3 are commonly used second messengers by a variety of cell types. Second messengers can either be released from intracellular stores, produced enzymatically or move in or out the cell through diffusion. Irrespective of their origin, transient changes in the concentration of second messengers propagate the signal and send it to appropriate intracellular compartments. Notably, many - but not all - second messengers are able to diffuse freely within the cell and bind to specific effector proteins, which in turn stimulate the synthesis of other second messengers. As a consequence, the external signal is amplified. Signal amplification constitutes an important step in the process of signal transduction, as it enables cells to respond properly to very low concentrations (10^{-8} M) of extracellular stimuli in the environment [20,21,43].

Second messengers can either directly evoke a defined cellular response or activate protein kinases. These enzymes transfer phosphoryl groups from adenosine triphosphate (ATP) to threonine, serine or tyrosine residues of various proteins. Structurally, protein kinases are made of a number of different regulatory and catalytic subunits [44]. As long as the regulatory subunits are attached to the catalytic subunits, the enzyme remains inactive. Binding of second messengers to the regulatory portion of the protein kinase liberate the catalytic subunits, which are then activated by phosphorylation. Subsequently, the activated kinase phosphorylates other target proteins in the signaling cascade. These target proteins undergo conformational changes which causes a binding site or catalytic site to become accessible for other signaling proteins. If the target protein is also a kinase, the signaling circuit is referred to as a phosphorylation cascade [21].

Note that the process of protein phosphorylation is reversible and results from a balanced interplay between kinases and phosphatases. This dynamic process constitutes a general mechanism by which cells transfer information down a particular signal transduction pathway. However, other PTMs such as glycosylation, adenylation, and oxidation also play important roles in signal transduction [19,39]. For example, glycosylation plays a key role in determining protein structure and function and can occur in every step of the process of signal transduction, *e.g.* on the ligand, receptor, enzymes, and/or downstream effector proteins [45].

1.3.3 Termination of the signaling cascade

Once a cell has responded to a signaling molecule in its microenvironment, it should return to its non-stimulated state as quickly as possible. Various physiological mechanisms of signal termination have been unraveled so far. Intracellular signaling molecules are often enzymatically destroyed after they have exerted their action. For example, cAMP is de-cyclized to AMP by the enzyme phosphodiesterase [46]. Calcium ions do not follow this rationale, as they are not destroyed when they have served their role. Increased intracellular calcium levels are lowered by the action of calcium-binding proteins, or via calcium-uptake into the mitochondrial matrix [21,47].

Other mechanisms that attenuate signaling include internalization of receptor-ligand complexes via endocytic pathways. After internalization, the receptor is degraded or recycled back to the plasma membrane [48]. It should also be mentioned that physiological mechanisms of signal termination have not been investigated to the same extent as their activation counterparts. However, a growing number of researchers recognize that the balance between 'on' and 'off' signals plays a pivotal role in various disease-related processes. Therefore, improved knowledge on the mechanisms of signal termination could establish a new starting point for future drug development efforts.

1.3.4 Functional selectivity

Prokaryotic and eukaryotic cells are always surrounded by a plethora of signal molecules in their microenvironment. Intriguingly, they appear to integrate and process all this information and come up with a specific response. For a long time, it was unclear how cells were able to manage different signal transduction pathways simultaneously. Currently, there is a consensus that different pathways share several common elements, which gives them the opportunity to influence each other. This is more commonly known as molecular crosstalk [21]. Vert *et al*. demonstrated that, in some cases, the combinatorial signal from two pathways produces a different response in comparison to the response triggered by each pathway on its own [49].

In addition to molecular cross-talk events, receptor heterodimerization as well as a concept termed 'functional selectivity' further underscore the complexity of signal transduction. Functional selectivity, also called biased signaling or ligand-directed signaling, posits that a ligand possesses the intrinsic ability to direct a receptor toward a conformation that selectively activates or inhibits one or more signaling pathways [50]. It has been demonstrated that receptors such as GPCRs are pluridimensional proteins able to undergo conformational changes depending on the ligand to which they bind. Different ligands can stabilize different receptor conformations, leading to a selective activation or inhibition of a signal transduction pathway. For instance, a functionally selective agonist may produce a biased coupling to a G protein, whereas another agonist interacts allosterically with the same receptor but biases coupling to β-arrestin [51,52].

To date, various GPCR families have been analyzed in the context of functional selectivity, including adrenergic, cannaboid, serotonin, and muscarinic receptors [51]. Given its complicated influence on signaling, the detection of biased (ant)agonism holds great promise in GPCR-based drug development. Exploiting functional selectivity can help improve the development of more specific drugs, while additionally lowering the chance of side effects. This is of particular interest in the treatment of neuropsychiatric diseases [50].

1.4 Methodology

1.4.1 Devising a strategy to elucidate the mode of action of candidate peptides

As mentioned before, the research group of prof. Schoofs houses a large collection of candidate bioactive peptides. Each candidate peptide from our collection can potentially serve as a novel drug design template. Improving peptide properties or discovering new routes of administration are often required before a peptide can be used clinically [5]. The process of peptide drug development involves four phases: discovery and research (i), development (ii), regulatory review (iii), and drug approval (iv). This project covers the first fundamental steps of this process.

We combined several methods and techniques to unravel the mechanism of action of a candidate peptide on a variety of cultured cell lines (figure 1.5). We first employed EIS to screen for bioactivity of candidate peptides, as this technique is capable of detecting cell activation, regardless of the intracellular signal transduction pathway that is activated. Second messenger and membrane potential assays, as well as western blots, were then used to identify key players in the signal transduction cascade. Subsequently, pharmacological agents were administered to cell lines observed to respond to a candidate peptide, which delivers information about the molecular target of a candidate peptide. In some cases, structure-activity relationship (SAR) studies were also

performed on promising peptides to characterize the role of each amino acid in the peptide sequence and to discover more selective, stable and/or potent analogues.

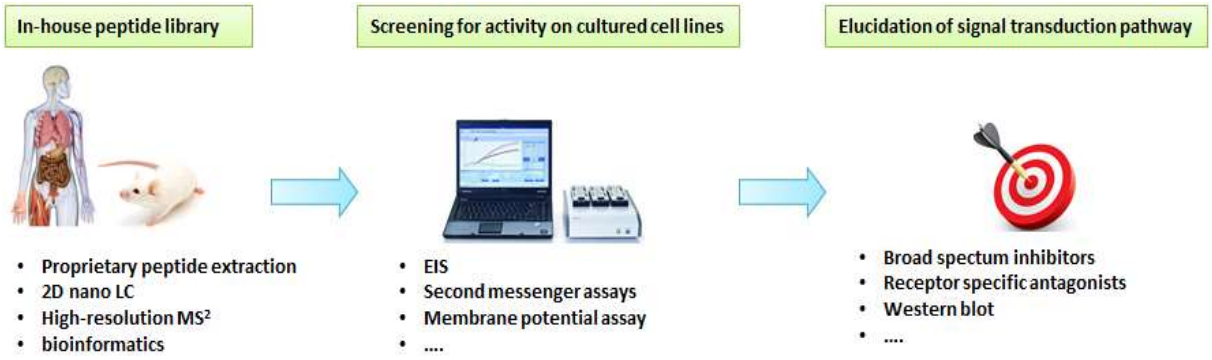

Fig.1.5. Overview of the workflow used in this study. The laboratory of prof. Schoofs houses a peptide library of approximately 700 peptides. These candidate peptides were tested on a panel of cultured cell lines. Several methods and techniques were combined in order to demonstrate the bioactive nature of a putative bioactive peptide and unravel its mode of action.

1.4.2 EIS vs traditional cell-based assays

Present-day scientists can choose among a wide variety of cell-based assays to gain more insight into the function of a candidate peptide. However, the utility of traditional end-point assays is often diminished by various factors, such as their requirement to use labels or the exclusive focus on a specific part of the signal transduction pathway. Additionally, only one or a few time-points are analyzed, thereby providing just a snapshot of the effect of a test compound [53,54]. For instance, fluorogenic calcium mobilization assays are routinely used to measure agonist-evoked increases in intracellular calcium concentrations. Even though this assay proved to be a valuable technique to monitor the release of intracellular calcium as a second messenger, the information it provides is limited because (i) the intracellular calcium levels are only monitored for a short time, (ii) other signaling pathways are not monitored and (iii) it can be difficult to fully comprehend the dye addition effect on a cell's behavior. Furthermore, multiple assays need to be combined in order to reconstruct the complete cellular response induced by a particular test compound. This increases the cost, complexity, and duration of experimental work.

To deal with these challenges, we applied an assay based on EIS to study peptide-induced cellular responses in a real-time and label-free manner. In this approach, an electrical potential is applied across gold electrodes embedded in the bottom of a microtiter plate (figure 1.6A). The gold electrodes are connected to the measurement system and attached to the system under study (*e.g.* adherent cell lines). The resulting electron flow caused by the applied voltage passes through the conductive culture medium and is then used to calculate the impedance, which is the complex generalisation of the resistance and thus given by Ohm's law (voltage divided by current). A change

in impedance is measured when cells adhere and spread on gold electrodes. Interestingly, Giaever and Keese showed that impedance changes correlate with morphological changes occurring within cells [55]. Further research indicated that the magnitude of the impedance is dependent on a broad range of cellular parameters, such as cell size, shape, and number. In essence, the technique can be used to study every cellular process that affects cell morphology, even processes that cannot be detected with high-resolution microscopy. To date, EIS has been successfully employed as a monitoring tool for a variety of cellular processes, including cell proliferation, adhesion, migration, and invasion [53-55].

The course of a typical impedance experiment is depicted in figures 1.6A and B. First, a baseline is measured after which cells are seeded at a certain density. Cells then anchor and spread on the bottom of the well, thereby causing the measured impedance to increase. When cells reach confluency, a compound under study can be added after which the impedance response is tracked as a function of time. For instance, addition of a compound that induces cell death typically causes a decrease in impedance due to cell detachment from the well bottom. However, more subtle cellular processes such as receptor signaling can also be captured by EIS, as shown by Stallaert *et al* [53]. This is because ligand binding to a receptor may alter cellular metabolism which in turn leads to subtle changes in cell size and/or morphology. The suitability of impedance measurements for studying receptor signaling is illustrated in figure 1.6C (impedance data from our lab). Here serotonin, which act through the $G\alpha_i$-class of G proteins, is added to Chinese hamster ovary (CHO) cells and the impedance response is monitored for 15 minutes. The activity of serotonin can be blocked by the $G\alpha_i$-antagonist pertussis toxin (PTX), indicating that the observed phenomena reflect GPCR activation. A dimensionless parameter termed cell index (CI) is used to express the relative change in electrical impedance (more information about CI can be found in the material and methods sections of chapters 4 and 5). Because peptides often elicit a cellular response through interacting with a cell surface receptor, we investigated whether EIS could be used in the context of elucidating the mode of action of candidate peptides on cultured cells.

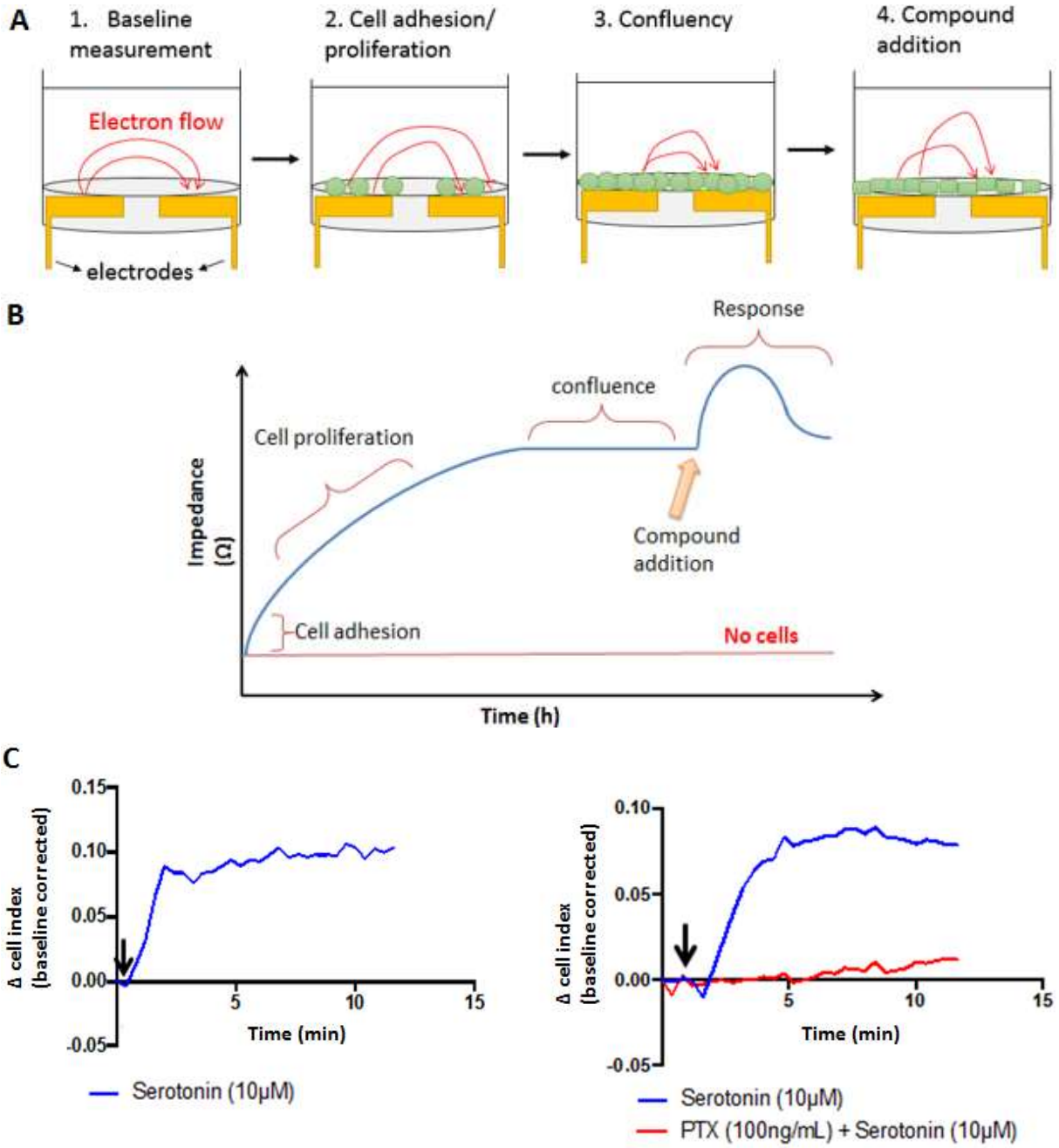

Fig.1.6. Simplified single-well view used in cellular impedance assays (**A**). After measuring a baseline (culture medium without cells), cells are seeded and left to proliferate until they reach confluency. The number of cells as well as their size, shape and adhesion strength affects the measured impedance. In a next step, compounds (*e.g*. peptides) are typically added which may lead to drastic or subtle morphological changes. (**B**) Example of a prototypical impedance readout. An initial rapid increase in impedance due to cell adhesion is followed by a slow increase in impedance due to cell proliferation and spreading. When cells reach confluency, the impedance plateaus and the cell's impedance response to the compound under study can be analyzed. (**C**) Real-time impedance response of CHO cells to serotonin (blue). The impedance response of CHO cells to serotonin is blocked by pretreating cells with the $G\alpha_i$-inhibitor PTX (red) for 24 hours. Arrows indicate the moment of serotonin addition.

Arguably the biggest advantage that EIS has over conventional cell-based assays is that it can be used as a sensitive filtering method for identifying a cell line that responds to a particular compound regardless of the signal transduction pathway that is triggered. This eliminates the time and resource

consuming need to evaluate each downstream signal transduction pathway separately during the intial screening stages of the research. In addition, EIS can also deliver information about the toxicological behavior of drug candidates during the early stages of drug development. To date, a significant number of late-stage clinical failures are attributed to toxicological issues [56]. EIS may alleviate this problem by detecting cytotoxic behavior in an early stage of the drug development process. This of particular interest to the pharmaceutical industry, as drug discovery is an expensive and time consuming process.

Another advantage is that EIS enables researchers to obtain an integrative assessment of ligand activity in a single assay [53]. Studies of Kammermann *et al*. and Stallaert *et al*. show that impedance responses contain complex real-time information on the underlying modes of action by which test compounds induce a certain cellular response [53,57]. Knowledge about the complete cellular response to a test compound is also valuable in the context of functional selectivity, as it may facilitate the identification of biased ligands [53]. The detection of biased signaling holds great promise in GPCR-based drug development and could enhance the feasibility of the development of safer and more specific GPCR-based drugs.

Despite the clear advantages, EIS has some characteristic limitations. Because the measurement by EIS is non-specific, it can be challenging to accurately interpret or dissect the impedance response profiles generated by test compounds. Data analysis also becomes increasingly complex when cells are preincubated with pharmacological agents, as some antagonists induce an impedance response on their own. In line with this, it can be difficult to analyze pleiotropic signaling when multiple pathways have opposing effects.

In the author's opinion, the benefits of EIS outweigh the drawbacks since EIS can be used as a filtering method and potentially provides greater biological insights in an early stage of the research in comparison to conventional end-point assays. This is especially important as we do not have any prior information regarding the mechanism of action of our newly discovered putative peptides. However, follow-up experiments using second messenger assays or western blots are required to validate hypotheses based on impedance measurements.

References

[1] D.A. Benson, I. Karsch-mizrachi, D.J. Lipman, J. Ostell, E.W. Sayers, GenBank, Nucleic Acids Res. 37 (2009) 26–31. doi:10.1093/nar/gkn723.

[2] C.A. Hutchison, R. Chuang, V.N. Noskov *et al.*, Design and synthesis of a minimal bacterial genome, Science. 351 (2016). doi:10.1126/science.aad6253.

[3] F. Baluška, G. Witzany, Life is more than a computer running DNA software, World J. Biol. Chem. 5 (2014) 275–278. doi:10.4331/wjbc.v5.i3.275.

[4] K. Boonen, B. Landuyt, G. Baggerman, S.J. Husson, J. Huybrechts, L. Schoofs, Peptidomics: the integrated approach of MS, hyphenated techniques and bioinformatics for neuropeptide analysis, J. Sep. Sc. 31 (2008) 427-445. doi:10.1002/jssc.200700450.

[5] K. Fosgerau, T. Hoffmann, Peptide therapeutics: Current status and future directions, Drug Discov. Today. 20 (2015) 122–128. doi:10.1016/j.drudis.2014.10.003.

[6] P. Feist, A.B. Hummon, Proteomic challenges: sample preparation techniques for microgram-quantity protein analysis from biological samples, Int. J. Mol. Sci. 16 (2015) 3537-3563. doi: 10.3390/ijms16023537.

[7] K. Sarfo, G.B.G. Moorhead, R.J. Turner, A novel procedure for separating small peptides on polyacryalamide gels, Lett. Pept. Sci. 10 (2003) 127-133. doi: 10.1007/BF02443652.

[8] G. Zilberstein, L. Korol, I. Shlar, P.G. Righetti, S. Bukshpan, High-resolution separation of peptides by sodium dodecyl sulfate-polyacrylamide gel “focusing”, 29 (2008) 1749-1752. doi:10.1002/elps.200700625.

[9] R. Edmondson, J.J. Broglie, A.F. Adcock, L. Yang, Three-dimensional cell culture systems and their applications in drug discovery and cell-based biosensors, Assay. Drug Dev. Technol. 12 (2014) 207-218. doi: 10.1089/adt.2014.573.

[10] M. Ravi, V. Paramesh, S.R. Kaviya, E. Anuradha, F.D. Paul Solomon, 3D cell culture systems: advantages and applications, J. Cell. Physiol. 230 (2015) 16-26. doi:10.1002/jcp.24683.

[11] International Human Genome Sequencing Consortium, Finishing the euchromatic sequence of the human genome, Nature. 50 (2005) 162–168. doi:10.1038/nature03001.

[12] R.H. Waterston, K. Lindblad-Toh, E. Birney *et al.*, Mouse Genome Sequencing, Initial sequencing and comparative analysis of the mouse genome, Nature. 420 (2002) 520–562. doi:10.1038/nature01262.

[13] M.D. Adams, S.E Celniker, R.A. Holt *et al.*, The genome sequence of Drosophila melanogaster, Science. 287 (5461) 2185–2195. doi:10.1126/science.287.5461.2185.

[14] The *C. elegans* Sequencing Consortium, Genome Sequence of the Nematode *C . elegans* : A platform for investigating Biology, Science. 2012 (2012) 2012–2019. doi:10.1126/science.282.5396.2012.

[15] J.K. Myers, C.N. Pace, J.M. Scholtz, A direct comparison of helix propensity in proteins and peptides, Proc. Natl. Acad. Sci. USA. 94 (1997) 2833-2837. PMC20282.

[16] T.M. O’Connor, J. O’Connell, D.I. O’Brien, T. Goode, C.P. Bredin, F. Shanahan, The role of substance P in inflammatory disease, J. Cell. Physiol. 201 (2004) 167-180. doi:10.1002/jcp.20061.

[17] Q. Wu, Y.O. Xu-Cai, S. Chen, W. Wang, Corin: new insights into the natriuretic peptide system, Kidney Int. 75 (2009) 142-146. doi:10.1038/ki.2008.418.

[18] F. Petraglia, P. Florio, C. Nappi, A.R. Genazzani, Peptide signaling in human placenta and membranes:

autocrine, paracrine, and endocrine mechanisms, End. Rev. 17 (1996) 156-186. doi:10.1210/edrv-17-2-156.

[19] K.M. Wagstaff, D.A. Jans, Protein transduction: cell penetrating peptides and their therapeutic applications, Curr. Med. Chem. 13 (2006) 1371-1387. doi:10.2174/092986706776872871.

[20] J.M. Cooper, The cell, a molecular approach, 2nd edition, Sunderland (MA): Sinauer Associates; 2000.

[21] J. T. Hancock, Cell signaling, third edition. New York, Oxford University Press Inc., 2009.

[22] P.G. Strange, Agonist binding, agonist affinity and agonist efficacy at G protein-coupled receptors, Br.J. Pharmacol. 153 (2008) 1353-1363. doi:10.1038/sj.bjp.0707672.

[23] F. Siso-Nadal, J.J. Fox, S.A. Laporte, T.E. Hébert, P.S. Swain, cross-talk between signaling pathways can generate robust oscillations in calcium and cAMP, PLoS One. 4 (2009) 1-10. doi:10.1371/journal.pone.0007189.

[24] H. Nishi, E. Demir, A.R. Panchenko, Crosstalk between signaling pathways provided by single and multiple protein phosphorylation sites, J. Mol. Biol. 427 (2015) 511–520. doi:10.1016/j.jmb.2014.11.001.

[25] S.R. George, B.F. O'Dowd, S.P. Lee, G-protein-coupled receptor oligomerization and its potential for drug discovery, Nat. Rev. Discov. 1 (2002) 808–820. doi:10.1038/nrd913.

[26] N. Tuteja, Signaling through G protein coupled receptors., Plant Signal. Behav. 4 (2009) 942–7. doi:10.4161/psb.4.10.9530.

[27] D.M. Rosenbaum, S.G.F Rasmussen, B.K.Kobilka, The structure and function of G protein-coupled receptors, Nature. 21 (2009) 356-363. doi:10.1038/nature08144.

[28] A. Thathiah, B. De Strooper, The role of G protein-coupled receptors in the pathology of Alzheimer's disease, Nat. Rev. Neurosci. 12 (2011) 73–87. doi:10.1038/nrn2977.

[29] Y. Huang, A. Skwarek-Maruszewska, K. Horre, E. Vandewyer, L. Wolfs, A. Snellinx, T. Saito, E. Radaelli, N. Corthout, J. Colombelli, A.C. Lo, L. Van Aerschot, Z. Callaerts-Vegh, D. Trabzuni, K. Bossers, J. Verhaagen, M. Ryten, S. Munck, R. D'Hooge, D.F. Swaab, J. Hardy, T.C. Saido, B. De Strooper, A. Thathiah, Loss of GPR3 reduces the amyloid plaque burden and improves memory in Alzheimer's disease mouse models, Sci. Transl. Med. 7 (2015) 309ra164. doi:10.1126/scitranslmed.aab3492.

[30] K. Bellmann-Sickert, A.G. Beck-Sickinger, Peptide drugs to target G protein-coupled receptors, Trends in Pharm. Sci. 31 (2010) 434-441.doi:10.1016/j.tips.2010.06.003

[31] H.L. Brinks, A.D. Eckhart, Regulation of GPCR signaling in hypertension, Biochim. Biophys. Acta, 1802 (2010) 1268-1275. doi:10.1016/j.bbadis.2010.01.005.

[32] M. Jiang, N.S. Bajpayee, Molecular Mechanisms of Go signaling, Neurosignals. 17 (2009) 23-41. doi: 10.1159/000186688.

[33] N. Suzuki, N. Hajicek, T. Kozasa, Regulation and physiological functions of G12/13-mediated signaling pathways, Neurosignals. 17 (2009) 55-70. doi:10.1159/000186690.

[34] S.G.F. Rasmussen, B.T. DeVree, Y. Zou, A.C. Kruse, K.Y. Chung, T.S. Kobilka, F.S.Thian, P.S. Chae, D. Calinski, J.M. Mathiesen, S.T.A. Shah, J.A. Lyons, M.Caffrey, S.H. Gellman, J. Steyaert, G. Skiniotis, W.I.Weis, R.K. Sunahara, B.K. Kobilka, Crystal Structure of the B2 Adrenergic Receptor-Gs protein complex, Nature. 477 (2012) 549–555. doi:10.1038/nature10361.

[35] S.G.F. Rasmussen, H.-J. Choi, D.M. Rosenbaum, T.S. Kobilka, F.S. Thian, P.C. Edwards, M. Berghammer, V.R.P. Ratnala, R. Sanishvili, R.F. Fischetti, G.F.X Schertler, W.I. Weis, B.K. Kobilka, Crystal structure of the human B2 adrenergic G-protein-coupled receptor, Nature. 450 (2007) doi:10.1038/nature06325.

[36] D.P. Staus, L.M. Wingler, R.T. Strachan, S.G. Rasmussen, E. Pardon, S. Ahn, J. Steyaert, B.K. Kobilka, R.J. Lefkowitz, Regulation of β2-adrenergic receptor function by conformationally selective single-domain intrabodies, Mol. Pharmacol. 85 (2014) 472-481. doi: 10.1124/mol.113.089516

[37] I.N. Maruyama, Mechanisms of activation of receptor tyrosine kinases: monomers or dimers, Cells 3 (2014) 304-330. doi:10.3390/cells3020304.

[38] M.A. Lemmon, J. Schlessinger, Cell signaling by receptor tyrosine kinases, Cell. 141 (2010) 1117–1134. doi:10.1016/j.cell.2010.06.011.

[39] A. Ullrich, J. Schlessinger, Signal transduction by receptors with tyrosine kinase activity, Cell. 61 (1990) 203–212. doi:10.1007/s00497-011-0177-9.

[40] S. Li, A.H.C. Wong, F. Liu, Ligand-gated ion channel interacting proteins and their role in neuroprotection, Front. Cell. Neurosci. 8 (2014) 125. doi:10.3389/fncel.2014.00125.

[41] F. López-Muñoz, R. Ucha-Udabe, C. Alamo, The history of barbiturates a century after their clinical introduction, Neuropsychiatr. Dis. Treat. 1 (2005) 329–43.

[42] E. Bearud, K.G. Chandy, Therapeutic potential of peptide toxins that target ion channels, Inflamm. Allergy Drug Targets. 10 (2011) 322-342. doi:10.2174/187152811797200696.

[43] B. Alberts, A. Johnson, J.Lewis, M. Raff, K. Roberts, P. Walter. Molecular biology of the cell, 4th edition, New York, Garland Science, 2002.

[44] K. Ueki, D. a Fruman, S.M. Brachmann, Y. Tseng, L.C. Cantley, C.R. Kahn, Molecular Balance between the Regulatory and Catalytic Subunits of Phosphoinositide 3-Kinase Regulates Cell Signaling and Survival Molecular Balance between the Regulatory and Catalytic Subunits of Phosphoinositide 3-Kinase Regulates Cell Signaling and survival, Mol. Cell. Biol. 22 (2002) 965–977. doi:10.1128/MCB.22.3.965.

[45] B.J. Arey, The role of glycosylation in receptor signaling, Chemistry, 12 (2012). doi: 10.5772/50262.

[46] M. Georget, P. Mateo, G. Vandecasteele, L. Lipskaia, N. Defer, J. Hanoune, J. Hoerter, C. Lugnier, R. Fischmeister, Cyclic AMP compartmentation due to increased cAMP-phosphodiesterase activity in transgenic mice with a cardiac-directed expression of the human adenylyl cyclase type 8 (AC8), Faseb J. 17 (2003) 1380–1391. doi:10.1096/fj.02-0784com.

[47] R. Rizzuto, D. De Stefani, A. Raffaello, C. Mammucari, Mitochondria as sensors and regulators of calcium signalling, Nat. Rev. Mol. Cell Biol. 13 (2012) 566–578. doi:10.1038/nrm3412.

[48] B.D. Grant, J.G. Donaldson, Pathways and mechanisms of endocytic recycling, Nat. Rev. Mol. Cell. Biol. 10 (2009) 597-608. doi:10.1038/nrm2755.

[49] G. Vert, J. Chory, Crosstalk in Cellular Signaling: Background Noise or the Real Thing?, Dev. Cell. 21 (2011) 1179. doi:10.1016/j.devcel.2011.11.006.

[50] S.D. Chang, M.R. Bruchas, Functional selectivity at GPCRs: new opportunities in psychiatric drug discovery, Neuropsychopharmacology, 39 (2014) 248–249. doi:10.1038/npp.2013.205.

[51] T. Kenakin, Functional selectivity and biased receptor signaling, J. Pharmacol. Exp. Ther. 336 (2011) 296–302. doi:10.1124/jpet.110.173948.

[52] L.M. Luttrell, D. Gesty-Palmer, Beyond Desensitization : Physiological Relevance of Arrestin -Dependent Signaling, Pharmacol. Rev. 62 (2010) 1-27. doi:10.1124/pr.109.002436.

[53] W. Stallaert, J.F. Dorn, E. van der westhuizen, M. Audet, M. Bouvier, Impedance responses revael β2-adrenergic receptor signaling pluridimensionality and allow classification of ligands with distinct signaling profiles, PLoS ONE 7 (2012) 1-14. doi:10.137/journal.pone.0029420.

[54] E. Verdonk, K. Johnson, R. McGuinness, G. Leung, Y.-W. Chen, H.R. Tang, J.M. Michelotti, V.F. Liu,

Cellular dielectric spectroscopy: a label-free comprehensive platform for functional evaluation of endogenous receptors, Assay and Drug Develop. Techn. 4 (5) (2006) 609-619. doi:10.1089/adt.2006.4.609.

[55] I. Giaever, C.R. Keese, A morphological biosensor for mammalian cells, Nature, 366 (1993) 591- 592. doi:10.1038/366591a0.

[56] S.M. Paul, D.S. Mytelka, C.T. Dunwiddi, C.C. Persinger, B.H. Munos, S.R. Lindborg, A.L. Schacht, How to improve R&D productivity: the pharmaceutical industry's grand challenge, Nat. Rev. Drug. Discov. 9 (2010) 203-214. doi:10.1038/nrd3078.

[57] M. Kammermann, A. Denelavas, A. Imbach, U. Grether, H. Dehmlow, C.M. Apfel, C. Hertel, Impedance measurement: a new method to detect ligand-biased receptor signaling, biochem. Biophys. Res. Comm. 412 (2011) 419-429. doi:1.1016/j.bbrc.2011.07.087.

Chapter II

Testing the peptide library for activity on cultured cell lines

Abstract

By exploiting a classical peptide discovery strategy, the research group of prof. Schoofs created a peptide library containing more than 700 potentially bioactive peptides. These candidate peptides were screened for activity using various cellular, organ, and behavioral assays. For cost reasons, screening experiments were initially conducted with peptide material from a small scale crude (purity > 70%) synthesis. Once activity was observed with crude peptide material, the same peptide was re-used at a higher purity level (> 95%) in order to reproduce the original observation. In many cases, confirmation of previously obtained results turned out to be challenge, suggesting that peptide quality is a critical attribute for interpretation of results. However, a significant number of purified peptides were shown to be biologically active, which opens ample perspectives to study their mechanism of action. This chapter summarizes the results obtained from screening experiments and highlights promising peptides upon which further research efforts can be based.

2.1 Introduction

Over the past two decades, the field of peptidomics progressed rapidly due to major advances in chromatography, MS, and bioinformatics. Combining these techniques enables present-day researchers to determine the mass of a peptide in highly complex biological samples with an ever-increasing accuracy. Information about the mass of a peptide, together with a search against the genome from which the peptide originates, often suffices to deduce the correct amino acid sequence of a peptide [1]. However, sequence confirmation with tandem mass spectrometry (MS/MS) is required to reliably confirm the primary sequence.

The laboratory of prof. Schoofs identified more than thousand putative peptide sequences from various human and mouse tissue samples and body fluids. In parallel, a significant number of putative peptides were predicted using *in silico* algorithms. If a particular amino acid sequence was not described in the scientific literature and possessed several hallmarks of known signaling peptides (short coding region, consensus cleavage sites flanking the candidate bioactive peptide, PTMs), it was commercially synthesized using the latest fluorenylmethyloxycarbonyl chloride (FMOC) solid-phase technology (ThermoFisher Scientific (Waltham, MA, USA)). This work resulted in the formation of a library which contained approximately 700 putative bioactive peptides.

To increase the chances of discovering a functional effect of our putative bioactive peptides, an inter-university consortium was founded, including experts in distinct fields of *in vitro* and *in vivo* cell biology. For example, the research group of prof. Cammue (KU Leuven) tested candidate peptides for antifungal activity on *Candida albicans* and *Aspergillus flavus*. In addition, the peptide collection was tested in platelet aggregation studies (Freson lab, KU Leuven), as well as on gastro-intestinal organ preparations (Depoortere lab, KU Leuven). In the latter experiments, peptide-induced smooth muscle responses of rat duodenal strips were investigated. The organ preparations were also stimulated electrically to evaluate the effects of candidate peptides on neurally mediated contractions. More information on the outcome of these screening experiments can be found in the appendix of this doctoral dissertation (see table 1 (p. 229). For a short summary of the most promising findings, the reader is referred to section 2.3.4 (p.40)).

The research group of prof. Schoofs contributed by testing the complete peptide collection on a panel of approximately 40 cultured cell lines representative for almost all cell types present in humans or mice. In order to detect a cellular response evoked by candidate peptides, an assay based on EIS was used. This technique detects cellular responses in a real-time and label-free manner, regardless of the type of receptor or signal transduction pathway that is triggered [2]. In addition,

second messenger assays were employed to study peptide-induced changes in the intracellular concentration of second messengers such as calcium or cAMP.

Initial screening experiments put the spotlight on several dozens of candidate peptides which showed a promising *in vitro* and/or *in vivo* activity. A summary of these results is provided in the appendix (table 1) of this thesis. For cost reasons, these screening experiments were carried out with crude peptides (purity > 70%) synthesized on a small scale (2-5 mg). Once activity was observed with crude peptide material, peptides with a purity level greater than 95% were synthesized and tested to confirm prior observations. This is of utmost importance because activity could be evoked by byproducts of peptide synthesis (linkers, protective groups, contaminants, etc.) or shorter (prematurely terminated synthesis) peptide fragments rather than by the peptide itself [3,4].

At the start of this project (October 2012), preliminary data obtained through the combined effort of several research groups needed to be reproduced with peptides of a higher quality. The contribution of this project to these ongoing 'confirmation experiments' was threefold. First, activity originally observed with crude peptides on a panel of cultured cell lines was compared to the activity induced by purified peptides. In most cases, EIS and second messenger assays were used and these results are presented in section 3.1.

Second, preliminary results obtained by the research group of prof. Dotti (Vlaams Instituut voor Biotechnologie (VIB), center for the biology of disease, KU Leuven) were investigated in more detail. The lab of prof. Dotti screened the complete peptide collection (crude quality) for effects on the secretion of the amyloid-β peptide (Aβ) from primary hippocampal neurons (PHNs) using a commercially available Aβ Enzyme-Linked Immuno Sorbent Assay (ELISA; Wako Pure Chemical Industries, Osake, Japan). They identified 10 candidate peptides with a potential effect on the secretion of Aβ from PHNs. Secretion of Aβ from neural cells to the extracellular environment plays a key role in the formation of neuritique plaques, one of the pathological hallmarks of Alzheimer's disease (AD) [5]. Aβ is a peptide that is cleaved from the amyloid precursor protein (APP) by β-secretase and γ-secretase in neurons. Because cleavage by γ-secretase is somewhat imprecise, Aβ peptides of varying lengths exist. The 40-residue peptide (Aβ (40)) is the most abundant, followed by the 42-residue peptide (Aβ (42)). Because Aβ (42) is more hydrophobic and fibrillogenic, it is more prone to aggregate than Aβ (40) [6]. Even though the relationship between Aβ deposition and AD progression is complex and not yet completely understood, many reports suggest that the generation of toxic oligomers during the aggregation of Aβ into senile plaques plays an important role in the development of AD [5,6].

We tried to reproduce the findings of Dotti's lab and used ELISA to measure Aβ (40) and Aβ (42) levels following exposure of PHNs to purified candidate peptides. Longer-term (10-days old) cultures of PHNs obtained from rat embryos (E18) were used because they are a good model for normal, mature neurons [7]. Two pure peptides, named P318 and P649, exerted a significant effect on the secretion of Aβ from PHNs. These peptides were then subjected to further analysis (such as cytotoxicity assays) to disclose whether they can potentially serve as a template for further optimization studies.

Third, candidate peptides which previously showed an effect (as measured by EIS, ELISA, or second messenger assays) on neurons or neuron-like cells were screened for effects on the outgrowth of neurites in rat pheochromocytoma PC-12 cells using a neurite outgrowth assay (NOA). NOA is an immunofluorescence-based technique that uses a primary antibody which labels neurites from various cell types, including PC-12 cells. PC-12 cells can easily differentiate into neuron-like cells upon stimulation with nerve growth factor (NGF), which induces neurite outgrowth by promoting Gβγ-microtubule interaction [8]. Neurites are essential for communication between neurons. Therefore, compounds that affect neurite outgrowth hold great promise in central nervous system drug discovery research.

Once a reproducible effect of a pure peptide was detected, the cell's response to this candidate peptide was studied in more detail. For example, dose-response curves were measured to ascertain that cell activation was dose-dependent and to determine which cell type was the most sensitive. Figure 2.1 outlines the selection process involved to find an appropriate starting point for further peptide characterization. Even though confirmation of previously obtained results turned out to be a major challenge, the bioactive nature of several pure peptides was demonstrated. This opens ample perspectives for follow-up research such as SAR studies on the peptide or pharmacological characterization of the receptor. An overview of all the effects induced by pure peptides on various cultured cell lines is provided in section 3.3. Ultimately, one of these peptides, termed P318, was selected for further analysis based on its pleiotropic effects on several cultured cell lines.

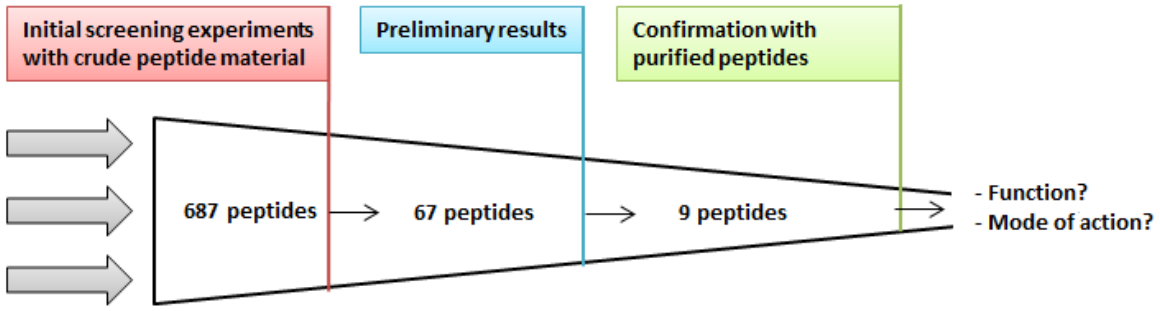

Fig.2.1. Visual representation of the steps required to discover candidate peptides with promising activities. 687 crude peptides were tested for activity on a number of mammalian cell lines, and approximately 10% of them evoked a certain cellular response. Further investigation indicated that the use of crude peptides often led to false-positive functionality conclusions. However, at least 9 pure peptides were found to be active and the cell's response to these peptides was examined in more detail using pharmacological agents.

2.2 Material and methods

Reagents

Dulbecco's modified medium (DMEM), Eagles minimum essential medium (EMEM), Roswell park memorial institute (RPMI) medium, EMEM with Ham's F12 (1:1), phosphate buffered saline (PBS), fetal bovine serum (FBS), horse serum (HS), goat serum (GS), L-glutamine, non-essential amino acids (NEAA), sodium pyruvate (NaP), penicillin/streptomycin (P/S), ethylenediamine tetraacetic acid (EDTA), collagen type IV, paraformaldehyde (PFA), and bovine serum albumin (BSA) were purchased from Sigma-Aldrich (St.-Louis, MO, USA). All peptides used in this study, as well as human β-nerve growth factor (NGF) and Alexa fluor 488 dye were acquired from ThermoFisher Scientific (Waltham, MA, USA). Anti-β-III tubulin primary antibody was obtained from Abcam (Cambridge, MA, USA). Neurobasal medium, B27 supplement, and N-[N-(3,5-Difluorophenacetyl)-L-alanyl]-S-phenylglycine t-butyl ester (DAPT) were kindly provided by the laboratory of prof. C. Dotti (VIB, center for the biology of disease, KU Leuven).

Cell cultures

B16 mouse melanoma, TE671 human rhabdomyosarcoma, Neuro2A mouse neuroblastoma, CTXTNA2 rat astrocyte, SK-HEP1 human hepatocellular carcinoma, PC-12 rat adrenal gland phaeochromocytoma cells, and SH-SY5Y human neuroblastoma cells were purchased from the European Collection of Authenticated Cell cultures (ECACC; Porton Down, Wiltshire, UK) and stored in a liquid N2 tank.

Cells were cultured according to their respective cell culture protocols, which can be found on the website of the supplier (www.phe-culturecollections.org.uk/collections/ecacc.aspx). B16, TE671 and CTXTNA2 cells were cultured in DMEM containing 10% FBS and 100 units penicillin/0.1 mg streptomycin. Neuro2A and SK-HEP1 cells were grown in EMEM supplemented with 10% FBS and 100 units penicillin/0.1 mg streptomycin. PC-12 cells were cultured in RPMI containing 1% HS and 100 units penicillin/0.1 mg streptomycin. SH-SY5Y cells were cultured in Ham's F12/EMEM containing 15% FBS, 1% NEAA, 2 mM glutamine and 100 units penicillin/0.1 mg streptomycin. Each cell line used in this study was incubated in a 37°C, 5% CO_2, humidified atmosphere.

To collect cells, cells were washed with PBS and then removed from the culture flask with trypsin-EDTA; 0.25% trypsin, 0.02% EDTA. Low-density dissociated PHNs were cultured as described by Kaech and Banker [3]. After isolation, PHNs from embryonic rats (E18) were grown overnight in EMEM supplemented with HS. The following day, the medium was replaced with neurobasal medium containing B27 supplement and L-glutamine. On day 10, PHNs were incubated with candidate peptides.

Fluorometric calcium mobilization assay

Intracellular [Ca^{2+}] was determined using the Fluo-Forte calcium assay kit (Enzo Life Sciences, NY, USA) as described by the manufacturer. B16, TE671, Neuro2A, CTXTNA2 and SK-HEP1 cells were seeded in a 96-well plate (B16, TE671, Neuro2A and SK-HEP1: 40000 cells/well; CTXTNA2: 60000 cells/well) and incubated in a 37°C, 5% CO_2, humidified atmosphere. The next day, the culture medium was removed and 100 µL of dye loading solution was added. The 96-well plate containing the cells was incubated for 45 minutes in a 37°C, 5% CO_2, humidified atmosphere and then incubated for another 15 minutes at room temperature. Finally, a 25 µL aliquot of the peptide solution, diluted in HBSS buffer, was automatically transferred from the compound plate to the plate containing the cells. The fluorophore was excited at 485 nm and the calcium response was measured for two minutes at 520 nm using a FlexStation II (Molecular Devices, New Milton, Hampshire, UK).

Human β-amyloid ELISA

A sandwich ELISA was performed to detect secreted Aβ levels (Wako Pure Chemical Industries, Osake, Japan). The monoclonal antibody BNT77 is pre-coated on a 96-well surface of a separable microplate which serves as a capture antibody for both Aβ 40 and 42. Captured Aβ is recognized by another antibody (BA27) labeled with horseradish peroxidase (HRP) to specifically detect Aβ (40). Similarly, HRP-conjugated antibody BC05 specifically detects the C-terminal portion of Aβ (42). On day one, test and standard solutions were added to the appropriate wells and incubated at 4°C overnight. The following day, solutions were discarded from the wells and then washed with washing solution. HRP-conjugated antibody solution was then added at 4°C for 1 hour. After a second washing step, TMB solution was added in the dark for 30 minutes and positive solutions developed a blue color. After terminating the reaction via the addition of stop solution, the absorbance of each well was measured at 450 nm.

Neurite outgrowth assay

PC-12 suspension cells were transferred to collagen IV-coated 96-well plates at a cell density of 7500 cells per well. Undifferentiated cells were cultured in standard PC-12 growth medium for six days. For PC-12 cell differentiation to occur, PC-12 cells were cultured in growth medium supplemented with NGF (100 ng/ml), thereby inducing the neuronal phenotype. PC-12 cells were treated with candidate peptides 30 minutes after adding cells to the 96-well plate. At the end of the neurite outgrowth culture period (day 6), PC-12 cells were fixed and stained directly in the 96-well plate. Cells were fixed in paraformaldehyde (PFA; 4%) for 15 minutes, after which the fixative was aspirated and washed with PBS 3 times. Next, blocking buffer (1x PBS, 5% GS) was added for 1 hour. After applying

the diluted (1:400) primary β-III tubulin antibody solution and subsequent washing with PBS, the secondary Alexa fluor 488 dye (excitation: 499 nm; emission: 519 nm) solution was added for 2 hours in the dark. The fluorescence intensity signal was monitored using a FlexStation II (Molecular devices, Sunnyvale, CA, USA).

Statistical analysis

Raw data from fluorometric calcium mobilization, ELISA, and neurite outgrowth assays were analyzed by GraphPad Prism 5.0 (GraphPad software, La Jolla, CA.). All experiments were performed in triplicate and repeated twice, unless stated otherwise. Student's t-tests were conducted to detect significant differences between experimental conditions, unless stated otherwise.

2.3 Results

2.3.1 Screening experiments using second messenger assays

At the start of this project, screening experiments to detect bioactivity of candidate peptides on cultured cell lines reached their final stage. In order to detect cell activation by candidate peptides, EIS and second messenger assays were often used. At the time, several observations obtained with crude peptide material needed to be reproduced with peptides of a higher purity to confirm that the observed effects were truly evoked by candidate peptides and not by contaminants. For clarity reasons, only the most recent results will be discussed in this chapter. The interested reader is referred to the supplementary information at the end of this manuscript (table 1) for a more complete overview of the results from screening experiments conducted so far.

Peptides 303, 384, 433, 438, and 444 (crude quality) were previously shown to induce the release of intracellular calcium in a number of cell types. In order to confirm these results, peptides of a higher quality were synthesized and tested on the same cell types (figure 2.2).

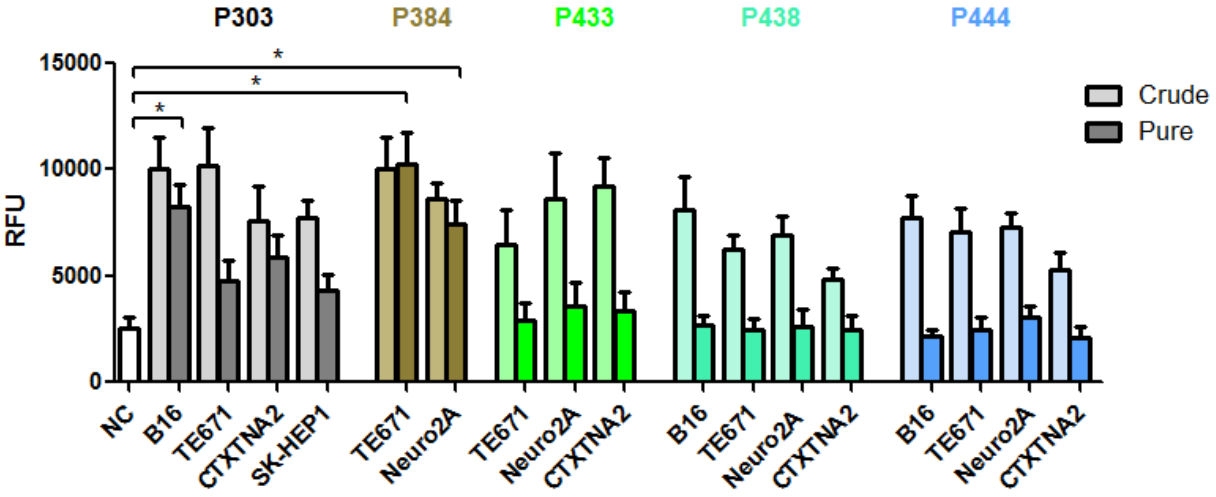

Fig.2.2. Comparison of the activity profiles of peptides with a different purity level on various cultured cell lines, as measured by a calcium flux assay. Note that an arbitrary unitless relative fluorescence unit (RFU; maximum peak height) value of 3000 is used as a minimum to judge if calcium is released. Error bars represent the standard error of mean (SEM). All experiments were performed in triplicate and repeated twice (*N*=6). Significance levels are depicted by asterisks which indicate p-value from Student's t-test: *, $p < 0.05$. Peptides were added at a final concentration of 5 µM (NC: negative control).

As depicted in figure 2.2, purified P303 induced the release of intracellular calcium as a secondary messenger in B16 melanoma cells. Purified P303 also evoked a weak calcium response in TE671, CTXTNA2, and SK-HEP1 cells, although this effect was not significant. Purified P384 induced a similar calcium response as crude P384 in TE671 and Neuro2A cells. These cells were then incubated with a dilution series (0.1 – 40 µM) of pure P384 in order to determine the half maximal effective concentration (EC_{50}) in TE671 and Neuro2A cells (figure 2.3). The EC_{50} value (4.7 µM) for purified P384 in TE671 cells was lower than the EC_{50} value (6.3 µM) in Neuro2A cells. Consequently, it is

possible that TE671 cells are more suitable for studies on signal transduction mechanisms as they may be more sensitive to pure P384 than Neuro2A cells. However, given the small differences in EC_{50} values, more data needs to be collected before this conclusion can be drawn.

Stimulating TE671, B16, Neuro2A, or CTXTNA2 cells with 5 µM of purified P433, 438, or 444 did not mobilize intracellular calcium. These results challenge the assumption that the calcium response induced by crude-peptide material was truly evoked by the peptide under study.

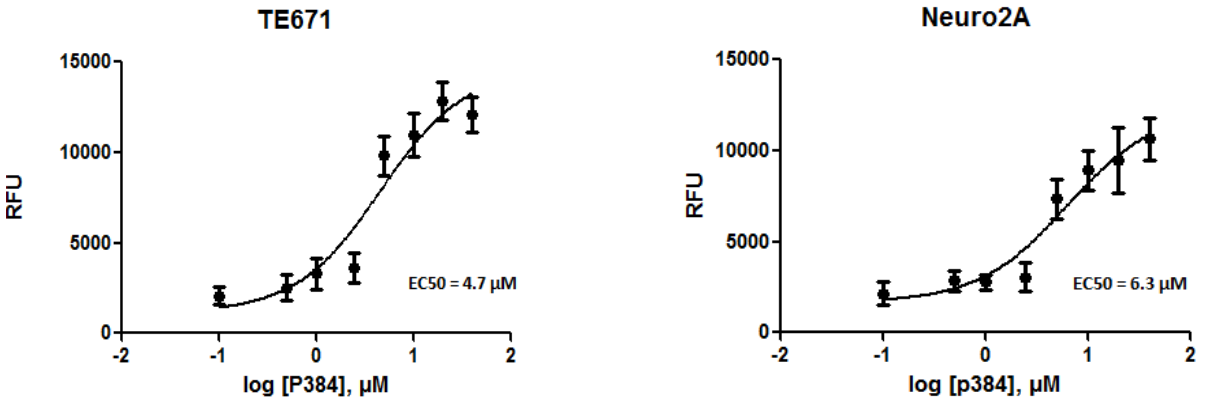

Fig.2.3. Dose-response curve of pure P384 in TE671 (EC_{50} = 4.7 µM) and Neuro2A (EC_{50} = 6.3 µM) cells as measured by calcium flux assay. Data expressed as the mean ± SEM (*N*=6).

2.3.2 Screening experiments using human Aβ ELISA

The research group of prof. Dotti identified 10 crude peptides that modulate the secretion of Aβ from longer-term cultures of PHNs. Peptides 77, 98, 112, 113, 296, 318, and 372 exerted an inhibitory effect on the secretion of Aβ, whereas peptides 614, 646 and 649 stimulated the secretion of Aβ in the culture medium.

Peptides of a higher purity level were synthesized in order to reproduce these results. After isolation, PHNs were cultured for ten days. PHNs were then incubated with purified peptides overnight and cell-secreted Aβ in the culture medium was determined by ELISA (figure 2.4). A functional γ-secretase inhibitor (DAPT) was used as a positive control.

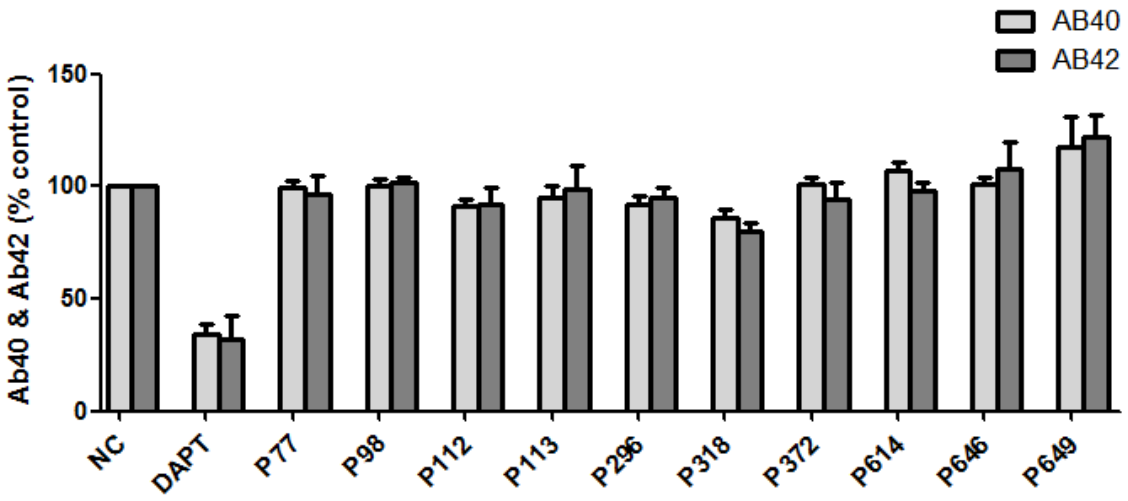

Fig.2.4. Human Aβ ELISA results. After 10 days of culture, pure peptides were added to the culture medium at a concentration of 10 µM. A γ-secretase inhibitor, DAPT, was used to block Aβ secretion. The next day, Aβ 40- and Aβ 42-levels were determined by ELISA. (*N*=3, data are mean ± SEM. All values are shown in percentage with respect to the negative buffer control).

Based on the results displayed in figure 2.4, P318 (mean= 86.1 (Aβ-40) and 79.6 (Aβ-42)) and P649 (mean= 117.4 (Aβ-40) and 120.9 (Aβ-42)) were selected for further analysis as they may modulate the secretion of Aβ from PHNs. To ascertain that these effects were dose-dependent, a dilution series (1 – 100 µM) of P318 and P649 were added to PHNs (figure 2.5).

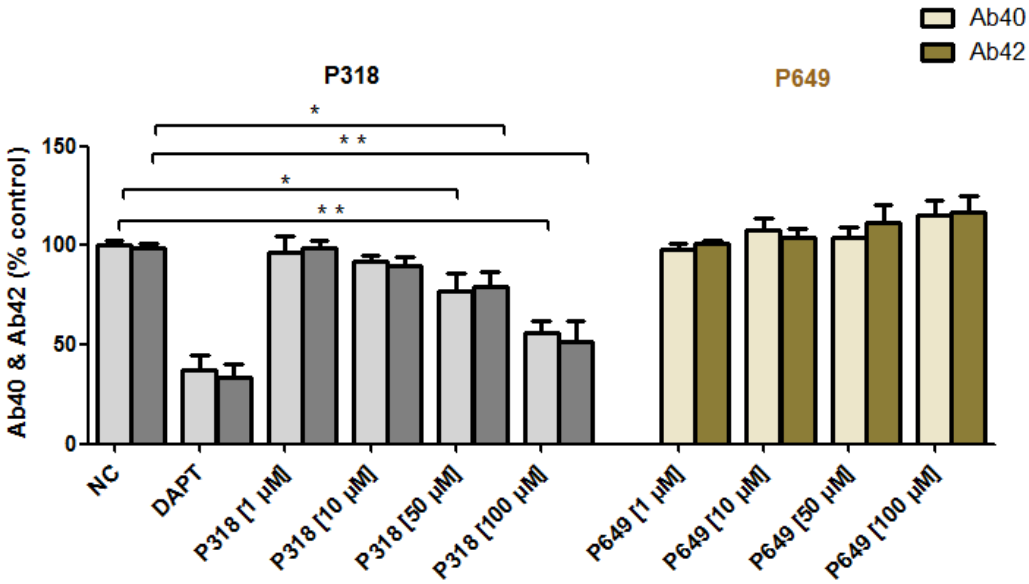

Fig.2.5. PHNs were treated with a concentration series of pure P318 and P649 upon which Aβ 40- and Aβ 42-levels were determined by ELISA. A γ-secretase inhibitor, DAPT, was used to block Aβ secretion. Significance levels are indicated by asterisks which represent p-values from Student's t-test: *, $p < 0.05$ and **, $p < 0.005$ (*N*=6; data are mean ± SEM).

P318 is a novel fragment of the mouse Cathelicidin-Related Antimicrobial Peptide (mCRAMP). Dürr *et al*. showed that cathelicidin-derived peptides can mediate cytotoxic effects against eukaryotic host cells by forming transmembrane pores which trigger various mechanisms of cell death [9]. Therefore, it is possible that the inhibitory effect of P318 on the secretion of Aβ from PHNs was caused by

cytotoxicity. To test this hypothesis, an ATP-based luminescence assay was employed to measure P318-induced cytotoxicity. Because ATP is present in metabolically active cells, it can be used as an indicator of cell viability [10].

At the time, PHNs were often difficult to obtain. Therefore, cytotoxicity tests were conducted in the neuroblastoma cell line SH-SY5Y. SH-SY5Y cells are commonly used for studies of neuronal function and differentiation [11]. SH-SY5Y cells express APP as well as the secretases required for cleavage of APP into Aβ peptides. First, it was confirmed that P318 (> 50 µM) also exerted an inhibitory effect on the secretion of Aβ from SH-SY5Y cells (figure 2.6-A). However, high concentrations (> 50 µM) of P318 negatively affected cell viability of SH-SY5Y cells following overnight exposure (figure 2.6-B).

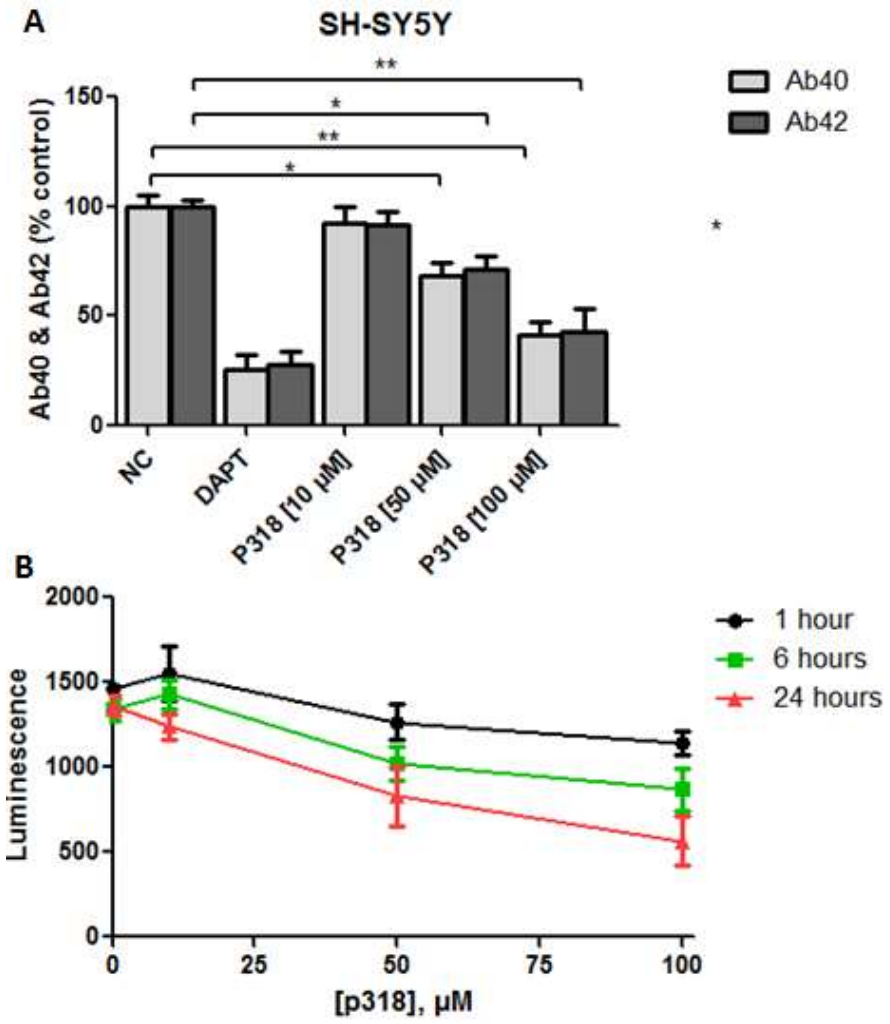

Fig.2.6. Human Aβ ELISA results (**A**). SH-SY5Y cells were treated with a concentration series of pure P318 upon which Aβ 40- and Aβ 42-levels were determined by ELISA. DAPT is an inhibitor of γ-secretase. Significance levels are indicated by asterisks which represent p-values from Student's t-test: *, $p < 0.05$ and **, $p < 0.005$ (*N*=6; data are mean ± SEM). Characterization of the toxic effect of P318 on SH-SY5Y cells using the CellTiter-Glo luminescent cell viability assay (**B**). The luminescence was measured at different timepoints after the addition of varying concentrations (10, 50, or 100 µM) of P318 (*N*=3).

The addition of high concentrations (100 µM) of purified P649 to PHNs elevated Aβ-levels (mean ± SEM = 114.9 ± 7.772 (Aβ-40) and 116.7 ± 8.50 (Aβ-42)) in the culture medium (figure 2.5). For practical reasons, SH-SY5Y cells instead of PHNs were treated with a dilution series of purified P649. The stimulatory effect of P649 on SH-SY5Y cells was comparable to the effect of P649 on PHNs (figure 2.7).

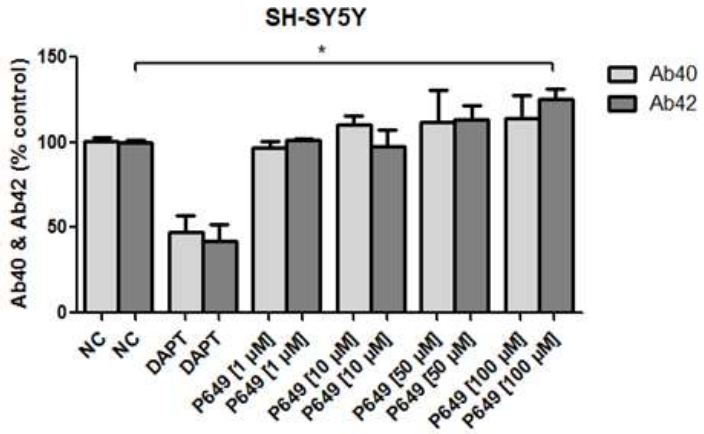

[P649] (µM)	Aβ40 Mean ± SEM	Aβ42 Mean ± SEM
1	97.00 ± 3.679	101.3 ± 1.145
10	110.2 ± 5.250	97.67 ± 9.376
50	112.0 ± 18.81	113.2 ±8.788
100	114.3 ± 13.38	125.3 ± 5.84

Fig.2.7. Human Aβ ELISA results. SH-SY5Y cells were treated with a concentration series of P649. After 24 hours, Aβ 40- and Aβ 42-levels were measured. Significance levels are indicated by asterisks which represent p-values from Student's t-test: *, p <0.05 (*N*=6; experiments performed in triplicate and repeated twice; Mean ± SEM values are shown in table).

2.3.3 Screening experiments using a neurite outgrowth assay

The combined efforts of several research groups identified 67 crude candidate bioactive peptides which formed a robust basis for further research. At least 25 peptides (P5, 24, 33, 71, 77, 98, 112, 113, 125, 218, 223, 296, 303, 318, 331, 372, 384, 433, 438, 444, 493, 571, 614, 646, and 649) exerted an effect (see appendix, table 1) on neurons or neuron-like cells such as Neuro2A, CTXTNA2, SH-SY5Y, PHNs, and/or primary cortical neurons. To evaluate whether these peptides stimulated or inhibited neurite formation in PC-12 cells, an immunofluorescence-based NOA was used. For PC-12 cell differentiation and neurite outgrowth to occur, undifferentiated cells were exposed to growth medium containing NGF (100 ng/ml) (figure 2.8). Under these conditions, PC-12 cells were cultured for 6 days after which the outgrowth of neurites was measured by labeling cells with a βIII-tubulin primary antibody. This antibody specifically labels neurites and neuronal cell bodies.

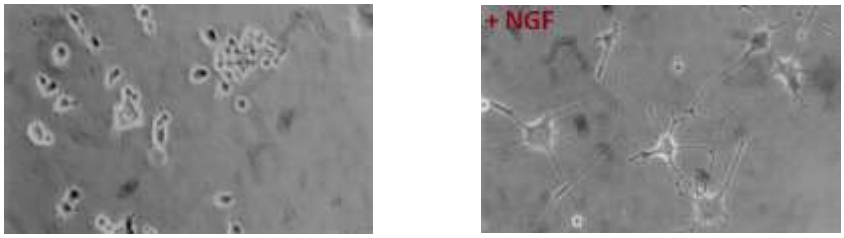

Fig.2.8. Undifferentiated (**left**) versus differentiated PC-12 cells (**right**).

When the culture medium of PC-12 cells was replaced with NGF-containing growth medium, candidate peptides (purity > 95%) were added in order to screen for effects on NGF-induced outgrowth of neurites. In addition, candidate peptides were added to undifferentiated PC-12 cells and tested for their ability to induce neurite outgrowth in PC-12 cells. As shown in figure 2.9, none of the 25 peptides tested inhibited or stimulated neurite formation in PC-12 cells.

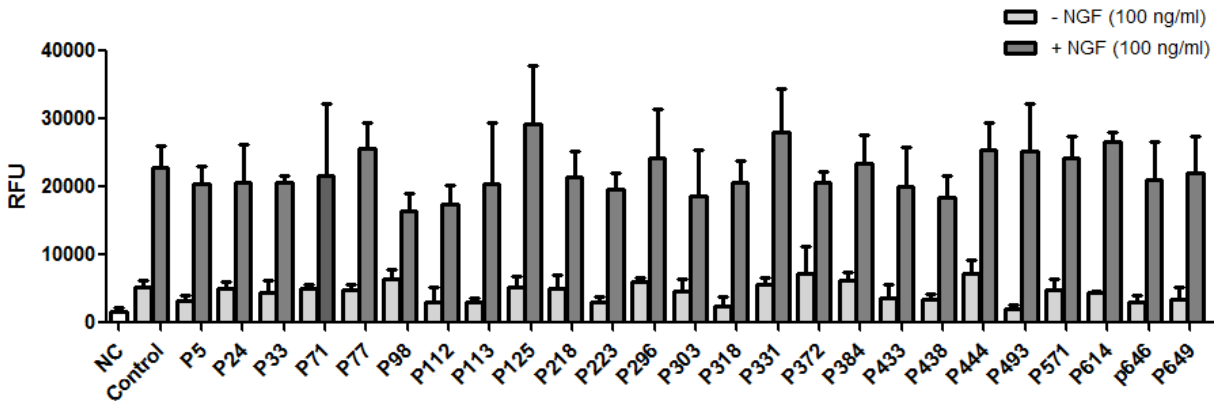

Fig.2.9. Immunofluorescence-based NOA results. Undifferentiated (-NGF) and differentiated (+NGF) PC-12 cells were cultured in the presence of purified putative bioactive peptides (5 µM) for six days (*N*=3; data are mean ± SEM) (NC: no primary antibody control; control: HBSS buffer).

2.3.4 Overview of promising candidate bioactive peptides

Once at least one cell type is found that is sensitive to a purified peptide, it is assumed that this cell line possesses a (cell surface) receptor for the candidate peptide in question. This allows us to proceed to the next stage, which comprises a detailed study of the response of the cell line to the candidate peptide. Through the years, a large number of experiments were conducted to screen for effects of candidate peptides on cultured cell lines (for a concise summary, see appendix table 1 (p. 229)). Because it can be challenging to keep track of all of these results, an overview of candidate peptides (purity > 95%) with a confirmed bioactive nature is given, along with some background information. This could serve as a source of inspiration for future experimental work.

1.) P24: a 14-residue fragment from mouse secretogranin 3 (Scg3). Scg3 is a neuroendocrine secretory protein, expressed in the hypothalamus and various endocrine cells such as pituitary cells and pancreatic β-cells [12]. The protein functions as helper protein in sorting and proteolytic processing of prohormones. We analyzed *Scg3* expression using a search engine for publicly available gene expression data (GENEVESTIGATOR). GENEVESTIGATOR integrates thousands of microarray and RNA-Seq gene expression data which enables biologists to visualize gene expression across a wide variety of biological contexts, including disease, cell lines, tissues, and genotypes. *Scg3* gene expression was analyzed across different stages of development (figure 2.10). Note that for each stage, mean and standard deviations are derived from all microarrays annotated for that particular

stage. Upregulated mRNA expression of Scg3 was observed in the first pre-natal stage (first week of embryonic development). Based on this information, it would be interesting to investigate whether P24 plays a role in pre-natal development processes.

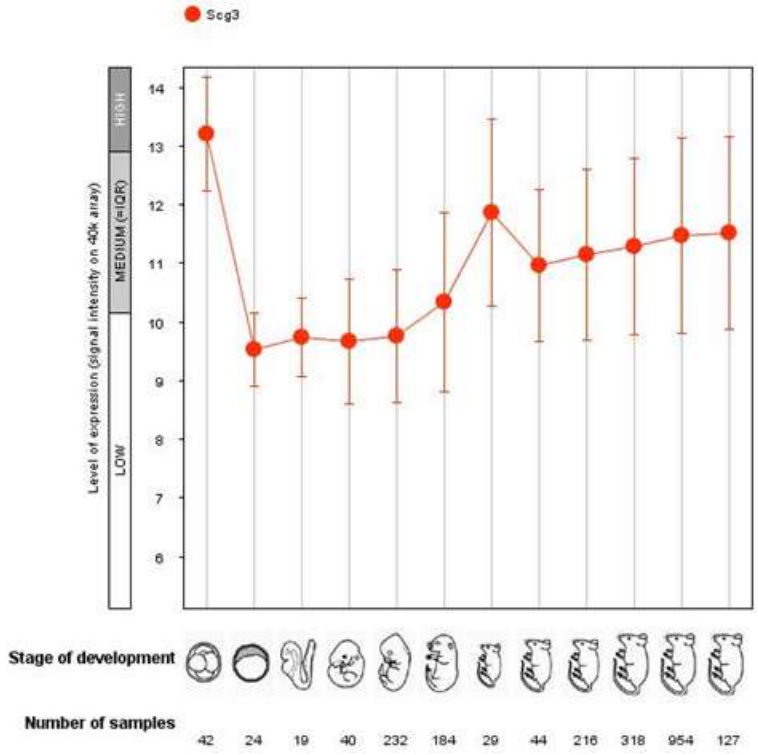

Fig.2.10. *Scg3* gene expression at different stages of mouse development. For each developmental stage, expression values and standard deviations are calculated from all microarrays annotated for that particular stage. Image created by GENEVESTIGATOR.

Scg 3 serves as a precursor protein for various biologically active peptides, possibly including P24. Previous research indicated that P24 induced the release of intracellular calcium and impedance changes in mouse neuroblastoma cells (Neuro2A; EC_{50}= 1 µM) and mouse Sertoli cells (TM4; EC_{50} = 4 µM) (Erwin Lauwers, Schoofs lab, personal communication). Crude peptide material was fractionated and the active fragment was identified as P24_4 ([H]FPKPEGSQ[OH]). To determine whether a GPCR was responsible for the observed calcium flux, Neuro2A cells were incubated with different inhibitors of GPCRs. However, these antagonists were unable to block the calcium response of Neuro2A cells to P24. P24 was also tested in various screening assays, including NOA, human Aβ ELISA, antimicrobial tests (Lavigne lab, KU Leuven), and contractility experiments (Depoortere lab, KU Leuven). However, no effect of P24 or P24_4 could be detected in any of these assays.

2.) P33: a 19-residue fragment of Agouti-signaling peptide (ASIP). ASIP is a paracrine signaling molecule that has a role in the regulation of human pigmentation. It acts as an antagonist of the melanocyte-stimulating hormone (MSH) [13,14]. P33 induced calcium flux and impedance changes in Neuro2A cells (EC_{50} = 3 µM; Erwin Lauwers, Schoofs lab, personal communication). Neuro2A cells

were incubated with broad-spectrum GPCR inhibitors, but these did not inhibit the response of Neuro2A cells to P33.

3.) P174: predicted peptide (22 amino acids) from colipase, which is a cofactor required for optimal enzyme activity of pancreatic lipase [15]. *In situ* hybridization studies revealed expression of the precursor mRNA in the hippocampus, intestines, and stomach (Arckens lab, KU Leuven). Impedance changes were detected on TE671 (EC_{50} = 1 µM) and DOK (dysplastic oral keratinocytes; EC_{50} = 5 µM) cells. An alanine scan was performed, and amino acids essential for the activity of P174 were identified (Erwin Lauwers, Schoofs lab, personal communication). No effect of P174 was observed in antimicrobial (Lavigne lab, KU Leuven) or contractility experiments (Depoortere lab, KU Leuven).

4.) P221: a 28-residue fragment of cocaine and amphetamine regulated transcript protein (CART), which is a neuropeptide that functions as an endogenous psychostimulant [16]. P221 induced the release of intracellular calcium in TM4 Sertoli (EC_{50} = 5 µM) and OLN93 oligodendroglia cells (EC_{50} = 10 µM) cells (Erwin Lauwers, Schoofs lab, personal communication). Experiments using pharmacological agents to elucidate the signal transduction pathway on these cell lines have not yet been conducted.

5.) P223: a decapeptide from the tachykinin-4 precursor protein. P223 was identified as hemokinin-1, an agonist of neurokinin receptors. P223 induced smooth muscle contractions on rat duodenal strips in a dose-dependent manner (Depoortere lab, KU Leuven). Because neurokinin-1 receptors are abundantly present in the rat intestines, it is not surprising that smooth muscle responses were observed after treatment with P223. However, P223 also activated B16 mouse melanoma cells and primary cortical neurons (Kamila Rzewucka, Schoofs lab, personal communication). Future experiments should focus on exploring the effects induced by P223 on these cell lines.

6.) P272: a predicted tetrapeptide derived from the mouse interleukin 1 receptor antagonist (IL1RN). Several proteins contain the amino acid sequence of P272 within their primary sequence, but the sequence of P272 is only flanked by predicted dibasic cleavage sites in IL1RN. Expression of precursor mRNA was detected by *in situ* hybridization experiments in the cortex, hippocampus, cerebellum, pancreas, spleen, thymus, stomach, and intestines (Arckens lab, KU Leuven). Alanine scan and truncated variants of P272 are available. Dose-dependent effects were detected by EIS and calcium mobilization measurements in B16 cells (EC_{50} = 0.5 µM; Erwin Lauwers, Schoofs lab, personal communication). These intracellular calcium increases evoked by P272 were inhibited by preincubating cells with SCH-202676, a general allosteric GPCR inhibitor, as well as with GPAnt-2, a G protein inhibitor specific for $G\alpha_i$, $G\alpha_o$, and $G\alpha_t$. The calcium response was not affected by GPAnt-2A, which is a G protein inhibitor for $G\alpha_q$. These results suggest that P272 activates a $G\alpha_i$- or $G\alpha_t$-coupled GPCR in B16 cells. To verify this hypothesis, receptor pull-down experiments were conducted with a

biotinylated version of P272 (Erwin Lauwers, Schoofs lab, personal communication). After confirmation of the bioactivity of the biotinylated peptide by EIS, pull-down experiments with streptavidin-coupled agarose beads and streptavidin-coupled magnetic beads were conducted to isolate the receptor for the peptides. These experiments resulted in a list of possible interaction proteins for P272. However, this list did not include GPCRs.

7.) P318: a novel fragment from mCRAMP, identified in the islets of Langerhans of the pancreas. CRAMP shares 67% identity with LL-37, the only human member of the cathelicidin family of antimicrobial peptides (AMP). Aside from antimicrobial (Lavigne lab, KU Leuven), antifungal (Cammue lab, KU Leuven), and antibiofilm (Vanderleyden lab, KU Leuven) activity, P318 evoked a response (as measured via EIS or second messenger assays) of several cultured cell lines (Schoofs lab, KU Leuven), and exerted inhibitory effects on electrical field-stimulated neural contractile responses of smooth muscle strips from the rat duodenum (Depoortere lab, KU Leuven). To gain more insight into the mechanism of action of P318 on cultured cell lines, efforts were made to identify its cognate receptor and elucidate the signaling cascade that it activates (chapter 5).

8.) P384: an 18-residue fragment derived from the eukaryotic translation initiation factor 3 subunit A (eIF3a), which is required for initiation of protein synthesis and regulates the extracellular signal-regulated kinase (ERK) pathway [17]. P384 induced the release of intracellular calcium in TE671 (EC_{50} = 4.7 µM) and Neuro2A cells (EC_{50} = 6.3 µM).

9.) P649: a 15-residue peptide from secretogranin 2 (Scg2), which participates in the sorting and packaging of peptide hormones and neuropeptides into secretory granules [18]. P649 stimulated the secretion of Aβ from PHNs and SH-SY5Y neuroblastoma cells (figure 2.4, 2.5, and 2.7).

2.4 Discussion

The research group of prof. Schoofs extracted a large number of novel candidate bioactive peptides from various human and mouse tissues and determined their amino acid sequence using different methods and techniques such as MS, liquid chromatography, and bioinformatics. In parallel, several *in silico* predicted peptides were synthesized for functional testing. These candidate peptides contain several important hallmarks of known bioactive peptides, but their function and mode of action remain to be established.

In order to assign a particular function to a candidate peptide, the complete peptide collection was screened for activity in different labs using a various *in vitro* assays. In this project, we employed EIS, NOA, ELISA, and second messenger assays to determine the activity profile of candidate peptides across various cultured cell lines. 67 candidate peptides were shown to be active in at least one of these assays (see appendix, table 1). Subsequently, the cell's response to these candidate peptides was analyzed in more detail.

For cost reasons, initial screening experiments were conducted with crude peptide material (> 70% purity) and needed to be reproduced with purified peptides (> 95% purity). As depicted in figures 2.2 and 2.4, several of the effects evoked by crude peptides could not be reproduced when repeated with pure peptides. Other research groups encountered the same problem, suggestive of a more general problem that could lead to wrong fail/pass decisions [3,4].

De Spiegeleer *et al*. elaborated on this issue and evaluated impurity profiles of obestatin peptides obtained from five different manufacturers [3]. They demonstrated that one peptide was a totally different peptide and that the quality of two-thirds of the other peptides was not sufficient to ensure high quality reproducible experimental data. In addition, De Spiegeleer *et al*. suggest that the presence of impurities account for the divergent conclusions about the activity of obestatin [3].

Verbeken *et al*. also showed that the quality of a peptide can affect the outcome of functionality tests [4]. They used a crude peptide from our peptide collection, P215_7, and demonstrated that this peptide triggered a contractile response in guinea pig ileum longitudinal smooth muscle preparations using tissue-organ baths. P215_7 is an 11-mer peptide derived from insulin-like peptide 6 (Insl6), a member of the insulin/relaxin family with unknown biological function [4]. However, the effect of crude P215_7 could not be reproduced using a high purity peptide (> 95% purity). Verbeken *et al*. also tested crude peptide material obtained from three different suppliers and showed that each sample evoked a different contractile response. In order to explain this observation, the purity profiles of the crude peptide samples were investigated using high-performance liquid chromatography (HPLC) and MS. Mass spectral interpretation revealed that each peptide sample possessed a different major impurity, which could account for the observed differences in

contraction behavior. This implies that peptide quality cannot be neglected and is of paramount importance for accurate and reliable interpretation of results.

To deal with these challenges, it is strongly recommended to check the quality control results provided by the manufacturer. The intactness of the peptide can also be verified by MS at the end of the experiment or the crude peptide material can be chromatographically separated. In the latter case, all fractions can be tested for activity and the active fraction can be identified by MS. We demonstrated that, in some cases, prematurely terminated synthesis fragments of the original peptide accounted for the observed activity (Erwin Lauwers, Schoofs lab, personal communication).

Taken together, there is a need for a clear strategy that tackles the root causes of this 'reproducibility crisis'. More reproducible and translatable data can be obtained by setting clear specifications for peptide impurities as well as developing improved research practice standards and guidelines for functional screening tests using peptides with different purity levels.

However, a number of pure peptides showed a reproducible effect on one or more cultured cell lines, which opened ample perspectives to study their mode of action. For instance, P384 increased intracellular calcium levels in TE671 cells (EC_{50} = 4.7 µM) and Neuro2A cells (EC_{50} = 6.3 µM) at a concentration of 5 µM. P384 is an 18-residue fragment from eIF3a, which is a polycistronic peptide that regulates the translation of various mRNAs involved in cell cycle and tumorigenesis [17]. Future experiments can be directed toward determining the effect of P384 on the cell cycle, *e.g*. using flow cytometry. In addition, SAR studies can be performed on P384 to evaluate the importance of each amino acid in the peptide sequence.

Two pure peptides (P318 and P649) were shown to modulate the secretion of Aβ from longer-term cultures of PHNs. Extracellular plaques deposits of Aβ are one of the hallmark pathologies required for diagnosis of AD [6]. Therefore, compounds that inhibit or modulate the process of Aβ generation are of great clinical interest. P318 exerted an inhibitory effect on PHN-secreted Aβ, but follow-up experiments showed that this effect was most likely induced by a cytotoxic effect of the peptide. P318 corresponds to the C-terminal fragment of mCRAMP, which is a well-known AMP known to cause membrane damage.

Addition of P649 to PHNs stimulated the release of Aβ from PHNs as well as SH-SY5Y neuroblastoma cells. From a clinical viewpoint, it seems counterintuitive to examine a candidate peptide that stimulates the secretion of Aβ from neurons. However, understanding the molecular mechanisms underlying this stimulatory effect could open new avenues for therapies targeting AD. The peptide *in se* has no direct therapeutic potential, but its cognate receptor and/or processing enzymes could be promising targets for new drugs.

It must be noted that P649 originates from Scg2, which is a precursor protein for many bioactive peptides, including secretoneurin. Secretoneurin is a well-characterized neuropeptide which is involved in various cellular processes such as chemotaxis and neuroprotection [21]. Interestingly, secretoneurin has also been linked to AD. Marksteiner *et al*. showed that approximately 20 % of amyloid-immunoreactive plaques co-labeled with secretoneurin [18]. The authors also suggest that secretoneurin has potential as a neuronal marker for synaptic degradation in AD [18].

It remains difficult to judge whether to proceed with testing on P649. Only physiologically irrelevant concentrations (100 µM) of P649 significantly increased cell-secreted Aβ in the culture medium. The low apparent potency of P649 can be caused by a low affinity ligand-receptor interaction or by a non-specific effect. It appears the suboptimal pharmacological properties of P649 need to improve before P649 can proceed to the next stage of the research. For example, SAR studies or sequence modification studies on P649 can be performed in a search for more potent and/or selective peptide analogues.

We also screened for effects of candidate bioactive peptides on the outgrowth of neurites from both differentiated and undifferentiated PC-12 cells. We employed an immunofluorescence-based technique that uses βIII-tubulin as a marker for neurites and neuronal cell bodies. Because it is known that tubulin is equivalently distributed along neurites, the intensity of the fluorescence emission reflects the length of neurites. During NGF-induced PC-12 cell differentiation, NGF increases total tubulin levels which correlates with increases in neurite length [22].

However, we were unable to observe any effect of the tested peptides on the formation of neurites from PC-12 cells. It remains a possibility that the concentration of NGF (100 ng/ml) used in this study was too high and already induced a maximal effect on the formation of neurites, thereby leaving subtle synergistic or inhibitory effects of candidate peptides in the dark. Therefore, it is recommended to preincubate PC-12 cells with lower concentrations of NGF before evaluating the effects of candidate peptides. It is also relevant to mention that cAMP and NGF have a synergistic effect on the outgrowth of neurites in PC-12 cells [23]. At present, several candidate bioactive peptides have been identified which lead to increased levels of cAMP (see appendix table 1). Further research is required to monitor the fluorescence signal when PC-12 cells are simultaneously treated with (lower concentrations of) NGF and candidate peptides that stimulate the production of cAMP.

Taken together, the activity profiles of several purified candidate peptides were determined on a panel of mammalian cell lines. The upcoming challenge is to elucidate the function and to figure out how these newly discovered bioactive peptides exert their action. This project primarily focuses on one peptide, codenamed P318. P318 was chosen based on its ability to activate a wide variety of cultured cell lines (see chapter 5) [24]. To gain more insight into the function of P318, knowledge

about the receptor and signal transduction cascade that is activated is of great value. Determination of the receptor type and unraveling the signal transduction pathway provides a starting point for functional elucidation and potential future drug development.

Aside from its amino acid sequence and some information about its precursor protein (mCRAMP), not much is known about P318. However, a lot of valuable information is available for the human orthologue of mCRAMP, termed LL-37. LL-37 is a cationic host defense peptide with pleiotropic effects on the innate and adaptive immune system [25]. In the following chapter, a summary of the current knowledge on the molecular mechanisms underlying LL-37-induced receptor activation is provided. This information can help to formulate hypotheses on the molecular mechanism behind the action of P318 to activate mammalian cell lines.

References

[1] K. Boonen, B. Landuyt, G. Baggerman, S.J. Husson, J. Huybrechts, L. Schoofs, Peptidomics: the integrated approach of MS, hyphenated techniques and bioinformatics for neuropeptide analysis, J. Sep. Sc, 31 (2008) 427-445. doi:10.1002/jssc.200700450.

[2] I. Giaever, C.R. Keese, A morphological biosensor for mammalian cells, Nature, 366 (1993) 591- 592. doi:10.1038/366591a0.

[3] B. De Spiegeleer, V. Vergote, A. Pezeshki, K. Peremans, C. Burvenich, Impurity profiling quality control testing of synthetic peptides using liquid chromatography-photodiode array-fluorescence and liquid chromatography-electrospray ionization-mass spectrometry: the obestatin case, Anal. Biochem., 15 (2008) 229-234. doi:10.1016/j.ab.2008.02.014.

[4] M. Verbeken, E. Wynendaele, R.A. Lefebvre, E. Goossens, B. De Spiegeleer, The influence of peptide impurity profiles on functional tissue-organ bath response: the 11-mer peptide INSL6 [151-161] case, Anal. Biochem., 421 (2012) 547-555. doi:10.1016/j.ab.2011.09.031.

[5] V.W. Chow, M.P. Mattson, P.C. Wong, M. Gleichmann, An overview of APP processing enzymes and products, Neuromolecular Med., 12 (2010) 1-12. doi:10.1007/s12017-009-8104-z.

[6] M.P. Murphy, H. LeVine, Alzheimer's disease and the β-amyloid peptide, J. Alzheimers. Dis. 19 (2010) 311. doi:10.3233/JAD-2010-1221.

[7] S. Kaech, G. Banker, Culturing hippocampal neurons, Nature protocols 1 (2006) 2406-2415. doi:10.1038/nprot.2006.356.

[8] J.A. Sierra-Fonseca, O. Najera, J.M. Martinez-Jurado, E.M. Walker, A. Varela-Ramirez, A.M. Khan, M. Miranda, N.S Lamango S. Roychowdhury, Nerve groth factor induces neurite outgrowth of PC12 cells by promoting Gβγ-microtubule interaction, BMC Neurosc., 15 (2014) 1-19. doi:101186/s12868-014-0132-4.

[9] U.H.N. Dürr, U.S. Sudheendra, A. Ramamoorthy, LL-37, the only human member of the cathelicidin family of antimicrobial peptides, Biochim. Biophys. Acta. 1758 (9) (2006) 1408–25. doi:10.1016/j.bbamem.2006.03.030.

[10] J.M. Posimo, A.S. Unnithan, A.M. Gleixner, H.J. choi, Y. Jiang, S.H. Pulugulla, Viability assays for cells in culture, J. Vis. Exp. 83 (2014) e50645. doi:10.3791/50645.

[11] K. Hohenauer, S. Anani, A. Marcil, P. Roby, S. Parent, S. Dahan, Secreted APP and amyloid beta quantification in SH-SY5Y cell media using high sensitivity AlphaLISA kits, FASEB journal, 24 (2010) 1-9.

[12] K. Hotta, M. Hosaka, A. Tanabe, T. Takeuchi, Secretogranin II binds to secretogranin III and forms secretory granules with orexin, neuropeptide Y, and POMC, J. Endocrinol., 202 (2009) 111-121. doi:10.167/JOE-08-0531.

[13] I. Suzuki, A. Tada, M.M. Ollmann, G.S. Barsh, S. Im, M.L. Lamoreux, V.J. Hearing, J.J. Nordlund, Z.A. Abdel-Malek, Agouti signaling protein inhibits melanogenesis and the response of human melanocytes to alpha –melanotropin, J. Invest. Dermatol., 108 (1997) 838-842. doi: 10.1093/hmg/ddm191.

[14] D. Lu, D. Willard, I.R. Patel, S. Kadwell, L. Overton, T. Kost, M. Luther, W. Chen, R.P. Woychik, W.O. Wilkison *et al*., Agouti protein is an antagonist of the melanocyte-stimulating hormone receptor, Nature, 371 (1994) 799-802. doi: 10.1038/371799a0.

[15] M.E. Lowe, Structure and function of pancreatic lipase and colipase, Annu. Rev. Nutr. 17 (1997) 141-158. doi:10.1146/annurev.nutr.17.1.141.

[16] M.J. Kuhar, S. Adams, G. Dominguez, J. Jaworski, B. Balkan, CART peptides, Neuropeptides 36 (2002) 1-8. doi:10.1054/npep.2002.0887.

[17] J.-Y. Yin, Z. Dong, J.-T. Zhang, EIF3A (eukaryotic translation initiation factor 3, subunit A, Atlas genet. Cytogenet. Oncol. Haematol. 15 (2011) 1-3. doi:10.4267/20242/45982.

[18] J. Marksteiner, W.A. Kaufmann, P. Gurka, C. Humpel, Synaptic proteins in Alzheimer's disease, J. Mol. Neurosc., 18 (2002) 53-63. doi:10.1385/JMN:18:1-2:53.

[19] D.W. Shineman, A.S. Dain, M.L. Kim, V.M.-Y. Lee, Constitutively active akt inhibits trafficking of amyloid precursor protein and amyloid precursor protein metabolites through feedback inhibition of phosphoinositide 3-kinase, Biochemistry, 48 (2009) 3787-3794. doi:10.1021/bi802070j.

[20] H.-K. Lee, P. Kumar, Q. Fu, KW. Querfurth, The insulin/Akt signaling pathway is targeted by intracellular B-amyloid, Mol. Biol. Cell. 20 (2009). 1533-1544. doi: 10.1091/mbc.E08-07-0777.

[21] W.D. Shyu, S.Z. Lin, M.F. Chiang, D.C. Chen, C.Y. Su, H.J. Wang, R.S. Liu, C.H. Tsai, H. Li, Secretoneurin promotes neuroprotection and neuronal plasticity via the Jak2/Stat3 pathway in murine models of stroke, J. Clin. Invest. 118 (2008) 133-148. doi:10.1172/JCI32723

[22] D.G. Drubin, S.C. Feinstein, E.M. Shooter, M.W. Kirschner, Nerve growth factor-induced neurite outgrowth in PC12 cells involves the coordinate induction of microtubule assembly and assembly-promoting factors, J. Cell biol., 101 (1985) 1799-1807.

[23] S.R. Heidemann, H.C. Joshi, A. Shechter, J.R. Fletcher, M. Bothwell Synergistic effects of cyclic AMP and nerve growth factor on neurite outgrowth and microtubule stability of PC12 cells, J. Cell biol., 100 (1985) 916-927.

[24] K. De Brucker, N. Delattin, S. Robijns, H. Steenackers, N. Verstraeten, B. Landuyt, L. Schoofs, B. Dovgan, M. Fröhlich, J. Michiels, J. Vanderleyden, B.P. Cammue, K. Thevissen, Derivatives of the mouse cathelicidin-related antimicrobial peptide (CRAMP) inhibit fungal and bacterial biofilm formation, Antimicrob. Agents Chemother. 58 (2014) 5395-5404. doi:10.1128/AAC.03045.

[25] D. Vandamme, B. Landuyt, W. Luyten, L. Schoofs, A comprehensive summary of LL-37, the factotum human cathelicidin peptide, Cell. Immunol. 280 (2012) 22–35. doi:10.1016/j.cellimm.2012.11.009.

Chapter III

Molecular mechanisms of LL-37-induced receptor activation: An overview.

E.-T. Verjans, S. Zels, W. Luyten, B. Landuyt, L. Schoofs.

Peptides, 85 (2016) 16-26. doi:10.1016/j.peptides.2016.09.002.

Abstract

The human cathelicidin peptide LL-37 plays a crucial role in the immune system on many levels, from the first line of defense in epithelial cells to restoring the tissue after infection. On host cells, the majority of LL-37-induced effects are mediated via direct or indirect activation of several structurally unrelated cell surface receptors or intracellular targets. How LL-37 is able to affect multiple receptors is currently not well understood. So far, the mechanistic details underlying receptor activation are poorly investigated and evidence for a conventional ligand/receptor interaction is scarce. Over the past few decades, a large number of studies have reported on the activation of a receptor and/or components of the downstream signal transduction pathway induced by LL-37. This chapter summarizes the current knowledge on molecular mechanisms underlying LL-37-induced receptor activation.

3.1 Introduction

Antimicrobial peptides and proteins (AMPs) are key components of the innate immune system, warding off invading pathogens such as bacteria, fungi, viruses and parasites [1,2]. More than hundred human AMPs have been identified and characterized from various host tissues and epithelial surfaces (for an overview see the Antimicrobial Peptide Database (APD)) [1]. AMPs are customarily positively charged and amphipathic low molecular weight proteins with a broad-spectrum antibiotic activity [1,3]. A wide variety of cell types express AMPs in a constitutive fashion or after exposure to a specific stimulus, such as vitamin D or interferon (IFN) γ [2,3]. In vertebrates, a small number of AMPs can also modulate and/or stimulate adaptive immunity via the specific activation of cell surface receptors or intracellular targets. Because of their prominent role in the human immune system and low inherent toxicity, AMPs are considered attractive templates to engineer new antimicrobials or therapeutics [1,4].

Cathelicidins are among the most studied classes of AMPs. In humans, there is only one representative, called LL-37, that exerts its function in concert with defensins [5]. The cathelicidin peptide plays a prominent role in innate host defense mechanisms against bacteria and some specific viruses, fungi and parasites [3,6–9]. LL-37 is expressed by cell types that are likely to encounter pathogens, such as epithelial cells of the skin, intestine, airway, ocular surface or reproductive tract, but is also localised in innate immune cells like neutrophils, dendritic cells (DC), mast cells, B-cells, natural killer (NK)-cells, γδ-T-cells, monocytes and macrophages [10,11]. The direct microbicidal activity of LL-37 is predominantly mediated by disrupting the integrity of microbial membranes, due to its inherent cationic and amphipathic nature [12]. Additionally, a multi-hit mechanism in which the peptide also interacts with several cytoplasmic targets appears to enhance microbial extirpation [13,14].

The discovery that LL-37 acts as a potent chemoattractant to guide monocytes, neutrophils and T cells to the site of infection led to a more thorough understanding of the role of the peptide [15]. LL-37 is not only involved in the innate immune system, but also exerts immunostimulatory and immunomodulatory effects. Upon infection, LL-37 acts as a danger signal and bridges the innate and adaptive immune system by recruiting immunocompetent cells to the site of infection. Additionally, LL-37 modulates the levels of inflammatory cytokines, serving to control the delicate balance between pro- and anti-inflammatory responses [16-18]. This ‘alarming’ effect of the peptide complements its role as endogenous antibiotic. Moreover, LL-37 is implicated in many key biological processes involving non-immune cells such as apoptosis, angiogenesis, re-epithelialization, wound closure and the maintenance of the intestinal epithelial barrier integrity [11,19–23]. Defects in LL-37

expression or processing are therefore frequently associated with the pathogenesis of several human diseases including psoriasis, rosacea, cystic fibrosis and cancer [18,24,25]. Detailed knowledge about the exact molecular mode of action on a variety of host cells and tissues is therefore a prerequisite to understand the pathology of these diseases.

Considering its small size and low structural complexity, it is remarkable that LL-37 contains all the necessary information to perform its pleiotropic tasks. In host cells, the majority of LL-37-induced effects are mediated via specific activation of various putative cell surface receptors, membrane channels or intracellular targets. LL-37 has been associated with at least nine receptors belonging to different receptor classes, including four G protein-coupled receptors (GPCRs), three receptor tyrosine kinases (RTKs), a ligand-gated ion channel (LGIC) and Toll-like receptors (TLRs) [2,26]. Recently, it has been demonstrated that LL-37 also inhibits the CD36 fat receptor in adipocytes and hepatocytes [27].

It remains a conundrum how one peptide is able to directly activate multiple receptors belonging to different receptor classes, especially since most 'ligand-receptor' interactions are classically thought to occur in a very specific manner. The current general consensus hypothesis appears to be that LL-37 activates eukaryotic cells by virtue of at least five distinctly different mechanisms, including direct and indirect modes of action.

LL-37 either acts as a surrogate ligand for a specific receptor or influences the formation or stabilization of membrane microdomains containing the receptor [3,28]. Transactivation of epidermal growth factor receptors (EGFRs) via metalloproteinase-mediated cleavage of membrane-anchored EGFR ligands has also been reported for LL-37 (*e.g.* 'triple-membrane-passing-signaling' model) [29]. More recently, LL-37 was found to contribute to the activation of receptors by promoting their incorporation in LRs [30]. Receptors that congregate in LRs can be more sensitive for their cognate agonists or even show activation in the absence of agonists. Furthermore, LL-37 and LL-37 aggregates can penetrate a variety of host cells, mainly via receptor-mediated endocytic pathways [26]. This provides a mechanism for the selective uptake of extracellular anionic molecules such as deoxyribonucleic acid (DNA) or lipopolysaccharide (LPS) and allows access for LL-37 to several intracellular targets, such as glyceraldehyde-3-phosphate dehydrogenase (GAPDH) [31].

Because of the large number of publications reporting on a specific receptor and/or components of the downstream signaling transduction pathway of LL-37, as well as functional effects on host cells, this chapter primarily intends to provide the reader with an updated and comprehensive synopsis on the subject. Also, during the last few years, novel molecular targets of LL-37 have been identified which have not been reviewed before, as exemplified by studies from Hoang-Yen Tran *et al.*, Zhang

et al., and Gambade *et al* [27,32,33]. Our aim is to review these recent findings in order to acquire a more thorough understanding of the complex modes of action of LL-37 on host cells. Finally, many studies rely on a collection of broad-spectrum or receptor-selective antagonists to identify the cognate receptor of LL-37. Administration of receptor-selective antagonists to cell lines displaying a response to LL-37 suggests direct interaction between the peptide and its receptor, but true functional coupling of LL-37 to a defined receptor binding pocket has been questioned by several research groups.

Currently, it is believed that LL-37 operates in a non-canonical manner by first binding to the membrane interface and then interacting with receptor transmembrane domains, but consensus on this matter has not yet been attained [2,10,26]. In order to establish a starting point for novel drug development efforts, improved knowledge on the interaction mechanism of LL-37 with its putative receptors is imperative.

Therefore, we want to provide the reader with an overview of the receptors reported to be activated by LL-37 and investigate whether there is compelling evidence for a direct interaction between receptor and peptide. This chapter will help researchers to compare their data with the current scientific literature (as of May 2017), or provide a source of inspiration for future experiments on this fascinating peptide.

3.2 GPCRs

GPCRs, also known as seven-transmembrane domain receptors, constitute a large and diverse family of cell surface proteins that mediate a wide variety of physiological processes in multiple cell types. In 2000, De Yang and colleagues identified *N*-formyl peptide receptor 2 (FPR2; formerly known as formyl peptide receptor like-1) as the first functional receptor for LL-37 [15]. FPR2 belongs to a class of G_i protein-coupled receptors activated by a wide range of structurally diverse pro- and anti-inflammatory ligands and plays a key role in many biological processes including chemotaxis, angiogenesis, phagocytosis, DC development, inflammation and the pathogenesis of amyloidosis, cancer, Alzheimer's disease and prion disease [34,35]. Complex functional properties constitute the foundation of FPR2's high promiscuity: activation of the receptor can either inhibit or trigger inflammatory responses depending on specific receptor domains targeted by different agonists [34].

At first, FPR2 was characterized as the receptor mediating the chemotactic response to LL-37 in human peripheral blood neutrophils, monocytes and T cells and this typically involves intracellular calcium flux [15]. Migration along a chemotactic gradient and subsequent accumulation of leukocytes at the site of infection constitutes an indispensable part of the inflammatory response in humans. However, the effects of LL-37 mediated via FPR2 surpass chemotaxis, as demonstrated by

Nagaoka *et al*. and Wan *et al.* in neutrophils [36,37]. In these reports, activation of FPR2 by LL-37 was found to suppress neutrophil apoptosis and stimulate leukotriene B4 (LTB4) production, which is a potent chemoattractant and stimulator of reactive oxygen species (ROS) formation. In line with this finding, LL-37 triggers the release of cysteinyl leukotrienes from eosinophils via FPR2 [38]. Furthermore, LL-37 uses FPR2 to increase neutrophil respiratory burst and neutrophil extracellular trap (NET) responses to mediate its defense against influenza A virus (IAV) [39].

Depending on the stimulated cell type, LL-37-induced activation of FPR2 may provoke different functional outcomes. For example, stimulation of FPR2 by LL-37 promotes angiogenesis and arteriogenesis in endothelial cells, induces the migration of corneal epithelial cells and stimulates healing of mechanically induced wounds in bronchial mucoepidermoid carcinoma-derived cells [34,40]. In IMR90 human fibroblasts, the predominant cell type in connective tissue responsible for the production of proteins that form the extracellular matrix, exposure to LL-37 activates extracellular signal-regulated kinases (ERKs), p47 (phox) phosphorylation and NADPH oxidase-dependent superoxide generation [41].
LL-37 also engages FPR2 to increase cell stiffness in lung epithelial cells which enforces the physical barrier to pathogens [42]. Moreover, emerging evidence from tumor biology studies indicate that activation of FPR2 by LL-37 promotes tumorigenesis in hepatocellular carcinoma cells. Stimulation with LL-37 triggers the G_i protein-mediated signaling cascade, which further activates Mitogen-Activated Protein Kinases (MAPKs), ROS signaling and the NF-κB transcription factor. These pathways subsequently evoke an increase in the expression of macrophage colony-stimulating factor (M-CSF) and monocyte chemotactic protein-1 (MCP1), promoting tumor growth and dissemination [35].

In addition to FPR2, at least three additional GPCRs have been associated with LL-37, namely CXC chemokine receptor type 2 (CXCR2), Mas-related gene X2 (MrgX2) and purinergic receptor P2Y11 (P2Y11) [2]. However, the LL-37 activation mechanism and downstream targets of these GPCRs have not been investigated to the same extent as for FPR2.

CXCR2 is a Pertussis Toxin (PTX)-sensitive $G\alpha_i$-coupled GPCR activated by various CXC-chemokines, including granulocyte chemotactic protein-2 and growth-related oncogenes [43]. Zhang *et al.* demonstrated that LL-37 acts in a similar fashion as CXCR2 selective ligands in terms of receptor downregulation and intracellular calcium mobilization in human neutrophils [44]. LL-37-induced neutrophil migration and activation could be completely blocked using a CXCR2-specific antagonist, whereas the FPR2-selective antagonist WRW4 did not exert the same effect. This report challenges the idea of FPR2 as the receptor of LL-37 on neutrophils and monocytes. Their hypothesis is supported by the fact that a considerable number of studies did not test for activity of CXCR2 and use

PTX as a specific blocker for FPR2, whereas this reagent is known to selectively block all $G\alpha_i$-coupled signaling. Furthermore, the suppression of neutrophil apoptosis by LL-37 was confirmed in another study by Barlow and co-workers, who reported signaling through a GPCR other than FPR2 [19]. The tacit assumption that FPR2 is the only GPCR activated by LL-37 in immune cells was further questioned by Subramanian *et al.* who identified MrgX2 as a novel GPCR for LL-37 in human mast cells [45]. Mast cells are important mediators of allergy and anaphylaxis, due to their granules containing histamine and heparin. Interestingly, MrgX2 is activated by a plethora of basic peptides, including human-β-defensins (hBDs), and substance P [46]. Given the basicity of LL-37, it is unsurprising that LL-37 can act as MrgX2 agonist. Finally, the rat homologue of LL-37 (rCRAMP) was shown to participate in brain immunity via the purinergic P2Y11 receptor. The peptide plays a prominent role in brain cell protection by stimulating cytokine production and glial cell activation [47].

Taken together, several GPCRs have been proposed to mediate the multitude of functional effects of LL-37 on a variety of cell types. However, the precise mechanism by which LL-37 activates these receptors is still subject to discussion. If there is an interaction with a cognate receptor, it remains unclear if specific binding to an orthosteric ligand-binding site is involved. Alternatively, the binding could be aspecific with one of the hydrophobic transmembrane domains of the GPCR, causing a conformational change that activates a downstream signal transduction pathway.
To date, FPR2 is suggested as a GPCR to which LL-37 can directly bind [3,15,40]. Supporting evidence for this hypothesis emerges from the fact that WRW4, a selective antagonist for FPR2 signaling which directly binds to the formyl peptide binding pocket, is able to block several functional effects of LL-37. Furthermore, LL-37-induced release of intracellular calcium can be cross-desensitized by FPR2-specific agonists in monocytes [15]. Nevertheless, the majority of publications raise questions on a direct interaction of the peptide with a specific ligand binding site, particularly since GPCRs are activated by ligands that possess unique structural characteristics. Therefore, the ability of LL-37 to activate more than one GPCR on a broad set of cell types argues against a highly structure-specific binding to a plasma membrane receptor.

To date, the general consensus hypothesis states that LL-37 resides in and accumulates at the cell membrane due to its amphipathic nature. Therefore, the peptide can activate the receptor by interacting with the hydrophobic transmembrane regions (figure 3.1-A) [26]. This hypothesized mode of action is supported by a recent study of Tripathi *et al.*, who developed a homology model for the binding of LL-37 to FPR2 employing known structures of related GPCRs [39]. Docking studies with the established nuclear magnetic resonance (NMR) structure of LL-37 suggested a binding of LL-37 to the membrane interface of FPR2 rather than to the orthosteric ligand binding site. Intriguingly, upon

substitution of all amino acids of LL-37 by their enantiomers, biological activity was retained. Enantiomeric substitution drastically changes the affinity of a ligand for its binding pocket in the receptor, but the structure and membrane insertion capacities remain unaltered**.** These observations indicate that LL-37 may not interact with FPR2 in a stereospecific manner. Nonetheless, the model of Tripathi and co-workers prompts the need for further research, especially since WRW4 is able to block the ability of LL-37 to potentiate the respiratory burst and NET responses in response to IAV infection. If LL-37 and WRW4 interact with different receptor domains, the inhibiting effect would not be expected. However, it remains a possibility that WRW4 prevents FPR2 to undergo the allosteric change mediated by LL-37, thereby inhibiting its ability to activate the receptor.

As mentioned before, the precise mechanisms by which LL-37 activates more than one GPCR are not fully delineated. Interestingly, the multiple basic residues of LL-37 may also play a previously unrecognized role in peptide binding and receptor activation. For instance, MrgX2 is promiscuously activated by basic peptides and a weak correlation between MrgX2 potency and peptide charge is observed [48]. Conducting site-directed mutagenesis to locate the important acidic amino acids that are involved in binding to basic centers could provide valuable information, although it will not explain the level of promiscuity in this receptor. Docking small molecule agonists to MrgX2 models *in silico* is another approach to obtain information on the properties of binding site, but docking peptides is virtually impossible due to the lack of knowledge of their bound conformation. NMR might be the only way, in combination with *in silico* approaches, to get a picture of the bound structure of a peptide, without using crystallization.

Recently, an alternative model for GPCR activation was discovered by Wu *et al* [30]. This model relies on the ability of LL-37 to increase the incorporation of CXC chemokine receptor type 4 (CXCR4) into specialized membrane microdomains called LRs. LRs contain high concentrations of cholesterol and glycosphingolipids and can contain the effectors of incomplete signal transduction pathways that can be triggered when a receptor is recruited into the raft [49]. A number of studies have revealed that LL-37 has membrane-active properties, possibly preferring LRs [26]. By increasing the incorporation of CXCR4 into LRs of human hematopoietic stem/progenitor cells (HSPCs), LL-37 enhanced the chemotactic responsiveness to a stromal-derived factor-1 (SDF-1) gradient. This phenomenon is known as the HSPC-priming effect and underlines a novel mechanism by which LL-37 exerts its action on eukaryotic host cells. Even though the mechanistic details appear to be complex and have not been fully elucidated, it is suggested that LL-37 disturbs the organization of the lipid bilayer via non-receptor mediated mechanisms that promote the formation of LRs (figure 3.1-B) [30].

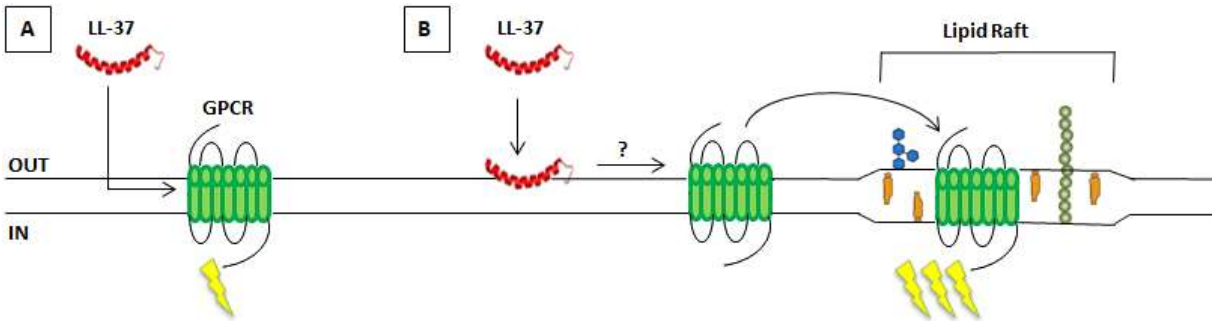

Fig.3.1. LL-37 activates multiple GPCRs. One mechanism to explain this involves initial binding to the membrane interface and then interacting with their receptor transmembrane domains. Based on this model, LL-37 exerts its action on GPCRs by inducing allosteric changes in the receptor rather than binding to an orthosteric binding site. According to Tripathi *et al.*, residues 24-32 of LL-37 make key contacts with the receptor (**A**). An alternative model for cell activation relies on the ability of LL-37 to increase the incorporation of GPCRs (CXCR4) into LRs containing cholesterol (orange) glycolipids (blue) and/or carbohydrates (green). It is suggested that LL-37 perturbs the organization of membrane lipids, leading to an enhanced inclusion of CXCR4 into LRs (**B**).

3.3 RTKs

RTKs are a family of cell surface receptors which depend on intracellular kinase activity upon binding of a ligand to propagate the signal inside the cell [50]. Using EGFR tyrosine kinase inhibitors and neutralizing anti-EGFR antibodies, Tjabringa and colleagues were the first to identify a functional association between LL-37 and a member of the EGFR family of RTKs (ErbBs), which are crucial for the development, growth and homeostasis of multicellular organisms [29,51]. Many physiological processes including corneal wound healing, gastric epithelial cell proliferation and ulcer healing, keratinocyte migration and skin wound closure, human pulp cell migration, innate immunity of airway and corneal epithelial cells as well as keratinocytes, airway mucus production in chronic obstructive pulmonary disease, LR-dependent endocytosis of LL-37/LPS complexes into lung epithelial cells and the growth of lung cancer cells, are influenced by LL-37-induced activation of ErbB1/EGFR [52–60].

Two other members of the RTK family are documented to respond to LL-37 in breast cancer cells, namely the Insulin-Like Growth Factor 1 Receptor (IGF1R) and ErbB2 [61,62]. The latter also belongs to the EGFR family of RTKs and plays a key role in the development of several human malignancies. In this respect, LL-37 could contribute to breast cancer progression through the activation of MAPK signaling via ErbB2. Exposure to LL-37 has the capacity to stimulate migration and alter cancer cell morphology, indicative of enhanced metastatic potential. Interestingly, the action of LL-37 could be competitively inhibited by a truncated fragment of LL-37, which opens up the possibility for therapeutic intervention [62]. IGF1R can also be activated by LL-37 and was identified by direct binding *in vitro* and co-immunoprecipitation experiments. The authors demonstrated that LL-37

works as a partial agonist for IGF1R. Activation of IGF1R by LL-37 led to increased migration and invasion of malignant cells [61].

Even though the majority of RTKs exhibit similar structures, it appears that LL-37 does not activate aforementioned RTKs by means of a common molecular mechanism. One of the proposed modes of action involves receptor 'transactivation', and relies on the ability of one receptor to activate another (figure 3.2-A). In this process, termed ectodomain shedding, LL-37-induced GPCR activation stimulates a currently unidentified member of the disintegrin and metalloproteinase (ADAM) family of metalloproteinases which subsequently cleaves a membrane-anchored ligand of EGFRs, *e.g.* heparin-binding EGF-like growth factor (HB-EGF) or transforming growth factor-alpha (TGF-α) [29,52]. Upon activation by this ligand, EGFR dimerizes and stimulates its intrinsic tyrosine kinase activity. Several of the ADAMs are known to be involved in ectodomain shedding, notably ADAM-9, -10, -12, -15, -17, and -19, but the molecular mechanisms underlying their activation are not fully clarified [63]. It is possible that LL-37 exerts a direct effect on ADAM by association with and modification of the cell membrane. However, EGFR transactivation is classically thought to be exclusively mediated through GPCR activation and HB-EGF has been demonstrated to undergo GPCR-stimulated release in various cell types [63,64].

The identity of the GPCR activated by LL-37 is still largely elusive in many cell types. For instance, in keratinocytes and airway epithelial cells, LL-37-induced EGFR phosphorylation could not be inhibited by PTX and FPR2-specific antagonists, which suggests that FPR2 is not involved in the transactivation of EGFR [29,56]. In agreement with these findings, LL-37 modulates the production of cytokines in human corneal epithelial cells through the activation of EGFR but not FPR2, excluding a FPR2-mediated transactivation mechanism [65]. Whether a GPCR other than FPR2 is involved in the LL-37-induced transactivation mechanism of EGFR remains to be determined and implicates the need for further research. Simultaneously, other hypotheses have been proposed to explain how EGFR is activated by LL-37. Most of these models point to the membrane-active properties of LL-37, which may induce specific changes in the overall activity pattern of receptors or membrane-associated molecules. These events could trigger EGFR signaling, especially since the activation of EGFRs is not unique among AMPs. For example, hBDs also phosphorylate EGFRs in keratinocytes, which may be suggestive of a more general mode of action [56]. Moreover, LL-37 has the ability to cross the cell membrane of keratinocytes using translocation mechanisms that do not require the activation of specific receptors [66]. Such perturbation of the cellular surface may alter receptor conformation, thereby activating downstream signaling cascades [56]. Until now, it is not clear whether the occurrence of cross-talk between GPCRs and EGFRs or the membrane activity of LL-37 is responsible for the activation of EGFR.

In breast cancer cells, both ErbB2 and/or IGF1R were identified as functional receptors for LL-37, but the molecular mechanism underlying this induction was not elucidated. It is postulated that LL-37 activates ErbB2 kinases via a still-uncharacterized receptor, especially since ErbB2 receptors do not have a functional ligand-binding domain [62,67]. However, this does not exclude a direct effect of LL-37 on the ErbB2 receptor, and further research efforts are needed before any definite conclusions can be drawn. A direct binding of LL-37 to IGF1R has been proposed by Girnita *et al.* This binding was demonstrated using a sandwich enzyme-linked immunosorbent assay (ELISA) and co-immunoprecipitation experiments (figure 3.2-B) [61]. A novel approach that could be useful to determine peptide-binding sites at domain level resolution was invented by Frei and colleagues [68]. In their strategy, called Ligand-Receptor-Capture (LRC), a trifunctional chemoproteomic reagent captures cell surface proteins bound to ligands followed by identification of captured receptors using quantitative mass spectrometry. Mapping the binding sites of LL-37 may be of utmost importance in light of potential future applications and for therapeutic exploitation.

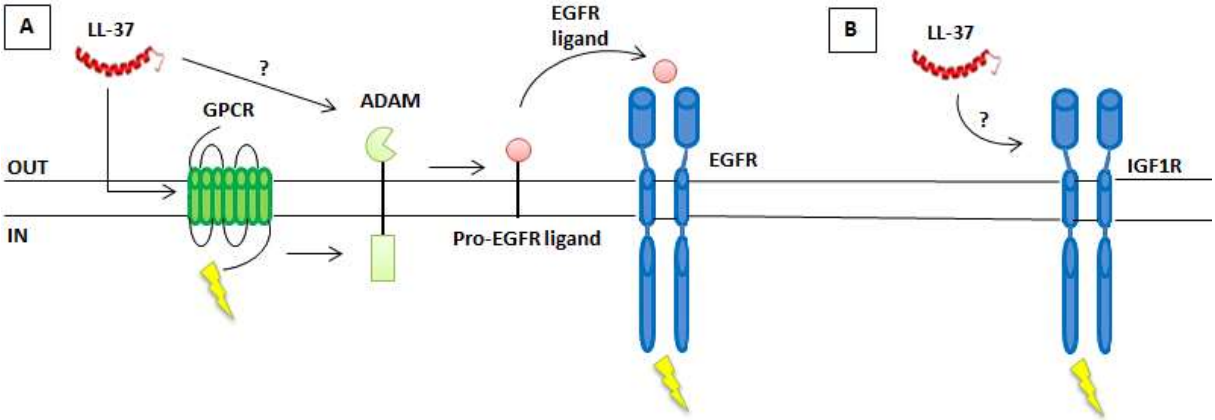

Fig.3.2. LL-37-mediated activation of RTKs. In the transactivation model, LL-37 stimulates the release of a membrane-anchored EGFR-ligand by activating a putative member of the ADAM family. The precise mechanism by which LL-37 mediates ADAM activation remains to be established (adapted from Ref. [24])(**A**). In breast cancer cells, LL-37 directly binds to IGF1R and behaves as a biased agonist for IGF1R. However, the peptide-binding sites have not yet been delineated (**B**).

3.4 Transmembrane channels

Besides GPCRs and RTKs, the human purinergic receptor $P2X_7$ is frequently associated with biological activity of LL-37. $P2X_7$ belongs to the family of ionotropic ATP-gated receptors and is highly expressed on immune cells. Within milliseconds, activation of $P2X_7$ by extracellular ATP leads to opening of a channel selective for small cations such as calcium, sodium and potassium. However, during prolonged exposure to ATP, a larger pore opens that allows permeation of molecules with a molecular weight up to 900 Da [69-71]. $P2X_7$ receptors play significant roles in multiple biological

processes linked to inflammation, mainly due to their ability to regulate processing and release of pro-inflammatory cytokines [72].

Among P2X receptors, $P2X_7$ is characterized by a significantly extended intracellular C-terminal tail [73]. Even though only a few subtype-specific agonists of $P2X_7$ have been discovered, Elssner and colleagues demonstrated that LL-37 acts as a $P2X_7$ activator in LPS-primed monocytes [74]. Subsequent research efforts indicated that several immunostimulatory and immunomodulatory effects of LL-37 could be explained by the specific activation of $P2X_7$, leading to the maturation and release of interleukin (IL) 1β and IL-8 [74,75]. Importantly, this effect was not deemed to be secondary to the extracellular release of ATP, because the ATP-hydrolyzing enzyme apyrase did not abrogate the action of LL-37 [16,36]. Furthermore, activation of $P2X_7$ by LL-37 could also mediate contrasting effects on apoptotic pathways in neutrophils and epithelial cells, contribute to maintenance and re-establishment of the intestinal barrier integrity, trigger a potassium flux from the cytoplasm in monocytes and promote proliferation along with pore-forming activity in $P2X_7$-expressing human embryonic kidney (HEK) cells [23,26,76]. Additionally, $P2X_7$ is involved in the extracellular uptake of LL-37 by human macrophages, where it promotes LTB4 and thromboxane A2 production or induces autophagy upon infection with intracellular pathogens such as *Mycobacterium tuberculosis* [77-79]. Due to its ability to regulate apoptosis and to mediate the secretion of proinflammatory cytokines, $P2X_7$ might also play a prominent role in pathogenesis of malignant tumors [80,81].

Remarkably, interactions between LL-37 and $P2X_7$ are more complex than previously estimated. For instance, LL-37 does not activate $P2X_7$ in mouse submandibular gland cells but modulates the response of $P2X_7$ to ATP in autocrine fashion, presumably by modifying the physicochemical state of the plasma membrane [82]. Moreover, Seil and colleagues reported that CRAMP, the unique murine antimicrobial cathelicidin-related peptide, is not the natural agonist of $P2X_7$ in murine peritoneal macrophages as binding of the peptide inhibits responses secondary to the activation of murine $P2X_7$ [83]. These results imply that the interaction between cathelicidins and $P2X_7$ are species-specific and CRAMP provokes the inhibition but not the activation of $P2X_7$ in mice. It remains difficult to explain why LL-37 and CRAMP inhibit or modulate certain responses coupled to $P2X_7$. One possibility is that mouse and human $P2X_7$ display a different sensitivity towards agonists or antagonists, evoking different responses to AMPs [83,84].

Numerous models have been proposed to explain how cathelicidins exert their effect on $P2X_7$, but the mechanistic details defining peptide and receptor interactions are not fully understood [85]. Like for GPCRs, it remains elusive whether this interaction occurs via specific interaction with an

orthosteric binding site [86]. Studies that favor the idea of direct ligand/receptor coupling mainly rely on the fact that specific antagonists of $P2X_7$ signaling inhibit various functional effects of LL-37. For example, neutrophil apoptosis was suppressed by oxidized ATP, a selective and irreversible inhibitor of $P2X_7$ signaling that binds to unprotonated lysine residues located near the ATP binding site [87]. Furthermore, LL-37 displayed strong binding potency for $P2X_7$ with a 2.99 kcal/mol binding potential while CRAMP only attains a binding potential of 1.74 kcal/mol [83]. These differences in energy could account for the versatility of effects exerted by LL-37 and CRAMP on $P2X_7$. Based on these findings, it is tempting to speculate that LL-37 and CRAMP interact directly with $P2X_7$ but the exact binding domains have yet to be identified.

Other studies suggest that LL-37 penetrates into the cell and interacts with the long C-terminal tail of the receptor. However, this hypothesis contradicts a study by Tomasinsig *et al.* who used a truncated form of the $P2X_7$ receptor lacking the C-terminus to show that the cytosolic domain is not necessary for LL-37 activity [76]. In the same study, the structural and aggregational requirements of LL-37 to modulate the activation state of $P2X_7$ were determined. The results indicate strong correlation between the helix-forming propensity of cathelicidin peptides and the extent to which $P2X_7$ is activated. Because helical peptides like LL-37 can insert deeply into the membrane and the all-D analog of LL-37 retained the capacity to stimulate $P2X_7$, it is reasonable to assume that the functional interaction between LL-37 and $P2X_7$ involves transmembrane segment-mediated binding rather than a high-stringency receptor interaction (figure 3.3).
Notably, it cannot be excluded that LL-37 changes $P2X_7$ function by inducing non-lytic alterations of the plasma membrane surrounding the receptor, particularly as $P2X_7$ function is known to be very sensitive to changes in membrane environment and a wide range of lipids have been demonstrated to increase agonist potency in both functional and binding studies [71]. However, in this model, the membrane activity needs to be specific because P2Y receptors are barely affected by the action of LL-37. It is currently unclear which of the proposed mechanisms are employed by LL-37 to activate $P2X_7$. In our view, further studies with more detailed imaging and biophysical techniques are needed to improve general understanding of this matter.

Recently, LL-37 was also characterized as a promoter of cancer cell migration by activating transient receptor potential cation (TRPV2) Ca^{2+}-permeable channels and Ca^{2+}-activated K^+-channels (BKCa) [33]. In this model, LL-37 binds to the cell membrane which induces a form of mechanical stress on the plasma membrane. As a consequence, the osmo- and mechanosensory TRPV channel is activated. Subsequently, Ca^{2+}-entry through TRPV2 is accompanied by K^+-efflux through BKCa, thereby further increasing the driving force of Ca^{2+} across TRPV2, leading to cancer cell migration.

Interestingly, the functional association between LL-37 and transmembrane channels could become a topic of future research on tumor development.

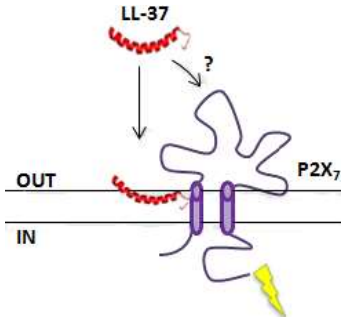

Fig.3.3. Activation of $P2X_7$ by LL-37. LL-37 activates $P2X_7$ through a currently unknown mechanism, possibly by inserting into the plasma membrane and interacting with receptor transmembrane domains rather than an orthosteric binding pocket.

3.5 TLRs and intracellular targets

TLRs represent a structurally conserved family of pattern-recognition receptors (PRRs) that recognize common structures (pathogen-associated molecular patterns (PAMPs)) shared by a vast majority of pathogens. In the human body, ten members have been identified to date, all of which are highly specific to a particular pathogen [88]. TLR1, TLR2, TLR4, TLR5, TRL6 and TLR10 are predominantly found on the cell surface whereas TLR3, TLR7, TLR8 and TLR9 are localized intracellularly [89]. Once a pathogen has evaded initial physical barriers such as the skin or gastrointestinal tract, the early innate immune responses are triggered by PRR/PAMP interaction. As mentioned before, LL-37 assists the immune system in combating disease and fulfills a critical role in maintenance of the delicate balance of inflammatory responses in homeostasis. The action of LL-37 could thus partly be mediated by members of the TLR family, depending on the presence of their conventional ligands [90]. The best-known example thereof is the anti-endotoxin activity of LL-37 to prevent TLR4 activation in monocytes and macrophages, which leads to a dampened production of proinflammatory cytokines and serves to protect against endotoxin shock in response to moderate pathogen challenge [91].
Another study by Di Nardo *et al.* also uncovered an immunosuppressive role for LL-37 and CRAMP using a mouse model of allergic contact dermatitis [92]. Their data indicate that cathelicidin peptides inhibit TLR4-mediated induction of DC maturation and cytokine release through a membrane-dependent mechanism. Here, the membrane-active properties of LL-37 selectively alter receptor motility and perturb DC membrane structures, thereby interfering with the assembly of the TLR4/CD14/MD2 receptor complex required for proper TLR4 signaling (figure 3.4-A).

As previously mentioned, LL-37 exerts numerous immunomodulatory effects and both anti-and pro-inflammatory functions have been assigned to the peptide [93]. For instance, LL-37 potentiates innate immune responses in polarized lung epithelial cells by increasing uptake and delivery of LPS to intracellular TLR4-enriched compartments [26,59]. This 'non-classical' TLR4 activation is restricted to the basolateral compartment of the epithelial membrane, providing a mechanism to keep sensors of infection and injury segregated from environmental microbes on the apical side unless the epithelial barrier is damaged. Interestingly, the ability of LL-37 to have an immunomodulatory effect on TLR4 might also depend on the sequence of LL-37 and LPS exposure, since macrophages primed with LPS prior to LL-37 treatment enhanced the release of tumor necrosis factor-alpha (TNF-α) [93].
Aside from TLR4, other TLR responses are modulated by the presence of LL-37. LL-37 enhances TLR3 signaling by translocating viral double-stranded (ds) RNA into host cells and complexes to extracellular self-RNA/DNA fragments to enhance signaling by TLR7/8 or 9 [94,95]. Furthermore, LL-37 also demonstrates synergy with flaggelin to regulate TLR5 and with Pam(3)CSK(4) to modulate TLR2/1 [96].

In order to access intracellular TLRs and mediate the delivery of nucleic acids or other types of cargo into host cells, LL-37 needs to cross the plasma membrane. Rather than directly penetrating the cell by inducing membrane deformations, LL-37 uses the endocytic machinery to enter host cells, assisted by interactions with a variety of putative cell surface receptors, *e.g.* EGFR, $P2X_7$, FPR2 or proteoglycans (figure 3.4-B) [26,77,97,98]. In most cases, clathrin-mediated and/or LR-dependent endocytic pathways are involved, consistent with the receptor-mediated endocytosis pathway hypothesis [26]. To date, considerable progress has been made towards understanding the mechanisms that contribute to the LL-37-induced modulation of TLR activity. Both the oligomeric state of LL-37 and the pH of the environment appear to be important factors to explain the differential effects on TLR signaling. For example, TLR4 predominantly signals from the plasma membrane, whereas TLR3 signaling occurs in acidified endosomes. Due to the action of proton pumps, the acidification of the endosome induces LL-37 to release viral dsRNA. Hereafter, the dsRNA acts as an agonist for TLR3 signaling while LL-37 is transferred to lysosomes and degraded [99]. Interestingly, internalization of LL-37 also allows access for LL-37 to other intracellular targets such as the cytosolic protein GAPDH, which can impact innate immune pathways including p38 MAPK. Even though GAPDH is considered to be a key glycolytic enzyme, mammalian GAPDH has been implicated in various biological processes such as membrane transport and microtubule assembly. Interaction of LL-37 interferes with the association of GAPDH with one or more activators of the p38 MAPK signaling pathway, without causing a complete inhibition of enzyme function. It is suspected that LL-37 binds directly to the surface of GAPDH, rather than to a specific binding pocket, especially since

responses to certain sequence unrelated cationic amphipathic peptides were found to be similar [31].

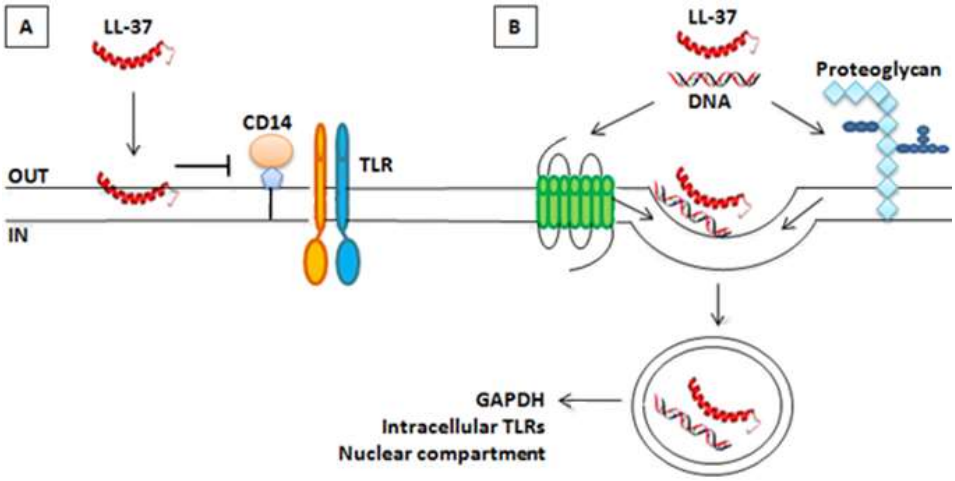

Fig.3.4. LL-37 influences TLR signaling. In DCs, LL-37 selectively inhibits TLR4 function, employing a receptor-independent mode of action. LL-37 impairs the movement of receptors and proteins in the cell membrane and hence interferes with the assembly of the TLR4/CD14/MD2 receptor complex (**A**). LL-37 or LL-37 aggregates are internalized via clathrin- or LR-mediated endocytosis, predominantly assisted by cell surface receptors (*e.g.* FPR2, EGFR or $P2X_7$) or proteoglycans. After penetration into the cell, LL-37 activates a variety of intracellular targets and/or traffics to specific compartments within the cell (adapted from Ref. [26]) (**B**).

3.6 Membrane interaction

As discussed in previous sections, the amphipathic nature of LL-37 enables it to reside in the zwitterionic membrane of eukaryotic cells [77,100,101]. In this position, LL-37 can modulate cellular activities by inducing allosteric changes of receptors, relocalizing them into LRs or influencing the motility of receptor complex components [26,30,39,92]. At higher concentrations, the peptide also exerts cytotoxic effects on various host cell types by creating transmembrane pores [2]. Therefore, the membrane activity of LL-37 needs to be tightly regulated.

Accumulated evidence, derived from experiments with D-enantiomers of LL-37 and fluorescence measurements with labeled LL-37, confirms the capacity of the peptide to attach to the membrane [33,42,76]. In addition, exposure to LL-37 modifies the fluidity of the plasma membrane, which can activate various downstream signal transduction pathways [16,33,82,102]. For example, Pochet and colleagues reported that LL-37 uses a membrane-dependent mechanism to potentiate the activation of phospholipase A_2 (PLA_2) in response to ATP in cells from mouse submandibular glands [82]. On the other hand, preincubation of LL-37 on these cells inhibits the activation of phospholipase D (PLD) upon exposure to ATP. According to Rao, these enzymes are sensitive to changes in the lipid packing in the plasma membrane in the presence of membrane-active peptides [103]**.** Notably, other amphipathic α-helical peptides such as melittin have also been documented to modulate PLA_2

activity by acting on the phospholipid bilayer [104]. It is therefore conceivable that LL-37 regulates cellular activities by modifying the physicochemical properties of the membrane.

In order to obtain more information about peptide-membrane interactions, model membranes of different lipid compositions are frequently used. Initially, the focus was put on the extent to which LL-37 perturbs anionic bacterial model membranes versus model membranes composed mainly of zwitterionic phospholipids to mimic the membrane of eukaryotic cells. It was demonstrated that electrostatic forces enable LL-37 to insert more efficiently into monolayers or bilayers made of negatively charged phospholipids. However, LL-37 also binds to neutral membranes by virtue of hydrophobic interactions between membrane phospholipids and apolar residues of the peptide [26,39,105]. Presumably, the four hydrophobic phenylalanine residues (F5, F6, F17, F27) of LL-37 participate in membrane binding [106].

Further characterization of LL-37 interaction with biological membranes revealed that its propensity to oligomerize strongly affects membrane binding [107]. Surface plasmon resonance (SPR) and cross-linking studies suggest that LL-37 interacts with host cell membranes as an oligomer and forms tetramers at elevated peptide concentrations. This is in line with studies using series of truncated LL-37 analogs, which show that the full oligomeric peptide is required for efficient binding to neutral membranes. Interestingly, the N-terminal fragment of LL-37 may play a key role in modulating membrane binding as removing the four N-terminal amino acids interferes with its capacity to adopt a helical oligomeric structure [26].

It has always been a major challenge to investigate membrane interactions at low concentrations of LL-37. One approach that might overcome this limitation is sum frequency generation (SFG) vibrational spectroscopy, as proposed by Ding *et al* [105]. Because of its superior sensitivity compared to other biophysical methods such as NMR, SFG intensity changes can be used to examine peptide-membrane interactions in the physiologically-relevant peptide concentration range. Ding and colleagues showed that low concentrations of LL-37 (0.46 µM) saturated a zwitterionic membrane bilayer model, most likely via hydrophobic interactions. However, it should be noted that model membranes do not completely mimic natural membranes which are made of heterogeneous mixtures of different lipid moieties. Therefore, experiments are difficult to reconcile and the choice of the model system and experimental conditions could profoundly influence the outcome of a peptide/lipid interaction experiment. Sevcsik and colleagues addressed this issue and demonstrated that LL-37 employs four distinctly different modes of action on bilayers composed of the four phospholipid species predominantly used in model membrane studies [108]. Consequently, it is

currently an unmet challenge to precisely determine the factors underlying the membrane interactions of LL-37.

Nonetheless, there is a consensus that the presence of cholesterol is one of the decisive parameters determining membrane intercalation of LL-37 [2,101,105]. Mammalian membranes contain a relatively high amount of cholesterol, which reduces the LL-37-induced impairment of the lipid bilayer and protects host cells from the membranolytic activity of the peptide. Some cancer cell types possess elevated levels of cholesterol-enriched LRs and are therefore less susceptible to lysis by LL-37 [109]. Intriguingly, several reports indicate that endocytosis of LL-37 may originate at LRs [26,77,98,110]. It remains unclear why LL-37 enters host cells via LRs while the presence of cholesterol attenuates the membrane association of the peptide. It is possible that sulfated proteoglycans play a key role in guiding the attachment and uptake of LL-37 at LRs, as suggested by Suzuki *et al* [110].

3.7 Conclusions and future prospects

Since the discovery of the human cathelicidin peptide LL-37 by Gudmundsson and colleagues, research on this peptide has progressed rapidly over the past two decades [111]. In hindsight, one can state that LL-37 transformed the general idea of what was considered purely an AMP into a multifunctional immunomodulator. The pleiotropic effects of LL-37 can be explained by the fact that the peptide operates by a wide diversity of complex mechanisms, ranging from non-specific membrane-damaging effects to specific activation of various putative cell surface receptors or intracellular targets. To date, at least nine receptors have been documented that mediate some of the multiple functional effects of LL-37. The existence of other unidentified receptors in human colon cancer cells, breast cancer cells, dermal fibroblasts and lung epithelial cells has even been hypothesized [62,112-114]. Moreover, novel molecular targets of LL-37 are continuously emerging, as exemplified in myeloid leukocytes, adipocytes, and melanoma cells [27,32,115-117]. It appears the ability to activate a broader set of cell types is directly derived from the cationic and amphipathic nature of the peptide. However, it remains difficult to understand how one single ligand can activate multiple structurally unrelated receptors. Most researchers favor the idea that LL-37 accumulates at and resides in the cell membrane, due to its membrane-active properties. Hereafter, LL-37 may affect or influence cell signaling via receptor-independent mechanisms or by inducing allosteric changes in receptor transmembrane domains rather than binding to an orthosteric binding site. This hypothesis is supported by the fact that D-enantiomers of LL-37 often maintain their activity, thereby arguing against a highly structure-specific binding to a cell surface receptor. Moreover, existing

studies provide little or no proof to demonstrate binding of LL-37 to a conventional ligand-binding pocket and the associated binding kinetics are lacking.

In our view, the proposed mechanism could explain the LL-37-induced effects on a variety of receptors (*e.g*. FPR2, CXCR4, TLR4) and transmembrane channels (*e.g.* $P2X_7$, TRPV2). Additionally, the membrane activity of LL-37 could also play a role in the transactivation mechanism of EGFR, as it may cause the activation of a putative member of the ADAM family. Therefore, it may prove valuable to thoroughly re-examine whether some of the previous observations underlying LL-37-induced receptor activation could be explained through indirect mechanisms of action, by which LL-37 first binds to the membrane interface.

However, this could also prove to be an oversimplified representation of the complex mode of action used by LL-37 and fails to explain how receptor-selective antagonists are able to inhibit various biological actions of LL-37. To further add to the complexity, a few molecular targets have been reported to which LL-37 could bind directly, including GAPDH and MAC-1, a member of the β_2-integrin family [31,32,115]. In addition, a recent study of Muñoz *et al*. suggested that LL-37 participates in the transcriptional regulation of melanoma cells by directly binding to gene promoter regions [117]. How this is possible, is the subject of ongoing discussion.

Considering future applications, a better understanding of how LL-37 activates its cognate receptor(s) is definitely required. So far, attempts to reveal peptide-binding sites have been hampered by the lack of characterized structures for most of the receptors of LL-37, thereby rendering a site-directed mutagenesis approach impossible. Additionally, docking peptides to a receptor model *in silico* is virtually unachievable due to the lack of knowledge of their bound conformation. However, it could be possible to build a homology model of receptors likely to be associated with LL-37, using known structures of structurally related receptors. Subsequently, conducting docking experiments with the established NMR structure of LL-37 could provide valuable information about the critical receptor domains involved in peptide binding. In a next step, this hypothesis can be validated using series of peptide fragments of LL-37 or by applying LRC technology. Finally, advanced *in silico* methods in combination with NMR spectroscopy experiments are expected to provide the necessary tools to increase the knowledge on the underlying molecular mechanisms behind LL-37-induced receptor activation.

References

[1] G. Wang, Human antimicrobial peptides and proteins, Pharmaceuticals, 7 (5) (2014) 545–594. doi:10.3390/ph7050545.

[2] D. Vandamme, B. Landuyt, W. Luyten, L. Schoofs, A comprehensive summary of LL-37, the factotum human cathelicidin peptide, Cell. Immunol. 280 (1) (2012) 22–35. doi:10.1016/j.cellimm.2012.11.009.

[3] F. Pinheiro da Silva, M.C. Machado, Antimicrobial peptides: clinical relevance and therapeutic implications, Peptides 36 (2) (2012) 308-314. doi:10.106/j.peptides.2012.05.014.

[4] M.A. Fox, J.E. Thwaite, D.O. Ulaeto, T.P. Atkins, H.S. Atkins, Design and characterization of novel hybrid antimicrobial peptides based on cecropin A, LL-37 and magainin II, Peptides 33 (2) (2012) 197-205. doi: 10.1016/j.peptides.2012.01.013.

[5] L. Frasca, R. Lande, Role of defensins and cathelicidin LL37 in auto-immune and auto-inflammatory diseases, Curr. Pharm. Biotechnol. 13 (10) (2012) 1882–1897. doi:10.2174/138920112802273155.

[6] M.D. Howell, J.F. Jones, K.O. Kisich, J.E. Streib, R.L. Gallo, D.Y.M. Leung, Selective killing of vaccinia virus by LL-37: implications for eczema vaccinatum, J. Immunol. 172 (3) (2004) 1763–1767. doi:10.4049/jimmunol.172.3.1763.

[7] B. Yasin, M. Pang, J.S. Turner, Y. Cho, N-N. Dinh, A.J. Waring, R.I. Lehrer, E.A. Wagar, Evaluation of the inactivation of infectious Herpes simplex virus by host-defense peptides, Eur. J. Clin. Microbiol. Infect. Dis. 19 (3) (2000) 187–194.doi:10.1007/s100960050457.

[8] A.L. den Hertog, J. van Marle, H.A. van Veen, W. Van't Hof, J.G.M. Bolscher, E.C.I. Veerman, A. V. Nieuw Amerongen, Candidacidal effects of two antimicrobial peptides: histatin 5 causes small membrane defects, but LL-37 causes massive disruption of the cell membrane, Biochem. J. 388 (Pt 2) (2005) 689–95. doi:10.1042/BJ20042099.

[9] B.S. McGwire, L. Olson, B.F. Tack, D.M. Engman, Killing of African trypanosomes by antimicrobial peptides, J. Infect. Dis. 188 (1) (2003) 146–152. doi:10.1086/375747.

[10] U.H.N. Dürr, U.S. Sudheendra, A. Ramamoorthy, LL-37, the only human member of the cathelicidin family of antimicrobial peptides, Biochim. Biophys. Acta. 1758 (9) (2006) 1408–25. doi:10.1016/j.bbamem.2006.03.030.

[11] R. Koczulla, G. Von Degenfeld, C. Kupatt, F. Krötz, S. Zahler, T. Gloe, K. Issbrücker, P. Unterberger, M. Zaiou, C. Lebherz, A. Karl, P. Raake, A. Pfosser, P. Boekstegers, U. Welsch, P.S. Hiemstra, C. Vogelmeier, R.L. Gallo, M. Clauss, R. Bals, An angiogenic role for the human peptide antibiotic LL-37 / hCAP-18, 111 (11) (2003) 1665–1672. doi:10.1172/JCI200317545.

[12] K.A. Henzler Wildman, D.K. Lee, A. Ramamoorthy, Mechanism of lipid Bilayer disruption by the human antimicrobial peptide, LL-37, Biochem. 42 (21) (2003) 6545–6558.doi:10.1021/bi0273563.

[13] M.-C. Chung, S.N. Dean, M.L. van Hoek, Acyl carrier protein is a bacterial cytoplasmic target of cationic antimicrobial peptide LL-37, Biochem. J. 470 (2) (2015) 243–253. doi:10.1042/BJ20150432.

[14] W. Liu, S.L. Dong, F. Xu, X.Q. Wang, T.R. Withers, H.D. Yu, X. Wang, Effect of intracellular expression of antimicrobial peptide LL-37 on growth of escherichia coli strain TOP10 under aerobic and anaerobic conditions, Antimicrob. Agents Chemother. 57 (10) (2013) 4707–4716. doi:10.1128/AAC.00825-13.

[15] De Yang, Q. Chen, A.P. Schmidt, G.M. Anderson, J.M. Wang, J. Wooters, J.J. Oppenheim, O. Chertov, LL-37, the neutrophil granule- and epithelial cell-derived cathelicidin, utilizes formyl peptide receptor-like 1 (FPRL1) as a receptor to chemoattract human peripheral blood neutrophils, monocytes, and T cells, J. Exp. Med. 192 (7) (2000) 1069–74. doi:10.1084/jem.192.7.1069.

[16] M. Seil, C. Nagant, J.P. Dehaye, M. Vandenbranden, M.F. Lensink, Spotlight on human LL-37, an

immunomodulatory peptide with promising cell-penetrating properties, Pharmaceuticals. 3 (11) (2010) 3435–3460. doi:10.3390/ph3113435.

[17] A. Nijnik, J. Pistolic, A. Wyatt, S. Tam, R.E.W. Hancock, Human cathelicidin peptide LL-37 modulates the effects of IFN-gamma on APCs, J. Immunol. 183 (9) (2009) 5788–5798. doi:10.4049/jimmunol.0901491.

[18] M. Reinholz, T. Ruzicka, J. Schauber, Cathelicidin LL-37 : An Antimicrobial Peptide with a Role in Inflammatory Skin Disease, Ann. Dermatol. 24 (2) (2012) 126–135. doi:10.5021/ad2012.24.2.126.

[19] P.G. Barlow, Y. Li, T.S. Wilkinson, D.M.E. Bowdish, Y.E. Lau, C. Cosseau, C. Haslett, a J. Simpson, R.E.W. Hancock, D.J. Davidson, The human cationic host defense peptide LL-37 mediates contrasting effects on apoptotic pathways in different primary cells of the innate immune system, J. Leukoc. Biol. 80 (3) (2006) 509–520. doi:10.1189/jlb.1005560.

[20] P.G. Barlow, P.E. Beaumont, C. Cosseau, A. Mackellar, T.S. Wilkinson, R.E.W. Hancock, C. Haslett, J.R.W. Govan, A.J. Simpson, D.J. Davidson, The human cathelicidin LL-37 preferentially promotes apoptosis of infected airway epithelium, Am. J. Respir. Cell Mol. Biol. 43 (6) (2010) 692–702. doi:10.1165/rcmb.2009-0250OC.

[21] J.D. Heilborn, M.F. Nilsson, G. Kratz, G. Weber, O. Sørensen, N. Borregaard, M. Ståhle-bäckdahl, The cathelicidin anti-microbial peptide LL-37 is involved in re-epithelialization of human skin wounds and is lacking in chronic ulcer epithelium, 120 (3) (2003) 379–389. doi:10.1046/j.1523-1747.2003.12069.x.

[22] R. Ramos, J.P. Silva, A.C. Rodrigues, R. Costa, L. Guardão, F. Schmitt, R. Soares, M. Vilanova, L. Comingues, M. Gama, Wound healing activity of the human antimicrobial peptide LL37, Peptides 32 (7) (2011) 1469-1476. doi:10.1016/j.peptides.2011.06.005.

[23] J-M. Otte, A-E. Zdebik, S. Brand, A.M. Chromik, S. Strauss, F. Schmitz, L. Steinstraesser, W.E. Schmidt, Effect of the cathelicidin LL-37 on intestinal epithelial barrier integrity, Regul. Peptides 156 (1-3) (2009) 104-117. doi:10.1016/j.regpep.2009.03.009.

[24] K. Kuroda, K. Okumura, H. Isogai, E. Isogai, The Human Cathelicidin Antimicrobial Peptide LL-37 and Mimics are Potential Anticancer Drugs, Front. Oncol. 5 (144) (2015) 1-10. doi:10.3389/fonc.2015.00144.

[25] C.I. Chen, S. Schaller-Bals, K.P. Paul, U. Wahn, R. Bals, Beta-defensins and LL-37 in bronchoalveolar lavage fluid of patients with cystic fibrosis, J. Cyst. Fibros. 3 (1) (2004) 45–50. doi:10.1016/j.jcf.2003.12.008.

[26] D. Xhindoli, S. Pacor, M. Benincasa, M. Scocchi, R. Gennaro, A. Tossi, The human cathelicidin LL-37 - A pore-forming antibacterial peptide and host-cell modulator, Biochim. Biophys. Acta - Biomembr. 1858 (3) (2015) 546-566. doi:10.1016/j.bbamem.2015.11.003.

[27] D. Hoang-Yen Tran, D. Hoang-Ngoc Tran, S.A. Mattai, T. Sallam, C. Ortiz, E.C. Lee, L. Robbins, S. Ho, J.E. Lee, E. Fisseha, C. Shieh, A. Sideri, D.Q. Shih, P. Fleshner, D.P.B. McGovern, M. Vu, T.C. Hing, K. Bakirtzi, M. Cheng, B. Su, I. Law, I. Karagiannides, S.R. Targan, R.L. Gallo, Z. Li, H.W. Koon, Cathelicidin suppresses lipid accumulation and hepatic steatosis by inhibition of the CD36 receptor, Int. J. Obes. (2016). doi:10.1038/ijo.2016.90. [Epub ahead of print]

[28] R.L. Gallo, Sounding the alarm: multiple functions of host defense peptides, J. Invest. Dermatol. 128 (1) (2008) 5–6. doi:10.1038/sj.jid.5701073.

[29] G.S. Tjabringa, J. Aarbiou, D.K. Ninaber, J.W. Drijfhout, O.E. Sørensen, N. Borregaard, K.F. Rabe, P.S. Hiemstra, The antimicrobial peptide LL-37 activates innate immunity at the airway epithelial surface by transactivation of the epidermal growth factor receptor, J. Immunol. 171 (12) (2003) 6690–6696. doi:10.4049/jimmunol.171.12.6690.

[30] W. Wu, C.H. Kim, R. Liu, M. Kucia, W. Marlicz, N. Greco, J. Ratajczak, M.J. Laughlin, M.Z. Ratajczak, The bone marrow-expressed antimicrobial cationic peptide LL-37 enhances the responsiveness of hematopoietic stem progenitor cells to an SDF-1 gradient and accelerates their engraftment after

transplantation, Leukemia. 26 (4) (2012) 736–745. doi:10.1038/leu.2011.252.

[31] N. Mookherjee, D.N.D. Lippert, P. Hamill, R. Falsafi, A. Nijnik, J. Kindrachuk, J. Pistolic, J. Gardy, P. Miri, M. Naseer, L.J. Foster, R.E.W. Hancock, Intracellular receptor for human host defense peptide LL-37 in monocytes, J. Immunol. 183 (4) (2009) 2688–96. doi:10.4049/jimmunol.0802586.

[32] X. Zhang, G. Bajic, G.R. Andersen, S.H. Christiansen, T. Vorup-Jensen, The cationic peptide LL-37 binds Mac-1 (CD11b/CD18) with a low dissociation rate and promotes phagocytosis, Biochim. Biophys. Acta 1864 (5) (2016) 471–478. doi:10.1016/j.bbapap.2016.02.013.

[33] A. Gambade, S. Zreika, M. Guéguinou, I. Chourpa, G. Fromont, A.M. Bouchet, J. Burlaud-gaillard, M. Potier-cartereau, S. Roger, V. Aucagne, S. Chevalier, C. Vandier, C. Goupille, G. Weber, Activation of TRPV2 and BKCa channels by the LL-37 enantiomers stimulates calcium entry and migration of cancer cells, Oncotarget. 7 (17) (2016) 23785-23800. doi:10.18632/oncotarget.8122.

[34] F. Cattaneo, M. Parisi, R. Ammendola, Distinct signaling cascades elicited by different formyl peptide receptor 2 (FPR2) agonists, Int. J. Mol. Sci. 14 (4) (2013) 7193–7230. doi:10.3390/ijms14047193.

[35] Y. Li, L. Cai, H. Wang, P. Wu, W. Gu, Y. Chen, H. Hao, K. Tang, P. Yi, M. Liu, S. Miao, D. Ye, Pleiotropic regulation of macrophage polarization and tumorigenesis by formyl peptide receptor-2., Oncogene. 30 (36) (2011) 3887–3899. doi:10.1038/onc.2011.112.

[36] I. Nagaoka, H. Tamura, M. Hirata, An antimicrobial cathelicidin peptide, human CAP18/LL-37, suppresses neutrophil apoptosis *via* the activation of formyl-peptide receptor-like 1 and P2X7, J. Immunol. 176 (5) (2006) 3044–52. doi:10.4049/jimmunol.176.5.3044.

[37] M. Wan, C. Godson, P.J. Guiry, B. Agerberth, J.Z. Haeggström, Leukotriene B4/antimicrobial peptide LL-37 proinflammatory circuits are mediated by BLT1 and FPR2/ALX and are counterregulated by lipoxin A4 and resolvin E1., FASEB J. 25 (5) (2011) 1697–1705. doi:10.1096/fj.10-175687.

[38] J. Sun, B. Dahlén, B. Agerberth, J.Z. Haeggström, The antimicrobial peptide LL-37 induces synthesis and release of cysteinyl leukotrienes from human eosinophils - Implications for asthma, Allergy Eur. J. Allergy Clin. Immunol. 68 (3) (2013) 304–311. doi:10.1111/all.12087.

[39] S. Tripathi, G. Wang, M. White, M. Rynkiewicz, B. Seaton, K. Hartshorn, Identifying the critical domain of LL-37 involved in mediating neutrophil activation in the presence of influenza virus: functional and structural analysis, PLoS One. 10 (8) (2015) 1–15. doi:10.1371/journal.pone.0133454.

[40] Y.J. Gordon, L.C. Huang, E.G. Romanowski, K.A. Yates, R.J. Proske, A.M. McDermotte, Human cathlecidin (LL-37), a multifunctional peptide, is expressed by ocular surface epithelia and has potent antibacterial and antiviral activity, Curr. Eye Res. 30 (5) (2005) 385–394. doi: 10.1080/02713680590934111.

[41] A. Iaccio, F. Cattaneo, M. Mauro, R. Ammendola, FPRL1-mediated induction of superoxide in LL-37-stimulated IMR90 human fibroblast, Arch. Biochem. Biophys. 481 (1) (2009) 94–100. doi:10.1016/j.abb.2008.10.026.

[42] F.J. Byfield, M. Kowalski, K. Cruz, K. Leszczyńska, A. Namiot, P.B. Savage, R. Bucki, P. a Janmey, Cathelicidin LL-37 increases lung epithelial cell stiffness, decreases transepithelial permeability, and prevents epithelial invasion by Pseudomonas aeruginosa, J. Immunol. 187 (12) (2011) 6402–6409. doi:10.4049/jimmunol.1102185.

[43] C.L. Addison, T.O. Daniel, M.D. Burdick, H. Liu, J.E. Ehlert, Y.Y. Xue, L. Buechi, A. Walz, A. Richmond, R.M. Strieter, The CXC chemokine receptor 2, CXCR2, is the putative receptor for ELR+ CXC chemokine-induced angiogenic activity, J. Immunol. 165 (9) (2000) 5269–5277. doi:10.4049/jimmunol.165.9.5269.

[44] Z. Zhang, G. Cherryholmes, F. Chang, D.M. Rose, I. Schraufstatter, J.E. Shively, Evidence that cathelicidin peptide LL-37 may act as a functional ligand for CXCR2 on human neutrophils, Eur. J. Immunol. 39 (11) (2009) 3181–3194. doi:10.1002/eji.200939496.

[45] H. Subramanian, K. Gupta, Q. Guo, R. Price, H. Ali, Mas-related gene X2 (MrgX2) is a novel G protein-coupled receptor for the antimicrobial peptide LL-37 in human mast cells: Resistance to receptor phosphorylation, desensitization, and internalization, J. Biol. Chem. 286 (52) (2011) 44739–44749. doi:10.1074/jbc.M111.277152.

[46] H. Wu, M. Zeng, E.Y.P. Cho, W. Jiang, O. Sha, The Origin, Expression, Function and Future Research Focus of a G Protein-coupled Receptor, Mas-related Gene X2 (MrgX2), Prog. Histochem. Cytochem. 50 (1-2) (2015) 11–17. doi:10.1016/j.proghi.2015.06.001.

[47] L.O. Brandenburg, S. Jansen, C.J. Wruck, R. Lucius, T. Pufe, Antimicrobial peptide rCRAMP induced glial cell activation through P2Y receptor signalling pathways, Mol. Immunol. 47 (10) (2010) 1905–1913. doi:10.1016/j.molimm.2010.03.012.

[48] H.J. Solinski, T. Gudermann, A. Breit, Pharmacology and Signaling of MAS-Related G Protein-Coupled Receptors, Pharmacol Rev. 66 (3) (2014) 570–597. doi:10.1124/pr.113.008425.

[49] L.J. Pike, Lipid rafts: bringing order to chaos, J. Lipid Res. 44 (4) (2003) 655–667. doi:10.1194/jlr.R200021-JLR200.

[50] M.A. Lemmon, J. Schlessinger, Cell signaling by receptor tyrosine kinases, Cell. 141 (7) (2010) 1117–1134. doi:10.1016/j.cell.2010.06.011.

[51] M.J. Wieduwilt, M.M. Moasser, The epidermal growth factor receptor family: Biology driving targeted therapeutics, Cell. Mol. Life Sci. 65 (10) (2008) 1566–1584. doi:10.1007/s00018-008-7440-8.

[52] J. Yin, F.S.X. Yu, Ll-37 *via* EGFR transactivation to promote high glucose-attenuated epithelial wound healing in organ-cultured corneas, Investig. Ophthalmol. Vis. Sci. 51 (4) (2010) 1891–1897. doi:10.1167/iovs.09-3904.

[53] R. Shaykhiev, C. Beisswenger, K. Kändler, J. Senske, A. Püchner, T. Damm, J. Behr, R. Bals, Human endogenous antibiotic LL-37 stimulates airway epithelial cell proliferation and wound closure., Am. J. Physiol. Lung Cell. Mol. Physiol. 289 (5) (2005) L842–L848. doi:10.1152/ajplung.00286.2004.

[54] Y. Zhang, Y. Jiang, C. Sun, Q. Wang, Z. Yang, X. Pan, M. Zhu, W. Xiao, The human cathelicidin LL-37 enhances airway mucus production in chronic obstructive pulmonary disease, Biochem. Biophys. Res. Commun. 443 (1) (2014) 103–109. doi:10.1016/j.bbrc.2013.11.074.

[55] Y.H. Yang, W.K. Wu, E.K. Tai, H.P. Wong, E.K. Lam, W.H. So, V.Y. Shin, C.H. Cho, The cationic host defense peptide rCRAMP promotes gastric ulcer healing in rats., J. Pharmacol. Exp. Ther. 318 (2) (2006) 547–554. doi:10.1124/jpet.106.102467.

[56] S. Tokumaru, K. Sayama, Y. Shirakata, H. Komatsuzawa, K. Ouhara, Y. Hanakawa, Y. Yahata, X. Dai, M. Tohyama, H. Nagai, L. Yang, S. Higashiyama, A. Yoshimura, M. Sugai, K. Hashimoto, Induction of keratinocyte migration *via* transactivation of the epidermal growth factor receptor by the antimicrobial peptide LL-37, J. Immunol. 175 (7) (2005) 4662–4668. doi:10.4049/jimmunol.175.7.4662.

[57] M. Carretero, M.J. Escámez, M. García, B. Duarte, A. Holguín, L. Retamosa, J.L. Jorcano, M.D. Río, F. Larcher, In vitro and in vivo wound healing-promoting activities of human cathelicidin LL-37, J. Invest. Dermatol. 128 (1) (2008) 223–236. doi:10.1038/sj.jid.5701043.

[58] M. Kajiya, H. Shiba, H. Komatsuzawa, K. Ouhara, T. Fujita, K. Takeda, Y. Uchida, N. Mizuno, H. Kawaguchi, H. Kurihara, The antimicrobial peptide LL37 induces the migration of human pulp cells: A possible adjunct for regenerative endodontics, J. Endod. 36 (6) (2010) 1009–1013. doi:10.1016/j.joen.2010.02.028.

[59] R. Shaykhiev, J. Sierigk, C. Herr, G. Krasteva, W. Kummer, R. Bals, The antimicrobial peptide cathelicidin enhances activation of lung epithelial cells by LPS, FASEB J. 24 (12) (2010) 4756–4766. doi:10.1096/fj.09-151332.

[60] J. von Haussen, R. Koczulla, R. Shaykhiev, C. Herr, O. Pinkenburg, D. Reimer, R. Wiewrodt, S. Biesterfeld,

A. Aigner, F. Czubayko, R. Bals, The host defence peptide LL-37/hCAP-18 is a growth factor for lung cancer cells, Lung Cancer. 59 (1) (2008) 12–23. doi:10.1016/j.lungcan.2007.07.014.

[61] A. Girnita, H. Zheng, A. Grönberg, L. Girnita, M. Ståhle, Identification of the cathelicidin peptide LL-37 as agonist for the type I insulin-like growth factor receptor, Oncogene. 31 (3) (2012) 352–365. doi:10.1038/onc.2011.239.

[62] G. Weber, C.I. Chamorro, F. Granath, A. Liljegren, S. Zreika, Z. Saidak, B. Sandstedt, S. Rotstein, R. Mentaverri, F. Sánchez, A. Pivarcsi, M. Ståhle, Human antimicrobial protein hCAP18/LL-37 promotes a metastatic phenotype in breast cancer, Breast Cancer Res. 11 (1) (2009) R6. doi:10.1186/bcr2221.

[63] D.K. Luttrell, L.M. Luttrell, Not so strange bedfellows: G-protein-coupled receptors and Src family kinases, Oncogene. 23 (48) (2004) 7969–7978. doi:10.1038/sj.onc.1208162.

[64] A. Gschwind, E. Zwick, N. Prenzel, M. Leserer, A. Ullrich, Cell communication networks: epidermal growth factor receptor transactivation as the paradigm for interreceptor signal transmission, Oncogene. 20 (13) (2001) 1594–1600. doi:10.1038/sj.onc.1204192.

[65] L.C. Huang, T.D. Petkova, R.Y. Reins, R.J. Proske, A.M. McDermott, Multifunctional roles of human cathelicidin (LL-37) at the ocular surface, Investig. Ophthalmol. Vis. Sci. 47 (6) (2006) 2369–2380. doi:10.1167/iovs.05-1649.

[66] M.H. Braff, M.A. Hawkins, A. Di Nardo, B. Lopez-Garcia, M.D. Howell, C. Wong, K. Lin, J.E. Streib, R. Dorschner, D.Y. Leung, R.L. Gallo, Structure-function relationships among human cathelicidin peptides: dissociation of antimicrobial properties from host immunostimulatory activities, J. Immunol. 174 (7) (2005) 4271–4278. doi:10.4049/jimmunol.174.7.4271.

[67] W.K. Wu, G. Wang, S.B. Coffelt, A.M. Betancourt, C.W. Lee, K. Wu, J. Yu, J.J. Sung, C.H. Cho,Emerging roles of the host defense peptide LL-37 in human cancer and its potential therapeutic applications, Int. J. Cancer. 127 (8) (2011) 1741–1747. doi:10.1002/ijc.25489.

[68] A.P. Frei, O.-Y. Jeon, S. Kilcher, H. Moest, L.M. Henning, C. Jost, A. Plückthun, J. Mercer, R. Aebersold, E.M. Carreira, B. Wollscheid, Direct identification of ligand-receptor interactions on living cells and tissues, Nat. Biotechnol. 30 (10) (2012) 997–1001. doi:10.1038/nbt.2354.

[69] C. Volonté, S. Apolloni, S.D. Skaper, G. Burnstock, P2X7 Receptors : Channels , Pores and More, CNS Neurol. Disord. - Drug Targets. 11 (6) (2012) 705–721. doi:10.2174/187152712803581137.

[70] J.S. Wiley, R. Sluyter, B.J. Gu, L. Stokes, S.J. Fuller, The human P2X7 receptor and its role in innate immunity, Tissue Antigens. 78 (5) (2011) 321–332. doi:10.1111/j.1399-0039.2011.01780.x.

[71] A.D. Michel, E. Fonfria, Agonist potency at P2X7 receptors is modulated by structurally diverse lipids, Br. J. Pharmacol. 152 (4) (2007) 523–537. doi:10.1038/sj.bjp.0707417.

[72] S.D. Skaper, P. Debetto, P. Giusti, P2X7 Receptors in Neurological and Cardiovascular Disorders, Cardiovasc. Psychiatry Neurol. 2009 (2009) 861324. doi:10.1155/2009/861324.

[73] R. Bartlett, L. Stokes, R. Sluyter, The P2X7 receptor channel: recent developments and the use of P2X7 antagonists in models of disease, Pharmacol. Rev. 66 (3) (2014) 638–675. doi:10.1124/pr.113.008003.

[74] A. Elssner, M. Duncan, M. Gavrilin, M.D. Wewers, A novel P2X7 receptor activator, the human cathelicidin-derived peptide LL37, induces IL-1β processing and release, J Immunol. 172 (8) (2004) 4987–4994. doi:10.4049/jimmunol.172.8.4987.

[75] P. Montreekachon, P. Chotjumlong, J.G.M. Bolscher, K. Nazmi, V. Reutrakul, S. Krisanaprakornkit, Involvement of P2X7 purinergic receptor and MEK1/2 in interleukin-8 up-regulation by LL-37 in human gingival fibroblasts, J. Periodontal Res. 46 (3) (2011) 327–337. doi:10.1111/j.1600-0765.2011.01346.x.

[76] L. Tomasinsig, C. Pizzirani, B. Skerlavaj, P. Pellegatti, S. Gulinelli, A. Tossi, F. Di Virgilio, M. Zanetti, The human cathelicidin LL-37 modulates the activities of the P2X7 receptor in a structure-dependent

manner, J. Biol. Chem. 283 (5) (2008) 30471–30481. doi:10.1074/jbc.M802185200.

[77] X. Tang, D. Basavarajappa, J.Z. Haeggström, M. Wan, P2X7 Receptor Regulates Internalization of Antimicrobial Peptide LL-37 by Human Macrophages That Promotes Intracellular Pathogen Clearance, J. Immunol. 195 (3) (2015) 1191–201. doi:10.4049/jimmunol.1402845.

[78] R. S. Rekha, S.S. Rao Muvva, M. Wan, R. Raqib, P. Bergman, S. Brighenti, G.H. Gudmundsson, B. Agerberth, Phenylbutyrate induces LL-37-dependent autophagy and intracellular killing of mycobacterium tuberculosis in human macrophages, Autophagy. 11 (9) (2015) 1688–1699. doi:10.1080/15548627.2015.1075110.

[79] M. Wan, O. Soehnlein, X. Tang, A.M. Van Der Does, E. Smedler, P. Uhlén, L. Lindbom, B. Agerberth, J.Z. Haeggström, Cathelicidin LL-37 induces time-resolved release of LTB4 and TXA2 by human macrophages and triggers eicosanoid generation in vivo, FASEB J. 28 (8) (2014) 3456–3467. doi:10.1096/fj.14-251306.

[80] B. Sainz, S. Alcala, E. Garcia, Y. Sanchez-Ripoll, M.M. Azevedo, M. Cioffi, M. Tatari, I. Miranda-Lorenzo, M. Hidalgo, G. Gomez-Lopez, M. Canamero, M. Erkan, J. Kleeff, S. Garcia-Silva, P. Sancho, P.C. Hermann, C. Heeschen, Microenvironmental hCAP-18/LL-37 promotes pancreatic ductal adenocarcinoma by activating its cancer stem cell compartment, Gut. 64 (12) (2015)1921-1935. doi:10.1136/gutjnl-2014-308935.

[81] E. Piktel, K. Niemirowicz, U. Wnorowska, M. Wątek, T. Wollny, K. Głuszek, S. Góźdź, I. Levental, R. Bucki, The Role of Cathelicidin LL-37 in Cancer Development, Arch. Immunol. Ther. Exp. 64 (1) (2015) 33–46. doi:10.1007/s00005-015-0359-5.

[82] S. Pochet, S. Tandel, S. Querriére, M. Tre-Hardy, M. Garcia-Marcos, M. De Lorenzi, M. Vandenbranden, A. Marino, M. Devleeschouwer, J.-P. Dehaye, Modulation by LL-37 of the responses of salivary glands to purinergic agonists, Mol. Pharmacol. 69 (6) (2006) 2037–2046. doi:10.1124/mol.105.021444.

[83] M. Seil, E. Kabré, C. Nagant, M. Vandenbranden, U. Fontanils, A. Marino, S. Pochet, J.-P. Dehaye, Regulation by CRAMP of the responses of murine peritoneal macrophages to extracellular ATP, Biochim. Biophys. Acta. 1798 (3) (2010) 569–78. doi:10.1016/j.bbamem.2009.11.002.

[84] M.T. Young, P. Pelegrin, A. Surprenant, Amino Acid Residues in the P2X7 Receptor that Mediate Differential Sensitivity to ATP and BzATP, Mol Pharmacol. 71 (1) (2007) 92–100. doi:10.1124/mol.106.030163.

[85] M.D. Wewers, A. Sarkar, P2X7 receptor and macrophage function, Purinergic Signal. 5 (2) (2009) 189–195. doi:10.1007/s11302-009-9131-9.

[86] Z. Hu, T. Murakami, K. Suzuki, H. Tamura, K. Kuwahara-Arai, T. Iba, I. Nagaoka, Antimicrobial cathelicidin peptide LL-37 inhibits the LPS/ATP-induced pyroptosis of macrophages by dual mechanism, PLoS One. 9 (1) (2014). doi:10.1371/journal.pone.0085765.

[87] M. Murgia, S. Hanau, P. Pizzo, M. Rippa, F. Di Virgilio, Oxidized ATP. An irreversible inhitibor of the macrophage purinergic P2Z receptor, J. Biol. Chem. 268 (1993) 8199–8203.

[88] B.A. Beutler, Review article TLRs and innate immunity, Blood. 113 (7) (2009) 1399–1407. doi:10.1182/blood-2008-07-019307.

[89] A.L. Blasius, B. Beutler, Intracellular Toll-like Receptors, Immunity. 32 (3) (2010) 305–315. doi:10.1016/j.immuni.2010.03.012.

[90] T. Into, M. Inomata, K. Shibata, Y. Murakami, Effect of the antimicrobial peptide LL-37 on Toll-like receptors 2-, 3- and 4-triggered expression of IL-6, IL-8 and CXCL10 in human gingival fibroblasts, Cell. Immunol. 264 (1) (2010) 104–109. doi:10.1016/j.cellimm.2010.05.005.

[91] N. Mookherjee, K.L. Brown, D.M.E. Bowdish, S. Doria, R. Falsafi, K. Hokamp, F.M. Roche, R. Mu, G.H. Doho, J. Pistolic, J.-P. Powers, J. Bryan, F.S. Brinkman, R.E. Hancock, Modulation of the TLR-Mediated

Inflammatory Response by the Endogenous Human Host Defense Peptide LL-37, J. Immunol. 176 (4) (2006) 2455–2464. doi:10.4049/jimmunol.176.4.2455.

[92] A. Di Nardo, M.H. Braff, K.R. Taylor, C. Na, R.D. Granstein, J.E. McInturff, S. Krutzik, R.L. Modlin, R.L. Gallo, Cathelicidin antimicrobial peptides block dendritic cell TLR4 activation and allergic contact sensitization, J. Immunol. 178 (3) (2007) 1829–1834. doi:10.4049/jimmunol.178.3.1829.

[93] J.M. Kahlenberg, M.J. Kaplan, Little peptide, big effects: the role of LL-37 in inflammation and autoimmune disease., J. Immunol. 191 (10) (2013) 4895–901. doi:10.4049/jimmunol.1302005.

[94] D. Ganguly, G. Chamilos, R. Lande, J. Gregorio, S. Meller, V. Facchinetti, B. Homey, F.J. Barrat, T. Zal, M. Gilliet, Self-RNA-antimicrobial peptide complexes activate human dendritic cells through TLR7 and TLR8, J Exp Med. 206 (9) (2009) 1983–1994. doi:10.1084/jem.20090480.

[95] M. Gilliet, R. Lande, Antimicrobial peptides and self-DNA in autoimmune skin inflammation, Curr. Opin. Immunol. 20 (4) (2008) 401–407. doi:10.1016/j.coi.2008.06.008.

[96] N.C. Filewod, J. Pistolic, R.E. Hancock, Low concentrations of LL-37 alter IL-8 production by keratinocytes and bronchial epithelial cells in response to proinflammatory stimuli, FEMS Immunol. Med. Microbiol. 56 (3) (2009) 233–240. doi:10.1111/j.1574-695X.2009.00571.x.

[97] D. Singh, R. Qi, J.L. Jordan, L. San Mateo, C.C. Kao, The human antimicrobial peptide LL-37, but not the mouse ortholog, mCRAMP, can stimulate signaling by poly(I:C) through a FPRL1-dependent pathway, J. Biol. Chem. 288 (12) (2013) 8258–8268. doi:10.1074/jbc.M112.440883.

[98] S. Sandgren, A. Wittrup, F. Cheng, M. Jönsson, E. Eklund, S. Busch, M. Belting, The Human Antimicrobial Peptide LL-37 Transfers Extracellular DNA Plasmid to the Nuclear Compartment of Mammalian Cells *via* Lipid Rafts and Proteoglycan-dependent Endocytosis, J. Biol. Chem. 279 (17) (2004) 17951–17956. doi:10.1074/jbc.M311440200.

[99] D. Singh, R. Vaughan, C.C. Kao, LL-37 peptide enhancement of signal transduction by toll-like receptor 3 is regulated by pH identification of a peptide antagonist of LL-37, J. Biol. Chem. 289 (40) (2014) 27614–27624. doi:10.1074/jbc.M114.582973.

[100] Z. Oren, J.C. Lerman, G.H. Gudmundsson, B. Agerberth, Y. Shai, Structure and organization of the human antimicrobial peptide LL-37 in phospholipid membranes: relevance to the molecular basis for its non-cell-selective activity, Biochem. J. 341 (PT3) (1999) 501-513. doi:10.1042/bj3410501.

[101] R. Sood, Y. Domanov, M. Pietiäinen, V.P. Kontinen, P.K.J. Kinnunen, Binding of LL-37 to model biomembranes: insight into target vs host cell recognition, Biochim.Biophys.Acta 1778 (4) (2008) 983-996. doi:10.1016/j.bbamem.2007.11.016.

[102] X. Zhang, K. Oglecka, S. Sandgren, M. Belting, E.K. Esbjörner, B. Nordén, A. Gräslund, Dual functions of the human antimicrobial peptide LL-37- Target membrane perturbation and host cell cargo delivery, Biochim. Biophys. Acta – Biomembr. 1798 (12) (2010) 2201-2208. doi: 10.1016/j.bbam.2009.12.011.

[103] N.M. Rao, differential susceptibility of phosphatidylcholine small unilamellar vesicles to phospholipases A2, C and D in the presence of membrane active peptides, Biochem. Biophys. Res. Commun. 182 (2) (1992) 682-688. doi:10.1016/0006-291X(92)91786-P.

[104] R. Bucki, J.J. Pastore, P. Randhawa, R. Vegners, D.J. Weiner, P.A. Janmey, Antibacterial activities of rhodamine B-conjugated gelsolin-derived peptides compared to those of the antimicrobial peptides cathelicidin LL37, magainin II and melittin, Antimicrob. Agents Chemother. 48 (5) (2004) 1526-1533. doi:10.1128/AAC.48.5.1526-1533.2004.

[105] B. Ding, L. Soblosky, K. Nguyen, J. Geng, X. Yu, A. Ramamoorthy, Z. Chen, Physiologically-relevant modes of membrane interactions by the human antimicrobial peptide, LL-37, revealed by SFG experiments, Sci Rep. 3 (1854) (2013) 1-8. doi:10.1038/srep01854.

[106] G. Wang, B. Mishra, R.F. Epand, R.M. Epand, High-quality 3D structures shine light on antibacterial, anti-biofilm and antiviral activities of human cathelicidin LL-37 and its fragments, Biochim. Biophys. Acta - Biomembr. 1838 (9) (2014) 2160-2172. doi:10.1016/j.bbamem.2014.01.016.

[107] D. Xhindoli, S. Pacor, F. Guida, N. Antcheva, A. Tossi, Native oligomerization determines the mode of action and biological activities of human cathelicidin LL-37, Biochem J. 457 (2) (2014) 263-275. doi:10.1042/BJ20131048.

[108] E. Sevcsik, G. Pabst, W. Richter, S. Danner, H. Amenitsch, K. Lohner, Interaction of LL-37 with model membrane systems of different complexity: influence of the lipid matrix, Biophys J. 94 (12) (2008) 4688-4699. doi:10.1529/biophysj.107123620.

[109] D.W. Hoskin, A. Ramamoorthy, Studies on anticancer activities of antimicrobial peptides, Biochim.Biophys.Acta 1778 (2) (2008) 357-375.doi:10.1016/j.bbamem.2007.11.008.

[110] K. Suzuki, T. Murakami, Z. Hu, H. Tamura, K. Kuwahara-Arai, T. Iba, I. Nagaoka, Human host defense cathelicidin peptide LL-37 enhances the lipopolysaccharide uptake by liver sinusoidal endothelial cells without cell activation, J. Immunol. 196 (3) (2016) 1338-1347. doi:10.1049/jimmunol.1403203.

[111] G.H. Gudmundsson, B. Agerberth, J. Odeberg, T. Bergman, B. Olsson, R. Salcedo, The human gene FALL39 and processing of the cathelin precursor to the antibacterial peptide LL-37 in granulocytes, Eur.J.Biochem 238 (2) (1996) 325-332. doi:10.1111/j.1432-1033.1996.0325z.x.

[112] S.X. Ren, J. Shen, A.S. Cheng, L. Lu, R.L. Chan, Z.J. Li, X.J. Wang, C.C. Wong, F.L. Zhang, S.S. Ng, F.L. Chan, F.K. Chan, J. Yu, J.J. Sung, W.K. Wu, C.H. Cho, FK-16 derived from the anticancer peptide LL-37 induces caspase-independent apoptosis and autophagic cell death in colon cancer cells, PLoS One. 8 (5) (2013) 1–9. doi:10.1371/journal.pone.0063641.

[113] H.J. Park, D.H. Cho, H.J. Kim, J.Y. Lee, B.K. Cho, S.I. Bang, S.Y. Song, K. Yamasaki, A. Di Nardo, R.L. Gallo, Collagen synthesis is suppressed in dermal fibroblasts by the human antimicrobial peptide LL-37, J. Invest. Dermatol. 129 (4) (2009) 843–850. doi:10.1038/jid.2008.320.

[114] Y.E. Lau, A. Rozek, M.G. Scott, D.L. Goosney, D.J. Davidson, R.E.W. Hancock, Interaction and Cellular Localization of the Human Host Defense Peptide LL-37 with Interaction and Cellular Localization of the Human Host Defense Peptide LL-37 with Lung Epithelial Cells, Infect. Immun. 73 (1) (2005) 583–591. doi:10.1128/IAI.73.1.583-591.2005.

[115] V.K. Lishko, B. Moreno, N.P. Podolnikova, T.P. Ugarova, identification of human cathelicidin peptide LL-37 as a ligand for macrophage integrin αMβ2 (Mac-1, CD11b/CD18) that promotes phagocytosis by opsonizing bacteria, Res. Rep. Biochem. 6 (2016) 39-55. PMC5157691.

[116] J. Jia, Y. Zheng, W. Wang, Y. Shao, Z. Li, Q. Wang, H. Yan, Antimicrobial peptide LL-37 promotes YB-1 expression, and the viability, migration and invasion of malignant melanoma cells. Mol. Med. Rep. 15 (1) (2017) 240-248. doi: 10.3892/mmr.2016.5978.

[117] M. Muñoz, M. Craske, P. Severino, T.M. de Lima, P. Labhart, R. Chammas, I.T. Velasco, M.C.C. Machado, B. Egan, H.I. Nakaya, F.P. da Silva, Antimicrobial peptide LL-37 participates in the transcriptional regulation of melanoma cells, J. Cancer. 7 (15) (2016) 2341-2345. doi: 10.7150/jca.16947.

Chapter IV

Gaining insight into the mechanism of action of the human cathelicidin peptide LL-37.

Abstract

The human cathelicidin peptide LL-37 plays a vital role in the innate and adaptive immune system. In addition to its non-specific membranolytic effect against a broad range of bacteria, LL-37 activates host cells through specific molecular interactions. Numerous studies report on the interaction of LL-37 with various structurally unrelated cell surface receptors, but the mechanisms underlying this activation are not well understood. A growing number of researchers suggest that LL-37 induces host cell responses by first binding to the plasma membrane. In this position, LL-37 can modulate cellular activities by inducing allosteric changes of receptors or affecting the motility of receptor complex components. Other studies suggest that LL-37 has membrane-penetrating properties and interacts with specific intracellular targets. Because LL-37 does not always appear to act through the same mode of action, we used an assay based on cellular impedance (EIS) to study LL-37 activity. EIS is a non-specific technique which captures the total integrated cellular response regardless of the intracellular signal transduction cascade that is activated. Based on the impedance response of cultured cell lines to LL-37, hypotheses concerning the mechanism of action of LL-37 were formulated and tested using a collection of pharmacological agents. With this strategy, we aimed to obtain a better understanding of the different mechanisms by which LL-37 modulates cellular activity or elucidate previously unknown modes of action on various cultured cell lines. Given the evolving role of LL-37 in several autoimmune diseases, a detailed understanding of the effect of LL-37 on different cell types is of great value.

4.1 Introduction

The human cathelicidin peptide LL-37 was first discovered as an AMP which participates in the innate immune system to combat invasive microbial infection [1,2]. Several years later, it became apparent that LL-37 also exerts chemotactic, immunostimulatory, and immunomodulatory effects [3]. Further exploration of the role of the peptide revealed that LL-37 is involved in crucial cellular processes such as wound healing, angiogenesis, and apoptosis [2,3,4,5]. In tumor biology, LL-37 participates in the tumor suppressing immune surveillance system under normal circumstances. However, dysregulation of LL-37 expression contributes to the development of cancer through the stimulation of proliferation, migration, and angiogenesis [2,3,6].

The pleiotropic effects of LL-37 can be explained by the ability of LL-37 to (in)directly activate various structurally unrelated cell surface receptors and/or intracellular targets in a wide variety of cell types [2,5,7]. At least 9 receptors have been documented to mediate some of the functional effects of LL-37 and novel molecular targets are continuously emerging [2,5]. The result is a large number of publications, reporting on either a receptor and/or components of the signaling transduction pathway (a more complete overview is provided in chapter 3).

The interactions of LL-37 with host cells are cell type-, context-, and concentration-dependent [2,8]. Second messenger assays such as fluorescence-based calcium assays are often used to study the effect of LL-37 on cultured cell lines. Measurement of the cytosolic calcium concentration following compound treatment is considered as a benchmark approach to the pharmacological characterization of receptors and compounds [9]. Because many effects of LL-37 are established through the release of intracellular calcium, calcium mobilization assays are commonly used to monitor the activity of LL-37 in cultured cell lines [2,3,5].

Second messenger assays such as fluorometric calcium mobilization assays have several limitations, as they only monitor a limited part of a signal transduction pathway, often at a single or a few timepoints, in addition to requiring labels. Furthermore, several assays with different sensitivities and dynamic ranges need to be combined in order to ‘reconstruct’ the complete cellular response to LL-37. This increases the cost, complexity, and duration of experiments. In order to overcome these challenges, a more aspecific method is required that captures the global signaling profile of LL-37 in a single assay.

In the present study, we use a real-time and label-free assay based on cellular impedance (EIS) to capture the overall cellular response to LL-37. EIS measures changes in the impedance of a voltage applied to a cell culture. Since impedance changes correlate with morphological changes occurring in

the cells, EIS can be used to monitor a variety of cellular processes, including receptor signaling, cell proliferation, cell adhesion, endothelial cell barrier function, and cytotoxicity [10-14]. Thanks to the non-specific nature of the technique, EIS allows for the measurement of a global cellular response in a fast, continuous, and label-free manner. Additionally, the technique is compatible with 96-well plates, thereby fitting in a high-throughput strategy and enabling researchers to screen a large number of cell types for their ability to respond to a test compound [10,11].

Kammermann *et al*. showed that impedance responses are characteristic for the receptor and activated intracellular pathway [12]. In agreement with this study, Stallaert *et al.* demonstrated that impedance responses are predictive of the signaling profiles of β-adrenergic ligands previously shown to display ligand-biased signaling [10]. Ciambrone *et al*. as well as Peters *et al*. evaluated ligand-induced impedance responses mediated by the three major G proteins ($G\alpha_s$, $G\alpha_i$ and $G\alpha_q$) within and across various cultured cell lines and demonstrated pathway-distinguishing capacity [13,14]. Even though both studies indicated that further research is required in regards to distinguishing subtle response patterns across different cell lines or converging signaling pathways, all 4 aforementioned studies suggest that impedance measurements can provide high content information about the underlying mode of action of a test compound. This is of particular interest to the study of LL-37, because the precise molecular mechanisms by which LL-37 exerts its effect on host cells are incompletely understood. Based on the impedance response generated by EIS, hypotheses can be devised and tested in order to elucidate the mechanism of action of LL-37 on cultured cell lines. Possible leads are then explored using a collection of broad-spectrum and receptor-selective antagonists. Notably, performing real-time impedance measurements enables the detection of possible short-term (*e.g.* receptor activation) as well as long-term (*e.g.* cytotoxicity) effects of LL-37 on a particular cell type.

We administered LL-37 to 6 commonly used cultured cell lines and recorded their impedance-based response profile. Next to confirming known activity on a number of cell lines, EIS enabled the detection of novel activity on HEK293T cells. Subsequent dissection of the impedance response led to the identification of a calcium-mediated signaling event immediately after LL-37 treatment. In addition, a long-term effect of LL-37 was observed which could be related to the pore-forming activity of LL-37, causing cell swelling followed by membrane breakdown and leakage of intracellular components. This cytotoxic effect was completely inhibited by preincubating HEK293T cells with suramin or suramin analogues.

Each cell line included in this study displayed a unique impedance response to LL-37 which may reflect different signaling events induced by LL-37. For example, a distinctly different impedance

response of A549 lung carcinoma cells to LL-37 was observed in comparison to the impedance response of HEK293T cells. Further experiments using pharmacological agents indicated that endocytic pathways play a role in the mode of action of LL-37 on A549 cells. These results imply that different cell types can respond in a different way to LL-37, as suggested by others [2-7].

Finally, we used EIS to further characterize the pleiotropic effects of LL-37. Wu *et al*. recently proposed a novel mechanism of action of LL-37 involving the inclusion of the human chemokine receptor CXCR4 into LRs [15]. Incorporation of CXCR4 into membrane LRs enhanced signaling in response to low doses of CXCR4's ligand stromal-derived factor-1 (SDF-1). We discovered that LL-37-primed U87 glioblastoma cells which were stably transfected with CXCR4 evoked a stronger impedance response to SDF-1 than unprimed cells. Moreover, this priming effect could be completely abrogated using cholesterol-depleting agents causing the disruption of LRs. Taken together, our results suggest EIS is a suitable technique to monitor the activity of LL-37 on various cultured cell lines.

4.2 Material and Methods

Reagents

The synthetic peptide LL-37 (NH_2-LLGDFFRKSKEKIGKEFKRIVQRIKDFLRNLVPRTES-$CONH_2$), the LL-37-derived peptide KI-26 (NH_2-KIGKEFKRIVQRIKDFLRNLVPRTES-$CONH_2$), and P318, a 26-amino-acid truncated form of mCRAMP (NH_2-KIGEKLKKIGQKIKNFFQKLVPQPEQ-$CONH_2$), were synthesized by Thermo Scientific (Ulm, Germany) at a purity of at least 95% as determined by liquid chromatography and MS. CRAMP (NH_2-GLLRKGGEKIGEKLKKIGQKIKNFFQKLVPQPEQ-$CONH_2$) was acquired from Innovagen (Lund, Sweden), and SDF-1α was purchased from Peprotech (Princeton, NJ, USA). Protease-activated receptor 1 activating peptide (PAR1-AP), forskolin (FSK), carbachol, HBSS, PBS, DMEM, FBS, GS, penicillin/streptomycin, puromycin, geneticin, 3-isobutyl-1-methylxanthine (IBMX), Krebs-Ringer bicarbonate glucose buffer (KRBG), fibronectin, diamidino-2-phenylindole (DAPI), paraformaldehyde (PFA), and trypsin-EDTA (T/E) were purchased from Sigma Aldrich (St.-Louis, MO, USA).

The following antagonists were acquired from the same manufacturer: pertussis toxin (PTX), U73122, curcumin, GM6001, methyl-β-cyclodextrin (MBCD), (2-hydroxypropyl)-β-cyclodextrin (HBCD), monodansylcadaverine (MDC), dynasore hydrate, 1,2-Bis(2-aminophenoxy)ethane-N,N,N',N'-tetraacetic acid acetoxymethyl ester (BAPTA-AM), lanthanum (III) chloride ($LaCl_3$), 8-(Diethylamino)octyl-3,4,5-trimethoxybenzoate (TMB-8), suramin, pyridoxalphosphate-6-azophenyl-2'-4'-disulfonic acid (PPADS), NF449, erlotinib hydrochloride, 5-(N-ethyl-N-isopropyl)amiloride (EIPA), paclitaxel, cycloheximide, BAY 11-7082, filipin III, cytochalasin B, brefeldin A, and z-VAD-fmk. Other pharmacological agents such as A-438079, WKYMVm, WRW4, MMK-1, SB225002, SB265610, G protein antagonist 2 (GPant-2), gallein, genistein, 2-aminoethoxydiphenyl borate (2-APB), dantrolene, tetraethyl ammonium (TEA), 10-[4'-(*N,N*-diethylamino)butyl]-2-chlorophenoxazine (10-DEBC), and AY9944 were purchased from Tocris Bioscience (Bristol, UK). The antagonist tyrphostin AG-1478 (Tyr AG-1478) was obtained from MedChem Express (NJ, USA) whereas AG-1024 and CP-724714 were purchased from Selleckchem (Munich, Germany). NF-157 and STA-21 were obtained from Santa Cruz Biotechnology (Dallas, Texas, USA). Heparinase and heparitinase were purchased from Seikagaku Corp. (Tokyo, Japan).

All the peptides, antagonists, and toxins used in the experiments along with their effects in cell signaling are listed at the beginning of this manuscript. Extra information was obtained from the product information sheet provided by the manufacturer.

Cell cultures

Human embryonic kidney 293T (HEK293T), A549 human lung carcinoma, RAW264.7 mouse leukemic monocyte macrophage, MRC-5 human fetal lung fibroblasts, B16 4A5 mouse melanoma, and A431 human squamous carcinoma cells were purchased from ECACC (Porton Down, Wiltshire, UK). U-87 human glioblastoma cells which were stably transfected with CXCR4 were a gift from the Rega Institute for Medical Research (Prof. D. Schols, KU Leuven). HEK293T, A549, RAW264.7, MRC-5, B16, and A431 cells were propagated at 37°C in a humidified atmosphere at 5% CO_2 in DMEM plus FBS (10 %), and 100 units penicillin/0.1 mg streptomycin. U87 (CXCR4+) cells were cultured in DMEM complemented with FBS (10%), puromycin (1 mg/ml), and geneticin (600 µg/ml). All cells were freshly thawed and underwent a limited number of passages. To collect cells, cells were first washed with PBS and then removed from the cell culture flask with T/E (0.25 % trypsin, 0.02% EDTA).

Electrical impedance spectroscopy

Impedance measurements were performed on a proprietary EIS device (CellSine) using 96-well electronic microtiter plates from ACEA Biosciences Inc. (San Diego, CA, USA). For time-dependent cell response profiling, 50 µL of culture medium was added to each well to obtain background readings. Next, 50 µL of a cell suspension was transferred to the 96-well plate (40000 cells/well for HEK293T, A549, RAW264.7, MRC-5, B16 cells, and 20000 cells/well for U87 (CXCR4+) cells), followed by overnight incubation at 37°C in a humidified atmosphere at 5% CO_2. The next day, the culture medium was replaced by medium without FBS, and 3 hours after this medium change, 10 µL of peptide solution was added. Depending on the type of experiment, antagonists were added one hour prior to peptide administration. Note that incubation times may vary depending on antagonist used. The addition of compounds was done manually inside the incubator via a modified 96-well microtiter plate cover that allows faster and more reproducible compound addition. Cells were monitored with a temporal resolution of 8 seconds per well. At the start of the experiment, each well was measured once before peptides were added. Raw impedance data were converted into a dimensionless parameter called cell index (CI), which reflects the relative change in measured electrical impedance to represent cell status [16]. The impedance is measured at 3 frequencies (10, 25, and 50 kHz). Data visualization was done by plotting the difference of the CI value at timepoint x with the first CI measurement ($\Delta CI = CI_{[x]} - CI_{[1]}$).

$$CI = \max_{i=1,\ldots,N} \left(\frac{R_{cell}(f_i)}{R_0(f_i)} - 1 \right)$$

N = 3 for each utilized frequency (f_i).
R_{cell} = real part of the impedance behavior in presence of cells
R_0 = real part of impedance behavior during background measurement

Fluorometric calcium flux assay

Intracellular calcium levels were determined using the Fluo-Forte calcium assay kit (Enzo Life Sciences, NY, USA) as described by the manufacturer. Cells were detached with T/E and subsequently seeded in 96-well plates at a density between 20000 to 60000 cells per well. After overnight incubation at 37°C, the cells were loaded with the fluorogenic calcium binding dye FluoForte for 45 minutes at 37°C and then incubated for 15 minutes at room temperature prior to assay. A 25-µl aliquot of various concentrations of the peptides, diluted in HBSS, was transferred from the compound plate to the 96-well plate containing the cells. The fluorophore was excited at 490 nm. The calcium response was monitored at 525 nm for two minutes using a FLEXStation II (Molecular Devices, New Milton, Hampshire, UK) and data were analyzed using the Softmax Pro software (Molecular Devices, New Milton, Hampshire, UK).

cAMP competitive immunoassay

The CatchPoint cAMP fluorescence assay (Molecular Devices, Sunnyvale, CA, USA) was used according to the manufacturer's instructions. Briefly, cells were seeded in standard 96-well plates and incubated overnight under standard conditions (37°C, 5% CO_2). The following day, cells were washed with KRBG buffer and then incubated with stimulation buffer supplemented with the phosphodiesterase antagonist IBMX. Next, peptides and control samples were added to the cells and allowed to incubate for twenty minutes at 37°C. After a lysis step, the resulting homogenate and calibrator series were transferred to a 96-well plate pre-coated with goat anti-rabbit immunoglobulin G. Hereafter, the rabbit anti-cAMP antibody and horse radish peroxidase-cAMP conjugate were added and allowed to incubate for two hours at room temperature. Finally, the fluorescent substrate was added and the resulting signal monitored by the FLEXstation II device (Molecular devices, New Milton, Hampshire, UK).

Human RTK phosphorylation array

The human phosphorylation antibody array C1 was purchased from Ray Biotech (Norcross, Georgia, USA) and used according to the manufacturer's instructions. This kit allows for the semi-quantitative detection of 71 phosphorylated human RTKs in cell and tissue lysates. HEK293T cells were cultured in T25 cell culture flasks until they were approximately 80% confluent. On the day of the experiment, the culture medium was replaced with serum-free culture medium for three hours. Cells were incubated with HBSS or with LL-37 at a concentration of 5 µM for one, five, or ten minutes. The culture medium was then removed and cells were rinsed twice with ice-cold PBS and solubilized with lysis buffer containing protease inhibitor cocktail and phosphatase inhibitor cocktail set II. The lysates

were then transferred to Eppendorf tubes, and centrifuged (14000g for ten minutes). Next, the sample protein concentrations were determined using Qubit 2.0 fluorometer (ThermoFisher Scientific, Walthalm, MA, USA). After blocking the array membranes with blocking buffer for one hour, 400 µg of total protein was loaded onto each antibody-printed nitrocellulose membrane for 24 hours at 4°C. Longer incubations may help maximize spot signal intensities, but can also increase the background signal. The next day, HEK293T cells were rinsed with washing buffer and 1 ml of biotinylated antibody cocktail was added to each membrane for two hours at room temperature. Membranes were then washed and incubated with 2 ml of HRP-streptavidin for two hours at 4°C. Finally, 500 µL of detection reagent was added to each membrane for two minutes at room temperature, after which RTK spots were visualized using the ChemiDoc MP imager (Bio-Rad, Hercules, California, USA).

Confocal imaging of EGFR

HEK293T and A431 cells were seeded in 8-well Millicell EZ slides (Merck Millipore, Darmstadt, Germany) at a density of 20000 cells per well and incubated overnight under standard growth conditions (37°C, 5% CO_2). The next day, cells were washed with HBSS and fixed with 4% PFA for twenty minutes at room temperature. After another washing step, slides were incubated with 10% goat serum blocking solution for one hour to prevent non-specific staining. Finally, cells were stained with 10 µg/ml of anti-human EGFR (clone AY13) Alexa Fluor 488 (Biolegend, San Diego, CA, USA) which has a maximum emission of 519 nm when it is excited at 488 nm. Nuclei were counterstained with DAPI (1:5000). Images were captured by a confocal imaging system using a 40X objective.

RNA-extraction and RNA-Seq

RNA extraction was performed with one million HEK293T cells using the RNeasy mini kit from Qiagen (Hilden, Germany) following the manufacturer's instructions. The sequencing was performed by the Genomics Core UZ Leuven using Illumina HiSeq system. For a detailed description of the workflow, the reader is referred to the material and methods section of chapter seven.

Statistical analysis

GraphPad Prism 5.1 (GraphPad software, La Jolla, CA, USA) was used to analyze raw data from EIS, calcium mobilization assays, cAMP measurements, human phospho-RTK array, and RNA-Seq. Note that the temporal resolution of EIS measurements was eight seconds per well. In contrast to commercially available EIS devices, our final temporal resolution was dependent on the number of wells. Unless stated otherwise, one example of a cell's impedance response to LL-37 of at least two independent experiments was displayed. Raw data from calcium and cAMP assays were analyzed

using Student's t-tests in order to determine whether there was a statistically significant difference between the means of experimental groups, unless stated otherwise. In most cases, experiments were performed in triplicate and repeated twice. Hence six datapoints were obtained to reflect the effect of a peptide on a cell line. Error bars represent the standard error of mean (SEM).

4.3 Results

4.3.1 The effect of LL-37 on cultured cell lines as measured by EIS

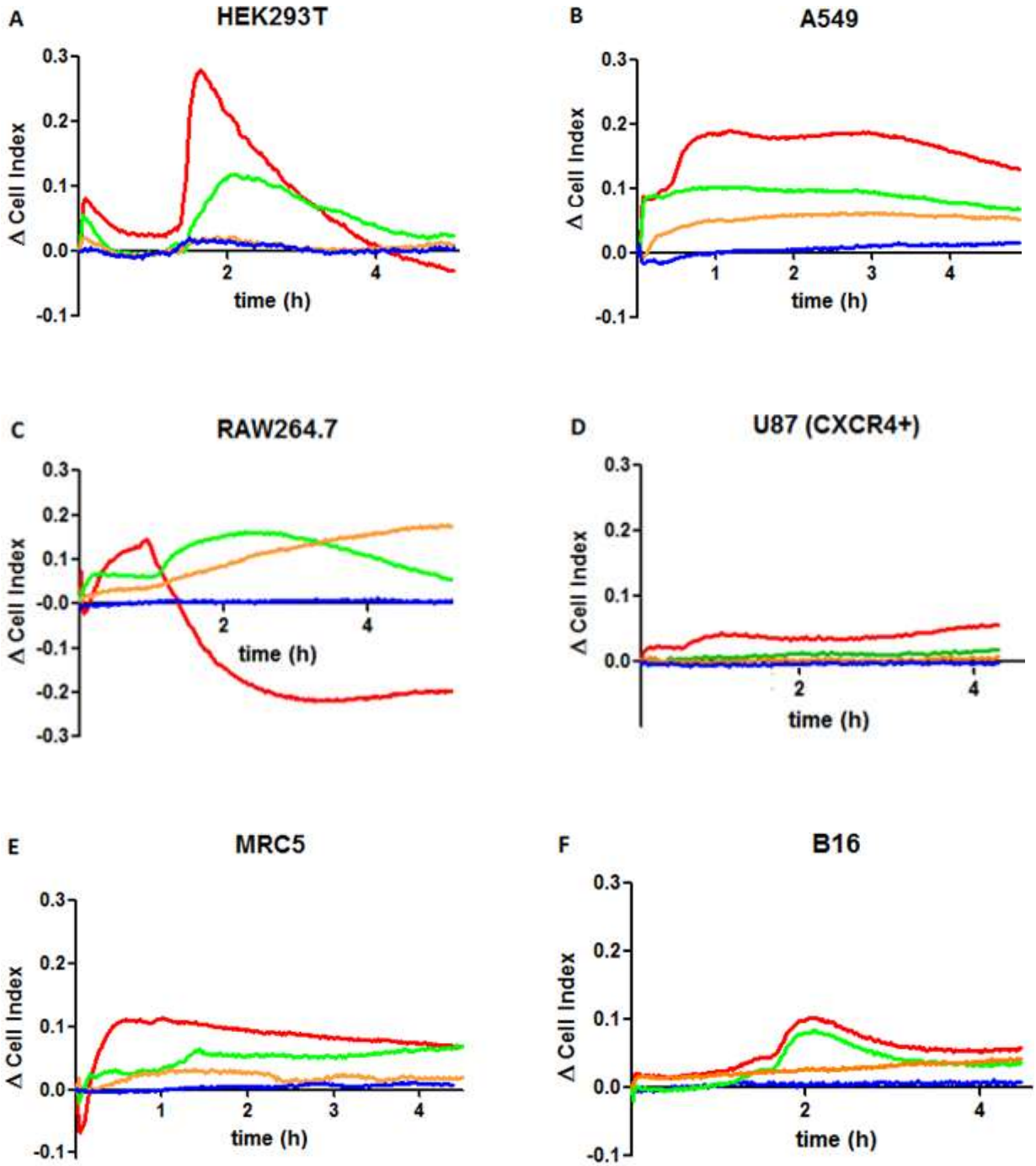

Fig.4.1. Plot of ΔCI over time (hours), reflecting the effect of 0.5 µM (orange), 1.5 µM (green), and 5 µM (red) of LL-37 on various mammalian cell lines. HBSS (blue) was used as a negative control. Graphs A to F respectively show the cell status of HEK293T, A549, RAW264.7, U87 (CXCR4+), MRC-5, and B16 cells. Experiments were repeated three times and one example of the impedance response to LL-37 is displayed.

Impedance measurements were made in various cultured cell lines of human (HEK293T, A549, MRC-5, U87 (CXCR4+) cells) and mouse (RAW264.7, B16 cells) origin following treatment with physiologically relevant concentrations (0.5, 1.5, and 5 µM) of LL-37 (figure 4.1). To see whether LL-

37 was able to evoke a response in different cell types, a diverse set of cultured cell lines was used, including a macrophage cell line (RAW264.7), a fibroblast cell line derived from normal lung tissue (MRC-5), a fibroblast-like melanoma cell line (B16), an epithelial cell line derived from lung carcinoma (A549), as well as the commonly used HEK293T cell line. Note that, despite its widespread use in cell biology studies, the authentic origin of HEK293T cells is still unknown [17]. In addition, U87 glioblastoma cells stably transfected with the human chemokine receptor CXCR4 were used for a particular purpose (see section 4.3.6).

A parameter called CI is used to reflect cell status [16]. When cells attach onto the electrodes, the CI values increase. For the same number of cells, morphological changes induced by test compounds lead to changes in cell-cell or cell-electrode contacts which will lead to changes in CI.

Other studies made impedance measurements for 1 or 2 hours to assess receptor-mediated ligand activity on cultured cell lines [11-14]. We recorded LL-37-induced changes in impedance over a longer period of time (at least 4 hours) in order to detect potential longer term effects of LL-37 as well.

As depicted in figure 4.1 , a reproducible effect of LL-37 was detected on HEK293T, A549, RAW264.7, MRC-5, and B16 cells. Note that each impedance profile contains complex real-time information on the mechanism of action by which LL-37 induces a cellular response. In U87 (CXCR4+) glioblastoma cells, only a small effect of LL-37 was observed at a concentration of 5 µM (figure 4.1-D).

Treatment of HEK293T cells with 5 µM of LL-37 led to an immediate increase in impedance within 10 minutes post-stimulation, followed by a decrease in impedance (figure 4.1-A). A second maximum was achieved approximately 90 minutes after LL-37 administration, upon which the ΔCI values decreased again towards the baseline level. LL-37 most likely activated HEK293T cells in a dose-dependent manner, since a relatively smaller impedance response of HEK293T cells to 1.5 µM of LL-37 was observed. At a lower concentration of LL-37 (0.5 µM), no impedance response of HEK293T cells to LL-37 was observed.

A549 cells were also exposed to a dilution series of LL-37 and a dose-dependent relationship was detected (figure 4.1-B). LL-37 induced a rapid increase in impedance, followed by a second increase until (signs of) a plateau was achieved. Note that the impedance response of A549 cells to various concentrations of LL-37 differs from the impedance response of HEK293T cells, suggesting that the mechanism of action of LL-37 is cell-type dependent.

RAW264.7 cells strongly responded to LL-37 (figure 4.1-C). At a concentration of 5 µM, an immediate increase in impedance was followed by a sharp decrease in impedance. This may indicate that LL-37

negatively affects cell viability or proliferation. This impedance response profile was not observed when RAW264.7 cells were exposed to lower concentrations of LL-37. At a concentration of 1.5 µM, a maximum was achieved 2 hours post-addition, after which the impedance decreased again. Notably, the impedance gradually increased upon treatment with 0.5 µM of LL-37, suggesting that the response to LL-37 not only differs among cell types, but also over concentrations.

In MRC-5 cells, only a small response to lower concentrations (0.5 and 1.5 µM) of LL-37 was observed, whereas a clear impedance response to LL-37 was detected at a concentration of 5 µM (figure 4.1-E).

Stimulation of B16 4A5 cells with LL-37 at concentrations of 1.5 and 5 µM led to a positive impedance response immediately after addition (figure 4.1-F). The maximum activity occurred at 2 hours post-stimulation, upon which the impedance decreased again. At a concentration of 0.5 µM of LL-37, the impedance gradually increased upon LL-37 treatment.

In the following sections, experiments were conducted to determine whether the changes in impedance induced by LL-37 were reflective of its mechanism of action on cultured cell lines.

4.3.2 LL-37 dose-dependently increases intracellular calcium levels

Second messengers are one of the initiating components of intracellular signaling cascades. In order to gain more insight into the mode of action of LL-37, identifying second messengers that transduce the signal inside the cell is of great value. A fluorometric calcium mobilization assay was used to test whether calcium ions are involved in the signal transduction pathway activated by LL-37 (figure 4.2). To allow for a more comprehensive comparison with data displayed in figure 4.1, the same cell lines were used in this set of experiments.

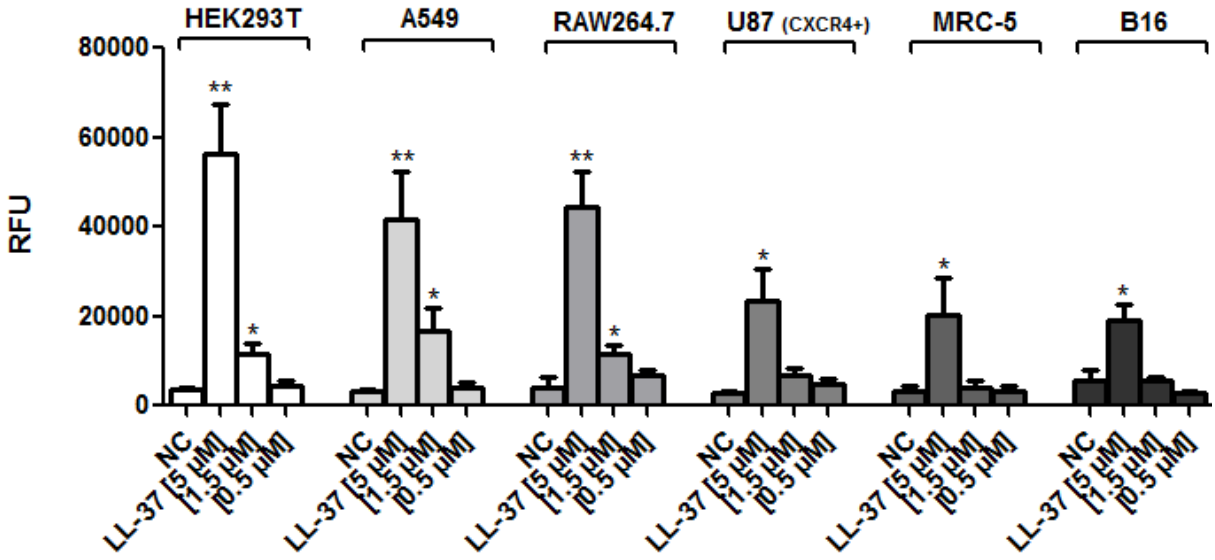

Fig.4.2. Graphs representing data from a calcium mobilization assay, plotted as relative fluorescence units (RFU, maximum peak height) values per concentration of LL-37. At a concentration of 5 µM, LL-37 induced calcium mobilization in HEK293T, A549, RAW264.7, U87 (CXCR4+), MRC-5, and B16 cells. Experiments were performed in triplicate and repeated twice, hence the mean of 6 datapoints was plotted (data are mean ± SEM). Significance levels are indicated by asterisks which represent p-values from Student's t-test: *, $p < 0.05$ and **, $p < 0.005$ when compared with the negative buffer control (NC).

At a concentration of 5 µM, LL-37 induced calcium release in all cell types tested. A significant calcium response of HEK293T (p-value from Student's t-test when comparing calcium response to LL-37 with the negative buffer control is 0.01), A549 (p-value = 0.02), and RAW264.7 cells (p-value = 0.04) to 1.5 µM of LL-37 was also detected. At a concentration of 0.5 µM, LL-37 did not increase intracellular calcium levels.

Intracellular cAMP levels following LL-37 (0.5 – 5 µM) treatment were also measured in the same set of cell lines using a competitive cAMP immunoassay, but increased cAMP production was not detected. The results of cAMP measurements in HEK293T cells are displayed in figure 4.3-B. The cAMP-activator forskolin (FSK) was used as a positive control.

4.3.3 Unraveling the short-term effect of LL-37 on HEK293T cells

4.3.3.1 Deciphering the calcium network

EIS measurements revealed that LL-37 (5 µM) exerted a short- and long-term effect in HEK293T cells (fig. 4.1-A). Subsequent fluorescence-based calcium assays showed that the short-term response involved the release of intracellular calcium (fig. 4.2). In addition, no cAMP production was measured upon exposure to LL-37 using a competitive cAMP immunoassay (figure 4.3-B). In a next set of experiments, the calcium response of HEK293T cells to LL-37 was examined in more detail.

Figure 4.3-A shows the calcium response of HEK293T cells to a dilution series (0.5 – 10 µM) of LL-37. Immediately after LL-37 treatment, a dose-dependent transient increase in cytoplasmic calcium levels in HEK293T cells was observed. The maximum fluorescence signal was reached approximately 25 seconds post-stimulation, upon which the fluorescence emission intensity decreased again. It is possible that the declining phase correlates with the cytosolic calcium buffering capacity of mitochondria.

Note that a sustained calcium response rather than a transient calcium response was observed when HEK293T cells were stimulated with higher doses (≥ 20 µM) of LL-37 (figure 4.3-C). This could be due to the pore-forming activity of LL-37, which causes dye leakage into the extracellular environment. To validate this hypothesis, HEK293T cells were microscopically inspected to check for signs of deterioration (granularity, cell detachment) 4 hours after exposure to a toxic concentration (50 µM) of LL-37 (figure 4.3-C). As depicted in figure 4.3-C, drastic morphological changes were noticed which were likely caused by the membrane-damaging effect of LL-37.

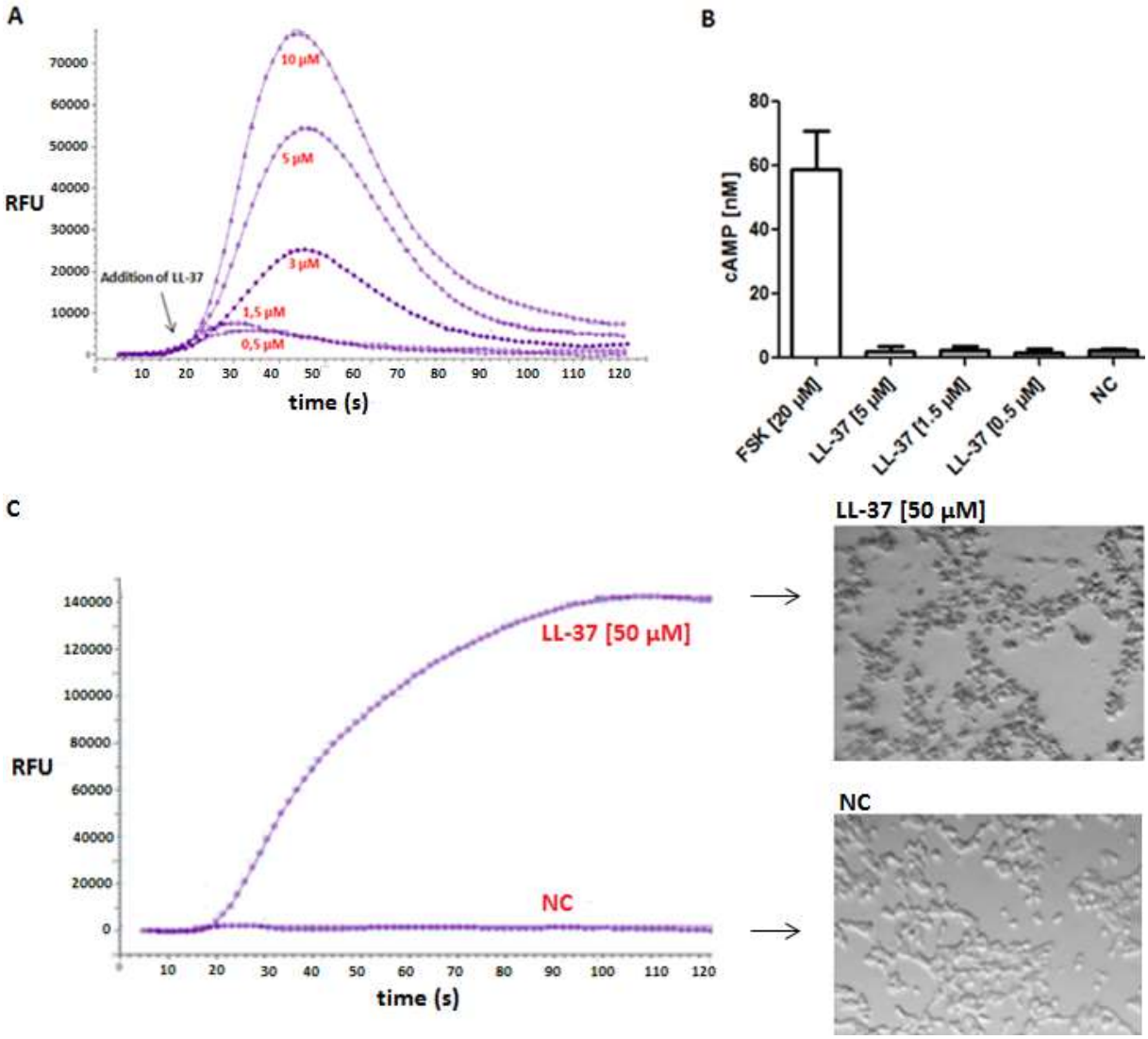

Fig.4.3. Graph A shows an example of calcium-based fluorescence in HEK293T cells after addition of 0.5 µM (◊), 1,5 µM (□), 3 µM (•), 5 µM (o), or 10 µM (Δ) of LL-37. An arbitrary unitless RFU value of 3000 was used as a cut-off value to judge if intracellular calcium was released. Graph B displays the cAMP production in nanomolar concentration. Forskolin (FSK) was used as a positive control. Note that untreated HEK293T cells (NC) contain basal levels of cAMP. Error bars represent SEM (*N*=3). Graph C shows the calcium response to a toxic concentration (50 µM) of LL-37, along with a phenotypic view of the cells after peptide addition (pictures taken 4 hours after exposure to 50 µM of LL-37. Control cells were treated with HBSS buffer).

Transient increases in cytosolic calcium concentration can be caused by endogenous calcium release from intracellular stores and/or influx of extracellular calcium ions across the plasma membrane [18]. Experiments to distinguish between these two general mechanisms were conducted. HEK293T cells were preincubated with 2-APB, a membrane-permeable inhibitor of IP_3R-induced calcium release from intracellular stores (IC_{50} = 42 µM) [18]. As depicted in figure 4.4-B, we observed a significant inhibitory effect of 2-APB (≥ 25 µM) on the calcium response of HEK293T cells to LL-37. In addition, 2-APB inhibited the initial transient impedance response of HEK293T cells to 5 µM of LL-37 (figure 4.4-A). The second impedance response to LL-37, which occurred approximately 1 hour after LL-37

treatment, was not completely inhibited by 2-APB. However, preincubating HEK293T cells with 100 µM of 2-APB partially blocked (or delayed) the long-term effect of LL-37.

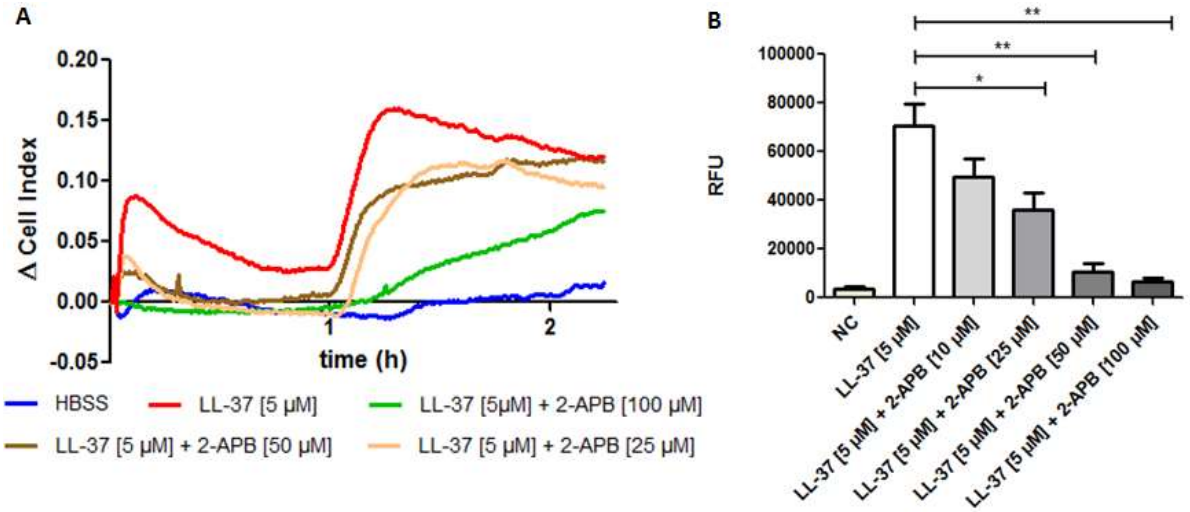

Fig.4.4. Graph A shows the effect of the membrane-permeable IP_3R-antagonist 2-APB on the impedance response of HEK293T cells to LL-37 (5 µM). Graph B shows that 2-APB (> 25 µM) is capable of blocking the calcium response of HEK293T cells to LL-37. HBSS was used as a negative control. Significance levels are represented by asterisks: * indicate p-value < 0.05, ** indicate p-value < 0.005 as analyzed by the Student's t-test (*N*=6; data are mean ± SEM).

Notably, 2-APB might have a dual mode of action as it also exerts a concentration-dependent effect on store-operated channels (SOCs) [19]. Because of this dual mechanism of action, HEK293T cells were preincubated with varying concentrations of $LaCl_3$. Lanthanides are widely used as inhibitors for calcium-permeable SOCs [20]. $LaCl_3$ was unable to inhibit the short-term impedance or calcium response to LL-37 (figures 4.5-A and B). Only a small effect on the long-term impedance response of HEK293T cells to LL-37 was observed when cells were preincubated with 10 or 30 µM of $LaCl_3$.

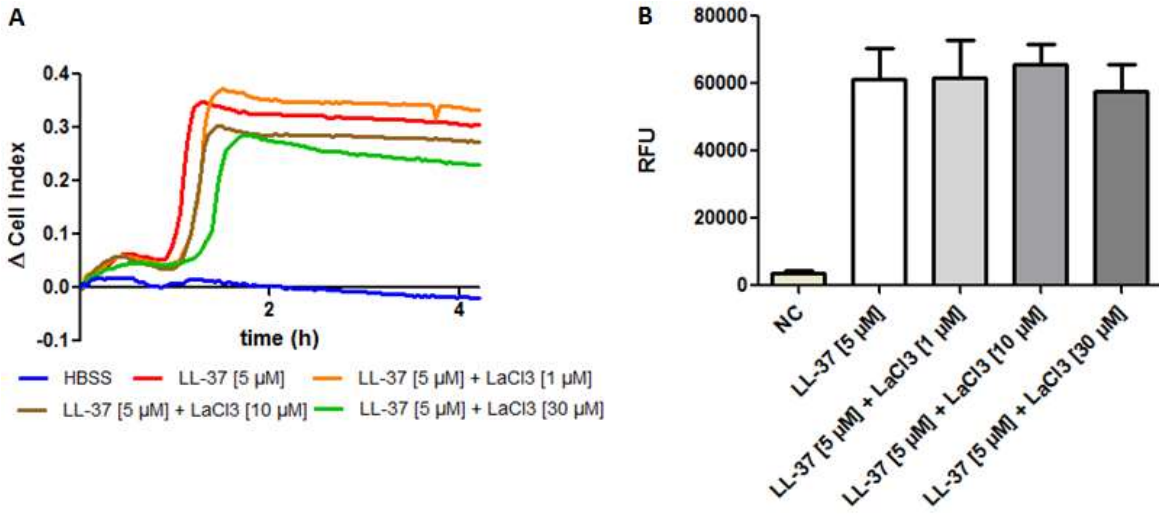

Fig.4.5. Graphs showing the effect of lanthanides on the impedance (**A**) and calcium (**B**) response of HEK293T cells to LL-37. Lanthanides are commonly used SOC antagonists. $LaCl_3$ could not abrogate the effect induced by LL-37 (*N*=6; data are mean ± SEM).

To further clarify whether the intracellular calcium elevation induced by LL-37 was caused by an endogenous calcium release and/or an extracellular calcium influx, HEK293T cells were preincubated

with 2-APB in calcium-free medium to prevent the entry of extracellular calcium into the cells. These experiments do not exclude a potential role for extracellular calcium in the mode of action of LL-37 on HEK293T cells. However, if the intensity of the fluorescence signal decreases in a calcium-free situation, a contribution of calcium influx across the plasma membrane through calcium-permeable ion channels becomes more likely.

In the absence of extracellular calcium, LL-37 retained its ability to activate HEK293T cells through the rapid release of intracellular calcium (figure 4.6). HEK293T cells were pretreated with 50 µM of 2-APB and this completely blocked the calcium response evoked by LL-37 (p-value = 0.04). This suggests that IP_3R plays a role in the mode of action of LL-37 on HEK293T cells. Carbachol was used as a positive control since it is known to release calcium ions from intracellular stores [21].

Noteworthy, HEK293T cells were also preincubated with dantrolene (1-100 µM), a ryanodine receptor (RyR) calcium release channel inhibitor. RyRs are receptors used in releasing calcium from intracellular stores. No effect of dantrolene on the calcium response of HEK293T cells to LL-37 was observed, suggesting that RyRs are not involved in the molecular mechanism by which LL-37 induces a calcium response of HEK293T cells.

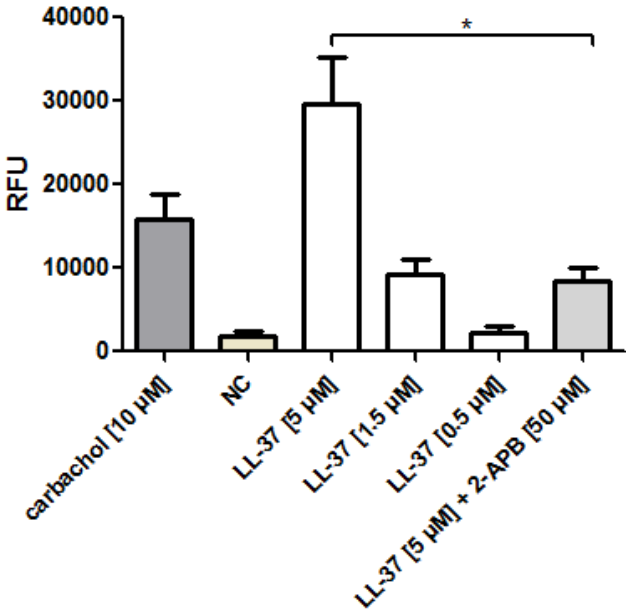

Fig.4.6. In a calcium-free situation, LL-37 elevated intracellular calcium concentrations in HEK293T cells. The calcium release from the ER was (at least partially) mediated by IP_3R. Experiments were performed in triplicate and repeated twice, hence the mean of 6 datapoints is displayed. Significance levels are represented by asterisks: * indicate p-value from Student's t-test < 0.05 (data are mean ± SEM). Carbachol was used as a positive control (*N*=3).

The primary mechanism by which cells release calcium ions from intracellular stores is via the PLC pathway. PLC hydrolyses PIP_2 into DAG and IP_3, which are important second messengers that regulate numerous cellular processes [3]. At a concentration of 10 µM, the PLC inhibitor U73122 partially partially inhibited the initial impedance response of HEK293T cells to LL-37, whereas the second

impedance response was not altered (figure 4.7-A). In agreement with this result, the calcium response of U73122 (10 and 20 µM)-treated HEK293T cells to LL-37 was partially inhibited relative to the calcium response of untreated HEK293T cells to LL-37 (p-values obtained from Student's t-tests on U73122-treated vs untreated cells are 0.052 (10µM) and 0.01 (20µM) respectively). These results point to a possible role for PLC in the mechanism of action of LL-37 (figure 4.7-B).

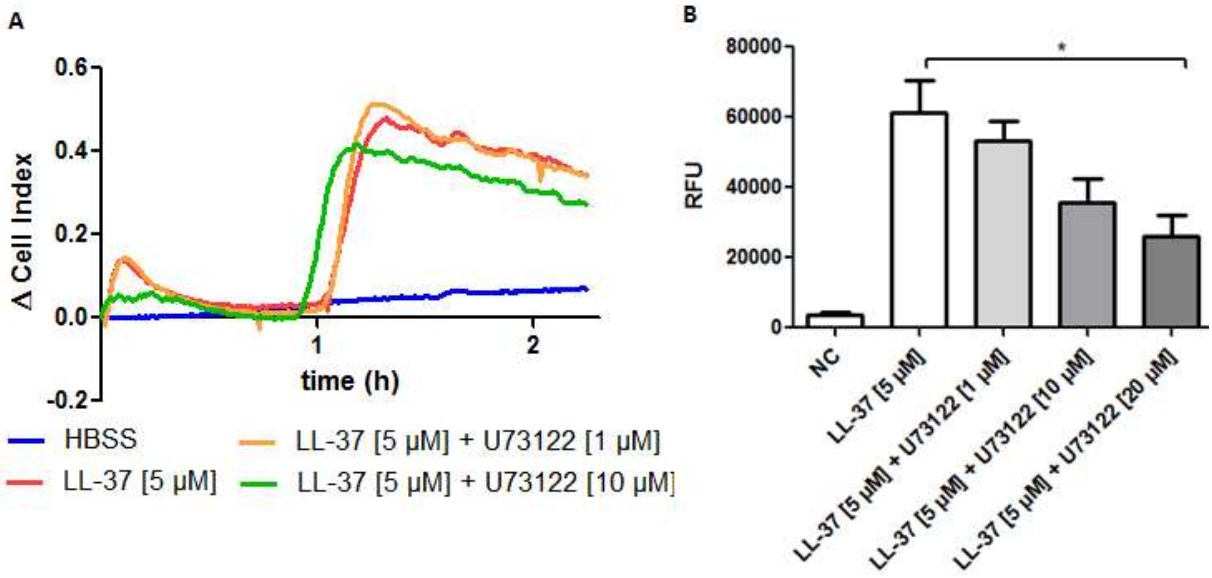

Fig.4.7. Data obtained with EIS (**A**) and calcium mobilization assay (**B**). Graph A depicts the impedance response of U73122-treated HEK293T cells to LL-37. U73122 is a commonly used small molecule for studying PLC signaling. Graph B shows the corresponding results as measured by a fluorometric calcium assay. U73122 (≥ 10 µM) partially decreased the calcium response to LL-37. Activation of PLC-mediated signaling pathways in non-excitable cells induces the release of endogenous calcium from intracellular stores. Significance levels are represented by asterisks: * indicate p-value < 0.05 (*N*=6; data are mean ± SEM).

4.3.3.2 Identifying the molecular target of LL-37

Several receptors have been proposed to mediate the multitude of functional effects of LL-37, including 4 GPCRs (FPR2, CXCR2, P2Y11R, MrgX2), 3 RTKs (IGF1R, EGFR, ErbB2), and 1 LGIC ($P2X_7$) [2,5]. In order to understand how LL-37 exerts its effect on HEK293T cells, it is of utmost importance to identify its cognate receptor. However, indirect mechanisms of action should also be considered, especially since evidence concerning the direct binding of LL-37 to cell surface receptors is scarce [2].

First, mRNA levels of candidate receptors for LL-37 in HEK293T cells were analyzed using RNA-Sequencing (RNA-Seq) (figure 4.8-C). Expression of FPR2, CXCR2, and MrgX2 were not detected. This is in agreement with microarray expression data provided by Atwood *et al* [22]. Furthermore, no endogenous expression of $P2X_7$ was detected. HEK293T cells expressed high mRNA levels of IGF1R, as well as (relatively little) mRNA of EGFR, ErbB2, and P2Y11R. For cost reasons, only 1 sample was sequenced and the total RNA counts per gene are displayed in figure 4.8-C. Note that the RNA-Seq read counts also depend on the length of the transcript. A long transcript will have more reads aligned to it compared to a shorter transcript of similar expression. Consequently, no strong

conclusions can be drawn from this exploratory study and each candidate receptor for LL-37 remained a potential target in later follow-up experiments to identify the cognate receptor for LL-37. However, IGF1R, EGFR, ErbB2, and P2Y11R are more likely candidates than others.

To investigate whether one of the purported cell surface receptors mediates the effect of LL-37 on HEK293T cells, a collection of broad-spectrum and receptor-selective inhibitors was used (figure 4.8-A-B). Differences in the effect of LL-37 in these experiments may deliver information whether or not a receptor is involved in the mode of action of LL-37.

Broad-spectrum GPCR inhibitors were applied to HEK293T cells to obtain an idea about the involved receptor family. Preincubating HEK293T cells with GPant2 or PTX did not lead to an altered calcium response to LL-37. PTX is toxin that inactivates $G\alpha_i$-coupled receptors by preventing the phosphorylation of the $G\alpha_i$-GDP complex [23]. FPR2 and CXCR2 are the only $G\alpha_i$-coupled GPCRs associated with biological activity of LL-37. However, the calcium response of HEK293T cells to LL-37 was not inhibited by FPR2- or CXCR2-selective antagonists (WRW4, SB225002, and SB265610 respectively), suggesting that these receptors are not involved in the recognition of the peptide. This observation is in agreement with our mRNA expression data, since we were unable to detect mRNA expression of FPR2 and CXCR2.

Many effects of LL-37 are mediated via the activation of FPR2 [2,3]. To exclude the possibility that FPR2 is the receptor for LL-37, cross-desensitization experiments were performed using two selective FPR2-agonists (WKYMVm and MMK 1). As displayed in figure 4.8-A, preincubating HEK293T cells with various concentrations of WKYMVm or MMK 1 for two minutes prior to LL-37 administration did not block the LL-37-induced calcium mobilization.

HEK293T cells were also preincubated with curcumin, a pigment from *Curcuma longa Linn* that downregulates EGFR via ubiquitination [24]. Upon treatment for 1 hour, the calcium response of HEK293T cells to LL-37 decreased significantly (p-value obtained from Student's t-test when comparing calcium response to LL-37 vs. LL-37 + curcumin (30 µM) is 0.001) (figure 4.8-B). Similar results were obtained when HEK293T cells were pretreated with the broad-spectrum RTK inhibitor genistein (p-value from Student's t-test when comparing LL-37 vs. LL-37 + genistein (50 µM) is 0.001). Subsequently, receptor-selective blockers for EGFR and IGF1R were applied to HEK293T cells, because these two members of the RTK family have previously been documented to respond to LL-37 [2,5]. Only the EGFR-specific antagonist erlotinib hydrochloride (EC_{50} 2 nM) exerted an inhibitory effect on the calcium response to LL-37 at a concentation of 10 µM. This effect was also significant (p-value obtained from Student's t-test is 0.02).

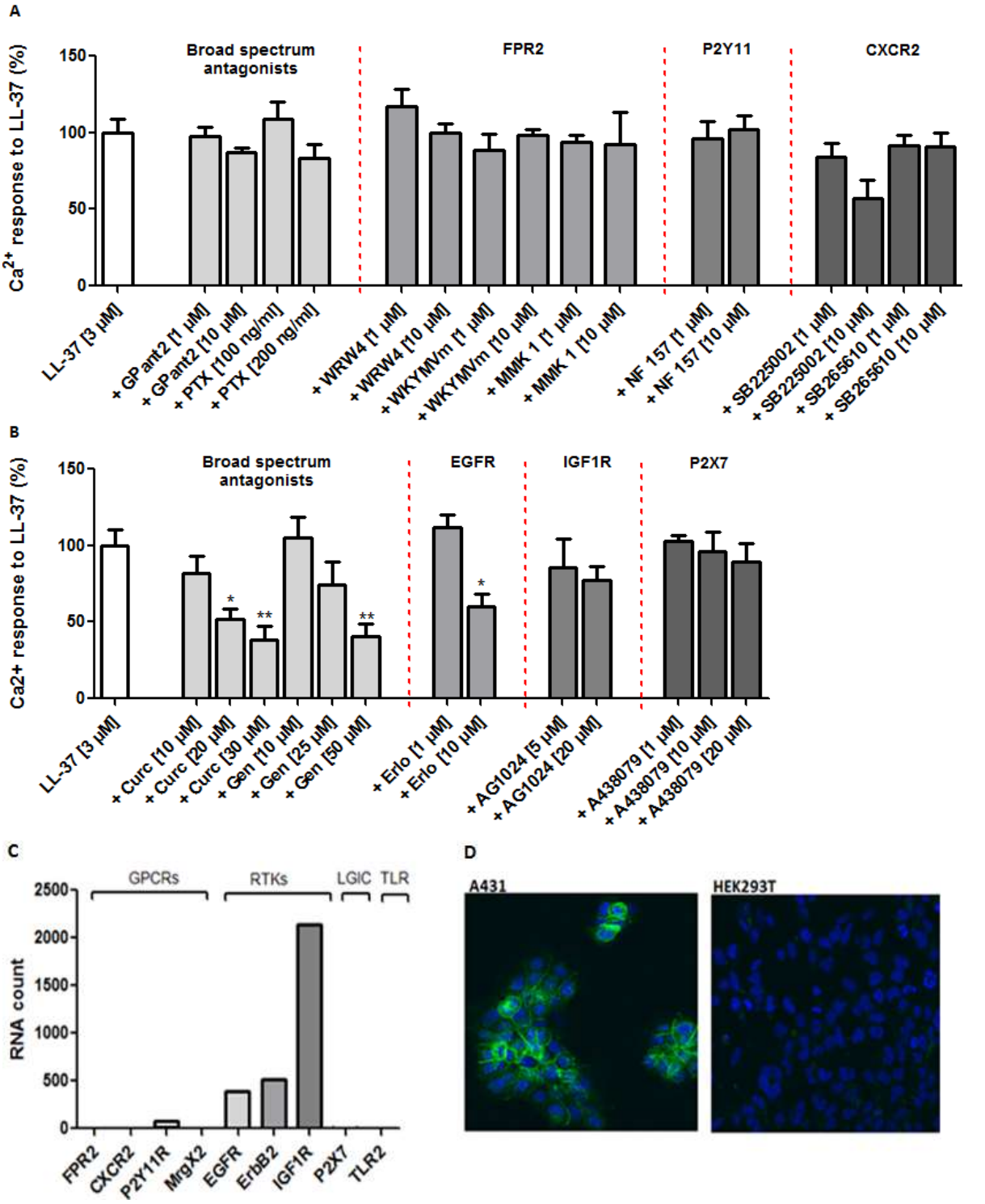

Fig.4.8. Graph **A** shows the effect of several broad-spectrum and receptor-specific GPCR antagonists on the calcium response of HEK293T cells to LL-37. Graph **B** displays the effect of broad-spectrum and receptor-selective RTK inhibitors, as well as the effect of the $P2X_7$-selective antagonist A438079. On HEK293T cells, curcumin (Curc) and genistein (Gen) partially blocked the calcium response evoked by LL-37. The EGFR-selective antagonist erlotinib (Erlo) also exerted a significant inhibitory effect at a concentration of 10 µM. Results are displayed as a percentage of the calcium response of HEK293T cells to LL-37 ($N \geq 6$; data are mean ± SEM). Significance levels are represented by asterisks: * indicate p-value from Student's t-test < 0.05, ** p-value < 0.005. Graph **C** shows mRNA expression data of candidate receptors for LL-37 ($N=1$). RNA counts reflect the number of aligned reads per gene. Graph **D** shows the results of a confocal imaging experiment. A431 cells, which are known to express high levels of EGFR, as well as HEK293T cells were stained with 10 µg/ml of anti-human EGFR chemically linked to a fluorophore (green). Nuclei were counterstained with DAPI (blue).

In order to verify whether EGFR was truly involved in the signal transduction pathway activated by LL-37, HEK293T cells were treated with another established EGFR antagonist: Tyr AG1478 (EC_{50} = 3 nM). At a concentration of 10 µM, only a small inhibitory effect of Tyr AG1478 on the calcium response to LL-37 was observed (figure 4.9-A). This effect was not significant (p-value obtained from Student's t-test when comparing groups Tyr AG1478 + LL-37 vs. LL-37 is 0.09).

The EGFR-selective antagonists used in this study have EC_{50} values in the low nanomolar range, whereas high concentrations (10 µM) were required to (partially) inhibit the calcium response to LL-37. Note that, at these concentrations, specificity is not always guaranteed and it remains a possibility that the inhibitory effect is caused by an off-target effect rather than a selective effect on EGFR. For instance, it is possible that another member of the EGFR family such as ErbB2 is targeted by the EGFR-specific antagonists. A functional association between LL-37 and ErbB2 in breast cancer has been demonstrated [25]. To test whether ErbB2 was involved in the signaling cascade activated by LL-37, HEK293T cells were preincubated with a selective antagonist of ErbB2 (CP-724714). However, CP-724714 could not block the calcium response of HEK293T cells to LL-37 (figure 4.9-A).

Another possible mechanism by which LL-37 activates EGFRs involves receptor transactivation [7]. In this process, LL-37 transactivates EGFRs via MPP-mediated cleavage of membrane-anchored ligands of EGFRs. To investigate whether LL-37 operates by virtue of the transactivation mechanism, HEK293T cells were preincubated with a broad-spectrum MPP inhibitor (GM6001) for 1 hour. However, GM6001 could not alter the effect of the peptide (figure 4.9-A).

The partial inhibitory effect on the calcium response to LL-37 exerted by high concentrations of EGFR-selective antagonists could also be related to low endogenous expression of EGFRs in HEK293T cells. In agreement with a study of Atwood *et al.*, we found that the expression of EGFR at the mRNA level is low [22]. However, we could not detect EGFR protein expression using a primary immunofluorescence approach (figure 4.8-D). On the other hand, EGFRs were easily visualized by the human anti-human EGFR antibody in A431 human epithelial carcinoma cells. This cell line is often used as a positive control for EGFR expression [27].

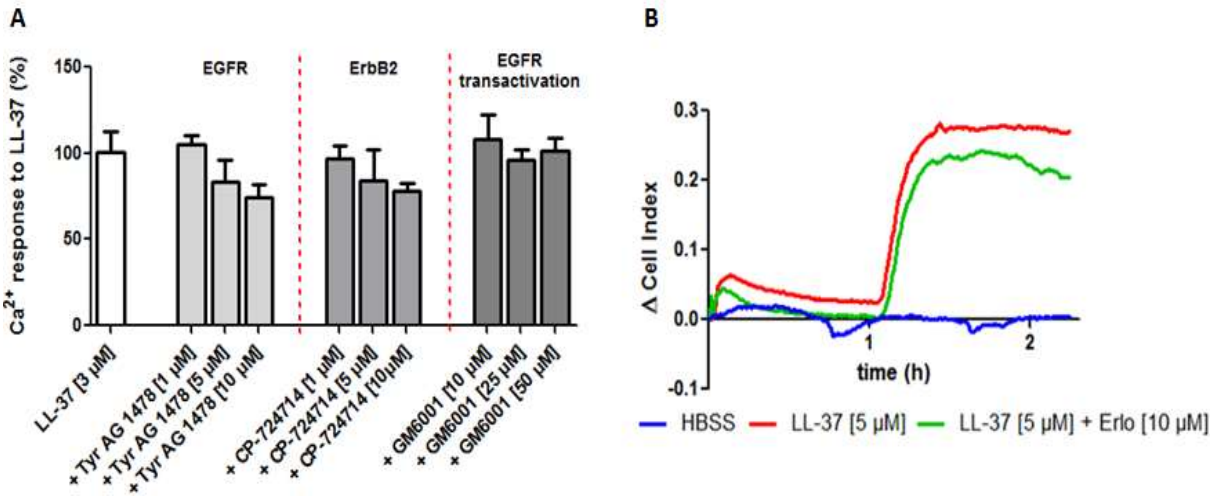

Fig.4.9. Graph **A** shows the effect of selective EGFR (Tyr AG1478) and ErbB2 (CP-724714) antagonists, as well as the effect of a broad-spectrum inhibitor of MMPs (GM6001), on the calcium response of HEK293T cells to LL-37 (N≥6). Graph **B** shows the impedance response of erlotinib-treated HEK293T cells to LL-37, as measured by EIS. The impedance measurement was repeated three times and one impedance response profile is shown.

Among the receptor-selective antagonists tested, only high concentrations of EGFR-selective inhibitors were able to partially inhibit the calcium response of HEK293T cells to LL-37. Remarkably, treatment of HEK293T cells with erlotinib (10 µM) did not completely inhibit the short- or long-term impedance response to LL-37 (figure 4.9-B).

In an attempt to explain these observations, a human RTK phosphorylation assay was used because it simultaneously identifies the relative levels of phosphorylation of 71 different human RTKs in cell lysates. If signaling by LL-37 involves activation of EGFR, specific tyrosine residues within the cytoplasmic domain of EGFR will be phosphorylated. These changes in EGFR tyrosine phosphorylation can then be visualized by chemiluminescence. However, when the signal densities of EGFR spots of LL-37-treated and untreated samples were compared, no differences were observed (figure 4.10). Noteworthy, changes in receptor tyrosine phosphorylation were not detected for other RTKs that have been documented to respond to LL-37, *e.g.* IGF1R and ErbB2.

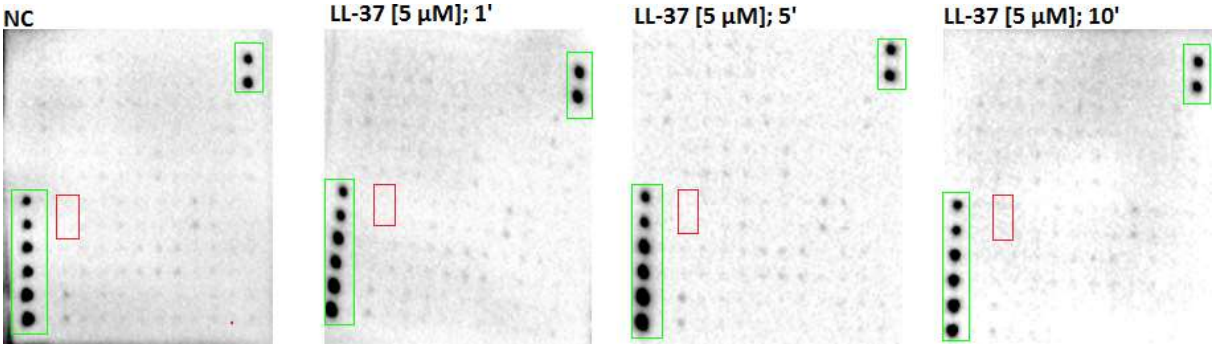

Fig.4.10. Human RTK phosphorylation assay results. HEK293T cells were either stimulated with HBSS (NC) or 5 µM of LL-37 for 1, 5, or 10 minutes respectively. Positive controls (green) are a controlled amount of biotinylated antibody printed onto the array. EGFR spots are marked in red (exposure time: 30 seconds).

4.3.3.3 LL-37 stimulates HEK293T cells via an indirect mechanism of action

By employing pharmacological antagonists, EGFR was initially proposed as a candidate receptor for LL-37. However, follow-up experiments to validate the role of EGFR in recognizing the peptide were inconclusive. A growing number of researchers suggest that LL-37 operates by virtue of a more complex signal transduction system than the classical mechanism in which one peptide activates a single receptor. LL-37 is an amphipathic peptide that can reside in the zwitterionic membrane of eukaryotic cells [2,5,7]. It is possible that the peptide induces cell signaling by altering the physicochemical state of the cell membrane. Experiments with D-enantiomers of LL-37 are usually conducted to investigate the membrane binding capacity of LL-37 [5]. If the D-enantiomer of LL-37 maintains the activity of the original peptide, it argues against a stringent ligand-receptor interaction. However, due to cost reasons, we were not able to test whether the D-enantiomer of LL-37 was able to elicit a calcium response in HEK293T cells.

Several studies suggest the involvement of LRs in the mode of action of LL-37 [5,28]. In order to determine whether LRs were involved in the signal transduction pathway activated by LL-37 in HEK293T cells, the plasma membrane cholesterol content was modified. This can be achieved through many ways, such as the addition of cholesterol-depleting (MBCD or HBCD) or cholesterol-sequestering (filipin) agents, or the inhibition of cholesterol synthesis (AY9944).

HEK293T cells were pretreated with 3 mM of MBCD for 1 hour prior to LL-37 treatment. As depicted in figures 4.11-A and 4.11-B, MBCD-treated HEK293T cells responded more strongly to LL-37 than untreated cells. MBCD did not reinforce the calcium response to the positive control (PAR1-AP). Administration of higher concentrations of MBCD (≥ 5 mM) to HEK293T cells resulted in the manifestation of a cytotoxic effect, characterized by a sustained calcium response and confirmed by EIS measurements. When HEK293T cells were pretreated with a lower concentration of MBCD (1.5 mM), no effect on the response to LL-37 was observed (figure 4.11-A).

Other pharmacological agents that manipulate cholesterol levels also augmented the calcium response of HEK293T cells to LL-37 (figure 4.11-C). For example, HEK293T cells were preincubated with a specific inhibitor of cholesterol synthesis (AY9944) for 24 hours. The next day, the calcium response of HEK293T cells to LL-37 was monitored. As depicted in figure 4.11-A, AY9944-treated cells responded more strongly to LL-37 than untreated cells. These results suggest that reducing the cholesterol levels in the plasma membrane leads to a stronger calcium response to LL-37.

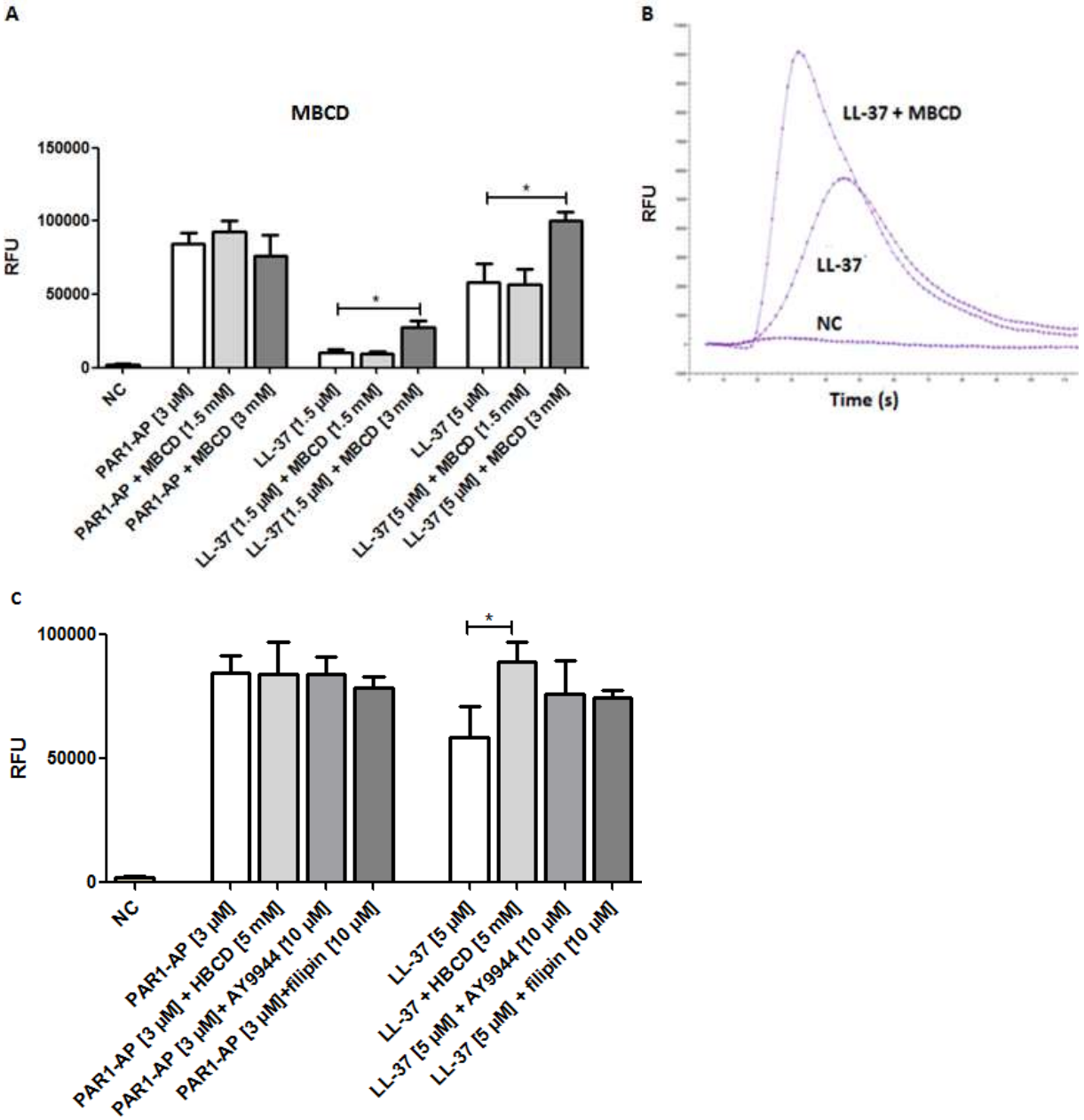

Fig.4.11. Pretreatment of HEK293T cells with the cholesterol-depleting agent MBCD (3 mM) reinforced the calcium response of HEK293T cells to LL-37, whereas the calcium response to the positive control (PAR1-AP) was not affected (**A**). Preincubating HEK293T cells with a lower concentration of MBCD (1.5 mM) could not augment the calcium response to LL-37. Significance levels are reflected by asterisks which indicate p-values from Student's t-test: *, $p < 0.05$ (*N*=6; data are mean ± SEM). Graph **B** shows a representative example of the calcium response of MBCD-treated HEK293T cells to 5 µM of LL-37 (Δ), or vehicles (o). HBSS was used as a negative control (□). Graph **C** shows the effect of another cholesterol-depleting agent (HBCD), a cholesterol biosynthesis inhibitor (AY9944), or a cholesterol-sequestering agent (filipin) on the calcium response of HEK293T cells to PAR1-AP or LL-37. Reducing the cholesterol levels in the plasma membrane evoked a stronger calcium response to LL-37, whereas the response to PAR1-AP was not reinforced. HBCD and filipin were preincubated for 1 hour, whereas AY9944 was added 24 hours prior to peptide exposure. Significance levels are reflected by asterisks which indicate p-values from Student's t-test: *, $p < 0.05$ (*N*=6; data are mean ± SEM).

Modifying the cholesterol content of cell membranes leads to changes in membrane fluidity which causes the disruption of LRs [28]. We hypothesized that removing cholesterol from the cell membrane alters the motility of receptors or unmasks receptors at the cell surface, thereby

improving the accessibility of LL-37 to its (their) cognate receptor(s). A member of the EGFR family was initially proposed as the most likely candidate receptor for LL-37 (see section 4.3.3.2). Therefore, HEK293T cells were simultaneously incubated with 3 mM of MBCD and 10 µM of either an EGFR-selective (erlotinib or Tyr AG1478) or an ErbB2-selective antagonist (CP-724714) for 1 hour (figure 4.12). In agreement with the results displayed in figures 4.8 and 4.9, only erlotinib significantly inhibited the calcium response of MBCD-treated HEK293T cells to LL-37 (p-value from Student's t-test comparing erlotinib+MBCD-treated HEK293T cells vs. MBCD-treated HEK293T cells is 0.009). The small inhibitory effect of Tyr AG1478 on the calcium response of MBCD-treated HEK293T cells to LL-37 was not significant (p-value from Student's t-test when comparing calcium response to LL-37 of Tyr AG1478+MBCD-treated HEK293T cells vs. MBCD-treated HEK293T cells is 0.23). In another set of experiments, we investigated whether syndecans were involved in the mode of action of LL-37. Syndecans are known to act as co-receptors for several of the purported receptors for LL-37, including EGFR and IGF1R [29]. To remove cell surface heparin sulfates, HEK293T cells were pretreated with 0.01 units/ml heparinase and/or 0.06 units/ml heparitinase for 40 minutes. However, removing cell surface syndecans did not block the action of LL-37 (figure 4.12).

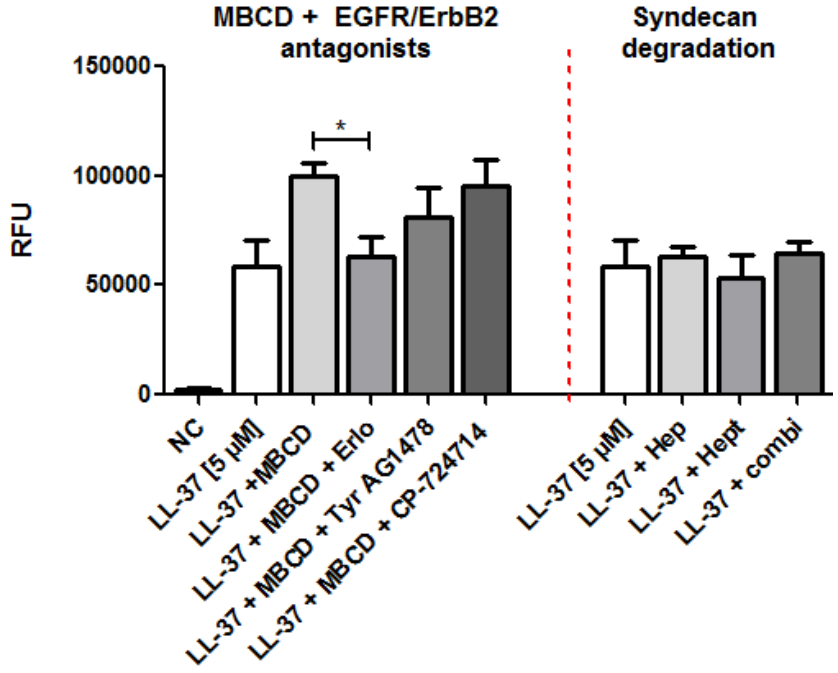

Fig.4.12. Pretreatment of HEK293T cells with a combination of the cholesterol-depleting agent MBCD [3 mM] and EGFR-selective antagonists [10 µM] or the ErbB2-selective antagonist CP-724714 (10 µM) could not completely inhibit the calcium response of HEK293T cells to 5 µM of LL-37. Only the EGFR-selective inhibitor erlotinib exerted a significant inhibitory effect on the calcium response of MBCD-treated HEK293T cells to LL-37. Significance levels are reflected by asterisks which indicate p-values from Student's t-test: *, $p < 0.05$ (N=6; data are mean ± SEM). To determine whether syndecans were involved in the signaling pathway activated by LL-37, HEK293T cells were pretreated with heparinase (Hep; 0.01 units/ml), heparitinase (Hept; 0.06 units/ml), or a combination (combi) of the enzymes. Removal of cell surface syndecans from HEK293T cells did not abrogate the effect of LL-37 ($N \geq 6$).

Lau *et al*. showed that LL-37 has the ability to enter mammalian cells via endocytic pathways [30]. To determine if signaling by LL-37 involved the activation of endocytic networks, HEK293T cells were preincubated with brefeldin A (20 µM), a fungal metabolite that is commonly used as an endocytosis inhibitor, and the impedance response to LL-37 was measured (figure 4.13).

HEK293T cells were also preincubated with dynasore (1-50 µM), a dynamin-dependent endocytosis inhibitor, or MDC (1-50 µM), a clathrin-mediated endocytosis antagonist, in order to examine their effect on the impedance response of HEK293T cells to LL-37. Even though the results obtained with dynasore and MDC are considered preliminary (experiments were only performed one time), no effect on the impedance response to LL-37 was observed when major endocytic pathways were blocked.

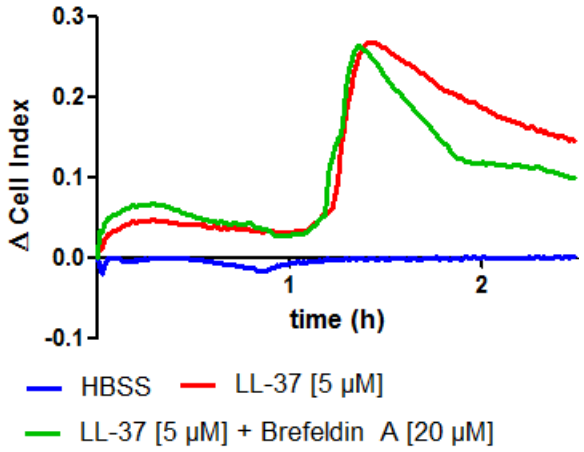

Fig.4.13. Impedance response profile of brefeldin A-treated HEK293T cells to 5 µM of LL-37 (green), as measured by EIS. Brefeldin A is commonly used as an endocytic inhibitor. HBSS is used as NC (blue). One example of three impedance measurements is displayed.

4.3.4 Unraveling the long-term effect of LL-37

When looking at the impedance response of HEK293T cells following treatment with LL-37, both short- and long-term effects of LL-37 were observed (figure 4.1-A). As mentioned before, the initial increase in impedance may correspond to morphological changes induced by calcium-mediated signaling events. The second impedance response was observed approximately one hour after LL-37 treatment (figure 4.1-A). Note that this long-term effect of LL-37 can easily be missed using traditional endpoint assays. In a next series of experiments, several hypotheses were devised and tested in order to understand the second impedance response to LL-37. Amongst the possibilities are the following hypotheses:

<u>Hypothesis 1</u>: LL-37-induced calcium overload exceeds the mitochondrial buffering capacity

LL-37 induced the rapid release of intracellular calcium in HEK293T cells (figure 4.2). It is known that mitochondria regulate the uptake of cytosolic calcium during physiological calcium signaling in various cell types [31]. However, when the calcium load exceeds the mitochondrial buffering capacity, mitochondrial swelling and rupture can occur [32]. We hypothesized that such cellular events might be associated with the long-term impedance response of HEK293T cells to LL-37.

Calcium uptake depends on the mitochondrial potential ($\Delta\psi_M$), which is defined by the calcium gradient between the cytosol and the mitochondrial matrix [31,32]. HEK293T cells were pretreated with paclitaxel, an antimitotic drug that depolarizes the mitochondrial membrane potential and prevents mitochondria from buffering cytosolic calcium [33]. Preincubating HEK293T cells with paclitaxel (10 µM) prior to LL-37 treatment could not inhibit the overall impedance response to LL-37 (figure 4.14). Pretreatment with higher concentrations (50 and 100 µM) of paclitaxel led to an altered impedance response to LL-37. Immediately following LL-37 treatment, the impedance response decreased below zero. This may point to a cytotoxic effect of paclitaxel (or the combination of paclitaxel and LL-37) on mitochondrial function and/or microtubule dynamics. However, the second impedance response to LL-37 still occurred in paclitaxel-treated HEK293T cells. Therefore, it is deemed unlikely that the long-term effect of LL-37 critically depends on the mitochondrial calcium uptake capacity.

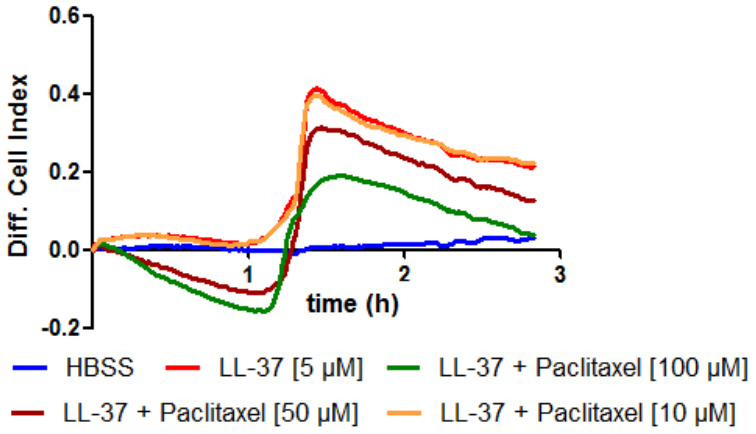

Fig.4.14. The impedance response profiles of paclitaxel-treated HEK293T cells to 5 µM of LL-37. One example of three EIS measurements is displayed. Paclitaxel interferes with cytosolic calcium signaling through depolarizing the mitochondrial membrane potential.

<u>Hypothesis 2</u>: LL-37 activates transcription factor(s) that regulate protein synthesis

The addition of LL-37 to HEK293T cells could impact gene expression, which in turn affects protein synthesis. It is possible that increased protein production and/or secretion by HEK293T cells caused the increase in impedance observed 1 hour after LL-37 treatment.

To put this hypothesis to the test, HEK293T cells were preincubated with BAY 11-7082, a selective NF-κB inhibitor. NF-κB plays a vital role in the regulation of more than 150 genes, including genes encoding chemokines and cytokines [34]. In addition, HEK293T cells were pretreated with STA-21, an antagonist of signal transducers and activators of transcription (STAT), as well as cycloheximide, an antagonist of eukaryotic translation [35]. As shown in figures 4.15-A and B, only cycloheximide was able to exert a partial inhibitory effect on the second impedance response of HEK293T cells to LL-37.

The 'second peak' as observed by EIS could also be a result of the induction of apoptosis. To test this hypothesis, HEK293T cells were pretreated with the broad-spectrum caspase inhibitor (Z-VAD-fmk) upon which the impedance response to LL-37 was monitored. However, we were not able to observe an effect of Z-VAD-fmk on the impedance response of HEK293T cells to LL-37 (figure 4.15-C).

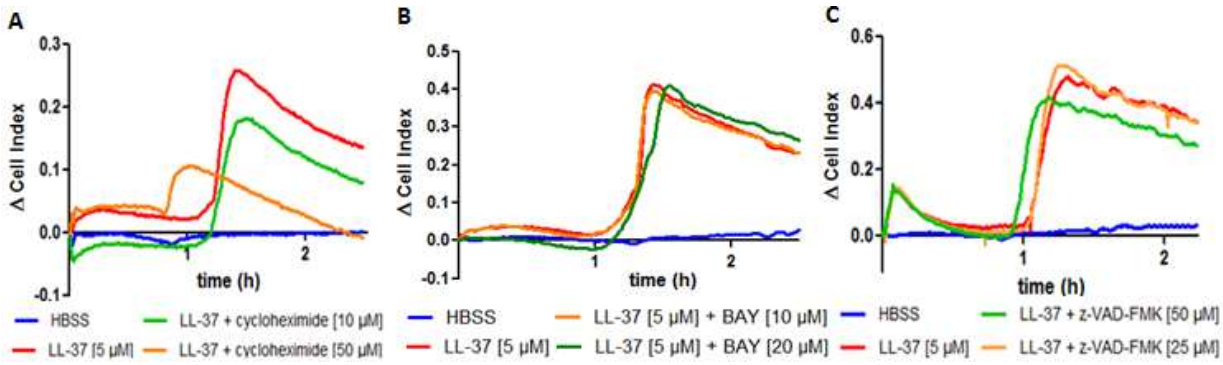

Fig.4.15. HEK293T cells were pretreated with respectively the protein synthesis inhibitor cyclocheximide (10 and 50 µM), the NF-κB inhibitor BAY 11-7082 (10 and 20 µM), and the broad-spectrum caspase inhibitor Z-VAD-fmk (25 and 50 µM), after which the impedance response to LL-37 was monitored. Cycloxheximide exerted a partial inhibitory effect on the long-term effect of LL-37. Each experiment was repeated at least two times.

Hypothesis 3: LL-37 forms pores in the plasma membrane

In order to determine whether $P2X_7$ or other ion channels were involved in the signal transduction pathway activated by LL-37, several ion channel antagonists were tested. For instance, HEK293T cells were pretreated with a competitive $P2X_7$ receptor antagonist (A438079), devoid of activity at other P2 receptors, prior to LL-37 treatment. No effect of A438079 on the calcium response of HEK293T cells to LL-37 was observed (figure 4.8). Because we were not able to detect mRNA of $P2X_7$ in HEK293T cells, it is deemed unlikely that $P2X_7$ is a cognate receptor for LL-37.

Other ion channel antagonists were also tested, including EIPA, TMB-8, and TEA. EIPA is derivative of amiloride that inhibits the Na^+/H^+ exchanger, a membrane protein found in many cell types. TMB-8 is a calcium and sodium channel inhibitor, and TEA blocks K^+-channels. As depicted in figure 4.16-C, none of these ion channel antagonists blocked the long-term impedance response of HEK293T cells to LL-37. Note that TMB-8 also acts as an intracellular calcium antagonist [36]. This might help to explain the inhibitory effect on the short-term impedance response (figure 4.16-C).

HEK293T cells were also preincubated with suramin. Suramin is a sulfonated napthylamine that has been widely used in studies of P2X ion channels [37,38]. As depicted in figure 4.16-A, suramin inhibited the calcium response of HEK293T cells to LL-37 in a dose-dependent manner, whereas no inhibitory effect on the calcium response evoked by the postivie control (PAR1-AP) was observed. Similar results were obtained using NF449, a commercially available suramin analogue, and PPADS, a non-selective P2 receptor antagonist [39-42]. Interestingly, the overall impedance response of HEK293T cells to LL-37 was completely blocked when HEK293T cells were pretreated with suramin (≥ 50 µM) (figure 4.16-B).

Suramin's inhibitory action on the impedance response of HEK293T cells to LL-37 was further explored in follow-up experiments. Suramin has multiple potential mechanisms of action [37-39,43]. For example, suramin disrupts receptor-G protein coupling by inhibiting the association of Gα- and Gβγ-subunits [43]. However, previous experiments using broad-spectrum and GPCR-selective inhibitors did not deliver any proof for a functional association between LL-37 and a member of the GPCR family (figure 4.8). HEK293T cells were also pretreated with an antagonist of Gβγ-subunit-dependent signaling (gallein; 1-100 µM) prior to LL-37 treatment, but this did not lead to an altered calcium response to LL-37 (preliminary results).

Suramin may also exert its effect by acting at P2 receptors [38]. To date, two purinergic receptors ($P2X_7$ and P2Y11R) have been documented to respond to LL-37. However, $P2X_7$- or P2Y11R-selective inhibitors were not able to block the impedance or calcium response of HEK293T cells to LL-37. These results suggest that $P2X_7$ and P2Y11R are not involved in the mechanism behind the action of LL-37. It must also be noted that PPADS is a non-selective P2 purinergic antagonist, whereas NF449 acts as a highly selective, potent $P2X_1$ receptor inhibitor (IC_{50} = 1 nM) [39-41]. $P2X_1$ is probably not a cognate receptor for LL-37, since mRNA of $P2X_1$ was not detected in HEK293T cells.

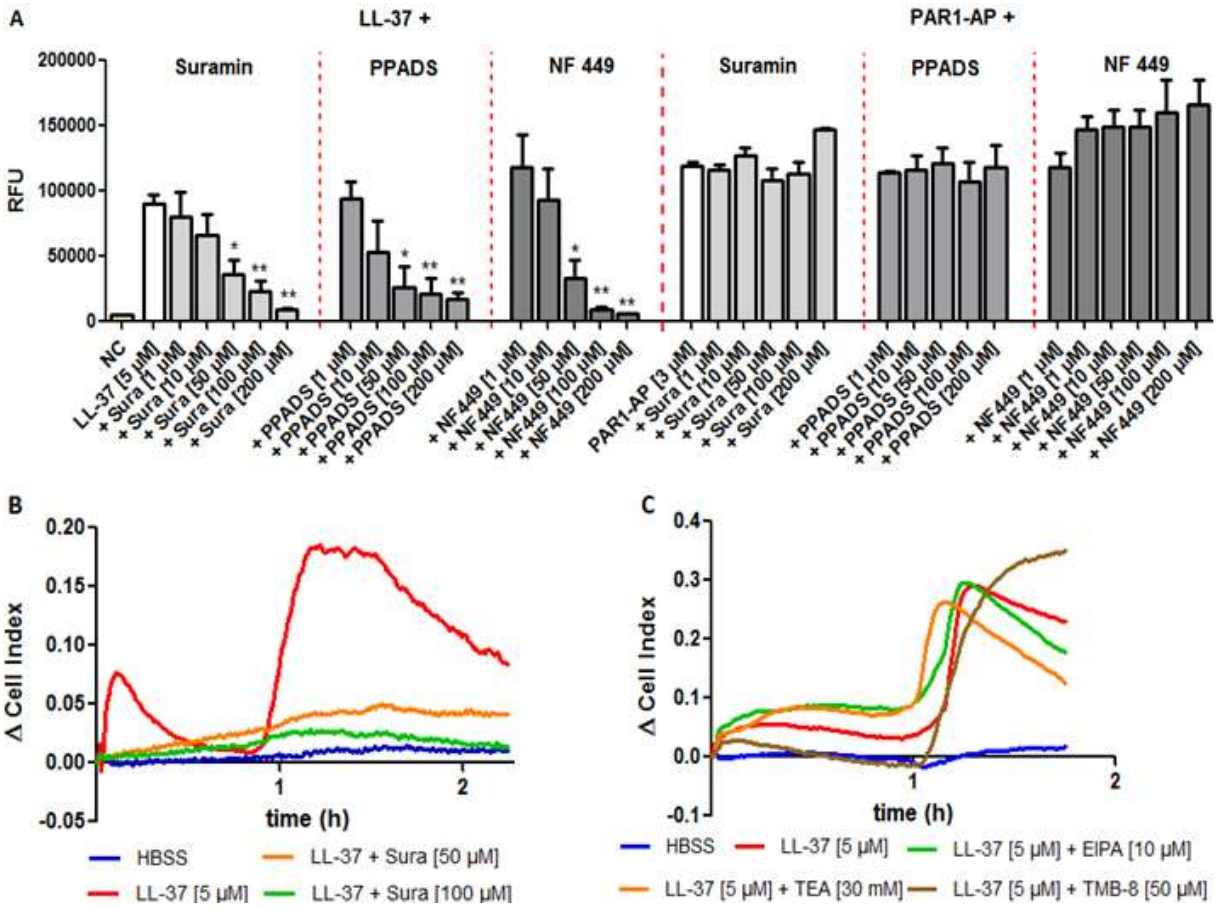

Fig.4.16. This panel of graphs represents data for LL-37 obtained with respectively a fluorescence-based calcium assay (**A**) and EIS (**B, C**). Graph A shows the inhibitory effect of respectively suramin, PPADS, and NF-449 on the calcium response of HEK293T cells to LL-37, whereas no effect on the response to PAR1-AP was observed. The activity spectrum of suramin and suramin analogues spans broadly, ranging from inhibition of activation of G proteins to inhibition of RTKs as well as P2 purinoceptors. Significance levels are represented by asterisks which indicate p-values from Student's t-test: *, $p < 0.05$. Suramin (50 or 100 µM) completely blocked the impedance response of HEK293T cells to LL-37, as depicted in graph B. Other commonly used ion channel antagonists such as EIPA (sodium-hydrogen antiport inhibitor), TEA (K^+-channel inhibitor), or TMB-8 (Ca_{2+} channel- and Na+ channel-blocker) were unable to inhibit the second impedance response to LL-37, as displayed in graph C.

Recent work by Chi *et al.* revealed that suramin protected cells from cell injury caused by α-hemolysin, a pore-forming toxin from *Staphylococcus aureus* [37]. The pore-forming activity of LL-37 has been widely reported [2,3,5,7]. Even though there were no indications of acute cytotoxicity (figure 4.3-A), there is a possibility that prolonged exposure of HEK293T cells to 5 µM of LL-37 results in the formation of pores in the plasma membrane. The resultant influx of water and ions then leads to cell swelling (increase in impedance) and rupture of the cell membrane (decrease in impedance). The combination of cell swelling, followed by membrane breakdown and loss of cellular integrity, is consistent with oncosis, an osmotically driven process [44].

In an attempt to track the LL-37-induced changes in cell morphology, HEK293T cells were treated with 5 µM of LL-37 and microscopically inspected for 6 hours using a standard inverted light

microscope (40X objective). Pictures were taken at an interval of 30 minutes. At first, no distinct morphological changes were observed. At the end of the experiment, clear changes in morphology were observed in a signficiant number of HEK293T cells which may be caused by the membrane-permeabilizing effect of LL-37 (figure 4.17-B). Notably, when looking at longer-term effects induced by 5 µM of LL-37, a decrease in impedance compared to untreated cells was observed (figure 4.17-A). Taken together, these results imply that LL-37 negatively affects cell viability.

The continuous decrease in impedance was not observed when HEK293T cells were pretreated with suramin (figure 4.17-A). Suramin might prevent cell injury by suppressing the membrane permeability induced by LL-37. This hypothesis is supported by the observation that LL-37 lost the ability to induce morphological changes in suramin-treated HEK293T cells (figure 4.17-B).

HEK293T cells were also exposed to a toxic concentration (50 µM) of LL-37 in order to examine the real-time cytotoxic response induced by the peptide. Following an initial increase in impedance, the impedance decreased below zero (figure 4.17-A). We hypothesized that HEK293T cells rapidly swell upon exposure to 50 µM of LL-37 due to its pore-forming activity, after which the continued swelling leads to the loss of cell membrane integrity.

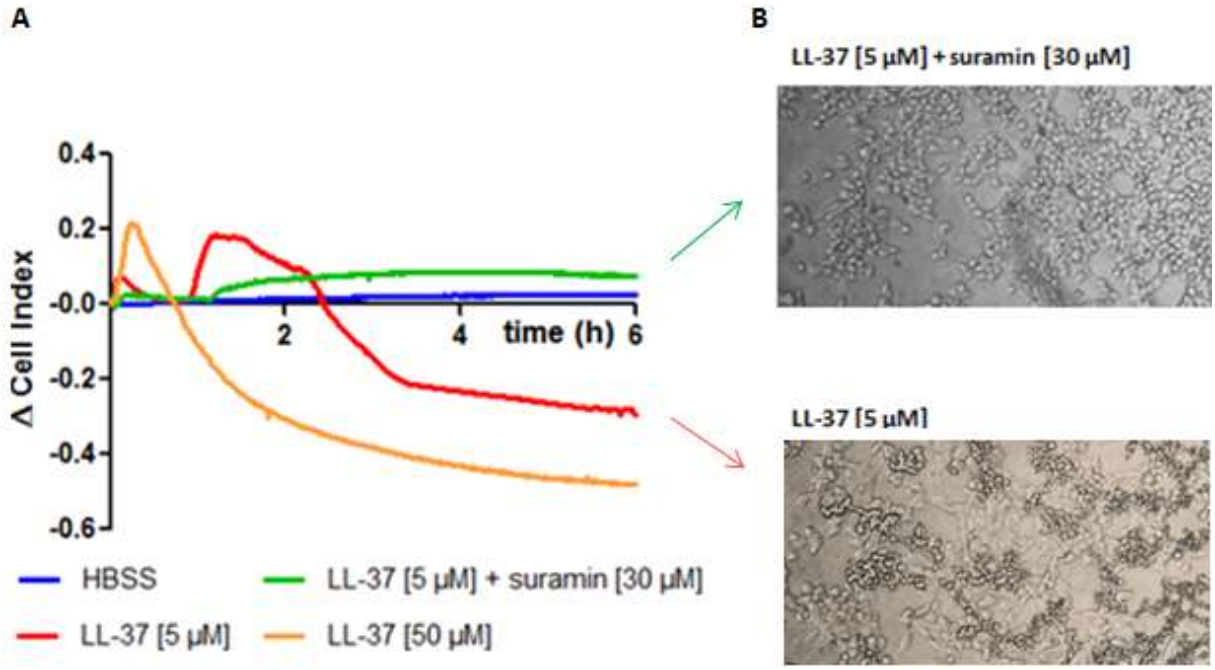

Fig.4.17. Graph **A** shows the inhibitory effect of suramin (green) on the impedance response of HEK293T cells to 5 µM of LL-37 (red). When looking at longer-term effects of LL-37, a decrease in impedance compared to control cells (blue) was observed. This suggests that LL-37 negatively affects cell viability. Morphological changes induced by LL-37 (5 µM) were observed by light microscopy (40X objective; pictures taken 6 hours after LL-37 treatment) (**B**). These changes in morphology were not observed when HEK293T cells were pretreated with suramin (30 µM). This suggests that suramin protects HEK293T cells from LL-37-elicited cell damage.

4.3.5 Pharmacological dissection of the effect of LL-37 on A549 cells

In a next set of experiments, we examined whether LL-37 employed a different mode of action in A549 cells in comparison to HEK293T cells. Following the same strategy as previously described (see section 4.3.3), we explored the role of candidate receptors for LL-37 using a collection of broad-spectrum and specific pharmacological agents. FPR2 has been suggested as the receptor for LL-37 on A549 cells [30,45]. However, Lau *et al*. reported that LL-37 was actively taken up by A549 cells and localized to the perinuclear region after 4 hours.

A549 cells were preincubated with broad-spectrum GPCR inhibitors such as PTX and GPant2 after which the calcium response to LL-37 was monitored. PTX partially inhibited the calcium mobilization induced by LL-37, suggesting the involvement of a $G\alpha_i$-coupled receptor in the signaling cascade (figure 4.18-A). PTX also exerted an inhibitory effect on the impedance response of A549 cells to LL-37 (figure 4.18-B). Based on the results of the foregoing, we hypothesized that FPR2 was the PTX-sensitive receptor for LL-37.

However, the FPR2-selective antagonist WRW4 failed to suppress the calcium or impedance response of A549 cells to LL-37. In addition, cross-desensitization experiments using the FPR2-agonist WKYMVm could not provide conclusive evidence that FPR2 was the cognate receptor for LL-37 (figure 4.18-A). Further experiments revealed that none of the inhibitors displaying selectivity for any of the purported receptors for LL-37 blocked the calcium response to the peptide. As a consequence, the identity of the PTX-sensitive GPCR remains undecided.

To examine whether LL-37 was internalized into A549 cells, A549 cells were pre-exposed to an endocytosis inhibitor (brefeldin A) for 1 hour upon which the impedance response to LL-37 was monitored for 4 hours. As shown in figure 20-B, brefeldin A almost completely inhibited the impedance response of A549 cells to LL-37. Interestingly, brefeldin A did not exert a similar effect on the impedance response of HEK293T cells to LL-37 (see figure 4.13).

It is also relevant to mention that no cytotoxic effects of LL-37 (5 µM) were observed on A549 cells using light microscopy and long-term impedance measurements. This is consistent with cytotoxicity data of LL-37 provided by Lau *et al* [30].

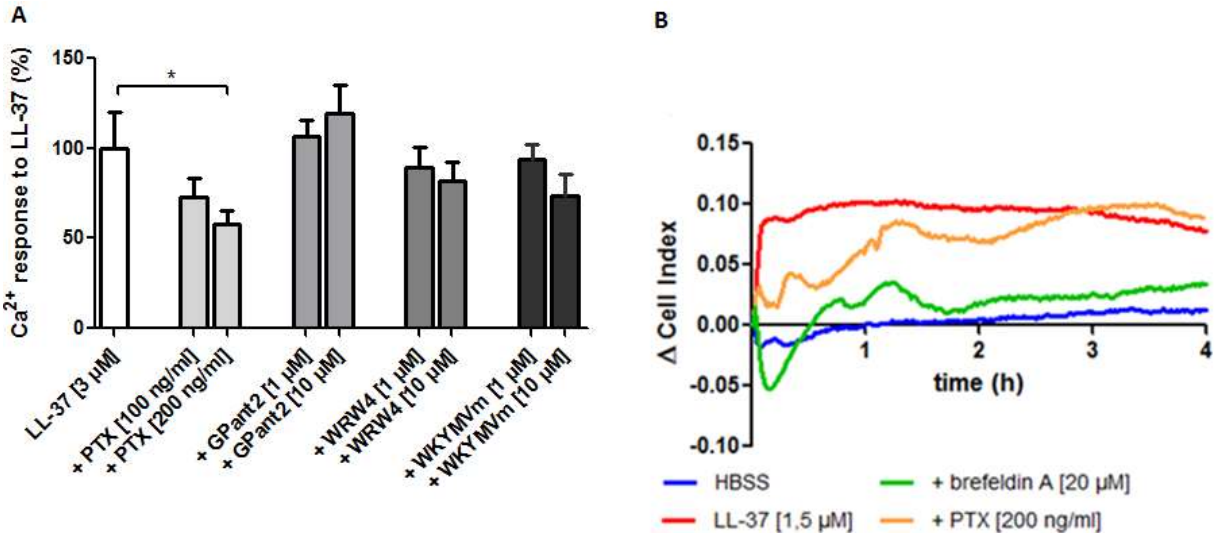

Fig.4.18. Graph **A** depicts the effect of the broad-spectrum GPCR antagonists PTX and GPant-2, as well as the effect of the FPR2-specific inhibitor WRW4 and FPR2-specific agonist WKYMVm on the calcium response of A549 cells to LL-37 (3 µM) (*N*=6; data are mean ± SEM). Significance levels are represented by asterisks which indicate p-values from Student's t-test: *, $p < 0.05$. Graph **B** shows an example of the impedance response of PTX-treated (orange) or brefeldin A-treated (green) A549 cells to LL-37 (*N*=3).

4.3.6 Pharmacological dissection of the effect of LL-37 on RAW264.7 and U87 (CXCR4+) cells

RAW264.7 macrophage cells strongly responded to a dilution series of LL-37, as determined by impedance measurements (figure 4.1-C). In addition, LL-37 (≥ 1.5 µM) evoked a calcium response (figure 4.2). Among the antagonists tested, only the broad-spectrum GPCR antagonist PTX exerted an inhibitory effect on the impedance response to the peptide (figure 4.19-B). However, PTX was not able to inhibit the calcium response evoked by LL-37 (figure 4.19-A).

Even though LL-37 has been demonstrated to be chemotactic for human neutrophils and monocytes through FPR2, FPR2-selective antagonists could not abrogate the effect of LL-37 (figures 4.19-A and B). Taken together, it appears a PTX-sensitive receptor is involved in recognizing LL-37 in RAW264.7 cells. However, the identity of this receptor remains unknown.

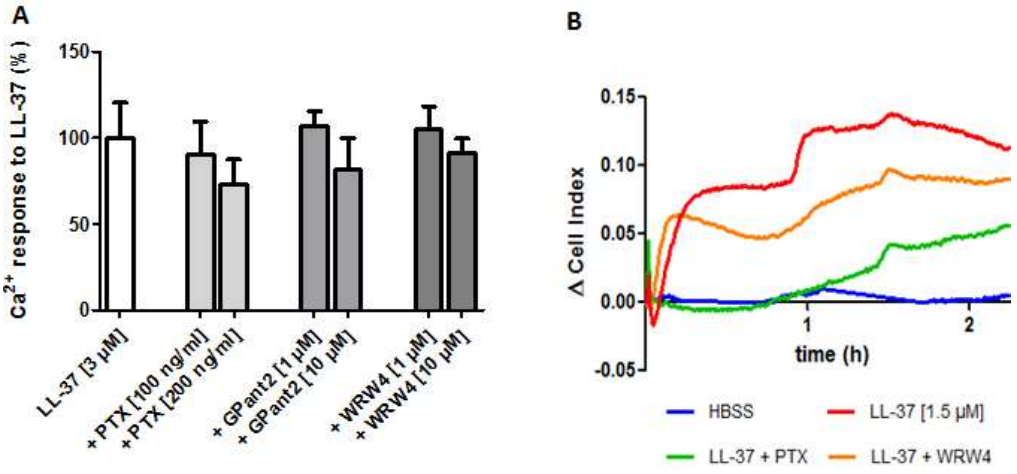

Fig.4.19. Graph **A** depicts the effect of the broad-spectrum GPCR antagonists PTX and GPant-2, as well as the FPR2-selective antagonist WRW4, on the calcium response of RAW264.7 cells to LL-37 (3 µM) (*N*=6; data are mean ± SEM). Graph **B** shows the impedance response of PTX-treated (green) or WRW4-treated (orange) RAW264.7 cells to LL-37 (*N*=2).

Based on a recent study of Wu *et al*., we included U87 glioblastoma cells transfected with CXCR4 in this study [15]. More specifically, we investigated whether impedance measurements can be used to detect increased responsiveness of U87 (CXCR4+) cells to nanomolar concentrations of SDF-1 by incorporating CXCR4 into LRs.

As shown in figure 4.1-D, a small impedance response of U87 (CXCR4+) cells to 5 µM of LL-37 was observed. However, lower concentrations of LL-37 (< 3 µM) were unable to induce a response of U87 (CXCR4+) cells, as measured by EIS and a fluorometric calcium mobilization assay (figures 4.1 and 4.2). U87 (CXCR4+) cells were pre-exposed to 1 µM of LL-37 for 30 minutes after which the impedance response to SDF-1 (125 nM) was monitored for 1 hour. As depicted in figures 4.20-A and

B , LL-37 exerted a stronger impedance response relative to cells which were not primed with LL-37. This could indicate that LL-37 increased the responsiveness to CXCR4's ligand SDF-1.

At a low concentration of 4 nM, U87 (CXCR4+) cells were unable to respond to SDF-1. However, when cells were primed with 1 µM of LL-37 prior to SDF-1 (4 nM) treatment, a clear impedance response to SDF-1 was observed, suggesting that LL-37 enhances SDF-1-dependent signaling (figure 4.20-B).

In order to investigate whether this priming effect could be due to an increased incorporation of CXCR4 into LRs, U87 (CXCR4+) cells were challenged with MBCD (3 mM) or filipin (10 µM) for 1 hour to interrupt formation of LRs. Cells were then primed with LL-37 for 30 minutes upon which the impedance response to SDF-1 was monitored. As depicted in figure 4.20-A, the SDF-1-CXCR4 axis priming effect was abrogated when LRs were destroyed. Note that a negative impedance response of MBCD-treated U87 (CXCR4) cells to SDF-1 was detected, suggestive of potential toxicity. It remains to be determined whether the inhibition of the priming effect induced by LL-37 is caused by the disruption of LRs or due to a toxic effect.

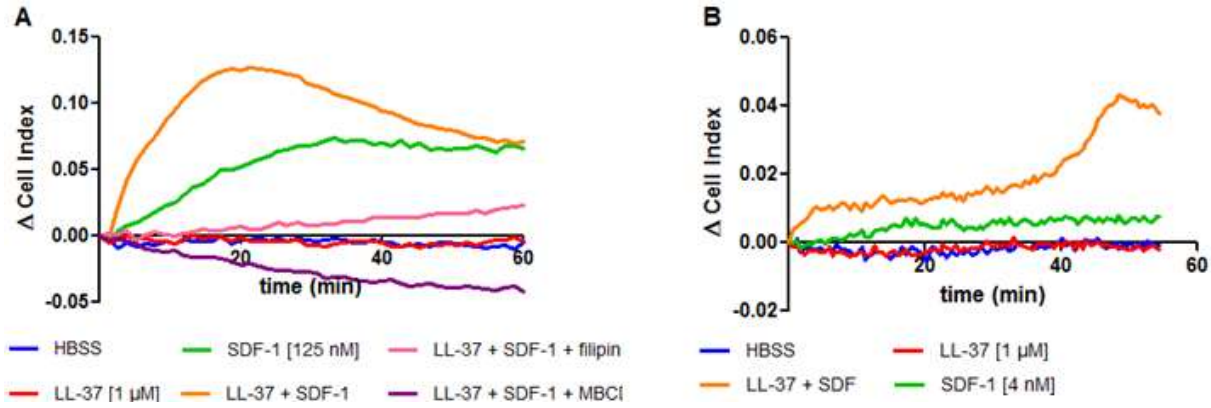

Fig.4.20. Graph **A** depicts the impedance response of U87 (CXCR4+) cells to 125 nM of SDF-1 (green) or 1 µM of LL-37 (red). HBSS (blue) was used as a negative control. LL-37-primed U87 (CXCR4+) cells exerted stronger signaling in response to SDF-1 as compared to unprimed cells (orange). The priming effect mediated by LL-37 was inhibited when U87 (CXCR4+) cells were preincubated with the cholesterol-sequestrating agent filipin (10 µM; pink) or the cholesterol-depleting agent MBCD (3 mM; purple) prior to LL-37 treatment, suggestive of the involvement of LRs in the mechanism of action. Graph **B** shows that LL-37 enhanced the responsiveness of U87 (CXCR4) cells to a low concentration (4 nM) of SDF-1 (orange) relative to cells which were not primed with LL-37 (green) (*N*=3).

4.4 Discussion

LL-37, the only human member of the cathelicidin family, is an amphipathic and cationic AMP with pleiotropic effects on the innate and adaptive immune system. In addition to its antimicrobial, -viral, -fungal, and –biofilm effects, LL-37 mediates various host defense responses and has complex immunomodulatory properties [2,5]. For instance, LL-37 acts as a potent chemoattractant to guide monocytes, neutrophils, and T cells to the site of infection, affects mast cell degranulation, and neutralizes bacterial LPS [2,46,47]. LL-37 also regulates the delicate balance between pro- and anti-inflammatory responses by modulating inflammatory cytokine levels [47-49]. Dysfunction of LL-37 is frequently associated with the pathogenesis of various diseases, including atopic dermatitis, rosacea, and cancer [2,5,50]. Therefore, it is important to gain an enhanced understanding of the molecular mechanisms by which LL-37 induces host cell responses.

How one peptide is able to have so many effects, has puzzled researchers for a long time. To date, various mechanisms of action have been proposed to explain how LL-37 exerts its effects on mammalian cells, including receptor-dependent and –independent mechanisms [7]. In the latter case, LL-37 modulates cellular activities by modifying the physical properties of the plasma membrane [2,5]. This can induce allosteric changes in receptors, affect receptor motility, or promote the inclusion of receptors into specialized membrane domains called LRs [5,15,50]. At higher concentrations of the peptide, LL-37 induces cytotoxic effects through the formation of transmembrane pores [2].

Because of its relevance in the immune system and several human diseases, we set out to elucidate the mode of action of LL-37 on various cultured cell lines. Even though many techniques and strategies have been developed to identify the receptor and/or elucidate the downstream signal transduction pathway of a test compound, there is no golden standard method. Second messenger assays such as fluorescence-based cAMP or calcium assays are routinely used as they respectively monitor cAMP production or calcium release upon stimulation with a test compound. However, the utility of these assays is diminished by their need to use fluorescent dyes, as well as incompatibility with continuous monitoring [10]. In addition, obtaining an overview of the overall cellular response involves the use of several assay formats with different sensitivities and dynamic ranges, which increases the costs and duration of experiments [10,11].

To deal with these shortcomings, an assay based on cellular impedance was used to study the effect of LL-37 on cultured cells. The reader is referred to chapter 1 for more information on the basic principles behind cellular impedance technology. Arguably the biggest advantage of EIS is that this technique is able to detect and measure cellular responses in real-time, regardless of the

downstream signaling cascade that is activated. Kammermann *et al*. suggest that impedance measurements generate a signature that reflects the intracellular pathways utilized [12]. Consequently, impedance responses can be used to formulate hypotheses concerning the mechanism of action of a test compound.

We discovered that LL-37 evoked an impedance response in various cultured cell lines, including HEK293T, A549, RAW264.7, U87 (CXCR4+), MRC-5, and B16 4A5 cells. The ability to activate a broader set of cell types may be related to its α-helical structure and/or amphipathic nature. Notably, LL-37 is expressed in all organs of the human body [6, 51]. Recently, a functional role for LL-37 in the central nerve system (CNS) was revealed for the first time [51]. Even though LL-37 activates a wide variety of cells, we observed that some cell lines were more sensitive to LL-37 than others. For instance, A549 and RAW264.7 cells strongly responded to a low concentration (0.5 µM) of LL-37, whereas U87 (CXCR4+) cells were less sensitive.

When looking at the impedance responses generated upon stimulation with LL-37, considerable differences were noticed among the cell types tested. For instance, the impedance response of HEK293T cells to 5 µM of LL-37 was characterized by an initial transient increase in impedance, followed by a second increase approximately 1 hour after LL-37 treatment. However, when RAW264.7 cells were exposed to 5 µM of LL-37, the impedance decreased below zero, suggestive of LL-37-induced cytotoxicity. A gradual increase in impedance was noticed when RAW264.7 cells were preincubated with 0.5 µM of LL-37. It is possible that, at this concentration, LL-37 promotes RAW264.7 cell migration or proliferation. Other research groups previously demonstrated that LL-37 has the potential to stimulate the migration of immune cells to the site of infection, where they play a crucial role in host defense against invading bacteria and other pathogens [2,5,46]. To study this hypothesis, more specialized techniques are required. For example, cell migration can be studied using the NANIVID (NANo IntraVital Imaging Device) [52].

It must be noted that the detection of a unique impedance response to LL-37 does not necessarily imply that LL-37 activates distinctly different signal transduction pathways in different cell types. It is possible that only one or a few components of the same multicomponent signaling pathway differ among cell types, leading to varying impedance responses. This flexibility may also enable cells to respond to LL-37 in a very specific manner. However, it is currently unclear how and to what extent different players in a signal transduction pathway contribute to distinct features of the impedance signature.

Previous studies aimed at dissecting impedance responses used pathway-specific inhibitors to link ligand-induced activation of signaling events to characteristic impedance changes [10-14]. In the

majority of cases, GPCR or RTK agonists with a well-defined mode of action were administered to cultured cell lines in order to demonstrate pathway-distinguishing capacity of cellular impedance assays. For example, Ciambrone *et al*. as well as Peters *et al*. demonstrated prototypical cellular impedance response profiles for $G\alpha_q$, $G\alpha_s$ and $G\alpha_i$ signaling [13,14]. These impedance responses can be used to reveal cell-specific differences in G protein coupling. One example hereof is the established $G\alpha_s$ coupling for the melanocortin 4 receptor (MC4R) in HEK293 cells, whereas signaling through $G\alpha_q$ was detected in Chinese hamster ovary (CHO) cells [14].

Peters *et al*. suggest that the activation of a particular G protein subtype leads to a series of molecular events that result in actin-dependent changes in cellular morphology which can be detected by EIS [14]. Polymerization of the actin cytoskeleton induced by stimulation of $G\alpha_q$- or $G\alpha_i$-coupled GPCRs generally increases the impedance. On the other hand, treatment of cells with compounds that activate $G\alpha_s$-coupled GPCRs leads to actin depolymerization which results in a rounded or stellated morphology. These morphological changes are typically associated with a decrease in impedance. Even though we did not investigate the effects of test compounds on actin (de)polymerization, preliminary results obtained in our lab are in agreement with these observations. For example, compounds that signal via $G\alpha_q$ or $G\alpha_i$ in HEK293T cells (PAR1-AP, carbachol, sphingosine-1-phosphate) increase the impedance, whereas compounds (FSK, isoproterenol) that propagate the signal via $G\alpha_s$ exert an opposite effect (unpublished data). However, this could also prove to be an oversimplified representation of the coupling diversity as the overall impedance response is most likely influenced by the expression and stoichiometry of receptors, G proteins, and downstream effector proteins.

Nevertheless, all aforementioned studies suggest an association between impedance responses and ligand-induced signal transduction events [10-14]. Because the modes of action of LL-37 on host cells are incompletely understood, we examined endogenous impedance responses of various cultured cell lines and discovered novel activity of LL-37 on HEK293T cells. More specifically, both short- and long-term impedance responses of HEK293T cells to LL-37 were observed. The ability of EIS to detect short- and long-term effects in a single assay underlines one of the key advantages of real-time impedance-based signals compared to traditional endpoint assays.

Using a calcium mobilization assay, we demonstrated that the short-term effect of LL-37 involved the mobilization of intracellular calcium. These results could have implications for conventional overexpression studies using HEK293T cells, as a functional endogenous receptor(s) for LL-37 might be present at the cell surface of HEK293T cells. However, it is also possible that LL-37 induces cell signaling by interacting with the cell membrane.

Because we were not able to find any previous reports concerning the activity of LL-37 on HEK293T cells, we set out to identify the cognate receptor and elucidate the intracellular transduction pathway. First, we investigated the calcium response of HEK293T cells to LL-37 in more detail. Calcium signals may arise from two possible sources: depletion of calcium stored within the ER and/or external calcium influx across the cellular membrane. To identify the source of intracellular calcium elevation induced by LL-37, HEK293T cells were preincubated with 2-APB in calcium-free medium, to prevent extracellular calcium entry into the cells. 2-APB was initially discovered as a membrane-permeable inhibitor of IP_3R. However, studies of Bootman *et al*. and DeHaven *et al*. showed that 2-APB also exerts complex effects on SOCs [18,53].

In a calcium-free situation, LL-37 elicited intracellular calcium mobilization. 2-APB completely inhibited the LL-37-induced calcium elevation in the absence of extracellular calcium, suggesting that the effect is (at least partially) mediated by IP_3R. Because 2-APB has a complex mode of action, HEK293T cells were also pretreated with $LaCl_3$, a potent inhibitor of SOCs, prior to LL-37 treatment [20]. We observed that $LaCl_3$ could not abrogate the effect of LL-37. These results imply that HEK293T cells release calcium ions from intracellular stores upon stimulation with LL-37. However, this does not exclude a potential contribution of extracellular calcium, as it is possible that calcium ions permeate across the cell membrane through ion channels activated by LL-37 or through pores formed by the peptide.

HEK293T cells were also pretreated with the PLC-antagonist U73122 to determine whether PLC is involved in the signaling cascade activated by LL-37. U73122 partially inhibited the calcium response of HEK293T cells, indicative of a role for PLC in the signal transduction pathway. Note that the initial impedance response to LL-37 was partially blocked by U73122, whereas the second impedance response was not affected. This suggests that the short- and long-term effects of LL-37 are independent of each other and reflect different cellular processes. In addition, this observation suggests that the cellular parameters as measured by EIS are influenced by the LL-37-induced release of intracellular calcium.

Identifying the molecular target of LL-37 turned out to be a major challenge. Among the candidate receptors for LL-37, HEK293T cells expressed mRNA of EGFR, IGF1R, and P2Y11R. The EGFR was initially put forward as a candidate receptor for LL-37, based on results obtained with the broad-spectrum RTK inhibitors curcumin and genistein, as well as the EGFR-selective inhibitor erlotinib.

However, follow-up experiments to validate the involvement of EGFR were inconclusive. It is known that curcumin and genistein do not display selectivity for EGFR and regulate a wide variety of cellular processes [54]. For instance, curcumin is involved in the regulation of transcription factors (such as

NF-κB), growth factor receptors (such as EGFR and ErbB2), protein kinases (such as Akt), and inflammatory cytokines (such as Il-1 and Il-6) [54]. Curcumin has also been demonstrated to insert into the membrane bilayer, thereby inducing a rigidifying effect on the plasma membrane [55].

Even though the EGFR-selective inhibitor erlotinib partially blocked the calcium response to LL-37, it showed almost no effect on the impedance response of HEK293T cells to the peptide. In addition, only a small and statistically insignificant inhibitory effect was observed when HEK293T cells were pretreated with another established EGFR-selective antagonist (Tyr AG1478). Furthermore, we were unable to detect EGFR protein expression using a primary immunofluorescence approach. Erlotinib and Tyr AG1478 have documented IC_{50} values of respectively 2 and 3 nM, whereas a concentration of 10 µM was used in this study. At this dose, EGFR-specificity cannot be guaranteed. It is known that many antagonists which display selectivity for receptors at pico- or nanomolar concentrations have a 'secondary pharmacology' at higher concentrations, thereby regulating other membrane proteins non-specifically. Altogether, the aforementioned results cast doubt on the hypothesis that EGFR is the cognate receptor for LL-37.

To further clarify whether the inhibitory effect of erlotinib was truly caused by an off-target effect rather than a specific effect on EGFR, possible changes in EGFR tyrosine phosphorylation upon activation by LL-37 were studied using a human RTK phosphorylation array. This assay is capable of detecting the phosphorylation of 71 human RTKs simultaneously. However, LL-37 treatment did not increase EGFR (or other candidate RTKs) phosphorylation compared to untreated cells. There is a possibility that the concentration of protein (400 µg/ml) loaded onto each membrane was not high enough to visualize subtle changes in RTK phosphorylation. In order to draw a definite conclusion, EGFR knockdown experiments can be performed using small interfering RNAs capable of suppressing EGFR signaling.

The inability of receptor-selective inhibitors to inhibit the calcium and impedance response of HEK293T cells to LL-37 may point to the existence of a more complex signaling system than the classical mechanism in which one peptide activates a single receptor. This is consistent with a study of Perregaux *et al*. who proposed that cationic AMPs induce host cell responses by interacting with the plasma membrane [56]. Given the amphipathic nature of LL-37, it is conceivable that LL-37 modulates activity of HEK293T cells by modifying the physicochemical state of the cell membrane rather than interacting with a cell surface receptor. To test this hypothesis, experiments with the all-D-analog of LL-37 need to be conducted to provide evidence for the attachment of the peptide to the membrane [5,57,58]. If LL-37 lacks a specific molecular target and instead binds to the cell

membrane, it is expected that the all-D-enantiomer of LL-37 is just as potent as the original peptide. However, due to cost reasons, experiments with D-enantiomers of LL-37 were not conducted.

It is also possible that LL-37 elicited calcium mobilization through a receptor-independent mechanism of action. We showed that LL-37 modulates PLC activity in HEK293T cells (figure 4.7). Interestingly, the modulation of phospholipase activity by amphipathic peptides is a well-known phenomenon. According to Rao, phospholipases are sensitive to alterations in the lipid packing in the plasma membrane induced by AMPs [59]. For example, the α-helical amphipathic peptide melittin shares with LL-37 a high content of basic residues and modulates PLA_2 activity by acting on the plasma membrane [60]. Pochet *et al*. demonstrated that LL-37 uses a membrane-dependent mechanism to potentiate the activation of PLA_2 in response to ATP in cells from mouse submandibular glands [68]. Pretreatment of these cells with LL-37 also blocked the activation of phospholipase D (PLD) upon exposure to ATP [61,62]. Taken together, the calcium response evoked by LL-37 may be caused by the membrane-active properties of LL-37 which modulate the activity of membrane-bound enzymes such as PLC.

Xhindoli *et al*. reported that cholesterol plays an important role in the peptide-membrane interaction process, as it protects eukaryotic cells from the cytolytic effects of cationic AMPs [5]. Cyclodextrins such as MBCD and HBCD are commonly used to modify the cholesterol content of cell membranes. We discovered that LL-37 evoked a stronger calcium response when HEK293T cells were exposed to cholesterol-depleting agents or a cholesterol biosynthesis inhibitor. One possible explanation for this observation is that cholesterol removal from the cell membrane alters the mobilization of receptors or improves the accessibility of LL-37 to its molecular target. To put this hypothesis to the test, HEK293T cells were simultaneously treated with 3 mM of MBCD and receptor-selective antagonists of candidate receptors for LL-37. However, the calcium response of MBCD-treated HEK293T cells to LL-37 was not inhibited by (a combination of) these inhibitors. Again, this observation favors the hypothesis that LL-37 exerts its action on HEK293T cells by interacting with the cell membrane. Noteworthy, cholesterol has been shown to attenuate the membrane association of LL-37 [63,64]. It is possible that depletion of cholesterol from the cell membrane leads to improved membrane binding of LL-37 which in turn triggers a stronger calcium response of HEK293T cells to LL-37.

Taken together, our data suggest that LL-37 dose-dependently activated HEK293T cells through the rapid release of intracellular calcium mediated via the PLC/IP_3R pathway. The calcium response to LL-37 could not be completely inhibited by preincubating cells with a collection of broad-spectrum and receptor-specific antagonists, suggestive of a membrane-dependent mechanism of action. It remains

a possibility that LL-37 modifies the physicochemical state of the cell membrane, thereby modulating phospholipase activity.

Aside from the initial impedance response, a second transient response was observed approximately 1 hour after LL-37 treatment. Various hypotheses were devised and tested in order to obtain a better understanding of the long-term effect induced by LL-37. HEK293T cells were preincubated with pharmacological agents that inhibit protein synthesis (cycloheximide), transcription factors (NF-κB and STAT3), caspase-dependent apoptosis (z-VAD-FMK), or ion channels (EIPA, TMB-8, TEA), but these were unable to completely block the long-term activity of LL-37. Because Z-VAD-fmk only targets caspase-dependent cell death pathways, it cannot be excluded that LL-37 induces apoptosis via caspase-independent cell death pathways. Furthermore, it must be noted that the shape of the curve generated by EIS suggests an acute (toxic?) response rather than a more long-lasting effect on HEK293T cells, *e.g.* enhancing the proliferative or migratory potential of HEK293T cells.

Because EIS provides a phenotypic view of cellular behavior, we hypothesized that the increase in impedance 1 hour after LL-37 treatment was caused by cellular swelling. Cell swelling often precedes cell death. The continued swelling of the cell eventually leads to membrane and organelle breakdown, causing the impedance to decrease (figure 4.21). This process of cell swelling and rupture is often referred to as oncosis, a non-apoptotic mode of cell death. Oncosis involves swelling of the cytoplasm, mitochondria, and nucleus, as well as coagulation of the cytoplasm [44,65,66]. To study this hypothesis, HEK293T cells were exposed to a toxic concentration of LL-37 (50 µM) in order to monitor the cytotoxic response kinetics on EIS. We observed an immediate increase in impedance upon which the impedance decreased below zero. This impedance signature may be characteristic for a mechanism of cell death by oncotic pathways.

At a lower concentration of 5 µM, the cytotoxic response of HEK293T cells occurred at a later point in time. It is possible that LL-37 covers the surface of the membrane until a local threshold concentration is reached and small pores are formed, causing leakage of intracellular components. This may explain why no acute cytotoxic activity was observed when HEK293T cells were treated with 5 µM of LL-37. Taken together, our results suggest that higher concentrations of LL-37 organize to form pores and trigger cell death mechanisms more quickly than lower concentrations of LL-37, and this is reflected in the corresponding impedance response profiles.

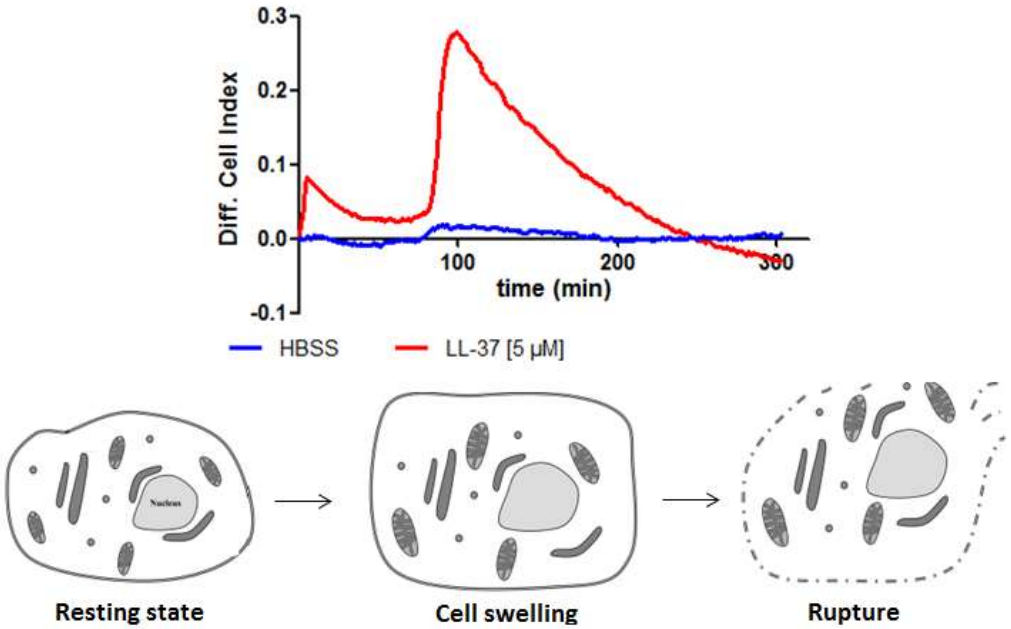

Fig.4.21. Hypothesis on the long-term effect of LL-37 on HEK293T cells. Before peptide administration, cells remained in a normal physiological state ('resting state'). When HEK293T cells were exposed to LL-37, both short- and long-term responses to the peptide were observed. Prolonged exposure to LL-37 may lead to the formation of pores, leading to cell swelling (impedance increases) and loss of integrity of the membrane (impedance decreases).

Suramin (30-100 µM), a well-known pharmacological antagonist of P2 purinoceptors, inhibited the long-term effect induced by LL-37 [37,38]. Suramin also blocked the calcium mobilization elicited by LL-37, but did not exert an effect on the calcium response to PAR1-AP. The suramin analogue (NF 449) as well as PPADS, a structurally different broad-spectrum P2 purinoceptor antagonist, also suppressed the calcium response of HEK293T cells to LL-37.

Because suramin is a multi-target compound, experiments were conducted to determine which of the known pharmacological actions of suramin could be responsible for this blocking effect. Our results indicated that the action of suramin was independent of its action on GPCRs and P2 purinoceptors. Chi *et al.* demonstrated that suramin significantly inhibited α-hemolysin-elicited membrane hyperpermeability and cell injury [37]. Data from microscopy analysis as well as EIS revealed that suramin (30 µM) protected HEK293T cells from LL-37-induced cell injury. Further research is required to determine whether suramin specifically interferes with membrane pores formed by LL-37, especially since suramin is negatively charged at physiological pH. The inhibitory effect on LL-37-induced activation of HEK293T cells can be caused by electrostatic interactions between positively charged residues of LL-37 and negatively charged residues of suramin. However, van der Does *et al.* demonstrated that suramin (30 µM) failed to suppress the effect of LL-37 on macrophage differentiation [67]. Moreover, Sun *et al.* showed that pretreatment of eosinophils with 30 µM of suramin did not affect LL-37-mediated cysteinyl leukotrienes release [68]. These studies

argue against the formation of a complex between LL-37 and suramin arising from electrostatic interactions.

We hypothesized that suramin protected HEK293T cells from the membrane-damaging effect of LL-37. The blocking effect of suramin on the pore permeability induced by LL-37 might prevent the swelling and rupture of HEK293T cells. Additional experimental evidence for the proposed cytotoxic action of LL-37 can be obtained using cytotoxicity assays*, e.g.* measuring the release of the intracellular enzyme lactate dehydrogenase (LDH) or monitoring the uptake of ethidium bromide following LL-37-induced pore formation. In addition, it may be worth to test suramin analogues with a lower negative charge in order to gain insight into the underlying mechanism by which suramin inhibits the activity of LL-37. A number of commercially available suramin analogues as well as truncated variants of suramin can be used for this purpose [69].

Subsequently, the impedance response of A549 non-small lung carcinoma cells to LL-37 was examined in more detail and compared to the impedance response of HEK293T cells. LL-37 might use a different mode of action to activate A549 cells than HEK293T cells, as distinct impedance responses were observed upon LL-37 treatment. A549 cells have been used before to study biological activity of LL-37 [30,45]. Lau *et al*. demonstrated that A549 cells have a high- and low-affinity receptor for LL-37 [30]. The identity of the high-affinity receptor is not known, but appears to be responsible for the internalization of LL-37 and its localization to the perinuclear region. Lau *et al*. identified FPR2 as the low-affinity receptor for LL-37 on A549 cells [30]. The interaction of LL-37 with a low-affinity receptor may have functional relevance as it directs cells of the immune system closer to inflammatory sites before their chemotactic receptors become desensitized.

Our results indicated that brefeldin A, an inhibitor of major endocytic pathways, completely abrogated the impedance response of A549 cells to LL-37. This is in agreement with results obtained by Lau *et al*. who demonstrated that brefeldin A blocked the uptake of LL-37 into A549 cells. The effect of brefeldin A appears to be target-specific, as brefeldin A did not exert an inhibitory effect on the impedance response of HEK293T cells to LL-37. However, identifying the exact molecular target of brefeldin A has been hampered by its pleiotropic nature and a broader set of inhibitors for different types of endocytic pathways need to be tested to gain additional information. For example, MBCD or nystatin can be used as inhibitors for LR-mediated endocytosis, whereas MCD can be administered as antagonist of clathrin coated pit-mediated endocytosis. In addition, the cell-permeable inhibitor of actin polymerization cytochalasin D can be used to investigate if actin is required for the internalization of LL-37 into A549 cells.

We also showed that PTX partially inhibited the calcium and impedance response of A549 cells to LL-37. The $G\alpha_i$-coupled receptor FPR2 was initially favored as the receptor responsible for mediating this effect. However, the FPR2-selective antagonist WRW4 could not inhibit the calcium or impedance response of A549 cells to the peptide, which leaves the identity of the $G\alpha_i$-coupled receptor activated by LL-37 undecided. These results are in line with previous reports which also hypothesize on the existence of other, yet unidentified receptors for LL-37 in various cell types [5,70,71]. It must be noted that A549 cells were pretreated with PTX for 2 hours, upon which the calcium or impedance response to LL-37 was monitored. Lau *et al*. also preincubated A549 cells with PTX for the same amount of time prior to LL-37 treatment [30]. However, several studies use longer incubation times (up to 24 hours) to evaluate the effects of PTX [72,73]. Further research is required to examine whether prolonged preincubation with PTX leads to a complete inhibition of the effect of LL-37.

Current unsolved questions include the identity of a $G\alpha_i$-coupled receptor involved in recognizing LL-37. In addition, it remains to be determined whether this receptor mediates the uptake of LL-37 by A549 cells. The use of ligand-receptor capture (LRC) technique can help to unambiguously identify the cognate receptor for LL-37 on A549 cells (for more information about LRC, see chapter 3) [74]. However, LRC is designed for the situation where a functional effect of a ligand is observed, but the binding partner at the cell membrane (receptor or other membrane protein) is unknown. There is a possibility that LL-37 non-specifically binds to the membrane interface and then induces allosteric changes in a $G\alpha_i$-coupled receptor. In this case, the use of LRC is less suited to identify the molecular target of LL-37. Experiments with the all-D-enantiomer of LL-37 can be conducted to gain insight into the membrane-binding properties of LL-37 before employing LRC.

Similar follow-up studies are required to unambiguously obtain the identity of the receptor(s) for LL-37 in RAW264.7 cells. In this cell line, PTX completely abrogated the impedance response to LL-37 (1.5 µM), suggesting the involvement of a $G\alpha_i$-coupled receptor. Since FPR2- and CXCR2-selective inhibitors could not block the action of LL-37, an FPR2- or CXCR2-mediated mechanism is deemed unlikely.

To gain more insight into the pleiotropic effects of LL-37 in modulating host cell responses, U87 stably transfected with CXCR4 were used. Wu *et al*. demonstrated that LL-37 contributed to the activation of CXCR4 in human HSPCs by promoting their incorporation in LRs. In agreement with this study, our results suggest that pretreatment of U87 (CXCR4+) cells with LL-37 evoked a stronger impedance response to CXCR4's ligand SDF-1 in comparison to unprimed cells [15]. This priming effect was completely abrogated when cells were exposed to cholesterol-depleting agents, which

causes the disruption of LRs. Note that our observations were made in the context of an exploratory study and need to be validated by complementary methods, *e.g.* separation of LRs by sucrose density gradients or visualization of LRs by confocal microscopy [75]. However, while writing this chapter, preliminary experiments showed that LL-37-primed U87 (CXCR4+) cells also exerted a stronger calcium response to SDF-1 than unprimed control cells.

Interestingly, the priming effect induced by LL-37 may have therapeutic potential, for instance in umbilical cord blood transplantation where the numbers of HSPCs are limited [15]. In light of potential follow-up studies, it would be interesting to investigate whether the proposed mechanism has a more general effect on how LL-37 modifies signal transduction and enhances the responsiveness of immune cells to inflammatory molecules. For example, LL-37 has been demonstrated to upregulate chemokine receptors in RAW264.7 cells, including CXCR2 and CXCR4 [76]. It is worth exploring whether LL-37 also enhances the responsiveness of RAW264.7 cells to CXCR2 ligands or SDF-1. To study this hypothesis, the impedance response of LL-37-primed RAW264.7 cells to CXCR2 ligands or SDF-1 can be compared to the impedance response of unprimed RAW264.7 cells.

In conclusion, EIS proved to be a convenient technique to study the complex mechanisms of action of LL-37 on cultured cell lines. Our impedance measurements confirm the ability of LL-37 to evoke a response in a variety of cultured cell lines. Moreover, we were able to detect novel activity of LL-37 in some cell types. Further dissection of the impedance responses using broad-spectrum and receptor-selective inhibitors revealed important clues about the molecular mechanisms behind the action of LL-37. Unsolved problems are primarily related to the identification of the precise molecular target of LL-37. In order to acquire more information about this matter, a number of hypotheses were formulated, accompanied by propositions for future experiments.

References

[1] G.H. Gudmundsson, B. Agerberth, J. Odeberg, T. Bergman, B. Olsson, R. Salcedo, The human gene FALL39 and processing of the cathelin precursor to the antibacterial peptide LL-37 in granulocytes, Eur.J.Biochem 238 (2) (1996) 325-332. doi:10.1111/j.1432-1033.1996.0325z.x.

[2] D. Vandamme, B. Landuyt, W. Luyten, L. Schoofs, A comprehensive summary of LL-37, the factotum human cathelicidin peptide, Cell. Immunol. 280 (1) (2012) 22–35. doi:10.1016/j.cellimm.2012.11.009.

[3] U.H.N. Dürr, U.S. Sudheendra, A. Ramamoorthy, LL-37, the only human member of the cathelicidin family of antimicrobial peptides, Biochim. Biophys. Acta. 1758 (9) (2006) 1408–25. doi:10.1016/j.bbamem.2006.03.030.

[4] M. Seil, C. Nagant, J.P. Dehaye, M. Vandenbranden, M.F. Lensink, Spotlight on human LL-37, an immunomodulatory peptide with promising cell-penetrating properties, Pharmaceuticals. 3 (11) (2010) 3435–3460. doi:10.3390/ph3113435.

[5] D. Xhindoli, S. Pacor, M. Benincasa, M. Scocchi, R. Gennaro, A. Tossi, The human cathelicidin LL-37 - A pore-forming antibacterial peptide and host-cell modulator, Biochim. Biophys. Acta - Biomembr. 1858 (3) (2015) 546-566. doi:10.1016/j.bbamem.2015.11.003.

[6] K. Kuroda, K. Okumura, H. Isogai, E. Isogai, The Human Cathelicidin Antimicrobial Peptide LL-37 and Mimics are Potential Anticancer Drugs, Front. Oncol. 5 (144) (2015) 1-10. doi:10.3389/fonc.2015.00144.

[7] R.L. Gallo, Sounding the alarm: multiple functions of host defense peptides, J. Invest. Dermatol. 128 (1) (2008) 5–6. doi:10.1038/sj.jid.5701073.

[8] A.J. Duplantier, M.L. van Hoek, The human cathelicidin antimicrobial peptide LL-37 as a potential treatment for polymicrobial infected wounds, Front. Immunol. 143 (3) (2013) 1-14. doi:10.3389/fimmu.2013.00143.

[9] J.P. Hughes, S. Rees, S.B. Kalindjian, K.L. Philpott, Principles of early drug discovery, Br. J. Pharmacol. 162 (6) (2011) 1239-1249. doi:10.1111/j.1476-5381.2010.01127.x.

[10] W. Stallaert, J.F. Dorn, E. van der Westhuizen, M. Audet, M. Bouvier, Impedance responses reveal β2-adrenergic receptor signaling pluridimensionality and allow classification of ligands with distinct signaling profiles, PLoS ONE, 7 (1) (2012) e29420. doi:10.1371/journal.pone.0029420.

[11] E. Verdonk, K. Johnson, R. McGuinness, G. Leung, Y.-W. Chen, H.R. Tang, J.M. Michelotti, V.F. Liu, Cellular dielectric spectroscopy: a label-free comprehensive platform for functional evaluation of endogenous receptors, Assay and Drug Develop. Techn. 4 (5) (2006) 609-619. doi:10.1089/adt.2006.4.609.

[12] M. Kammermann, A. Denelavas, A. Imbach, U. Grether, H. Dehmlow, C.M. Apfel, C. Hertel, Impedance measurement: a new method to detect ligand-biased receptor signaling, biochem. Biophys. Res. Comm. 412 (2011) 419-429. doi:1.1016/j.bbrc.2011.07.087.

[13] G.J. Ciambrone, V.F. Liu, .C. Lin, R.P. McGuinness, G.K. Leung, Cellular dielectric spectroscopy: a powerful new approach to label-free cellular analysis, J. Biomol. Screen. 9 (2004) 467-480.

[14] M.F. Peters, C.W. Scott. Evaluating cellular impedance assays for detection of GPCR pleiotropic signaling and functional selectivity, J. Biomol. Sc. 14 (2009) 246-255. doi:10.177/1087057108330115.

[15] W. Wu, C.H. Kim, R. Liu, M. Kucia, W. Marlicz, N. Greco, J. Ratajczak, M.J. Laughlin, M.Z. Ratajczak, The bone marrow-expressed antimicrobial cationic peptide LL-37 enhances the responsiveness of hematopoietic stem progenitor cells to an SDF-1 gradient and accelerates their engraftment after transplantation, Leukemia. 26 (4) (2012) 736–745. doi:10.1038/leu.2011.252.

[16] E. Urcan, U. Haertel, M. Styllou, R. Hickel, H. Scherthan, F.X. Reichl, Real-tim xCELLigence impedance

analysis of the cytotoxicity of dental composite components on human gingival fibroblasts, Dent. Mater. 26 (1) 2010 51-58. doi: 0.1016/j.dental.2009.08.007.

[17] A.A. Stepanenko, V.V. Dmitrenko, HEK293 in cell biology and cancer research: phenotype, karyotype, tumorigenicity, and stress-induced genome-phenotype evolution. Gene. 569 (2015) 182-190. doi: 10.1016/j.gene.2015.05.065.

[18] M.D. Bootman, T.J. Collins, L. Mackenzie, H.L. Roderick, M.J. Berridge, C.M. Peppiatt, 2-aminoethoxydiphenyl borate (2-APB) is a reliable blocker of store-operated Ca2+ entry but an inconsistent inhibitor of InsP3-induced Ca2+ release, FASEB J. 16 (10) (2002) 1145-1150. doi: 10.1096/fj.02-0037rev.

[19] Y. Dobrydneva, P. Blackmore, 2-Aminoethoxydiphenyl Borate directly inhibits store-operated calcium entry channels in human platelets, Mol. Pharmacol. 3 (2001) 541-552. doi:10.4172/2155-9538.1000e123.

[20] C.R. Halaszovich, C. Zitt, E. Jungling, A. Luckhoff, Inhibition of TRP3 channels by lanthanides block from the cytosolic side of the plasma membrane, 275 (48) (2000) 37423-37428. doi: 10.1074/jbc.M007010200.

[21] A. Mayerhofer, K.J. Föhr, K. Sterzik, M. Gratzl, Carbachol increases intracellular free caclium concentrations in human granulosa-lutein cells, J. Endocrinol. 135 (1992) 153-159.

[22] B.K. Atwood, J. Lopez, J. Wager-Miller, K. Mackie, A. Straiker, Expression of G protein-coupled receptors and related proteins in HEK293, AtT20, BV2, and N18 cell lines as revealed by microarray analysis, BMC Genomics. 12 (14) (2011) 1471-1479. doi:10.1186/1471-2164-12-14.

[23] S. Mangmool, H. Kurose, Gi/o Protein-dependent and -independent actions of Pertussis Toxin (PTX), Toxins (Basel) 3 (7) (2011) 884-889. doi:10.3390/toxins3070884.

[24] J.-Y. Lee, Y.-M. Lee, G.-C. Chang, S.-L. Yu, W.-Y. Hsieh, J.J.W. Chen, H.-W. Chen, P.-C. Yang, Curcumin induces EGFR degradation in lung adenocarcinoma and modulates p38 activation in intestine: the versatile adjuvant for gefitinib therapy, PLoS ONE. 6 (8) (2011) e23756. doi:10.1371/journal.pone.0023756.

[25] G. Weber, C.I. Chamorro, F. Granath, A. Liljegren, S. Zreika, Z. Saidak, B. Sandstedt, S. Rotstein, R. Mentaverri, F. Sánchez, A. Pivarcsi, M. Ståhle, Human antimicrobial protein hCAP18/LL-37 promotes a metastatic phenotype in breast cancer, Breast Cancer Res. 11 (1) (2009) R6. doi:10.1186/bcr2221.

[26] M. Tan, D. Yu, Molecular mechanisms of ErbB2-mediated breast cancer chemoresistance, Adv. in Exp. Med. and Biol. 608 (2007) 119-129. doi: 10.1007/978-0-387-74039-3_9.

[27] S. Derer, P. Baur, S. Lohse, A.H. Scheel, S. Berger, C. Kellner, M. Peipp, T.Valerius, Impact of EGFR cell surface expression on effector mechanisms of EGFR antibodies, J. Immunol. 189 (2012) 1-11. doi: 10.4049/jimmunol.1202037.

[28] S. Sandgren, A. Wittrup, F. Cheng, M. Jönsson, E. Eklund, S. Busch, M. Belting, The Human Antimicrobial Peptide LL-37 Transfers Extracellular DNA Plasmid to the Nuclear Compartment of Mammalian Cells *via* Lipid Rafts and Proteoglycan-dependent Endocytosis, J. Biol. Chem. 279 (17) (2004) 17951–17956. doi:10.1074/jbc.M311440200.

[29] A. Hienola, S. Tumova, E. Kulesskiy, H. Rauvala, N-syndecan deficiency impairs neural migration in brain, J. Cell Biol. 174 (4) (2006) 569-580. doi:10.1083/jcb.200602043.

[30] Y.E. Lau, A. Rozek, M.G. Scott, D.L. Goosney, D.J. Davidson, R.E.W. Hancock, Interaction and Cellular Localization of the Human Host Defense Peptide LL-37 with Interaction and Cellular Localization of the Human Host Defense Peptide LL-37 with Lung Epithelial Cells, Infect. Immun. 73 (1) (2005) 583–591. doi:10.1128/IAI.73.1.583-591.2005.

[31] M.R. Duchen, Mitochondria and calcium: from cell signalling to cell death, J. Physiol. 15 (529 Pt 1)

(2000) 57-68. doi:10.1111/j.1469-7793.2000.00057.x.

[32] G. Szabadkai, M.R. Duchen, mitochondria, the hub of cellular ca2+ signaling, Am. Physiol. Soc. 23 (2) (2008) 84-94. doi:10.1152/physiol.00046.2007.

[33] J.F. Kidd, M.R. Pilkington, M.J. Schell, K.E. Fogarty, J.N. Skepper, C.W. Taylor, P. Thorn, Paclitaxel affects cytosolic calcium signals by opening the mitochondrial permeability transition pore, J. Biol. Chem. 277 (8) (2002) 6504-6510. doi:10.1074/jbc.M106802200.

[34] H.L. Pahl, Activators and target genes of Rel/NF-κB transcription factors, Oncogene. 18 (1999) 6853-3866. doi:10.1038/sj.onc.1203239

[35] T. Schneider-Poetsch, J. Ju, D.E. Eyler, Y. Dang, S. Bhat, W.C. Merrick, R. Green, B. Shen, J.O. Liu, Inhibition of eukaryotic translation elongation by cycloheximide and lactimidomycin, Nat. Chem. Biol. 6 (3) (2010) 209-217. doi:10.1038/nchembio.304.

[36] M.D. Brand, S.M. Felber, The intracellular calcium antagonist TMB-8 [8-(NN-diethylamino)octyl-3,4,5-trimethoxybenzoate] inhibits mitochondrial ATP production in rat thymocytes, Biochem J. 224 (3) (1984) 1027-1030.

[37] Y. Chi, K. Gao, H. Zhang, M. Takeda, J. Yao, Suppression of cell membrane permeability by suramin: involvement of its inhibitory actions on connexin 43 hemichannels, BR. J. Pharmacol. 171 (14) (2014) 3448-3462. doi:10.1111/bph.12693.

[38] P.M. Dunn, A.G. Blakeley, Suramin: a reversible P2-purinoceptor antagonist in the mouse vas deferens, Br. J. Pharmacol. 93 (2) (1988) 243-245. doi:10.1111/j.1476-5381.1988.tb11427.x.

[39] M. Hüllsmann, P. Nickel, M. Kassack, G. Schmalzing, G. Lambrecht, F. Markwardt, NF449, a novel picomolar potency antagonist at human P2X1 receptors, Eur. J. Pharmacol. 471 (1-2) (2003) 1-7. doi:10.1016/S0014-2999(03)01761-8.

[40] K. Braun, J. Rettinger, M. Ganso, M. Kassack, C. Hildebrandt, H. Ullmann, P. Nickel, G. Schmalzing, G. Lambrecht, NF449: a subnanomolar potency antagonist at recombinant rat P2X1 receptors, Naunyn. Schmiedebergs Arch. Pharmacol. 364 (3) (2001) 285-290. doi:10.1007/s002100100463.

[41] S. Rost, C. Daniel, E. Schulze-Lohoff, H.G. Bäumert, G. Lambrecht, C. Hugo, P2 receptor antagonist PPADS inhibits mesangial cell proliferation in experimental mesangial proliferative glomerulonephritis, Kidney Int. 62 (5) (2002) 1659-1671. doi:10.1046/j.1523-1755.2002.00621.x.

[42] S. El-Ajouz, D. Ray, R.C. Allsopp, R.J. Evans, Molecular basisof selective antagonism of the P2X1 receptor for ATP by NF449 and suramin: contribution of basic amino acids in the cysteine-rich loop, Br. J. Pharmacol. 165 (2) (2012) 390-400. doi:10.1111/j.1476-5381.2011.01534.x.

[43] W.C. Chung, J.C. Kermode, Suramin disrupts receptor-G protein coupling by blocking association of G protein alpha and betagamma subunits, J. Pharmacol. Exp. Ther. 313 (1) (2005) 191-198. doi: 10.1124/jpet.104.078311.

[44] G. Majno, I. Joris, Apoptosis, oncosis, and necrosis. An overview of cell death. Am. J. Pathol. 146 (1) (1995) 3-15. doi:10.1177/019262339702500116.

[45] F.J. Byfield, M. Kowalski, K. Cruz, K. Leszczyńska, A. Namiot, P.B. Savage, R. Bucki, P. a Janmey, Cathelicidin LL-37 increases lung epithelial cell stiffness, decreases transepithelial permeability, and prevents epithelial invasion by Pseudomonas aeruginosa, J. Immunol. 187 (12) (2011) 6402–6409. doi:10.4049/jimmunol.1102185.

[46] De Yang, Q. Chen, A.P. Schmidt, G.M. Anderson, J.M. Wang, J. Wooters, J.J. Oppenheim, O. Chertov, LL-37, the neutrophil granule- and epithelial cell-derived cathelicidin, utilizes formyl peptide receptor-like 1 (FPRL1) as a receptor to chemoattract human peripheral blood neutrophils, monocytes, and T cells, J. Exp. Med. 192 (7) (2000) 1069–74. doi:10.1084/jem.192.7.1069.

[47] M. Seil, C. Nagant, J.P. Dehaye, M. Vandenbranden, M.F. Lensink, Spotlight on human LL-37, an immunomodulatory peptide with promising cell-penetrating properties, Pharmaceuticals. 3 (11) (2010) 3435–3460. doi:10.3390/ph3113435.

[48] A. Nijnik, J. Pistolic, A. Wyatt, S. Tam, R.E.W. Hancock, Human cathelicidin peptide LL-37 modulates the effects of IFN-gamma on APCs, J. Immunol. 183 (9) (2009) 5788–5798. doi:10.4049/jimmunol.0901491.

[49] M. Reinholz, T. Ruzicka, J. Schauber, Cathelicidin LL-37 : An Antimicrobial Peptide with a Role in Inflammatory Skin Disease, Ann. Dermatol. 24 (2) (2012) 126–135. doi:10.5021/ad2012.24.2.126.

[50] A. Di Nardo, M.H. Braff, K.R. Taylor, C. Na, R.D. Granstein, J.E. McInturff, S. Krutzik, R.L. Modlin, R.L. Gallo, Cathelicidin antimicrobial peptides block dendritic cell TLR4 activation and allergic contact sensitization, J. Immunol. 178 (3) (2007) 1829–1834. doi:10.4049/jimmunol.178.3.1829.

[51] M. Lee, X. Shi, A.E Barron, E. McGeer, P.L. McGeer, Human antimicrobial peptide LL-37 induces glial-mediated neuroinflammation, Biochem. Pharmacol. 94 (2) (2015) 130-141. doi: 10.1016/j.bcp.2015.02.003.

[52] W.K. Raja, B. Gligorijevic, J. Wyckoff, J.S. Condeelis, J. Castracane, A new chemotaxis device for cell migration studies, Integr. Biol. (Camb) 2 (11-12) (2010) 696-706. doi:10.1039/c0ib00044b.

[53] W.I. DeHaven, J.T. Smyth, R.R. Boyles, G.S. Bird, J.W.Jr. Putney, Complex actions of 2-aminoethyldiphenyl borate on store-operated calcium entry, J. Biol. Chem, 283 (28) 19265-19273. doi: 10.1074/jbc.M801535200.

[53] H. Zhou, C.S. Beevers, S. Huang, Targets of curcumin, Curr. Drug Targets. 12 (3) (2011) 332-347. doi: 10.2174/138945011794815356

[54] J. Barry, M. Fritz, J.R. Brender, P.E.S. Smith, D.-K. Lee, A. Ramamoorthy, Determining the effects of lipophillic drugs on membrane structure by solid-state NMR spectroscopy– the case of the antioxidant curcumin, J. Am. Chem. Soc. 131 (2) (2009) 4490-4498. doi:10.1021/ja809217u.

[55] Z. Oren, J.C. Lerman, G.H. Gudmundsson, B. Agerberth, Y. Shai, Structure and organization of the human antimicrobial peptide LL-37 in phospholipid membranes: relevance to the molecular basis for its non-cell-selective activity, Biochem. J. 341 (1999) 501-513. doi:10.1155/2015/679109.

[56] D.G. Perregaux, K. Bhavsar, L. Contillo, J. Shi, C.A. Gabel, Antimicrobial peptides initiate IL-1 beta posttranslational processing: a novel role beyond innate immunity, J. Immunol. 168 (6) (2002). 3024-3032. doi:10.4049/jimmunol.168.6.3024.

[57] L. Tomasinsig, C. Pizzirani, B. Skerlavaj, P. Pellegatti, S. Gulinelli, A. Tossi, F. Di Virgilio, M. Zanetti, The human cathelicidin LL-37 modulates the activities of the P2X7 receptor in a structure-dependent manner, J. Biol. Chem. 283 (5) (2008) 30471–30481. doi:10.1074/jbc.M802185200.

[58] S. Tripathi, G. Wang, M. White, M. Rynkiewicz, B. Seaton, K. Hartshorn, Identifying the critical domain of LL-37 involved in mediating neutrophil activation in the presence of influenza virus: functional and structural analysis, PLoS One. 10 (8) (2015) 1–15. doi:10.1371/journal.pone.0133454.

[59] N.M. Rao, differential susceptibility of phosphatidylcholine small unilamellar vesicles to phospholipases A2, C and D in the presence of membrane active peptides, Biochem. Biophys. Res. Commun. 182 (2) (1992) 682-688. doi:10.1016/0006-291X(92)91786-P.

[60] R. Bucki, J.J. Pastore, P. Randhawa, R. Vegners, D.J. Weiner, P.A. Janmey, Antibacterial activities of rhodamine B-conjugated gelsolin-derived peptides compared to those of the antimicrobial peptides cathelicidin LL37, magainin II and melittin, Antimicrob. Agents Chemother. 48 (5) (2004) 1526-1533. doi:10.1128/AAC.48.5.1526-1533.2004.

[61] S. Pochet, S. Tandel, S. Querriére, M. Tre-Hardy, M. Garcia-Marcos, M. De Lorenzi, M. Vandenbranden, A. Marino, M. Devleeschouwer, J.-P. Dehaye, Modulation by LL-37 of the responses of salivary glands to purinergic agonists, Mol. Pharmacol. 69 (6) (2006) 2037–2046. doi:10.1124/mol.105.021444.

[62] M. Seil, E. Kabré, C. Nagant, M. Vandenbranden, U. Fontanils, A. Marino, S. Pochet, J.-P. Dehaye, Regulation by CRAMP of the responses of murine peritoneal macrophages to extracellular ATP, Biochim. Biophys. Acta. 1798 (3) (2010) 569–78. doi:10.1016/j.bbamem.2009.11.002.

[63] B. Ding, L. Soblosky, K. Nguyen, J. Geng, X. Yu, A. Ramamoorthy, Z. Chen, Physiologically-relevant modes of membrane interactions by the human antimicrobial peptide, LL-37, revealed by SFG experiments, Sci Rep. 3 (1854) (2013) 1-8. doi:10.1038/srep01854.

[64] R. Sood, Y. Domanov, M. Pietiäinen, V.P. Kontinen, P.K.J. Kinnunen, Binding of LL-37 to model biomembranes: insight into target vs host cell recognition, Biochim.Biophys.Acta 1778 (4) (2008) 983-996. doi:10.1016/j.bbamem.2007.11.016.

[65] T. Vanden Berghe, S. Grootjans, V. Goossens, Y. Dondelinger, D.V. Krysko, N. Takahashi, P. Vandenabeele, Determination of apoptotic and necrotic cell death in vitro and in vivo, Methods (61 (2) (2013) 117-129/ doi:10.1016/j.ymeth.2013.02.011.

[66] P. Weerasinghe, L.M. Buja, Oncosis: An important non-apoptotic mode of cell death, Exp. Mol. Pathol. 93 (2012) 302-308. doi:10106/j.jexmp.2012.09.018.

[67] A.M. van der Does, H. Beekhuizen, B. Ravensbergen, T. Vos, T.H.M. Ottenhoff, J.T. van Dissel, J.W. Drijfhout, P.S. Hiemstra, P.H. Nibbering, LL-37 directs macrophage differentiation toward macropahges with a proinflammatory signature, J. Immunul. 185 (2010) 1442-1449. doi:10.4049/jimmunol.1000376.

[68] J. Sun, B. Dahlén, B. Agerberth, J.Z. Haeggström, The antimicrobial peptide LL-37 induces synthesis and release of cysteinyl leukotrienes from human eosinophils - Implications for asthma, Allergy Eur. J. Allergy Clin. Immunol. 68 (3) (2013) 304–311. doi:10.1111/all.12087.

[69] J. Trapp, R. Meier, D. Hongwiset, M.U. Kassack, W. Sippl, M. Jung, Structure-activity studies on suramin analogues as inhibitors of NAD+-dependent histone deacetylases (sirtuins), Chem. Med. Chem. 2 (2007) 1419-1431. doi: 10.1002/cmdc.200700003.

[70] S.X. Ren, J. Shen, A.S. Cheng, L. Lu, R.L. Chan, Z.J. Li, X.J. Wang, C.C. Wong, F.L.Zhang, S.S. Ng, F.L. Chan, F.K. Chan, J. Yu, J.J. Sung, W.K. Wu, C.H. Cho, FK-16derived from the anticancer peptide LL-37 induces caspase-independentapoptosis and autophagic cell death in colon cancer cells, PLoS One 8 (2013) 1–9. doi:101371/journal.pone.0063641.

[71] H.J. Park, D.H. Cho, H.J. Kim, J.Y. Lee, B.K. Cho, S.I. Bang, S.Y. Song, K.Yamasaki, A. Di Nardo, R.L. Gallo, Collagen synthesis is suppressed in dermalfibroblasts by the human antimicrobial peptide LL-37, J. Invest. Dermatol.129 (2009) 843–850. doi:10.1038/jid.2008.320.

[72] H. Tong, H.A. Rockman, W.J. Koch, C. Steenbergen, E. Murphy, G protein-coupled receptor internalization signaling is required for cardioprotection in ischemic preconditioning, Cir. Res. 94 (2004) 1133-1144. doi:10.1161/01.RES0000126048.32383.6B.

[73] T.R.H. Buch, D. Heling, E. Damm, T. Gudermann, A. Breit, Pertussis Toxin-sensitive signaling of melanocortin-4 receptors in hypothalamic GT1-7 cells defines agouti-related protein as a biased agonist, J. Biol. Chem. 284 (2009) 26411-26420. doi: 10.1074/jbc.M109.039339.

[75] A.P. Frei, O.-Y. Jeon, S. Kilcher, H. Moest, L.M. Henning, C. Jost, A. Plückthun, J. Mercer, R. Aebersold, E.M. Carreira, B. Wollscheid, Direct identification of ligand-receptor interactions on living cells and tissues, Nat. Biotechnol. 30 (10) (2012) 997–1001. doi:10.1038/nbt.2354.

[76] R.S. Ostrom, P.A. Insel, Methods for the study of signalin molecul in membrane lipid rafts and caveolae, Methods Mol. Biol. 332 (2006) 181-191. doi:10.1385/1-59745-048-0:181.

[77] M.G. Scott, D.J. Davidson, M.R. Gold, D. Bowdish, R.A.W. Hancock, The human antimicrobial peptide LL-37 is a multifunctional modulator of innate immune responses, J. Immunol. 169 (7) (2002) 3883-3891. doi:10.4049/jimmunol.169.7.3883.

Chapter V

Gaining insight into the molecular mechanism of P318

Abstract

P318 is a novel fragment of the mouse cathelicidin-related antimicrobial peptide (CRAMP) isolated from the pancreatic islets of Langerhans. Previous studies showed that P318 exerts diverse biological activities such as the activation of neural networks in the gut, induction of contractions of duodenum muscle strips, as well as antibacterial and antibiofilm activity. In addition, novel activity was discovered on HEK293T and B16 melanoma cells. To understand how P318 exerts its effects on HEK293T and B16 cells, a collection of pharmacological agents was applied to identify the cognate receptor and elucidate the signal transduction pathway. Structure-activity relationship (SAR) studies were also performed on P318 using an alanine scan library to determine the specific amino acid residues responsible for P318's activity. On HEK293T cells, strong indications were found that P318 and the human cathelicidin peptide LL-37 share a similar mechanism of action. However, it appears P318 uses a different mode of action to activate B16 melanoma cells. In these cells, the production of cAMP as a second messenger was observed upon P318 treatment. Furthermore, P318 elicited a transient calcium response and induced hyperpolarization of the cell membrane potential, upon which the signal was transduced via an Akt-dependent pathway. Taken together, our results revealed important information on the molecular mechanism behind the action of P318. This could be of great value in later stages of the research, in case P318 is implicated in a particular cellular process or pathology.

5.1 Introduction

Since the discovery of several hundred putative bioactive peptides from mammalian cells and tissues in our lab, the study of their function has been a major research topic. In this chapter, we focus on P318, which corresponds to the 318th sequence in our peptide library. P318 was discovered in the islets of Langerhans of the murine pancreas [1]. Sequence analysis revealed that P318 coincides with the C-terminal part of the mouse Cathelicidin-Related AntiMicrobial Peptide (CRAMP), a cationic host defense peptide that plays a vital role within the innate immune system [2,3]. P318 has a length of 26 amino acids and is positively charged (+5) at physiological pH. The peptide has a predicted α-helical conformation with 6 hydrophobic amino acid residues facing the same side [1,3].

Biologically active fragments of CRAMP and its human orthologue (LL-37) have been identified before, as exemplified by studies from Shin *et al.* and Murakami *et al* [4,5]. A selection of CRAMP and LL-37 derivatives along with their amino acid sequence alignment is provided in table 5.1. Some of these functional fragments were found to possess an increased antimicrobial activity in comparison to the original peptide [6]. Murakami *et al.* examined LL-37 in sweat and reported that it is further degraded by serine-proteases to yield functional fragments with enhanced antimicrobial activity [5]. Kuroda *et al.* showed that fragments of LL-37 display anticancer effects on various cancer cell lines [7]. This is in agreement with a study of Ren *et al.*, who demonstrated that a functional fragment of LL-37 suppressed the development of colon cancer [8]. Shin *et al.* reported that CRAMP analogues possessed potent antibiotic activity without increasing hemolysis [4]. In general, a variety of bioactive fragments of CRAMP and LL-37 have been demonstrated to perform important biological functions with potential clinical significance [6,7]. Understanding the precise molecular details by which cathelicidin derivatives induce functional effects on host cells can potentially provide information for the development of new drugs to treat autoimmune diseases or cancer.

Peptide	Sequence	AM, AB, AC	Ref
LL-37	LLGDFFRKSKEKIGKEF**K**R**I**V**Q**R**IK**DFLRN**LV**P**RTES	+, +, +/-	1,16-19
LL-31	LLGDFFRKSKEKIGKEF**K**R**I**V**Q**R**IK**DFLRN**L**---------	+, +, ND	1,9
FK-16	----------FKRIVQRIKDFLRNLV-------	ND, ND, +	8
KR-12	----------KRIVQRIKDFLR----------	+, ND, ND	6
CRAMP	----GLLRKGGEKIGEKL**K**K**I**G**Q**K**IK**NFFQK**LV**P**QPEQ	+, ND, +/-	1,16-19
P318	----------KIGEKL**K**K**I**G**Q**K**IK**NFFQK**LV**P**QPEQ	+, +, ND	1
AS10	----------KL**K**K**I**A**Q**K**IK**NFFQK**LVP**------	+, +, ND	1
CRAMP-18	----------GEKL**K**K**I**G**Q**K**IK**NFFQK**L**----------	+, ND, ND	1,10

Table 5.1. Amino acid sequences of LL-37 and CRAMP derivatives (conserved amino acids in bold). AM, reported antimicrobial activity in corresponding reference; AB, reported antibiofilm activity, AC, reported anticancer activity (+/- indicates that both pro- and anticancer effects of the peptide are documented); ND, not determined. KR-12 is the antibacterial core peptide of LL-37, *i.e.* the smallest peptide sequence that still displayed antimicrobial activity similar to the parent peptide.

For this reason, P318 was extensively tested for biological activity on a wide array of *in vitro* and *ex vivo* tests. For example, De Brucker *et al*. showed that P318 displayed antimicrobial and antibiofilm activity against the fungal pathogen *Candida albicans* (*C. albicans*) [1]. They demonstrated that concentrations as low as 0.15 µM of P318 prevented biofilm formation of *C. albicans* up to 2-fold without affecting planktonic survival. Additionally, the authors identified a shortened alanine-substituted variant of P318 as the most potent antibiofilm peptide which prevented biofilm formation of *C. albicans* and other Gram-positive and Gram-negative bacteria without exerting adverse effects on the viability of human endothelial cells, osteoblasts, and mesenchymal stromal cells [1]. This peptide, codenamed AS10, may have potential applications in a clinical context such as the development of biofilm-preventive coatings for medical devices and implants.

In addition to its antimicrobial, -fungal, and –biofilm effects, several other biological activities were attributed to P318. The research group of prof. Depoortere (KU Leuven) discovered inhibitory effects of P318 on electrical field-stimulated neuronal responses in rat duodenal strips, whereas the group of prof. Vanden Berghe demonstrated the ability of P318 to activate neuronal networks in the intestines of guinea pigs (unpublished data).

In the present study, the activity profile of P318 was investigated across a range of cultured cell lines using a variety of methods and techniques, including EIS, second messenger, and membrane potential assays. This activity profile may yield valuable suggestions for the role of P318 in an organism. However, in order to gain more insight into the function of P318 and to unravel the molecular mechanism(s) behind its action, knowledge about its molecular target(s) and signaling cascade is required.

A lot of valuable clues to elucidating the molecular mechanism of P318 can be deduced from the human orthologue of CRAMP, LL-37. However, even though P318 and LL-37 share 52% sequence similarity (see table 5.1), the mode of action of P318 cannot be readily deduced from knowledge of LL-37 [1,6]. On one hand, several parallel effects of CRAMP and LL-37 have been described, as exemplified by a study of Kurosaka *et al* [2]. They demonstrated that exogenous addition of CRAMP into dorsally generated air pockets on BALB/c mice resulted in the recruitment of neutrophils in a dose-dependent manner [2]. FPR2 was identified as the receptor responsible for mediating this chemotactic effect. Notably, LL-37 also uses FPR2 to induce leukocyte chemotaxis and activation [6,11]. Other cell surface receptors associated with biological activity of LL-37 also appear to recognize CRAMP. Sun *et al*. reported that CRAMP promoted pancreatic β-cell survival via EGFR activation [12]. Brandenbrug *et al.* showed that the rat homologue of LL-37 (rCRAMP) played a role in brain immunity through P2Y receptor signaling pathways [13]. Di Nardo *et al.* uncovered an

immunosuppressive role for LL-37 and CRAMP using a mouse model of allergic contact dermatitis [14]. They report that the membrane-active properties of the peptides altered receptor motility and interfered with the assembly of TLR4/CD14/MD2 receptor complex required for proper TLR4 signaling.

On the other hand, some interactions between cathelicidin peptides and receptors showed species-specific effects. For example, CRAMP provoked the inhibition but not the activation of $P2X_7$ in mice. It is possible that mouse and human $P2X_7$ have a different sensitivity towards agonists or antagonists, thereby evoking different responses to CRAMP or LL-37 [15,16]. These results imply that, depending on the cell type and context, the activation of cell surface receptors by CRAMP (or P318) and LL-37 can lead to different outcomes.

In this chapter, efforts to identify the cognate receptor(s) and elucidate the intracellular signal transduction pathway on cultured cell lines are described. Because P318 is a candidate ligand for receptors involved in various biological processes, broad-spectrum as well as receptor-selective inhibitors were administered to cultured cell lines observed to respond to P318. The results of these experiments were compared to results obtained with LL-37, to see whether P318 works through a different mode of action than LL-37. In addition, an alanine scan was performed on P318 in order to determine the contribution of each amino acid in the primary sequence to the function and/or stability of P318 [17]. The sequences of the alanine scan library used in this study are listed in table 5.2.

Peptide	Sequence
318_AS1	[H]**A**IGEKLKKIGQKIKNFFQKLVPQPEQ[NH2]
318_AS2	[H]K**A**GEKLKKIGQKIKNFFQKLVPQPEQ[NH2]
318_AS3	[H]KI**A**EKLKKIGQKIKNFFQKLVPQPEQ[NH2]
318_AS4	[H]KIG**A**KLKKIGQKIKNFFQKLVPQPEQ[NH2]
318_AS5	[H]KIGE**A**LKKIGQKIKNFFQKLVPQPEQ[NH2]
318_AS6	[H]KIGEK**A**KKIGQKIKNFFQKLVPQPEQ[NH2]
318_AS7	[H]KIGEKL**A**KIGQKIKNFFQKLVPQPEQ[NH2]
318_AS8	[H]KIGEKLK**A**IGQKIKNFFQKLVPQPEQ[NH2]
318_AS9	[H]KIGEKLKK**A**GQKIKNFFQKLVPQPEQ[NH2]
318_AS10	[H]KIGEKLKKI**A**QKIKNFFQKLVPQPEQ[NH2]
318_AS11	[H]KIGEKLKKIG**A**KIKNFFQKLVPQPEQ[NH2]
318_AS12	[H]KIGEKLKKIGQ**A**IKNFFQKLVPQPEQ[NH2]
318_AS13	[H]KIGEKLKKIGQK**A**KNFFQKLVPQPEQ[NH2]
318_AS14	[H]KIGEKLKKIGQKI**A**NFFQKLVPQPEQ[NH2]
318_AS15	[H]KIGEKLKKIGQKIK**A**FFQKLVPQPEQ[NH2]
318_AS16	[H]KIGEKLKKIGQKIKN**A**FQKLVPQPEQ[NH2]
318_AS17	[H]KIGEKLKKIGQKIKNF**A**QKLVPQPEQ[NH2]
318_AS18	[H]KIGEKLKKIGQKIKNFF**A**KLVPQPEQ[NH2]
318_AS19	[H]KIGEKLKKIGQKIKNFFQ**A**LVPQPEQ[NH2]
318_AS20	[H]KIGEKLKKIGQKIKNFFQK**A**VPQPEQ[NH2]
318_AS21	[H]KIGEKLKKIGQKIKNFFQKL**A**PQPEQ[NH2]
318_AS22	[H]KIGEKLKKIGQKIKNFFQKLV**A**QPEQ[NH2]
318_AS23	[H]KIGEKLKKIGQKIKNFFQKLVP**A**PEQ[NH2]
318_AS24	[H]KIGEKLKKIGQKIKNFFQKLVPQ**A**EQ[NH2]
318_AS25	[H]KIGEKLKKIGQKIKNFFQKLVPQP**A**Q[NH2]
318_AS26	[H]KIGEKLKKIGQKIKNFFQKLVPQPE**A**[NH2]
318_50_AS10+18+22	[H]KLKKI**A**QKIKNFF**A**KLV**A**[OH]

Table 5.2. Amino acid sequences of the alanine scan library of P318 as well as the sequence of a peptide codenamed P318_50_AS10+18+22. This peptide is an 18-amino acid truncated fragment of P318 derived from the truncated analog peptide 318_50 and containing alanine substitutions at positions 10, 18, and 22 of P318. P318_50_AS10+18+22 was shown to exhibit more potent antimicrobial activity in comparison to P318 (unpublished data). Its effect on mammalian cells has not yet been investigated.

Following this strategy, we discovered similarities between the modes of action of P318 and LL-37 on HEK293T cells. HEK293T cells were less sensitive to P318 than LL-37. Subsequent experiments using pharmacological agents sugggest that P318 interacts with the plasma membrane rather than specific receptor/ligand binding sites. This is in agreement with the proposed mechanism by which LL-37 induced impedance and calcium responses of HEK293T cells (chapter 4).

In addition, we demonstrated that P318 modulates activity of B16 mouse melanoma cells through a different mode of action than LL-37. Both calcium and cAMP were identified as second messengers when B16 cells were treated with P318. Further experiments revealed that P318 also caused hyperpolarization across the cell membrane of B16 cells. Strong indications were found that one or more GPCRs as well as potassium channels are involved in the signal transduction pathway activated by P318. Therefore, we suggest that P318 regulates B16 cell activity through a mechanism that is

more complex than the classical mechanism where a ligand is able to activate one single receptor type. It is important to obtain a thorough understanding of the molecular mechanism behind the action of P318 on melanoma cells, especially since the role of cathelicidin peptides in cancer development and metastasis is poorly understood [6,18-21].

5.2 Material and Methods

Reagents

All P318-derived peptides were synthesized by Thermo Fisher Scientific (Ulm, Germany) at a purity of at least 95% as determined by liquid chromatography and MS. All peptides were stored as a 3 mM stock solution in 70% acetonitrile at -20°C. All media and reagents including PBS, HBSS, DMEM, FBS, penicillin/streptomycin, fibronectin, puromycin, geneticin, and trypsin-EDTA (T/E) were purchased from Sigma Aldrich (St.-Louis, MO, USA). The following antagonists were also acquired from the same manufacturer: PTX, MBCD, dynasore hydrate, brefeldin A, suramin, GM6001, erlotinib HCl, BAY 11-7082, EIPA, and TMB-8. AG-1024 and CP-724714 were purchased from Selleckchem (Munich, Germany) and NF-157 and STA-21 were obtained from Santa Cruz Biotechnology (Dallas, Texas, USA). GPant-2, WKYMVm, MMK-1, WRW4, SB225002, A-438079, genistein, 10-[4'-(*N,N*-diethylamino)butyl]-2-chlorophenoxazine (10-DEBC), LOE908, TEA, 4,4'-Diisothiocyanato-2,2'stilbenedisulfonic acid (DIDS), and SCH-202676 were purchased from Tocris Bioscience (Bristol, UK). The EGFR-selective antagonist Tyrphostin AG-1478 (Tyr AG-1478) was obtained from MedChem Express (NJ, USA). To remove cell surface heparin sulfates, cells were treated with 0.01 units/ml heparinase I and/or 0.06 units/ml heparitinase (Seikagaku Corp., Tokyo, Japan) at 37°C for 40 minutes.

Cell cultures

HEK293T, A549 human lung carcinoma, RAW264.7 mouse leukemic monocyte macrophage, MRC-5 human fetal lung fibroblasts, and B16 4A5 mouse melanoma were purchased from ECACC (Porton Down, Wiltshire, UK). U-87 human glioblastoma cells transfected with a human chemokine CXCR4 receptor were a gift from the Rega Institute for medical research (Prof D. Schols, KU Leuven). All cells were freshly thawed from the liquid nitrogen stock and underwent a limited number of passages. HEK293T, A549, RAW264.7, B16 4A5, and MRC-5 cells were cultured in DMEM supplemented with 10% FBS, 100 U penicillin/0.1 mg streptomycin in a 5% CO2/95% air humidified atmosphere at 37°C. U87 (CXCR4+) cells were cultured in DMEM complemented with 10 % FBS, puromycin (1 mg/ml), and geneticin (600 µg/ml). To collect cells, they were washed with PBS and then removed from the cell culture flask with T/E (0.25 % trypsin, 0.02% EDTA).

Electrical impedance spectroscopy

Impedance measurements were performed on a proprietary EIS device (CellSine) using 96-well electronic microtiter plates purchased from ACEA Biosciences Inc (San Diego, CA, USA). For time-

dependent cell response profiling, 50 µL of culture medium was added to each well to obtain background readings. Next, 50 µL of a cell suspension was transferred to the electronic plate (40000 cells/well for HEK293T, A549, RAW264.7, MRC-5, B16 cells, and 20000 cells/well for U87 (CXCR4+) cells), followed by overnight incubation at 37°C in a humidified atmosphere at 5% CO_2. The culture medium was then replaced by medium without FBS, and 3 hours after this medium change, 10 µL of peptide solution was added. Depending on the type of experiment, antagonists were added one hour prior peptide treatment. Note that incubation times may vary depending on antagonist used. The addition of compounds was done manually inside the incubator via a modified 96-well microtiter plate cover that allows faster and more reproducible compound addition. Cells were monitored with a temporal resolution of 8 seconds per well. Once the experiment was started, each well was measured once before peptides were added. Raw impedance data were converted into a dimensionless parameter called cell index (CI), which is used to express the relative change in electrical impedance. The impedance is measured at 3 frequencies (10, 25, and 50 kHz). Data visualization was done by plotting the difference of the CI value at timepoint x with the first CI measurement, as illustrated in the following equation: $\Delta CI = CI_{[x]} - CI_{[1]}$.

$$CI = \max_{i=1,\ldots,N} \left(\frac{R_{cell}(f_i)}{R_0(f_i)} - 1 \right)$$

N = 3 for each utilized frequency (f_i).
R_{cell} = real part of the impedance behavior in presence of cells
R_0 = real part of impedance behavior during background measurement

Fluorometric calcium flux assay

Intracellular calcium levels were determined using the FluoForte calcium assay kit (Enzo Life Sciences, NY, USA) as described by the manufacturer. Cells were detached with T/E and subsequently seeded in 96-well plates at a density of 40000 cells per well. After overnight incubation at 37°C, the cells were loaded with the fluorogenic calcium binding dye for 45 minutes at 37°C and then incubated for 15 minutes at room temperature prior to assay. A 25-µl aliquot of various concentrations of the peptides, diluted in HBSS, was transferred from the compound plate to the 96-well plate containing the cells. The fluorophore was excited at 490 nm. The calcium response was monitored at 525 nm for 2 min using a FLEXStation II (Molecular Devices, New Milton, Hampshire, UK) and data were analyzed using the Softmax Pro software (Molecular Devices, New Milton, Hampshire, UK).

cAMP competitive immunoassay

The CatchPoint cAMP fluorescence assay (Molecular Devices, Sunnyvale, CA, USA) was used according to the manufacturer's instructions. Briefly, cells were seeded in standard 96-well plates and incubated overnight under standard conditions (37°C, 5% CO_2). The following day, cells were

washed with KRBG and then incubated with stimulation buffer supplemented with the phosphodiesterase antagonist IBMX. Next, peptides and control samples were added to the cells and allowed to incubate for twenty minutes at 37°C. After a lysis step, the resulting homogenate and calibrator series were transferred to a 96-well plate coated with goat anti-rabbit immunoglobulin G. Hereafter, the rabbit anti-cAMP antibody and horse radish peroxidase-cAMP conjugate were added and allowed to incubate for two hours at room temperature. Finally, the fluorescent substrate was added and the resulting signal monitored by the Flexstation II device (Molecular devices, Nem Milton, Hampshire, UK).

Fluorometric membrane potential assay

The FLIPR Membrane Potential Assay Kit (Molecular Devices, Sunnyvale, CA, USA) was used according to the manufacturer's instructions. Briefly, cells were seeded in a 96-well plate and allowed to grow overnight. The following day, the wells were loaded with a fluorescent indicator dye and allowed to incubate for thirty minutes at 37°C. Next, peptides were added to the cells by a pipetting robot included in the FLEXStation II, upon which changes in the membrane potential were measured. Instrument settings were as follows: addition volume was 50 µl, addition rate was set at 2, excitation and emission wavelengths were respectively 530 nm and 565 nm with an emission cut-off of 550 nm. Each well was measured for two minutes.

RNA-extraction and RNA-Seq

RNA extraction was performed with one million HEK293T or B16 4A5 cells using the RNeasy mini kit from Qiagen (Hilden, Germany) according to the manufacturer’s instructions. RNA-Seq was conducted by the Genomics Core UZ Leuven using Illumina HiSeq system. For a detailed description of the workflow, the reader is referred to the material and methods section of chapter seven.

Statistical analysis

GraphPad Prism 5.1 (GraphPad software, La Jolla, CA, USA) was used to analyze raw data from EIS, RNA-Seq, calcium mobilization, cAMP, and membrane potential assays. Note that the temporal resolution of EIS measurements was 8 seconds per well. As a consequence, the final temporal resolution depends on the number of wells. In most cases, 4 wells were measured and 1 example of the impedance response of at least two experiments was displayed. Statistical analysis of the results from cAMP, calcium mobilization, and membrane potential assays was performed using Student’s t-tests or one-way analysis of variance (ANOVA) followed by Dunnett’s multiple comparisons test. P-values < 0.05 were considered statistically significant. In most cases, experiments were performed in triplicate and repeated twice, unless stated otherwise.

5.3 Results

5.3.1 Characterizing the effect of P318 on HEK293T cells

P318 has previously been tested for activity on a panel of cultured cell lines, employing different methods such as EIS and second messenger assays. These screening experiments were conducted at a peptide concentration of 3 µM. At this concentration, HEK293T cells did not respond to P318 (Dieter Vandamme, Schoofs lab, personal communication). However, we discovered that LL-37 evoked an impedance and calcium response of various cell types (chapter 4). This observation prompted us to re-examine if higher concentrations of P318 were able to induce a calcium and/or impedance response of HEK293T cells.

As depicted in figure 5.1-A, P318-induced impedance responses of HEK293T cells were detected, which were likely dose-dependent. In addition, P318 elicited a dose-dependent transient calcium increase in HEK293T cells (figure 5.1-B). In analogy with the action of LL-37 on HEK293T cells (see chapter 4), the mouse orthologue of LL-37 (CRAMP) also evoked impedance and calcium responses in HEK293T cells (figures 5.1-C and E). The impedance responses shown in figure 5.1-C suggest that HEK293T cells respond more strongly to LL-37 than to CRAMP or P318. More specifically, P318 appears to be the least potent peptide, when comparing the calcium as well as the impedance response of HEK293T cells to P318 versus CRAMP (figures 5.1-C and E).

The impedance responses generated by P318 and CRAMP share common characteristics with the impedance signature of LL-37, since both short- and long-term effects of P318 and CRAMP were detected (figure 5.1-C). This suggests that cathelicidin peptides such as CRAMP, P318, and LL-37 work through a similar mechanism of action. However, the long-term impedance response of HEK293T cells to P318 was less pronounced than the long-term response to CRAMP and LL-37. As proposed in chapter 4, the second impedance response to LL-37 might be associated with the emergence of cytotoxic effects induced by peptide treatment. Therefore, it is conceivable that P318 has a different toxicity profile than CRAMP and LL-37. This hypothesis is supported by comparing the calcium response of HEK293T cells to a toxic concentration (25 µM) of LL-37 with the calcium response to the same concentration of P318 (figure 5.1-D). A sustained calcium response rather than a transient response was detected when HEK293T cells were treated with 25 µM of LL-37. This could be due to the membrane-damaging effect of LL-37, which causes dye leakage into the extracellular environment. However, a reversible calcium response was observed when HEK293T cells were treated with 25 µM of P318. Furthermore, we previously showed that LL-37 (≥ 20 µM) modified cell morphology and negatively affected HEK293T cell viability (chapter 4). These drastic morphological changes were not noticed when HEK293T cells were preincubated with a dilution series of P318 (1-50

μM) and microscopically inspected 6 hours post-stimulation to check for signs of deterioration. Taken together, these observations imply that HEK293T cells are better able to tolerate higher doses of P318 than LL-37.

Subsequently, a collection of broad-spectrum and receptor-selective antagonists were applied to gain insight into the mechanism of action of P318 on HEK293T cells. The results obtained with these pharmacological agents were largely similar to those of LL-37 (chapter 4). For example, pre-exposure of HEK293T cells to 2-APB (p-value from Student's t-test when comparing experimental groups LL-37 vs. LL-37 + 2-APB is 0.02) or suramin (p-value = 0.052) inhibited the calcium response to P318 (10 μM), whereas preincubation with MBCD (p-value = 0.14) reinforced the effect of P318 (figure 5.1-D). P318 also evoked a calcium response in medium depleted of free calcium, suggesting a contribution of calcium release from intracellular stores.

HEK293T cells expressed mRNA of EGFR, ErbB2, IGF1R, and P2Y11R (chapter 4). However, antagonists displaying selectivity for these candidate receptors were not able to block the effect of P318 (figure 5.1-D). Broad-spectrum GPCR and RTK inhibitors such as PTX (200 ng/ml), GPant2 (10 μM), genistein (10 μM), and curcumin (20 μM) as well as FPR2-, CXCR2-, and $P2X_7$-selective inhibitors (10 μM) were also unable to inhibit the calcium response of HEK293T cells to P318. These results point more into the direction of a membrane-dependent mechanism of action for P318, as we have suggested for LL-37 (chapter 4). However, it remains to be elucidated whether the decreased activity of P318 relative to LL-37 is due to a decreased capability of the peptide to interact with the plasma membrane.

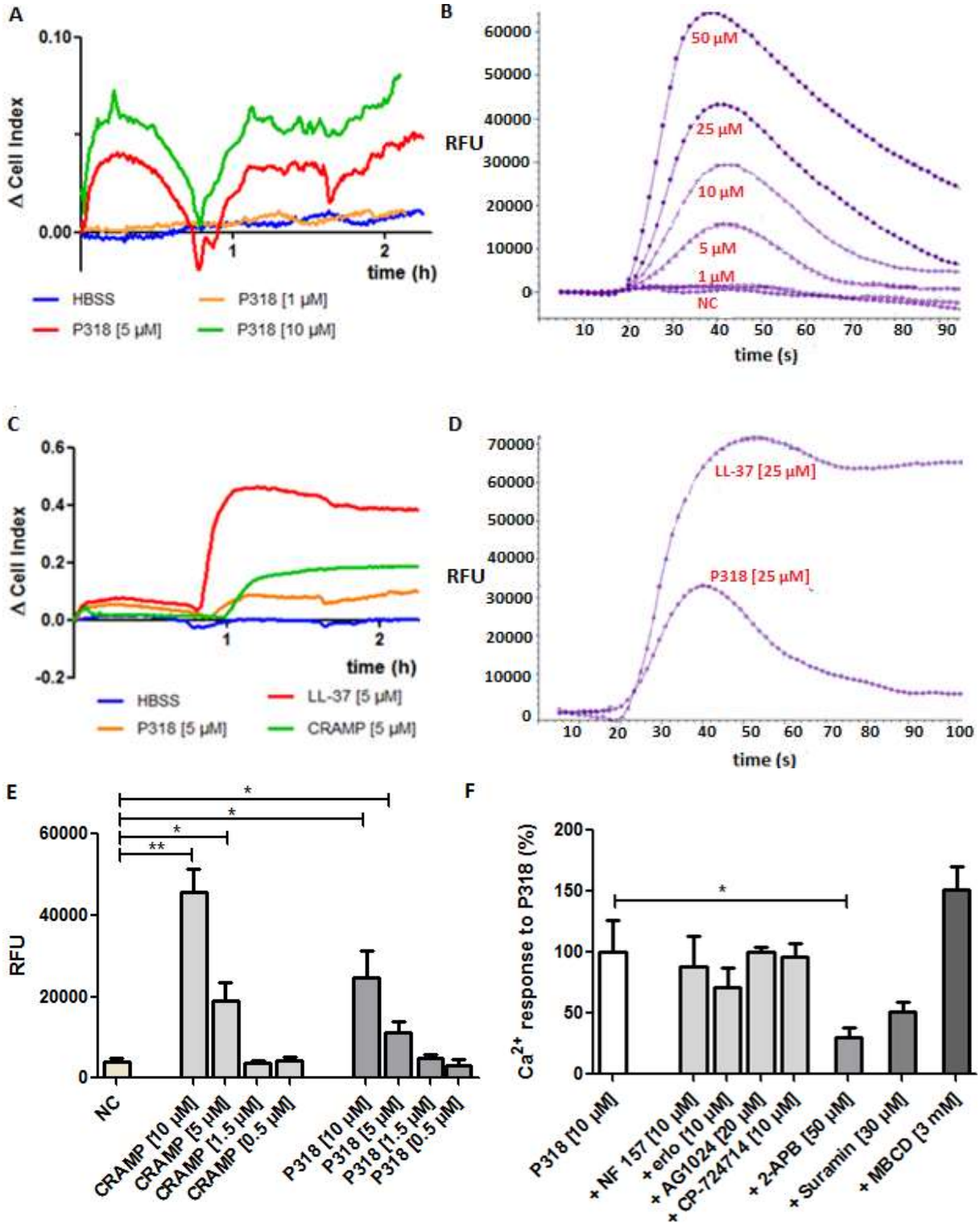

Fig.5.1. Plot of ΔCI over time (hours), reflecting the effect of 1 µM (orange), 5 µM (green), and 10 µM (red) of P318 on HEK293T cells. HBSS (blue) was used as a negative control (**A**). Raw data obtained with a fluorescence-based calcium assay showing the reversible calcium increase in HEK293T cells upon P318 administration (RFU value of peak height) (**B**). Graph **C** depicts the impedance response of HEK293T cells to 5 µM of LL-37 (red), CRAMP (green), or P318 (orange). HBSS (blue) was used as a negative control. Graph **D** shows the transient calcium response of HEK293T cells to P318 (25 µM) as well as the calcium response to 25 µM of LL-37. Cytotoxic effects induced by LL-37 can potentially occur, characterized by a sustained calcium plateau. CRAMP, the mouse orthologue of LL-37, evoked a stronger calcium response compared to P318 (*N*=6; results presented as mean± SEM). Significance levels are indicated by asterisks which represent p-values from Student's t-test: *, $p < 0.05$ and **, $p < 0.005$ when compared with the negative buffer control (NC) (**E**). Various antagonists for

several of the purported receptors for LL-37 were unable to block the calcium response of HEK293T cells to P318 (**F**). NF157 is a P2Y11R inhibitor, whereas erlotinib HCl (erlo) displays selectivity for EGFR. AG1024 inhibits IGF1R activation and CP-724714 is an ErbB2-selective antagonist. Pretreatment with 2-APB (antagonist of IP_3R) or suramin exerted an inhibitory effect on the calcium response to the peptide, whereas the cholesterol-depleting agent MBCD augmented the calcium response of HEK293T cells to P318. Significance levels are indicated by asterisks which represent p-values from Student's t-test: *, $p < 0.05$ (*N*=6; results are presented as mean ± SEM).

Next, SAR studies on P318 were performed in a search for more potent analogues. By performing an alanine scan of P318, important amino acid residues responsible for the activity of P318 can be identified. Peptides of the alanine scan library were tested at a concentration of 10 µM upon which the calcium response of HEK293T cells was monitored. The results are displayed as percentage of the calcium response to P318 (figure 5.2). The 3 peptides eliciting the strongest calcium response were those containing alanine substitutions at positions 11 (mean ± SEM: 145.8 ± 9.5), 18 (mean ± SEM: 134.8 ± 6.6), and 24 (mean ± SEM: 109.3 ± 9.2), whereas the 3 peptides eliciting the weakest calcium flux contained alanine substitutions at sites 13 (mean ± SEM: 42.7 ± 7.1), 16 (mean ± SEM: 51.5 ± 11.5), and 17 (mean ± SEM: 53.7 ± 8) of the original sequence.

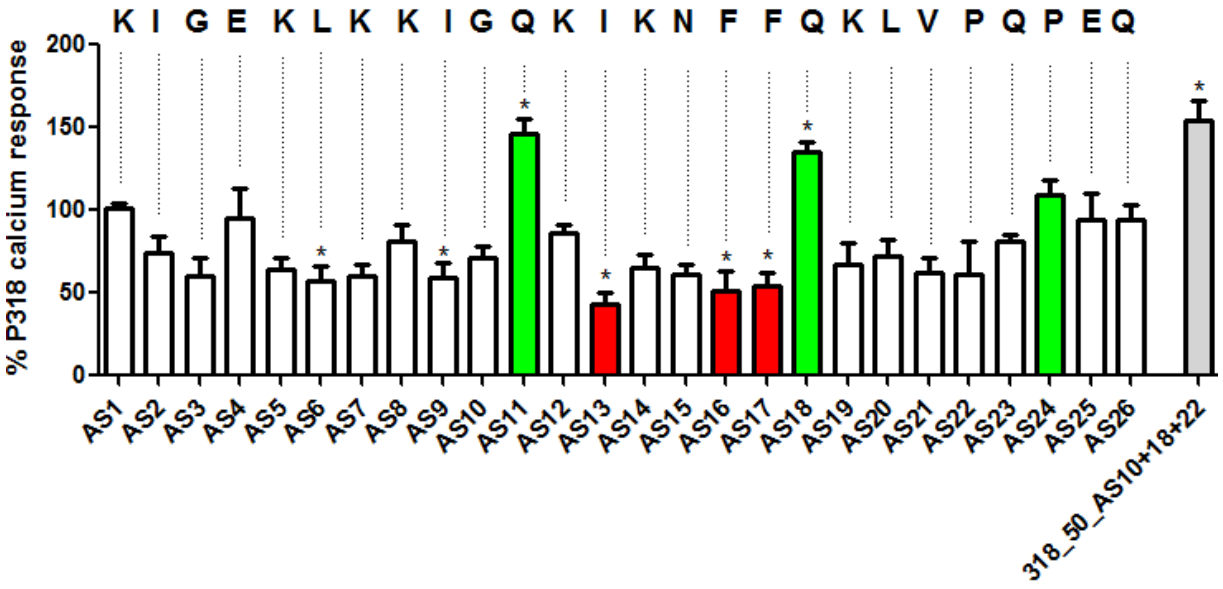

Fig.5.2. Graph displaying the calcium response of HEK293T cells to peptides of the alanine scan library of P318, as well as to P318_50_AS10+18+22. Each peptide was tested at a final concentration of 10 µM. Top 3 peptide analogues eliciting the highest (largest mean absolute RFU value) calcium flux are colored green, whereas top 3 peptides eliciting the lowest (smallest mean absolute RFU value) calcium flux are colored red. Results are shown as percentage of the original peptide (P318). Experiments were conducted in duplicate and repeated twice, hence 4 datapoints were obtained for each peptide. The statistical significance was tested with one-way analysis of variance (ANOVA) followed by Dunnett's test (*, $p < 0.05$). Error bars reflect SEM.

The peptide analogue P318_50_AS10+18+22 was also included in this study and this peptide variant elicited a stronger calcium response in comparison to P318 (figures 5.2 and 5.3-A). This difference was significant (p-value from Student's t-test when comparing P318 vs P318_50_AS10+18+22 is 0.03). It is relevant to mention that receptor-selective antagonists displaying selectivity for candidate receptors of P318 were also added to HEK293T cells prior to P318_50_AS10+18+22 treatment.

However, none of the receptor-specific antagonists exerted an inhibitory effect on the calcium response to P318_50_AS10+18+22.

HEK293T cells were treated with a dilution series of P318_50_AS10+18+22 and the mobilization of intracellular calcium was measured by a fluorometric calcium-flux assay (figure 5.3-A). Even though P318_50_AS10+18+22 evoked a stronger calcium response of HEK293T cells than P318, only a small change in the fluorescence intensity signal was detected when HEK293T cells were exposed to 1.5 µM of P318_50_AS10+18+22. At this concentration, HEK293T cells responded more strongly to 1.5 µM of LL-37 (chapter 4), highlighting the higher potency of LL-37 relative to P318_50_AS10+18+22. Next, cAMP assays were employed to investigate if the peptide analogues had gained the ability to produce cAMP. However, no changes in cAMP production compared to untreated HEK293T cells were observed (figure 5.3-B; only the cAMP production evoked by AS11, AS18, AS24, and P318_50_AS10+18+22 are displayed).

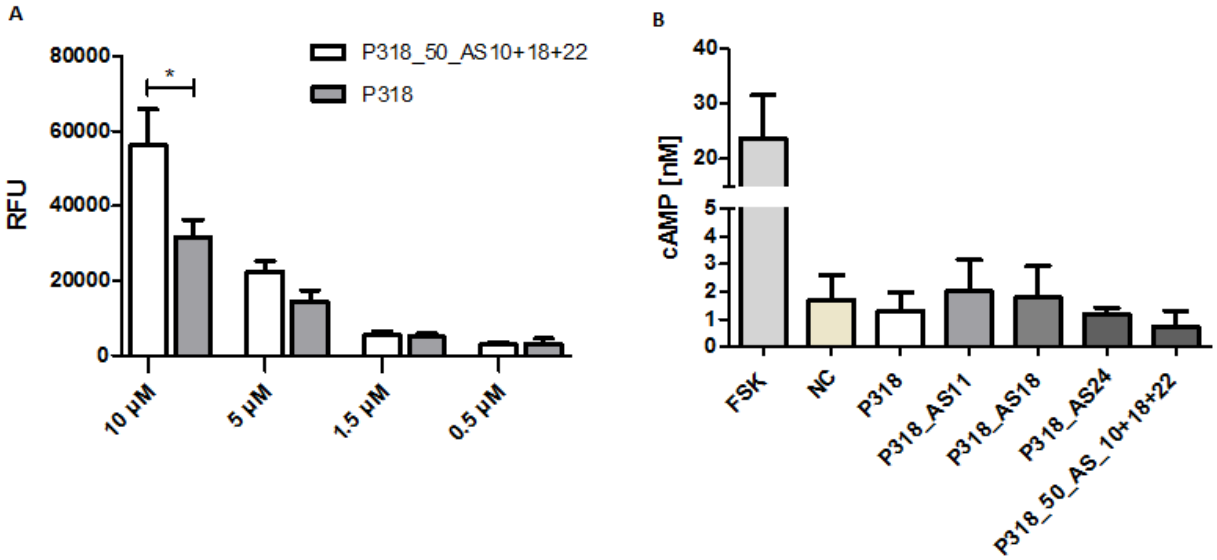

Fig.5.3. Graph **A** shows the calcium mobilization in response to a dilution series of P318_50_AS10+18+22 as well as P318 in HEK293T cells. Significance level is represented by an asterisk which indicates p-value from Student's t-test: *, $p < 0.05$. Results are mean ± SEM (*N*=6). Graph **B** shows the amount of cAMP (in nM) produced in HEK293T cells upon addition of P318 or 3 peptides of the alanine scan library of P318. FSK (20 µM) is used as a positive control. Graphs represent the mean of 3 measurements. Error bars represent SEM.

5.3.2 Characterizing the effect of P318 on B16 cells

After we discovered that P318 mobilized calcium from intracellular stores in HEK293T cells, other cell types were tested for their ability to respond to P318. To allow for a straightforward comparison with the effects of LL-37, only the calcium responses of HEK293T, A549, RAW264.7, U87 (CXCR4+), and MRC-5 cells are shown in figure 5.4. In addition, cAMP assays were performed to determine if P318 induced the production of cAMP by adenylyl cyclase in these cell types.

At a concentration of 10 µM, neither calcium mobilization nor cAMP production were detected or reached significant levels upon P318 treatment in RAW264.7, A549, U87 (CXCR4+), and MRC-5 cells (figure 5.4-A). However, P318 evoked a significant calcium response in HEK293T and B16 cells. Notably, P318 also induced the production of cAMP by adenylyl cyclase in B16 cells.

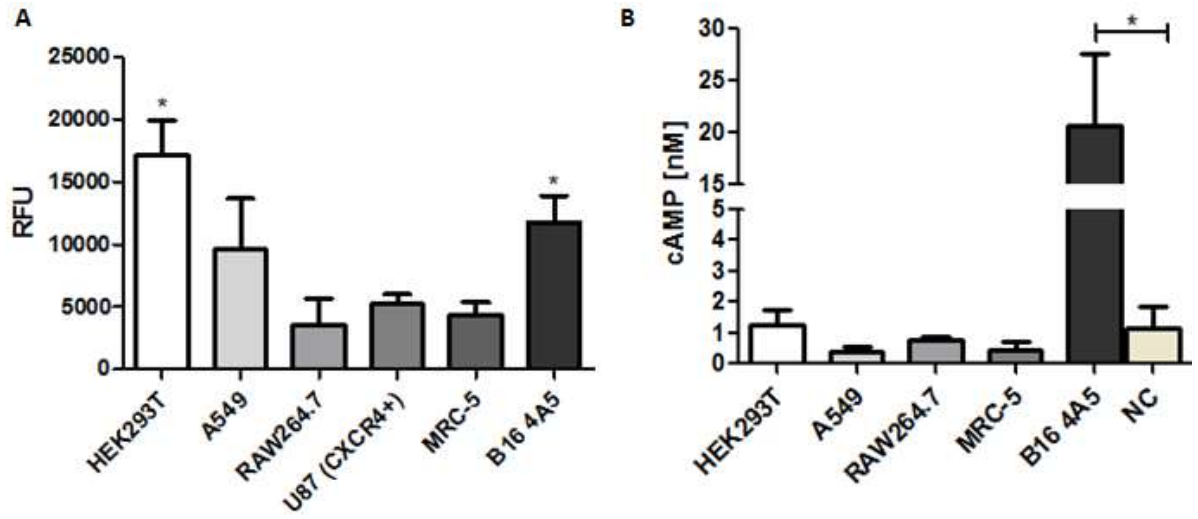

Fig.5.4. Graph **A** shows the calcium response of several cultured cell lines to P318 (10 µM). Results are presented as mean ± SEM (*N*=6). Graph **B** shows the cAMP production expressed in nanomolar concentration upon stimulation with P318. Error bars reflect SEM (*N*=3). In both graphs, significance levels are indicated by asterisks which represent p-values from Student's t-test: *, $p < 0.05$ when compared with the negative buffer control (NC).

Subsequent experiments focused on the effect of P318 on B16 cells, as the role of cathelicidin peptides in cancer is poorly understood. Previous research revealed that the FPR2-specific antagonist WRW4 (1 µM) completely inhibited the cAMP production induced by P318, favoring FPR2 as the cognate receptor for P318 on B16 cells (Dieter Vandamme, Schoofs lab, personal communication). However, follow-up experiments using Enzyme Fragment Complementation (EFC) technology to validate the role of FPR2 were inconclusive. EFC technology (DiscoveRx Corporation, Fremont, CA 94538, USA) relies on intracellular formation of an active β-galactosidase enzyme that hydrolyzes substrate to generate a chemiluminescent signal.

To explain these inconclusive results, a replication study was performed to investigate whether WRW4 was capable of abrogating the effect of P318. As depicted in figures 5-A and 5-B, WRW4 failed to suppress either the calcium or cAMP response of B16 cells to P318. The calcium mobilization and cAMP production evoked by P318 were also not cross-desensitized by stimulating B16 cells with the FPR2-specific ligands MMK-1 or WKYMVm. Furthermore, expression of FPR2 was not detected using RNA-Seq (figure 5.4-D). Taken together, these observations cast considerable doubt on the hypothesis that FPR2 is a cognate receptor for P318 in B16 cells.

Among the candidate receptors for LL-37, hence P318, only mRNA expression of IGF1R and $P2X_7$ was observed (figure 5.4-D). Based on this observation, IGF1R- and $P2X_7$-selective antagonists were added to B16 cells prior to P318 treatment. However, these antagonists were unable to exert an inhibitory effect on the calcium or cAMP response of B16 cells to P318 (figures 5.5-A and B).

However, the cAMP production upon addition of P318 to B16 cells was significantly inhibited by the broad-spectrum GPCR antagonist GPant-2. The allosteric GPCR inhibitor SCH-202676 exerted a similar inhibitory effect (figure 5.5-B). This observation suggests that one or more types of GPCRs are responsible for mediating the cAMP production in B16 cells. However, the identity of this low-affinity receptor for P318 is currently unknown.

None of the antagonists tested, including GPant-2 and SCH-202676, exerted a significant inhibitory effect on the calcium response to P318. This might indicate that P318 mobilizes intracellular calcium by first binding to the cell membrane. The binding of P318 to the plasma membrane could indirectly activate cell surface receptors, leading to calcium mobilization. However, it is also possible that P318 affects the lipid packing of the cell membrane and directly modulates the activity of membrane-bound enzymes such as PLC.

The effect of P318 on B16 cells was also detected by EIS. At a concentration of 10 µM, the maximum activity of P318 occurred approximately 2 hours post-addition upon which a plateau was reached which is sustained until the end of the measurement (figure 5.5-C). To confirm the hypothesis that GPCRs play a role in the mode of action of P318, B16 cells were preincubated with GPant-2 prior to P318 treatment. Despite the small effect of the GPant-2 antagonist itself on B16 cells (orange), conclusions on the ability to block the effect of P318 can be made when comparing the impedance response of GPant-2-treated versus untreated B16 cells to P318.

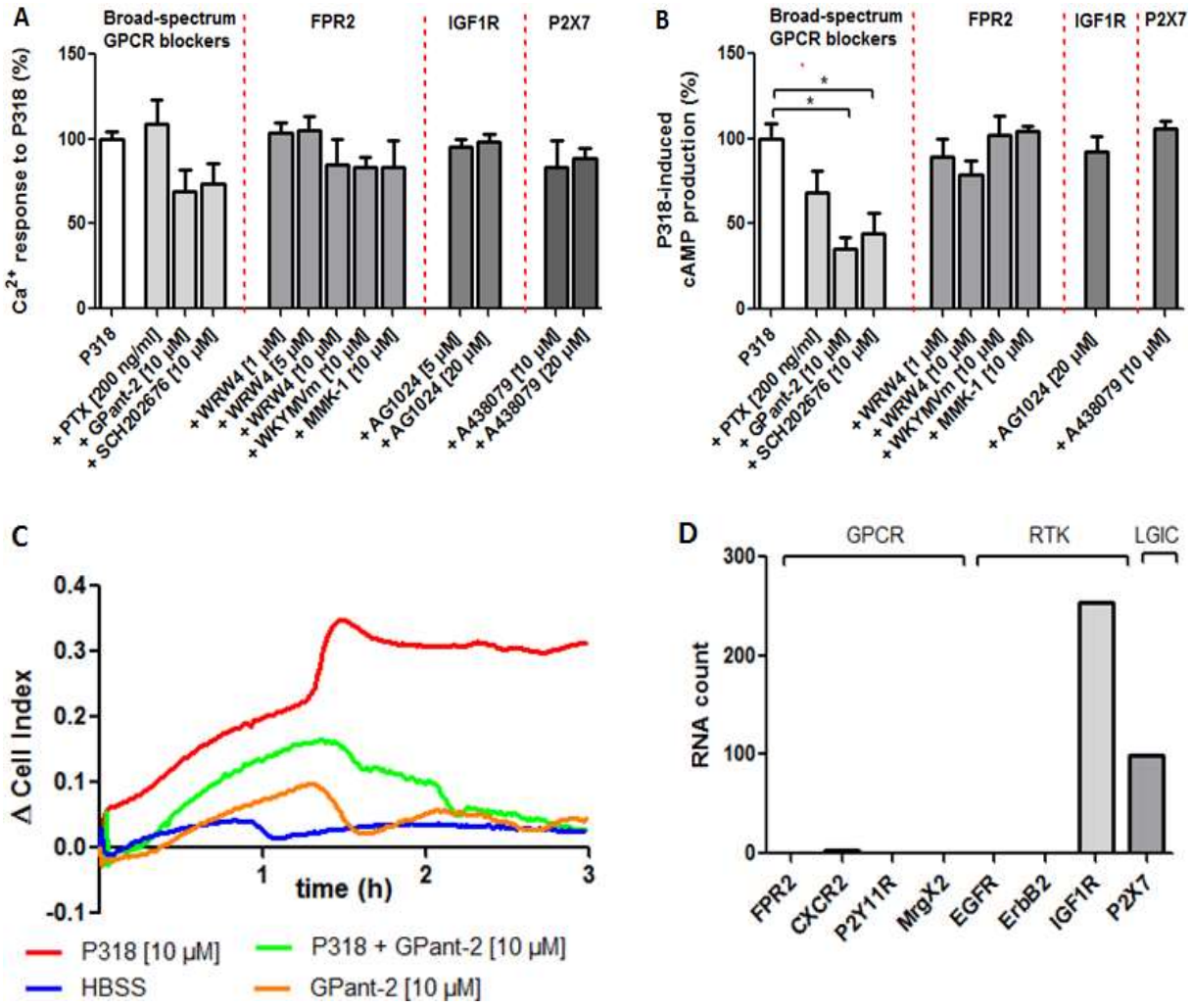

Fig.5.5. Graph **A** shows the effect of several broad-spectrum and receptor-selective inhibitors on the calcium response of B16 cells to 10 µM of P318 (*N*=6). PTX, GPant-2, and SCH202676 are broad-spectrum GPCR antagonists. WRW4, AG1024, and A438079 are selective antagonists of FPR2, IGF1R, and $P2X_7$ signaling respectively. WKYMVm and MMK-1 are selective agonists of FPR2 signaling. Graph **B** depicts the effect of the same set of pharmacological agents on the cAMP production induced by P318 (*N*=3; Significance level is represented by an asterisk which indicates p-value from Student's t-test: *, $p < 0.05$). GPant-2 and SCH202676 partially inhibited the cAMP response evoked by P318. The effect of P318 (red) as well as the inhibitory effect of GPant-2 on the impedance response to P318 (green) was also detected by EIS (graph **C**). The experiment was repeated twice and one representative example is shown. The calcium response and cAMP production upon addition of P318 to B16 cells was not blocked by the FPR2-selective antagonist WRW4 or desensitized by FPR2-selective agonists, indicating that FPR2 is not involved in the mode of action of P318. In agreement with this observation, expression of FPR2 was not detected in B16 cells (graph **D**).

We also excluded the possibility that the effect of P318 was mediated by syndecans. Syndecans act as co-receptors for several receptors, including EGFR, IGF1R, and GPCRs [21,22]. In mammals, 4 genes encode syndecans which are expressed in a cell-type-, development-, and tissue-specific manner. It is known that individual cell lines have different combinations of syndecan receptors as well as varying combinations of other cell surface receptors. This may contribute to the different activity profile of P318 on several cell lines. Because B16 cells expressed mRNA of all 4 syndecans, we hypothesized that this could be one of the reasons why B16 cells were more sensitive to P318 than

other cell types (figure 5.6-A). However, when syndecans were degraded by heparinase and/or heparitinase treatment, the calcium or cAMP response of B16 cells to P318 was not altered (figure 5.6-B).

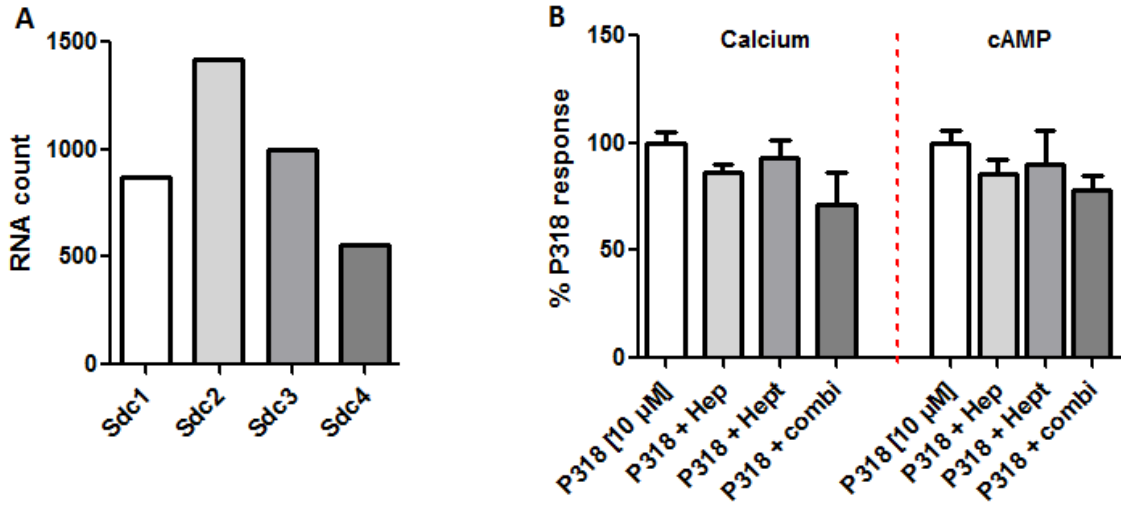

Fig.5.6. mRNA expression of genes encoding the four syndecans in B16 mouse melanoma cells (**A**). B16 cells were treated with 0.01 units/ml heparinase (Hep), 0.06 units/ml heparitinase (Hept), or a combination (combi) for 40 minutes prior to P318 treatment (**B**). Hep and Hept are enzymes which remove cell surface heparan sulfates. No effect on the calcium (N=6) or cAMP response (*N*=2) of B16 cells to P318 was observed.

Based on the literature concerning LL-37, several signal transduction pathways appear to be frequently involved, including the NF-κB pathway and the STAT3 pathway [23-25]. Because it is possible that the same pathways were activated by P318, we preincubated B16 cells with a specific NF-κB-antagonist (BAY 11-7082; 10 µM) or a specific STAT3-antagonist (STA-21; 10 µM) prior to P318 treatment. However, these antagonists were not able to alter the impedance response to P318 (data not shown). Notably, EGFR-selective antagonists such as erlotinib HCl (10 µM) and AG-1478 (10 µM) as well as the broad-spectrum MMP inhibitor GM6001 (25 µM) could not suppress the impedance response to P318, suggesting that P318 did not activate B16 cells via EGFR (trans)activation (data not shown). Several endocytic inhibitors were also tested, including brefeldin A (20 µM), dynasore (10 µM), and MDC (10 µM). Preliminary results indicated that these blockers were unable to inhibit the impedance response of B16 cells to P318.

However, the specific Akt-antagonist 10-DEBC inhibited the impedance response to P318 (figure 5.7-A). Interestingly, 10-DEBC did not exert the same effect on the impedance response of B16 cells to LL-37 (figure 5.7-B). These results imply that P318 activates an Akt-dependent pathway in B16 cells. In addition, it suggests that P318 and LL-37 do not share the same mechanism of action on B16 cells. This hypothesis is further supported by the observation that only P318 induced cAMP production (and not LL-37).

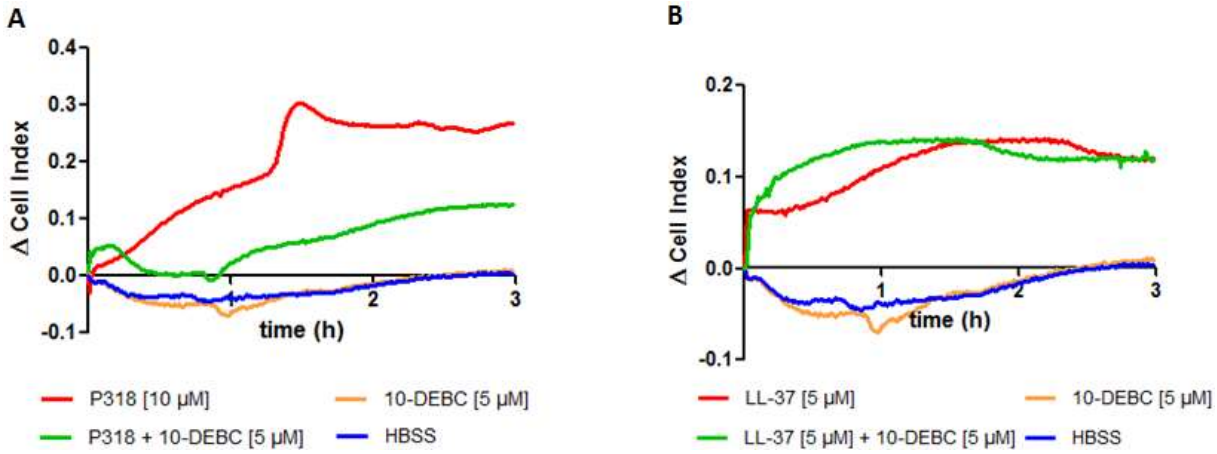

Fig.5.7. Panel of graphs showing the effect of the Akt antagonist 10-DEBC (5 µM) on the impedance response of B16 cells to P318 (**A**) or LL-37 (**B**). Experiments are repeated at least two times.

Previous research (Dieter Vandamme, Schoofs lab, personal communication) also indicated that P318 (10 µM) induced a hyperpolarization across the cell membrane of B16 cells, which could be related to the activation of certain ion channels. Hyperpolarization refers to the change of a cell's membrane potential that makes it more negative. This can be caused by an influx of anions such as chloride ions or an efflux of cations such as potassium ions. Figure 5.8 depicts the dose-response effect of P318 (1-10 µM) on B16 cells. KCl (30 mM) was used as a positive control, as it is known to depolarize cells.

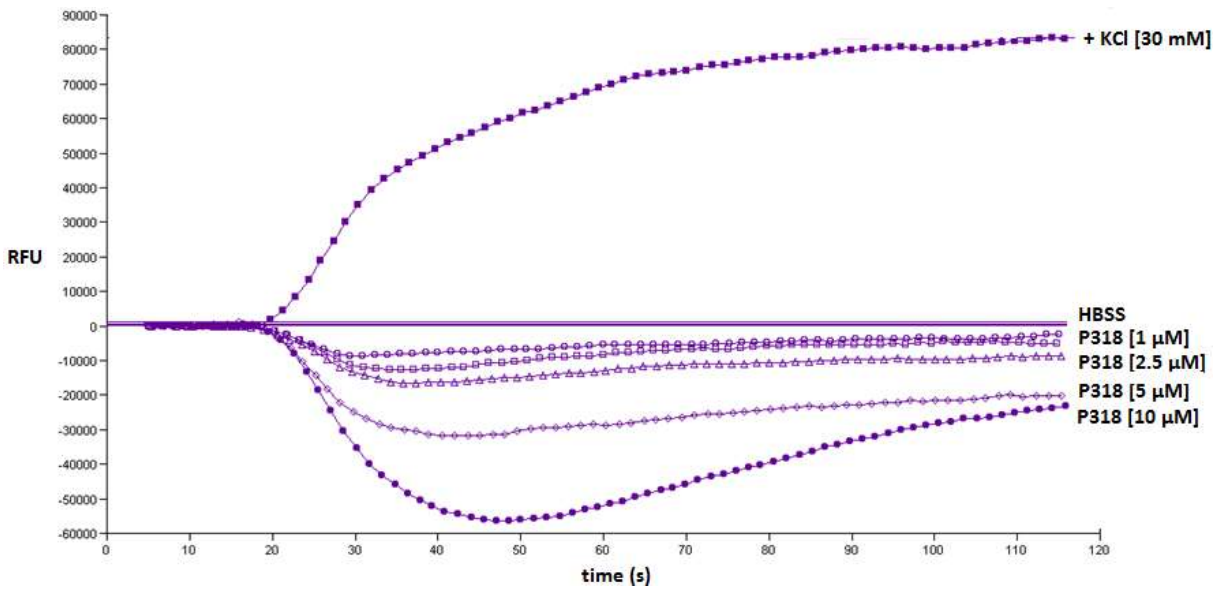

Fig.5.8. Dose-response curve of P318 (1-10 µM) on B16 mouse melanoma cells. During P318-induced membrane hyperpolarization, the fluorescent signal (expressed as RFUs) decreases in intensity as the dye follows the positively charged ions out of the cell. KCL-induced depolarization results in additional dye influx and an increase in fluorescence.

The only calcium-permeable channel identified so far as activated by LL-37 is the human purinergic receptor $P2X_7$ [4,5,6]. Because B16 cells expressed mRNA of $P2X_7$ (figure 5-D), a $P2X_7$-selective ion channel antagonist (A-438079) was applied to B16 cells and its effect on the hyperpolarization

induced by P318 was measured (figure 5.9-A). Additionally, EIS was used to examine whether A-438079 altered the impedance response to P318 (figure 5.9-B). Both assays revealed that A-438079 did not abrogate the effect of P318. Because A-438079 also failed to suppress the calcium or cAMP response to P318, it can be concluded that $P2X_7$ is not a cognate receptor for P318 in B16 cells (figures 5.9-A and B)

Subsequent experiments were conducted to determine if P318 induces the activation of ion channels via specific molecular interactions or operates by virtue of a passive process that involves the formation of pores. Previous research indicated that the nonselective cation channel antagonist LOE908 inhibited the hyperpolarization induced by P318 (figures 5.9-A and C). Since the effect of P318 can be diminished by an inhibitor, the possibility that P318 acts by permeabilizing the cell membrane becomes less likely.

To determine which type of ion channel might be activated by P318, several ion channel antagonists were used. B16 cells were pretreated with DIDS (a chloride channel blocker), $LaCl_3$ (a non-selective calcium channel blocker), TEA (a non-selective potassium channel blocker), EIPA (a blocker of the sodium-hydrogen antiport), or LOE908 (broad-spectrum cation channel blocker, including SOCs and voltage-operated calcium channels) prior to P318 administration. Among the antagonists tested, only TEA and LOE908 exerted an inhibitory effect on the hyperpolarization induced by P318 (figures 5.9-A and C).

The results obtained with TEA suggest that potassium channels play a role in the mechanism of action of P318. It is possible that P318-induced calcium mobilization activates calcium-activated potassium channels, which in turn leads to membrane hyperpolarization. A similar mode of action was recently proposed for LL-37 by Gambade *et al* [26]. The authors used D-enantiomers of LL-37 to demonstrate that no binding to a specific receptor was involved. This is in agreement with our observation that the calcium response of B16 cells to P318 could not be blocked by pretreating cells with receptor-selective antagonists for candidate receptors of LL-37/P318. Furthermore, Gambade *et al*. showed that LL-37 activated the Akt signal transduction pathway in breast cancer cells. This is in accordance with our observation that the specific Akt-antagonists 10-DEBC exerted an inhibitory effect on the impedance response to P318 (figure 5.7-A).

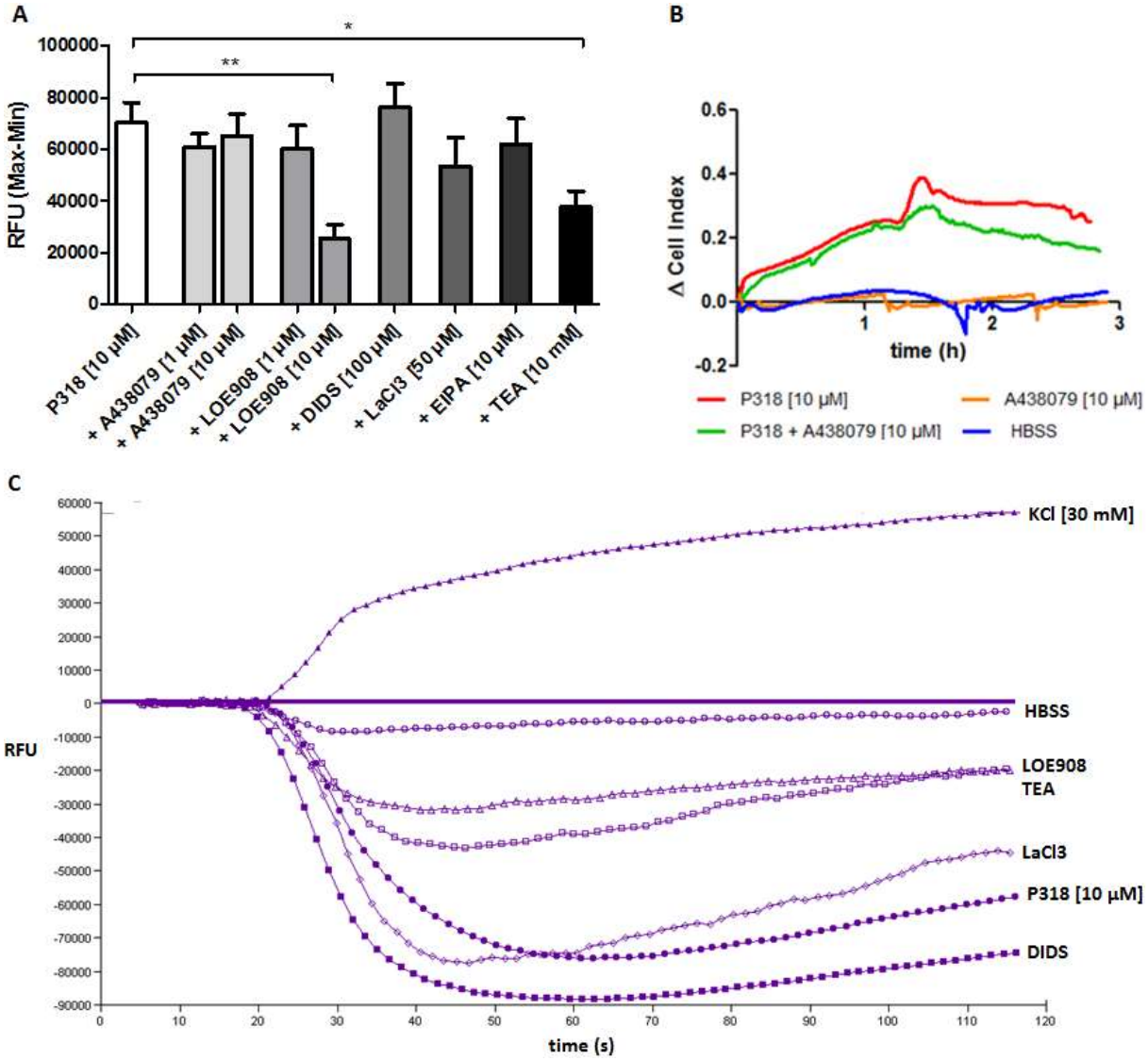

Fig.5.9. Graph **A** depicts the effect of several ion channel antagonists on the effect of P318 [10 µM] on B16 cells. The non-selective cation channel antagonist LOE908 [10 µM] and the potassium channel antagonist TEA [10 mM] exerted an inhibitory effect on the hyperpolarization induced by P318, whereas DIDS (a chloride channel inhibitor) and $LaCl_3$ (a non-selective calcium channel inhibitor) exerted no blocking effect. Bars represent the amount of hyperpolarization expressed as RFUs (*N*=6). Significance levels are reflected by asterisks which indicate p-values from Student's t-test: **, $p < 0.005$ and *, $p < 0.05$. Graph **C** shows raw data of a membrane potential experiment in which the activity of several ion channel antagonists was tested. The specific $P2X_7$ antagonist A-438079 could not block the hyperpolarization or impedance response to P318, suggesting that this receptor did not play a role in the mode of action of P318 (**B**).

SAR studies were also performed on P318 to identify more selective and/or more potent analogues. Previously, a library containing truncated series from the N-terminus, the C-terminus, or both termini were added to B16 cells. The most potent analogue was P318_30, as measured through a cAMP assay (Dieter Vandamme, Schoofs lab, personal communication). This peptide analogue exhibited a lower EC_{50} value (1.853 µM) than the original P318 (2.5 µM). Therefore, P318_30 can be seen as a full agonist and P318 as a partial agonist.

Furthermore, alanine scanning mutagenesis was used to determine the specific contribution of a particular amino acid to the stability or function of P318. These experiments revealed that most P318 analogues retained their activity to induce cAMP production in B16 cells, although most peptides show a decreased activity. However, P318_AS11 was shown to induce a higher cAMP production compared to the original peptide in B16 cells. Note that P318_AS11 also induced a stronger calcium response in HEK293T cells (figure 5.2).

Peptides of the alanine scan library were tested for their ability to mobilize intracellular calcium in B16 cells (figure 5.10). To allow for a more straightforward comparison with SAR studies of P318 on HEK293T cells, P318_50_AS10+18+22 was also included in this study. The three peptides eliciting the strongest calcium response were those with alanine substitutions at position 11 (mean ± SEM: 121.8 ± 8.3), 23 (mean ± SEM: 112.3 ± 4.3), and 25 (mean ± SEM: 105.8 ± 4.3), whereas the three peptides eliciting the weakest calcium flux contained alanine substitutions at positions 7 (mean ± SEM: 48.3 ± 10.3), 17 (mean ± SEM: 33.8 ± 5.9), and 19 (mean ± SEM: 42.9 ± 6.6).

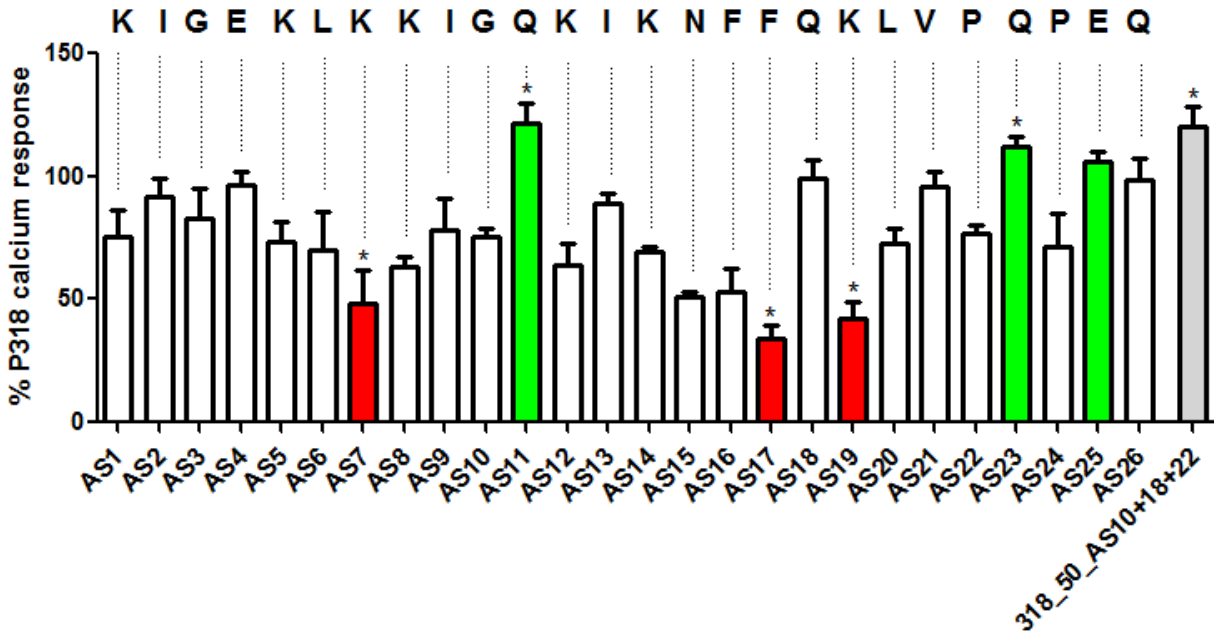

Fig.5.10. Graph displaying the calcium response of B16 cells to peptides of the alanine scan library of P318, as well as to P318_50_AS10+18+22. Each peptide was tested at a concentration of 10 µM. Results are shown as percentage of the calcium response induced by the original peptide. Peptides eliciting the strongest (largest mean absolute RFU values) calcium flux are highlighted in green, and peptide variants eliciting the weakest (smallest mean absolute RFU value) calcium response are marked in red. The statistical significance was tested with one-way analysis of variance (ANOVA) followed by Dunnett's test (*, $p < 0.05$). Error bars reflect SEM. Experiments were conducted in duplicate and repeated twice, hence 4 datapoints were obtained for each peptide. Error bars represent SEM.

5.4 Discussion

Cathelicidin peptides were originally investigated for their potential antimicrobial usefulness. Further exploration on the role of these peptides in cells and tissues of the host revealed that cathelicidins are ubiquitous in nature as components of the innate and adaptive immune system [4,5,6]. To date, considerable progress has been made toward understanding the mechanisms by which cathelicidin peptides activate host cells. However, the precise molecular details often remain undetermined, prompting the need for further research.

We identified a novel fragment of CRAMP in mouse pancreatic tissue. This peptide, codenamed P318, corresponds to the C-terminus of CRAMP. P318 was tested in different labs, employing various assays. Several promising activities were observed, *e.g.* antibacterial and antifungal effects, contraction of duodenum muscle strips, and activity in networks of intrinsic neurons in the intestinal wall. In addition, effects of P318 on several cultured cell lines were observed, including HEK293T and B16 cells. To gain more insight into the mechanism behind the action of P318, we set out to identify its cognate receptor(s) and the downstream signaling cascade that it activates in HEK293T and B16 cells.

In HEK293T cells, several similarities were noticed between the effects induced by P318 and the full length human counterpart of CRAMP, LL-37. First, intracellular calcium mobilization was observed in response to P318 as well as LL-37. Secondly, both short- and long-term impedance responses of HEK293T cells to P318 and LL-37 were observed. Kammermann *et al*. suggest that compounds with a similar mode of action produce similar impedance response profiles [27]. The initial impedance response may reflect changes in morphology induced by altered calcium homeostasis, whereas the second impedance response might be related to the emergence of cytotoxic effects induced by peptide treatment. However, the long-term impedance response to P318 (5 µM) was markedly less strong compared to the long-term effect induced by LL-37 (5 µM). This decrease in activity could be caused by a reduced ability of P318 to attach to the cell membrane and form pores. This hypothesis is favored as no phenotypic changes were observed 6 hours after exposure to 10 µM of P318, whereas drastic morphological effects were detected upon treatment with the same concentration of LL-37 (chapter 4). Taken together, our EIS data suggest that P318 and LL-37 share a similar mechanism of action on HEK293T cells, but differ in potency. Future experiments include performing cytotoxicity assays to assess the potential toxic effect induced by P318.

Thirdly, none of the antagonists displaying selectivity for candidate receptors of LL-37 inhibited the impedance or calcium response to 10 µM of P318. This is comparable to the results described in chapter 4. Only the IP_3R-inhibitor 2-APB significantly inhibited the calcium response of HEK293T cells

to P318 in the absence of extracellular calcium, which suggests that IP_3R is involved in the mode of action of P318 in HEK293T cells. Suramin also exerted a close to significant (p-value 0.052) inhibitory effect on the calcium response of HEK293T cells to P318. Because suramin is a negatively charged molecule, it is possible that electrostatic forces between negatively charged amino acids of suramin and the cationic residues of P318 play a role in this blocking effect. However, suramin (30 µM) failed to suppress the calcium response of B16 cells to 10 µM of P318. This observation suggests that suramin binds to a specific molecular target(s) on HEK293T cells rather than forming a complex through electrostatic interactions. The molecular identity of such molecule(s) is presently unknown. It is a genuine challenge to identify the molecular target of suramin, as suramin behaves as a multi-target compound, being able to block not only purinergic receptors, but also GPCRs, RTKs, membrane channels, and several enzymes [28,29].

Since none of the broad-spectrum GPCR (GPant-2, PTX) or RTK (genistein) antagonists as well as receptor-selective inhibitors for candidate receptors of LL-37 inhibited the calcium response to the peptide, a membrane-dependent mechanism of P318 becomes more likely. It is possible that P318 modifies the physicochemical state of the cell membrane, thereby modulating the activity of membrane-bound enzymes such as PLC in a receptor-independent manner. The membrane-active properties of P318 could also indirectly stimulate cell surface receptors and activate downstream signaling cascades. Possibly, suramin inhibits this indirect receptor activation, either via a specific molecular interaction with a receptor protein or by interfering with the binding of P318 to the plasma membrane. Further research is required in order to pharmacologically dissect the molecular basis of suramin's inhibitory action on the calcium response to P318, *e.g.* by conducting experiments with suramin analogues or with structurally different P2 purinoceptor antagonists.

Next, an alanine scan was performed on P318 in order to identify amino acids important for its calcium-mobilizing effect on HEK293T cells. In addition, the same experiment was performed in B16 melanoma cells. All peptide analogues in the alanine scan library retained their ability to mobilize intracellular calcium, although most analogues exhibited a decreased activity. This could be explained by local changes in amino acid side chain composition, thereby affecting the stability of the α-helix. Additionally, charge differences among peptide variants could play a role. Two peptide analogues, codenamed P318_AS16 and P318_AS17, exerted a markedly lower activity than the original peptide in HEK293T cells. In both cases, a phenylalanine was replaced by alanine. According to Wang *et al*., the 4 phenylalanines of LL-37 are all involved in membrane binding [30]. Phenylalanine residues are also more common than either tyrosine or tryptophan among AMPs collected in the Antimicrobial Peptide Database (APD). Therefore, replacement of phenylalanine by alanine might alter the binding and/or the surface orientation of P318 to the membrane interface, thereby decreasing the ability of

P318 to mobilize intracellular calcium. Interestingly, the calcium response of B16 cells to P318_AS16 and particularly P318_AS17 was also strongly reduced in comparison to the calcium response evoked by P318. These observations further demonstrate the importance of the replaced phenylalanines.

P318_AS13 also showed a decreased ability to release intracellular calcium ions in HEK293T cells. Here, an isoleucine was replaced by alanine. It remains difficult to explain this decrease in activity, as no changes in charge or hydrophobicity appear to be involved. Notably, a similar decrease in calcium mobilization was not observed when B16 cells were treated with P318_AS13.

On the other hand, P318_AS11 evoked a stronger calcium response in HEK293T and B16 cells than the original peptide. In this peptide analogue, a glutamine was substituted for alanine. Similarly, replacement of glutamine at position 18 (P318_AS18) led to an increased calcium response in HEK293T cells, whereas substitution of glutamine at position 23 (P318_AS23) strongly increased calcium mobilization in B16 cells. Since glutamine is a zwitterionic amino acid at neutral pH, replacement by alanine does not change the overall charge of these peptide variants. However, glutamine possesses a hydrophilic side chain, whereas alanine is characterized by a more hydrophobic nature. It is possible that this increase in hydrophobicity correlates with an enhanced ability to mobilize intracellular calcium. This hypothesis is further supported by the observation that the peptide analogue P318_50_AS10+18+22 evoked a stronger calcium release than P318 in HEK293T and B16 cells. P318_50_AS10+18+22 is characterized by a hydrophobicity ratio of 55%, whereas only 30% of the amino acids of P318 are hydrophobic. Furthermore, P318_50_AS10+18+22 is predicted to form an α-helix with 9 hydrophobic amino acids facing the same direction in the α-helix, while P318 only has 6 residues facing one side. Therefore, P318_50_AS10+18+22 has a more pronounced amphipathic nature than P318, which could facilitate the positioning of the peptide in the cellular membrane.

However, it must also be noted that P318_50_AS10+18+22 has a higher net charge (+6) than P318 (+5). This can be one of the underlying reasons why P318_50_AS10+18+22 exhibited a more potent antimicrobial activity compared to P318. Bacterial membranes are negatively charged due to the presence of anionic phospholipids [4,5]. Therefore, an additional positive charge could facilitate binding to the bacterial membrane, thereby enhancing the susceptibility of bacteria to the lytic actions of AMPs. However, the extra positive charge of P318_50_AS10+18+22 is not thought to affect the interaction with eukaryotic cells as their cell membrane primarily consist of neutral zwitterionic lipids. Notably, various cancer cells and red blood cells contain a high concentration of negatively charged cell membrane components. Further research is required to determine whether P318_50_AS10+18+22 has a higher affinity for these types of cells relative to P318.

Peptide analogues in which a lysine residue was replaced by an alanine residue (*e.g*. P318_AS1, P318_AS5, P318AS7, P318_AS8, P318_AS12, P318_AS14, P318_AS19) could deliver valuable information about the importance of the cationic net charge in the sequence of P318. In general, it appears that the calcium response of B16 cells to the aforementioned variant forms of P318 was more reduced compared to the calcium response of HEK293T cells. More specifically, alanine/lysine replacement at positions 7 or 19 resulted in a calcium response of B16 cells that was reduced more than 2-fold. Because B16 melanoma is a murine tumor cell line that posessess negative surface charge density, it is possible that electrostic peptide-membrane interactions between positively charged residues of the peptide and negatively charged cell surface molecules play a more pronounced role in B16 cells than HEK293T cells. However, further in-depth studies are required to validate this hypothesis and unambiguously identify the most important amino acids in the sequence of P318. For example, by combining the results obtained in figure 5.2 and 5.10, it may be worth to synthesize new peptide variants such as P318_AS7+16+17 (alanine substitutions at position 7 (A/K), 16 (A/F), and 17 (A/F)) or P318_AS11+18+25 (alanine substitutions at position 11 (A/Q), 18 (A/Q), and 25 (A/E)) and evaluate if these peptide variants elicit a weaker or stronger calcium response of HEK293T and B16 cells in comparison to the original peptide derivatives. In addition, P318 variants truncated at the N-terminus, the C-terminus, or both termini together may provide additional information.

In a next set of experiments, the effect of P318 on B16 melanoma cells was investigated in more detail. Effects of cathelicidin peptides on melanoma cells have been described before [19,20]. Kim *et al*. reported increased LL-37 expression in malignant melanoma cells [20]. The authors showed that LL-37 stimulated melanoma cell proliferation, migration, and invasion *in vitro*. These results suggest a function for LL-37 as a putative growth factor for malignant melanoma. However, the underlying mechanism by which LL-37 exerts its effect on melanoma cells has not yet been elucidated. Among the candidate receptors described for LL-37, only mRNA expression of IGF1R and $P2X_7$ was detected in B16 cells. However, administration of IGF1R- or $P2X_7$-selective antagonists to B16 cells prior to LL-37 treatment could not inhibit the calcium response of B16 cells to LL-37 (chapter 4).

P318 evoked a response of B16 cells that could be observed by EIS. The impedance response of B16 cells to P318 was distinctly different from the impedance response to LL-37. Verdonk *et al.* demonstrated that the curves generated by EIS reflect the intracellular pathways utilized by test compounds [31]. Therefore, it is conceivable that P318 and LL-37 do not share the same mechanism of action on B16 cells. This hypothesis is favored as P318 induced cAMP production in B16 cells (EC_{50} = 2.5 µM; Erwin Lauwers, Schoofs lab, personal communication), whereas intracellular cAMP levels were not increased following LL-37 treatment.

Previous research indicated that the small peptide with amino acid sequence WRWWWW (WRW4) completely blocked P318-induced cAMP production. Activation of FPR2 is functionally coupled to calcium mobilization rather than cAMP production [32]. However, this does not exclude the possibility that FPR2 is coupled to adenylyl cyclase in B16 cells. It is known that among different cell types, a receptor can be coupled to different possible signal transduction pathways. To which degree each pathway is activated depend on which ligand interacts with the receptor [32,33].

However, the hypothesis that P318 induced cell activation by acting on the FPR2 receptor was not confirmed by follow-up experiments using EFC technology and RNA interference (RNAi) (Dieter Vandamme, Schoofs lab, personal communication). In order to explain these paradoxical results, replication studies were performed to validate the inhibitory effect of WRW4 on the P318-induced cAMP production. The results from this study revealed that WRW4 (1-10 µM) failed to suppress cAMP production induced by P318. In addition, no effect on the cAMP response to P318 was observed when B16 cells were preincubated with the selective FPR2 agonist MMK 1 or WKYMVm for 2 minutes and re-challenged with P318. Because mRNA expression of FPR2 was not detected in B16 cells, it can be concluded that the effects of P318 were not mediated via activation of FPR2.

However, the broad-spectrum GPCR antagonists GPant-2 and SCH20267 exerted an inhibitory effect on the P318-induced cAMP production. Additionally, the impedance response to P318 was almost completely blocked when B16 cells were pretreated with GPant-2. These results suggest that P318 activates an as-yet-unidentified member (or multiple members) of the GPCR family on B16 cells. Because elevated cAMP concentrations were measured upon P318 treatment, GPCRs known to couple to the $G\alpha_s$-subunit are more likely candidate receptors for P318 than others. A possible next step in the receptor identification strategy is the use of transcriptomics data to list all $G\alpha_s$-protein coupled GPCRs in B16 cells. By employing receptor-selective antagonists, differences in the cAMP response to P318 can be detected. It is also recommended to measure cAMP production upon P318 treatment in cultured cell lines which have not been investigated before. If cAMP is produced after stimulation with P318, the list of candidate receptors for P318 can be narrowed down by comparing the expression of $G\alpha_s$-protein coupled receptors in these cultured cell lines.

We are not the first to speculate on the interaction of cathelicidin peptides with a currently unidentified cell surface receptor(s). For example, Barlow *et al*. demonstrated that LL-37 is a potent blocker of neutrophil apoptosis, signaling via $P2X_7$ and a GPCR other than FPR2 [34]. Weber *et al*. documented that LL-37 activates ErbB2 via a yet unidentified receptor [35]. Park *et al*. showed that GPCR activation is required for activities of LL-37 on fibroblasts [36]. Based on strong indications that a GPCR (or multiple GPCRs) is a putative receptor for P318, pull-down experiments with streptavidin-

coupled magnetic beads were previously performed (Erwin Lauwers, Schoofs lab, personal communication). P318 was synthesized with either an N-terminal or C-terminal biotin group, and, after confirming the bioactivity of the biotinylated peptide by EIS, enriched membrane proteins from B16 cells were added to the beads. The prey proteins were then identified by LC separation coupled to tandem MS. This resulted in a list of possible interaction proteins for P318. However, no GPCRs or other candidate receptors were identified. A possible explanation for these findings is the low affinity of P318 for its cognate receptor, as well as the fact that endogenous GPCRs are difficult to detect because they are often not abundantly expressed.

If P318 specifically engages a member of the GPCR family to mediate cAMP production, the use of LRC-technology can help to identify the molecular target of P318 in B16 cells. By coupling P318 to a trifunctional chemoproteomic reagent called TRICEPS, cell surface receptors can be identified on living cells by quantitative MS without the need for genetic manipulation [37]. According to Frei *et al.*, the LRC approach has the potential to detect multiple intended, as well as off-target effects. Because P318 potentially has several molecular targets or may induce signaling by acting on the cell membrane, the outcome of an LRC experiment can reveal important information about the identity of the interaction partner(s) of P318.

Aside from its cAMP-producing effect, P318 also elicited a calcium response and induced hyperpolarization of the cell membrane, suggesting a highly complex interplay between multiple signaling pathways. The signal was then transduced through an Akt-dependent pathway, since the Akt antagonist 10-DEBC suppressed the impedance response of B16 cells to P318. Activated Akt has mediates several downstream responses such as cell growth, proliferation, and migration [38]. This may point to a potential role for P318 as a putative growth factor for B16 cells. Follow-up research is required to determine whether P318 enhances the proliferative or migratory potential of B16 cells. Cell proliferation rates can be determined by measuring the overall metabolic activity inside a cell, whereas scratch assays can be used to measure cell migration *in vitro*. While writing this chapter, P318 (5 µM) was shown to stimulate the migration of human fibroblasts. It remains to be determined whether P318 exerts a similar effect on B16 melanoma cells.

Some of the questions that have arisen during our work remain difficult to answer. For example, it is currently not fully understood how P318 induced the rapid release of intracellular calcium as a second messenger. Based on the negative results obtained with receptor-selective pharmacological agents, one can speculate that P318 interacts with the cell membrane and indirectly activates signal transduction pathways. This hypothesis is favored as the peptide analogues P318_AS11 and P318_50_AS10+18+22 evoked a stronger calcium response than the original peptide. Both peptide

analogues are characterized by an increased hydrophobicity ratio, *i.e.* more amino acids in their sequence are hydrophobic. The physicochemical nature of these peptide analogues may favor a non-specific interaction with the membrane interface. Whether this is an oversimplified representation of the mechanism used by P318 to mobilize intracellular calcium in B16 cells, remains to be determined. D-enantiomers of P318 can be used to shed light on the membrane-binding properties of P318.

The ability of P318 to cause hyperpolarization in B16 cells can be related to a direct or indirect effect on ion channels. Hyperpolarization across the cell membrane can be caused by an influx of negatively charged ions, *e.g.* chloride ions, or an efflux of positively charged ions, *e.g.* potassium ions. The human purinergic receptor $P2X_7$ is the only calcium-channel identified so far as activated by LL-37 [4,5,6]. Because expression of $P2X_7$ was detected in B16 cells, the $P2X_7$-selective antagonist A-438079 was added to B16 cells prior to P318 treatment in order to determine whether $P2X_7$ was involved in the mode of action of P318. However, no effect of A-438079 on the P318-induced hyperpolarization of the plasma membrane of B16 cells was observed.

However, the broad-spectrum cation channel antagonist LOE908 inhibited the hyperpolarization induced by P318. This suggests that the movement of ions across the plasma membrane was mediated by active transport via ion channels rather than passive transport via pores. Gambade *et al*. recently reported that LL-37 stimulated breast cancer cell migration and metastasis by activating TRPV2 calcium-permeable channels [26]. TRPV channels are osmo- and mechanosensory channels that allow rapid movement of calcium ions from the extracellular compartment to the cytosol. Gambade *et al*. also showed that the D-enantiomer of LL-37 displayed identical effects as the L-enantiomer, suggesting that no binding to a defined receptor binding pocket was involved. Calcium entry into breast cancer cells activated calcium-activated potassium channels, leading to membrane hyperpolarization, thereby increasing the driving force for calcium across the cellular membrane. Furthermore, the binding of LL-37 to the membrane increased Akt signaling which induced the recruitment of TRPV2 channels from intracellular vesicles to the plasma membrane.

The mode of action of LL-37 on breast cancer cells as proposed by Gambade *et al.* shares common characteristics with the activity of P318 on B16 cells. First, we found that none of the receptor-selective antagonists displaying selectivity for candidate receptors of LL-37 inhibited the calcium response of B16 cells to P318, suggesting that P318 interacts with the plasma membrane. SAR studies on P318 also point more into the direction of a membrane-dependent mechanism, although no strong conclusions can be drawn from these tests. Secondly, stimulation of B16 cells with P318 resulted in the activation of the Akt signal transduction pathway. This observation still awaits confirmation, *e.g.* by conducting western blot experiments to detect Akt activation. Thirdly, the non-

selective antagonist of potassium channels TEA significantly reduced the magnitude of the hyperpolarization induced by P318, suggestive of a contribution of potassium channels. Gambade *et al.* used the selective BKCa channel inhibitor iberiotoxin (ibtx) to reveal the molecular identity of the potassium channel involved in the mechanism of LL-37 on breast cancer cells. They discovered that ibtx suppressed both the calcium entry and migration induced by LL-37. Further research is necessary to determine whether ibtx exerts a similar blocking effect on the P318-induced hyperpolarization-activated cation current in B16 cells.

Despite several similarities between the activity of P318 on B16 cells and the action of LL-37 on breast cancer cells, there are some significant differences which are difficult to explain. For example, Gambade *et al.* showed that pretreating cells with $LaCl_3$, a non-selective inhibitor of calcium channels, reduced the migratory potential of breast cancer cells. However, we did not observe an effect of $LaCl_3$ on the P318-induced hyperpolarization of the membrane, as depicted in figures 5.9-A and 5.9-C. One possible explanation for this discrepancy is that Gambade *et al*. used a higher concentration of $LaCl_3$ (100 µM) to block calcium-permeable channels [26]. Whether P318 induced calcium influx through the same calcium channel as proposed by Gambade *et al*, remains to be determined in future experiments. However, RNA-Seq measurements revealed expression of TRPV2 in B16 cells.

The results described and discussed above, do not allow drawing a simple conclusion. A schematic representation of the action of P318 on B16 cells is provided in figure 5.11. However, some of the steps in the proposed process are poorly understood. For instance, the membrane potential change induced by P318 is thought to occur via a membrane-dependent mechanism, whereas the cAMP response involves the activation of a ($G\alpha_s$-coupled?) GPCR. At this stage, we can also not entirely exclude the possibility that multiple GPCRs are involved. Nevertheless, we favor the hypothesis that the amphipathic nature of P318 plays an important part in the observed effects. By residing in the membrane, P318 may activate calcium-permeable channels and/or lead to changes in GPCR function such that it can signal without binding to its cognate ligand. At present, it is unclear whether this indirect GPCR activation has true functional relevance or is an off-target effect. The answer to this question includes identifying a functional effect of P318, *e.g.* by conducting cell migration or proliferation assays. B16 cells can then be treated with GPCR antagonists in order to obtain information on the functional importance of GPCR activation.

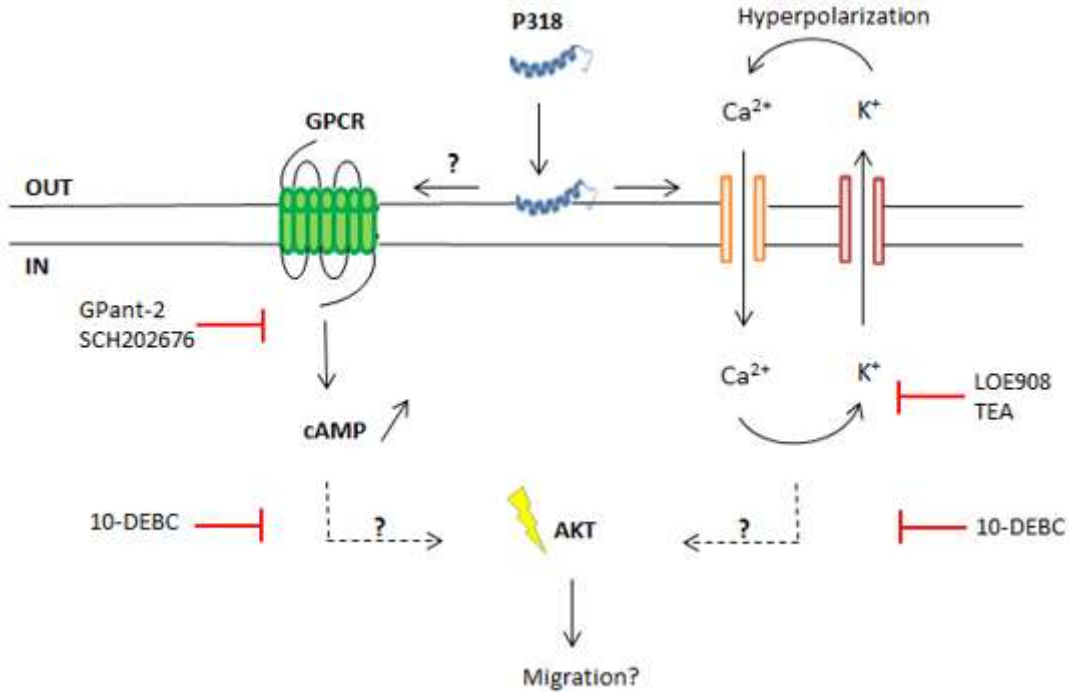

Fig.5.11. Proposed mechanism of action by which P318 evokes a cellular response in B16 melanoma cells. P318 interacts with the cell membrane and changes GPCR function, leading to the production of cAMP. The broad-spectrum GPCR inhibitors GPant-2 and SCH202676 were able to block the P318-induced cAMP synthesis. In addition, P318 induced hyperpolarization of the cell membrane potential. This effect was inhibited by the broad-spectrum ion channel antagonist LOE908 as well as TEA, a potassium channel antagonist. The signal was then further transduced via the activation of Akt. It remains to be determined whether this promotes the migratory potential of B16 cells. Other research questions include determining in what ways (direct or indirect?) P318 exerts its action on ion channels and GPCRs.

In summary, important parts of the whole image have become visible for the mechanism behind the action of P318 on HEK293T and B16 cells. However, many questions still remain. It is expected that the suggestions and recommendations as proposed in this chapter will provide a source of inspiration for future experiments on P318.

References

[1] K. De Brucker, N. Delattin, S. Robijns, H. Steenackers, N. Verstraeten, B. Landuyt, L. Schoofs, B. Dovgan, M. Fröhlich, J. Michiels, J. Vanderleyden, B.P. Cammue, K. Thevissen, Derivatives of the mouse cathelicidin-related antimicrobial peptide (CRAMP) inhibit fungal and bacterial biofilm formation, Antimicrob. Agents Chemother., 58 (2014) 5395-5404. doi:10.1128/AAC.03045.

[2] K. Kurosaka, Q. Chen, F. Yarovinsky, J.J. Oppenheim, De Yang, Mouse Cathelin-Related Antimicrobial Peptide chemoattracts leukocytes using formyl peptide receptor-like 1/mouse formyl peptide receptor-like 2 as the receptor and acts as an immune adjuvant, J. Immunol. 174 (2005) 6257-6265. doi: 10.4049/jimmunol.174.10.6257.

[3] R.L. Gallo, K.J. Kim, M. Bernfield, C.A. Kozak, M. Zanetti, L. Merluzzi, R. Gennaro, Identification of CRAMP , a cathelin-related antimicrobial peptide expressed in the embryonic and adult mouse, J. Biol. Chem. 16 (1997) 13088-13093. doi: 10.1074/jbc.272.20.13088.

[4] S.Y. Shin, S.-W. Kang, D.G. Lee, S.Y. Eom, W.K. Song, J.I. Kim, CRAMP analogues having potent antibiotic activity against bacterial, fungal, and tumor cells without hemolytic activity, Biochem. Biophys. Res. Commun. 275 (2000) 904-909. doi:10.1006/bbrc.2000.3269.

[5] M. Murakami, B. Lopez-Garcia, M. Braff, R.A. Dorschner, R.L. Gallo, Postsecretory processing generates multiple cathelicidins for enhanced topical antimicrobial defense, J. Immunol. 172 (2004) 3070-3077. doi:10.4049/jimmunol.172.5.3070.

[6] D. Vandamme, B. Landuyt, W. Luyten, L. Schoofs, A comprehensive summary of LL-37, the factotum human cathelicidin peptide, Cell. Immunol. 280 (1) (2012) 22–35. doi:10.1016/j.cellimm.2012.11.009.

[7] K. Kuroda, K. Okumura, H. Isogai, E. Isogai, The Human Cathelicidin Antimicrobial Peptide LL-37 and Mimics are Potential Anticancer Drugs, Front. Oncol. 5 (144) (2015) 1-10. doi:10.3389/fonc.2015.00144.7.

[8] S.X. Ren, J. Shen, A.S. Cheng, L. Lu, R.L. Chan, Z.J. Li, X.J. Wang, C.C. Wong, F.L. Zhang, S.S. Ng, F.L. Chan, F.K. Chan, J. Yu, J.J. Sung, W.K. Wu, C.H. Cho, FK-16 derived from the anticancer peptide LL-37 induces caspase-independent apoptosis and autophagic cell death in colon cancer cells, PLoS One. 8 (5) (2013) 1–9. doi:10.1371/journal.pone.0063641.

[9] S. Kanthawong, J.G. Bolscher, E.C. Veerman, J. van Marle, H.J. de Soet, K. Nazmi, S. Wongratanacheewin, S. Taweechaisupapong, Antimicrobial and antibiofilm activity of LL-37 and its truncated variants against *Burkholderia pseudomallei,* Int. J. Antimicorb. Agents. 39 (2011) 39-44. doi:10.1016/j.ijantimicag.2011.09.010.

[10] J.H. Wong, T.B. Ng, A. Legowska, K. Rolka, M. Hui, C.H. Cho, Antifungal action of human cathelicidin fragment (LL13–37) on Candida albicans, Peptides. 32 (2011) 1996-2002. doi:10.1016/j.peptides.2011.08.018.

[11] De Yang, Q. Chen, A.P. Schmidt, G.M. Anderson, J.M. Wang, J. Wooters, J.J. Oppenheim, O. Chertov, LL-37, the neutrophil granule- and epithelial cell-derived cathelicidin, utilizes formyl peptide receptor-like 1 (FPRL1) as a receptor to chemoattract human peripheral blood neutrophils, monocytes, and T cells, J. Exp. Med. 192 (7) (2000) 1069–74. doi:10.1084/jem.192.7.1069.

[12] J. Sun, M. Xu, H. Ortsäter, E. Lundeberg, L. Juntti-Berggren, Y.Q. Chen, J.Z. Haeggström, G.H. Gudmundsson, J. Diana, B. Agerberth, Cathelicidins postively regulate pancreatic β-cell fnctions, FASEB. J. 30 (2016) 884-894. doi:10.1096/fj.15-275826

[13] L.O. Brandenburg, S. Jansen, C.J. Wruck, R. Lucius, T. Pufe, Antimicrobial peptide rCRAMP induced glial cell activation through P2Y receptor signalling pathways, Mol. Immunol. 47 (10) (2010) 1905–1913. doi:10.1016/j.molimm.2010.03.012.

[14] A. Di Nardo, M.H. Braff, K.R. Taylor, C. Na, R.D. Granstein, J.E. McInturff, S. Krutzik, R.L. Modlin, R.L. Gallo, Cathelicidin antimicrobial peptides block dendritic cell TLR4 activation and allergic contact sensitization, J. Immunol. 178 (3) (2007) 1829–1834. doi:10.4049/jimmunol.178.3.1829.

[15] M. Seil, E. Kabré, C. Nagant, M. Vandenbranden, U. Fontanils, A. Marino, S. Pochet, J.-P. Dehaye, Regulation by CRAMP of the responses of murine peritoneal macrophages to extracellular ATP, Biochim. Biophys. Acta. 1798 (3) (2010) 569–78. doi:10.1016/j.bbamem.2009.11.002.

[16] M.T. Young, P. Pelegrin, A. Surprenant, Amino Acid Residues in the P2X7 Receptor that Mediate Differential Sensitivity to ATP and BzATP, Mol Pharmacol. 71 (1) (2007) 92–100. doi:10.1124/mol.106.030163.

[17] M.D. Boersma, J.D. Sadowsky, Y.A. Tomita, S.H. Gellman, Hydrophile scanning as a complement to alanine scanning for exploring and manipulating protein–protein recognition: Application to the Bim BH3 domain, Protein Sci. 17 (2008) 1232-1240. doi:10.1110/ps.032896.107.

[18] E. Piktel, K. Niemirowicz, U. Wnorowska, M. Wątek, T. Wollny, K. Głuszek, S. Góźdź, I. Levental, R. Bucki, The Role of Cathelicidin LL-37 in Cancer Development, Arch. Immunol. Ther. Exp. 64 (1) (2015) 33–46. doi:10.1007/s00005-015-0359-5.

[19] J.E. Kim, H.J. Kim, J.M. Choi, K.H. Lee, T.Y. Kim, B.K. Cho, J.Y. Jung, K.Y. Chung, D. Cho, H.J. Park, The antimicrobial peptide human cationic antimicrobial protein-18/cathelicidin LL-37 as a putative growth factor for malignant melanoma, Brit. J. Derm. 163 (2010) 959-967. doi:10.1111/j.1365-2133.2010.09957.x.

[20] D. Xhindoli, S. Pacor, M. Benincasa, M. Scocchi, R. Gennaro, A. Tossi, The human cathelicidin LL-37 - A pore-forming antibacterial peptide and host-cell modulator, Biochim. Biophys. Acta - Biomembr. 1858 (3) (2015) 546-566. doi:10.1016/j.bbamem.2015.11.003.

[21] U.H.N. Dürr, U.S. Sudheendra, A. Ramamoorthy, LL-37, the only human member of the cathelicidin family of antimicrobial peptides, Biochim. Biophys. Acta. 1758 (9) (2006) 1408–25. doi:10.1016/j.bbamem.2006.03.030

[22] J.-H. Lee, H. Park, H. Chung, S. Choi, Y. Kim, H. Yoo, T.-Y. Kim, H.-J. Hann, I. Seong, K.G. Kang, I.-O. Han, E.-S. Oh, Syndecan-2 regulates the migratory potential of melanoma cells, J. Biol. Chem. 284 (2009) 27167-27175. doi:10.1074/jbc.M109.034678.

[23] N. Mookherjee, K.L. Brown, D.M.E. Bowdish, S. Doria, R. Falsafi, K. Hokamp, F.M. Roche, R. Mu, G.H. Doho, J. Pistolic, J.-P. Powers, J. Bryan, F.S. Brinkman, R.E. Hancock, Modulation of the TLR-Mediated Inflammatory Response by the Endogenous Human Host Defense Peptide LL-37, J. Immunol. 176 (4) (2006) 2455–2464. doi:10.4049/jimmunol.176.4.2455.

[24] K.L. Brown, G.F.T. Poon, D. Birkenhead, O.M. Pena, R. Falsafi, C. Dahlgren, A. Karlsson, J. Bylund, R.E.W. Hancock, P. Johnson, host defense peptide LL-37 selectively reduces proinflammatory macrophage responses, J. Immunol. 186 (2011) 5497-5505. doi: 10.4049/jimmunol.1002508.

[25] S. Tokumaru, K. Sayama, Y. Shirakata, H. Komatsuzawa, K. Ouhara, Y. Hanakawa, Y. Yahata, X. Dai, M. Tohyama, H. Nagai, L. Yang, S. Higashiyama, A. Yoshimura, M. Sugai, K. Hashimoto, Induction of keratinocyte migration *via* transactivation of the epidermal growth factor receptor by the antimicrobial peptide LL-37, J. Immunol. 175 (7) (2005) 4662–4668. doi:10.4049/jimmunol.175.7.4662.

[26] A. Gambade, S. Zreika, M. Guéguinou, I. Chourpa, G. Fromont, A.M. Bouchet, J. Burlaud-gaillard, M. Potier-cartereau, S. Roger, V. Aucagne, S. Chevalier, C. Vandier, C. Goupille, G. Weber, Activation of TRPV2 and BKCa channels by the LL-37 enantiomers stimulates calcium entry and migration of cancer cells, Oncotarget. 7 (17) (2016) 23785-23800. doi:10.18632/oncotarget.8122.

[27] M. Kammermann, A. Denelavas, A. Imbach, U. Grether, H. Dehmlow, C.M. Apfel, C. Hertel, Impedance measurement: a new method to detect ligand-biased receptor signaling, biochem. Biophys. Res. Comm. 412 (2011) 419-429. doi:1.1016/j.bbrc.2011.07.087.

[28] W.C. Chung, J.C. Kermode, Suramin disrupts receptor-G protein coupling by blocking association of G protein alpha and betagamma subunits, J. Pharmacol. Exp. Ther. 313 (1) (2005) 191-198. doi: 10.1124/jpet.104.078311.

[29] P.M. Dunn, A.G. Blakeley, Suramin: a reversible P2-purinoceptor antagonist in the mouse vas deferens, Br. J. Pharmacol. 93 (2) (1988) 243-245. doi:10.1111/j.1476-5381.1988.tb11427.x.

[30] G. Wang, B. Mishra, R.F. Epand, R.M. Epand, High-quality 3D structures shine light on antibacterial, anti-biofilm and antiviral activities of human cathelicidin LL-37 and its fragments, Biochim. Biophys. Acta - Biomembr. 1838 (9) (2014) 2160-2172. doi:10.1016/j.bbamem.2014.01.016.

[31] E. Verdonk, K. Johnson, R. McGuinness, G. Leung, Y.-W. Chen, H.R. Tang, J.M. Michelotti, V.F. Liu, Cellular dielectric spectroscopy: a label-free comprehensive platform for functional evaluation of endogenous receptors, Assay and Drug Develop. Techn. 4 (5) (2006) 609-619. doi:10.1089/adt.2006.4.609.

[32] F. Cattaneo, M. Parisi, R. Ammendola, Distinct signaling cascades elicited by different formyl peptide receptor 2 (FPR2) agonists, Int. J. Mol. Sci. 14 (4) (2013) 7193–7230. doi:10.3390/ijms14047193.

[33] T. Kenakin, Functional selectivity and biased receptor signaling, J. Pharmacol. Exp. Ther. 336 (2011) 296–302. doi:10.1124/jpet.110.173948.

[34] P.G. Barlow, Y. Li, T.S. Wilkinson, D.M.E. Bowdish, Y.E. Lau, C. Cosseau, C. Haslett, a J. Simpson, R.E.W. Hancock, D.J. Davidson, The human cationic host defense peptide LL-37 mediates contrasting effects on apoptotic pathways in different primary cells of the innate immune system, J. Leukoc. Biol. 80 (3) (2006) 509–520. doi:10.1189/jlb.1005560.

[35] G. Weber, C.I. Chamorro, F. Granath, A. Liljegren, S. Zreika, Z. Saidak, B. Sandstedt, S. Rotstein, R. Mentaverri, F. Sánchez, A. Pivarcsi, M. Ståhle, Human antimicrobial protein hCAP18/LL-37 promotes a metastatic phenotype in breast cancer, Breast Cancer Res. 11 (1) (2009) R6. doi:10.1186/bcr2221.

[36] H.J. Park, D.H. Cho, H.J. Kim, J.Y. Lee, B.K. Cho, S.I. Bang, S.Y. Song, K. Yamasaki, A. Di Nardo, R.L. Gallo, Collagen synthesis is suppressed in dermal fibroblasts by the human antimicrobial peptide LL-37, J. Invest. Dermatol. 129 (4) (2009) 843–850. doi:10.1038/jid.2008.320.

[37] A.P. Frei, O.-Y. Jeon, S. Kilcher, H. Moest, L.M. Henning, C. Jost, A. Plückthun, J. Mercer, R. Aebersold, E.M. Carreira, B. Wollscheid, Direct identification of ligand-receptor interactions on living cells and tissues, Nat. Biotechnol. 30 (10) (2012) 997–1001. doi:10.1038/nbt.2354.

[38] B.D. Manning, L.C. Cantley, AKT/PKB signaling: navigating downstream, Cell. 129 (2007) 1261-1274. doi: 10.1016/j.cell.2007.06.009.

Chapter VI

An introduction to three-dimensional cell culture models: (dis)advantages and techniques.

Adapted version of this chapter accepted for publication.

E.-T. Verjans, J. Doijen, W. Luyten, B. Landuyt, L. Schoofs, Three-dimensional cell culture models for anticancer drug screening: worth the effort? J. Cell. Physiol. Accepted author manuscript (2017). doi:10.1002/jcp26052.

Abstract

High attrition of new drug candidates in clinical trials is partially caused by the poor predictive capacity of artificial monolayer cell culture assays used at early stages in drug discovery. Monolayer assays do not take the natural three-dimensional (3D) microenvironment of cells into account. As a result, false positive compounds often enter clinical trials, leading to high dropout rates and a waste of time and money. To deal with this challenge, there is great demand for new *in vitro* tools that better recapitulate *in vivo* cell and tissue biology. Over the past two decades, tissue engineers and cell biologists have developed a broad range of 3D cell culture techniques which preserve the 3D architecture of a cell more closely than conventional 2D approaches. 3D cell cultures are increasingly recognized as improved models for cell differentiation, migration, polarization, drug resistance, and survival. In addition, growing cells as multicellular spheroids reveals a more realistic drug response. However, the widespread implementation of 3D cell cultures into cell-based research programs has been limited by various factors, including their cost and reproducibility. In addition, different 3D cell culture techniques often produce spheroids of different size and shape, which can strongly influence drug efficacy and toxicity. Hence, it is imperative to morphometrically characterize multicellular spheroids to avoid generalizations among different spheroid types. Standardized 3D culturing procedures could further reduce data variability and enhance biological relevance. In this chapter, the benefits and challenges inherent to growing cells in 3D are described, along with an overview of the techniques used to form multicellular spheroids.

6.1 Introduction

Pharmaceutical research and development (R&D) has increased significantly over the last decade [1]. It is estimated that it may cost up to 2.6 billion dollar to get a new drug to the market [2]. Factors that boosted R&D expenditures are larger clinical trial sizes, enhanced clinical trial complexity and increasingly stringent regulatory landscapes. However, a significant part of expenditure in drug discovery is attributed to high attrition rates of drug candidates in clinical trials [3]. Even though it is possible to avoid false discoveries by adjusting and improving experimental design and practices, high failure rates appear to have a deeper underlying cause. This cause is represented by a large gap between *in vitro* hypotheses and *in vivo* 'veritas'.

In essence, only a small fraction of the incredibly complex nature of living organisms is currently understood by present-day science. To unpick this complexity, researchers rely on a broad range of techniques and model systems that mimic important features of human physiology. Each of these approaches strikes a delicate balance between usability, cost, and resemblance to *in vivo* circumstances. In addition, there is a huge demand for faster drug development due to urgent global health changes such as emerging pandemic viruses and the increase in antibiotic resistance [3].

Generally, standard screening procedures involve target identification of a compound on immortalized cell lines cultured in two dimensions (2D). Once a target has been identified, experiments of different complexity are performed using computational, *in vitro*, and *in vivo* models [4]. During this process, each technique or model system suffers from inherent limitations by which promising candidate drugs can be missed or by which adverse drug side effects can be overlooked.

Animal models such as *Caenorhabditis elegans* (*C. elegans*), *Drosophila melanogaster*, and *Rattus norvegicus* are commonly used to expand our understanding of similar physiological processes in other animals. For example, Beets *et al*. used *C. elegans* as a neurobiological model to study neuropeptidergic signaling and discovered that vasopressin/oxytocin-related peptides play a key role in the associative learning behavior of the roundworm. Interestingly, vasopressin and oxytocin also regulate cognitive processes in mammals, confirming the presumption that biochemical processes in the nervous system of *C. elegans* are similar to organisms of higher complexity [5]. Kobet *et al*. report that several oncogenic signaling pathways (Wnt, Notch, and Ras) in *C. elegans* are also highly conserved in vertebrates, including humans [6]. In addition, many genes known to be involved in human cancer have functional counterparts in well-characterized model organisms [6-8]. Studying these genes can provide insight into the molecular mechanisms underlying the formation of cancer.

However, the inadequacy of most *in vivo* models for predicting the clinical outcome of a drug candidate in humans is a recurrent issue. Experimental data from animal tests can be limited by interspecies differences which are likely to be theoretically and technically difficult to overcome. Knight elaborated on this issue and proposes a ban on using animal models that lack scientific evidence establishing human predictivity or utility [9]. This fact, in conjunction with strong ethical concerns, prompted research institutions to develop and implement alternative models to diminish animal testing.

Numerous *in vitro* test methods have been developed based on human cell and tissue cultures. The majority of cell-based assays rely on the growth of cells as immortalized 2D monolayers, which are easy to work with and allow for simple and efficient culturing workflows. 2D cell cultures serve as the main workhorse for basic cellular research and are being used for predictions of drug activity, metabolism and toxicity *in vivo* [10]. In many cases, transformed cell lines are used. These cell types often do not resemble the native cellular function found in normal primary cells, but instead are selected for a particular research purpose such as increased proliferative capacity or higher plating efficiency. Transformed cells have acquired a transient or permanent change in their phenotype by genetic changes, which may diminish their capacity as a model to predict the *in vivo* performance of a drug candidate.

To better understand native cellular function, primary cells are often used in cell-based research programs. Primary cultures are directly derived from living tissue and are therefore more likely to reflect the properties of native cells *in vivo*. However, primary cells have a limited lifespan and the preparation and culture workflows are much more challenging compared to permanent cell lines [8]. Moreover, primary cells often have to be isolated from a heterogeneous cell population, in order to study the cell type of interest [11].

The introduction of co-cultures, where multiple cell types are grown together in the same culture dish, represent a higher degree of *in vivo* resemblance compared to monocultures. Both immortalized cell lines and primary cells can be cultured in co-culture systems. These mixed populations can be used to study cell-cell interactions *ex vivo* [12]. Nevertheless, analyzing cellular interactions remains a major challenge, especially since these interactions tend to change in different environments and some interactions only occur within defined pH ranges [13].

All the aforementioned model systems, ranging from permanent 2D monocultures or primary cultures to co-culture approaches have one common drawback: cells are typically cultivated on plastic dishes or tissue culture flasks. Culturing cells on a polystyrene surface has serious limitations, as the cells adhere to an unnatural plastic substrate. The polystyrene surface is often pre-coated in

order to help the cells attach to the substrate. However, this configuration inadequately represents the complex physiological environment where cells interact with each other and with the ECM. The poor resemblance of *in vivo* architecture could lead to dubious conclusions and can endanger subsequent R&D efforts. For example, Gomez-Roman and colleagues evaluated whether glioblastoma-derived cells responded to radiotherapy more strongly when it was given in combination with molecular targeted agents for which clinical data was available. While the EGFR tyrosine kinase antagonist erlotinib enhanced the radiosensitivity of cells cultured in 2D, it had no efficacy in phase II clinical trials [14]. This does not necessarily mean that 2D models are wrong *per se*, as clinical failure could also be due to pharmacokinetic variability. However, this study underlines the need for better predictive *in vitro* models. Multiple studies suggest that drug responses of 2D cell cultures poorly predict the outcome of clinical studies [15-23].

A promising approach to deal with high failure rates in clinical trials is the development of 3D cell cultures. 3D models often closely reflect cell behavior in living tissues and tumors [10,24]. They possess many features by which they resemble *in vivo* tissues and tumors including physiologically relevant cell-cell and cell-ECM interactions, hypoxia and central necrosis, and drug resistance [10,20,25,26]. In addition to molecular drug resistance, spheroid cultures can help predict drug penetration, an important cause of resistance in tumors that is often overlooked [27]. Due to these features, the spheroid model is often seen as a more stringent and representative platform for *in vitro* drug screening [28]. Therefore, it might be useful to implement 3D studies in drug screening programs to support monolayer findings before advancing to animal testing. Such an approach might ensure more efficient animal testing and may reduce the number of animals used. However, 3D models cannot completely replace animal research as they still underappreciate the complex nature of living organisms.

As powerful as they are, some clear limitations prevent the integration of 3D cell culture models into mainstream drug discovery pipelines. Different 3D culturing techniques can be used to form spheroids, which have an impact on various spheroid parameters including size, shape, density, surface features, and internal textures [29]. Differences in spheroid configuration can in turn affect the outcome of drug delivery and efficacy studies. Consequently, there is a critical demand for an improved morphometric characterization of multicellular spheroids, which can reduce the variability between different experimental setups and increase the comparability of results.

In this chapter, the advantages and limitations inherent to 3D cell culture models are discussed in more detail. Additionally, commonly used techniques to maintain the 3D structure of a cell are described.

6.2 Merits and demerits of 3D cell cultures

3D cell culture models can be created by growing cells into larger 3D cell aggregates (spheroids) *via* a wide variety of scaffold and scaffold-free techniques. One of the main objectives of culturing 3D spheroids *in vitro* is to examine the pharmacodynamic effects of drug candidates before carrying out clinical trials [23]. Additional applications of 3D cell cultures include studying cancer, pharmacology, cell differentiation, and tissue engineering [10,16,17,20,22].

A powerful improvement of tumor spheroids over conventional 2D cell cultures is the presence of metabolic and proliferative gradients across their spherical geometry that can influence pharmacological efficacy. Spheroids of permanent cell types that reach sizes of 500 µm or more often undergo central necrosis. This necrosis evolves because nutrient and oxygen supply is limited in the center, the pH is low and there is an accumulation of waste. A viable layer of approximately 200 µm surrounds the outer surface of the necrotic core [30,31]. Before undergoing cell death, cells located more in the center adapt their metabolism and become quiescent in order to maintain homeostasis [32]. This leads to the typical zonation found in spheroids with proliferating cells found on the outside of the spheroid, whereas quiescent and necrotic cells are harbored within the spheroid (figure 6.1). Similarly, solid tumors often have regions with different proliferation rates and regions with mild to severe oxygen deficiencies, due to the lack of blood supply to growing tumor [33-35]. Therefore, spheroid models mimic avascular tumors and can be used to predict the efficacy of radiotherapy and chemotherapy and to predict the metastatic potential of certain tumors.

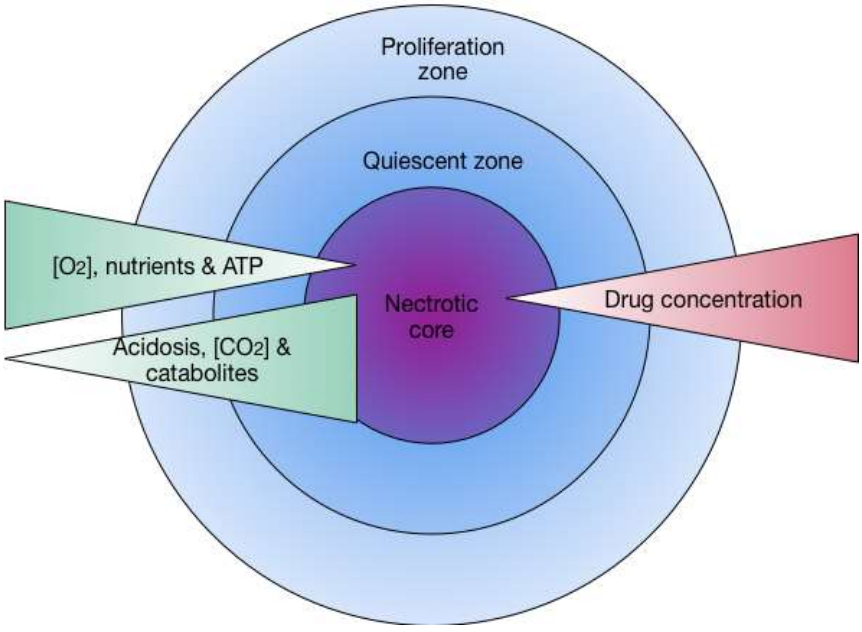

Fig.6.1. Schematic representation of multi-layered spherical geometry. Proliferation is higher on the outside due to high levels of oxygen and nutrients. The availability of nutrients and oxygen decreases towards the center of the spheroid resulting in growth arrest or cell necrosis (adapted from Ref. [35]).

The value of working with 3D cell culture models was highlighted by a study of Tung *et al* [36]. Two anticancer drugs, 5-fluorouracil (5-FU) and tirapazamine, with different modes of action produced distinct responses in 3D spheroids compared to conventional 2D cell cultures of human epithelial carcinoma cells. 5-FU is a well-characterized compound that inhibits cell proliferation, whereas tirapazamine is an anticancer drug that functions as a hypoxia-selective cytotoxin [36,37]. The 3D spheroids remained viable after 5-FU treatment, whereas cells grown as 2D monolayers did not survive the treatment. Because 2D cell cultures initially proliferate at a relatively uniform rate across the plastic substrate, 5-FU is able to exert its DNA-damaging effect. Instead, spheroids have a lower proliferation rate, leading to a reduced sensitivity to 5-FU.

At low oxygen levels, tirapazamine is activated and forms a toxic radical that is exclusively effective on cells cultured in 3D since they exhibit hypoxic regions inside the spheroid that promote radical formation [38]. Hypoxia in the center also stalls proliferation, indirectly making spheroids less susceptible to anti-proliferative drugs such as cisplatin [33]. Fayad *et al*. demonstrated that colorectal cancer HCT116 cells grown in 3D are indeed less susceptible to cisplatin than their monolayer counterparts [25]. Testing for synergistic effects of drugs that target hypoxic zones like tirapazamine and conventional anticancer drugs such as cisplatin may provide new strategies to oncology drug development. The former results show that the development of such strategies can potentially be improved using spheroid cultures.

Differential drug responses of cells grown in 3D vs 2D are not solely related to differential zones of proliferation or oxygen availability. Multiple studies report differences in gene and protein expression between 3D spheroids and 2D cultures that change drug efficacy, metabolism, and cell communication [15-17,22,39-45]. Aljitawi *et al*. showed that an increase in N-cadherin expression in spheroid co-cultures of leukemic and bone marrow mesenchymal stem cells reduces chemotherapy efficacy when compared to monolayer co-cultures [15]. The precise role of *N*-cadherin in mediating leukemic cell resistance is currently not well understood but may be an interesting target for leukemia therapy [15].

Monolayer cultures of hepatocytes quickly dedifferentiate and lose many characteristics of *in vivo* liver tissue such as the secretion of albumin [22,40,41]. Different groups have shown, using both protein and RNA studies, that various liver-specific functions are re-acquired when growing cells in spheroid cultures [23,40,41,44]. Of particular interest is the upregulation of metabolic genes in spheroid cultures as compared to hepatic cells cultured in 2D. The expression level of drug-metabolizing enzymes (DMEs) in spheroids more closely resembles the expression level of DMEs in native liver tissue, suggesting that spheroids are more adequate *in vitro* models than monolayer

cultures to study the metabolic breakdown of drugs [23,43,45]. DMEs are important for solubilizing drugs by means of hydroxylation and conjugation, which facilitates their transport and clearance. The biotransformation of drugs by the cytochrome P450 system often results in the production of reactive intermediates [46]. It is known that many drugs are initially inert but exert toxic side effects when they are converted to their metabolites by DMEs. Many drugs withdrawn from the market produce these types of reactive intermediates (*e.g*. benoxaprofen) emphasizing the necessity to find new, convenient and more accurate systems for hepatotoxicity testing [21].

Loessner *et al.* measured mRNA levels in ovarian cancer cells in 2D and 3D cultures and reported increased expression of receptors for $\alpha_3/\alpha_5/\beta_1$ integrins and matrix metalloprotease 9 (*MMP9*) in 3D cultures compared to cells grown in 2D monolayers [39]. Colorectal cancer (CRC) 3D spheroids showed altered EGFR expression as compared to monolayer cultures which impaired the efficacy of pharmacological EGFR inhibition [47]. In melanoma cells, genes encoding laminin, hyaluronic acid, CXCL1, IL-8, as well as pro-angiogenic genes were upregulated in 3D spheroids compared to conventional 2D monolayer cultures. These genes are associated with melanoma progression *in vivo* [48]. Maria *et al*. discovered that spheroid cultures of human submandibular salivary gland (HSG) cells increased the secretion of acinar proteins. This increase was not associated with enhanced transcription of the according genes, but rather a consequence of translational regulation. In this case, cells cultured in 2D experienced a protein translation defect, leading to a lower acinar protein production [49]. Stimulation of Fas/CD95 which is highly toxic *in vivo,* induces apoptosis in the hepatocyte cell line MhAT3F 3D spheroid model but is not effective in monolayer cultures due to increased NF-κB signaling downstream of the engaged death receptor [50]. These and many other reports indicate that changes in gene expression and proliferation can drastically alter the experimental outcome and thus determine whether a pharmaceutical compound is seen as effective or not.

Spheroid morphology and organization also affect cellular processes such as apoptosis and histone acetylation [51]. Morphology changes allow spheroid cultures to better represent the *in vivo* situation than 2D cultures in which cells flatten and proper cell-to-cell interactions are virtually eliminated [23,52]. For instance, cell polarization in spheroids is suggested to be more accurate than in monolayer cultures [10]. This could be of particular interest to study the behavior of polarized epithelial cell cultures [53].

Taken together, growing cells in a 3D environment changes its cell contacts and nutrient availability which in turn alters the expression of genes. Differences in gene expression affect different physical and physiological properties including metabolism and proliferation. It also influences different types

of cell behavior such as cell migration, differentiation, and communication [10,15,16]. The expression profiles of cells grown in 3D are often more similar to expression patterns found in native tissues or primary tumor samples [10,15,16,56,57]. Multiple studies compared protein or gene expression levels of liver monolayer cultures with liver tissues or spheroid cultures and suggest that expression patterns of spheroids more closely resemble those of native liver tissue [23,41,43,45]. Therefore, they are believed to be very promising for improved drug discovery.

Despite these promising findings, none of the 3D methods have been implemented in cell-based research programs on a large scale. This is due to their high costs, along with difficulties to create uniformly sized spheroids and develop spheroid co-cultures [16,33]. Commercially available assay formats are not always optimized for 3D cell culturing and data interpretation can be challenging due to the lack of standardized protocols [10]. In contrast to 2D cell cultures, researchers can also not rely on a rich scientific literature addressing mechanisms of drug interactions, cell differentiation, and cell signaling in a 3D environment.

Several studies suggest that a thorough characterization of the spheroid system is required to avoid generalizations among different types of spheroids [58]. For example, Mellor *et al*. examined the effect of different antitumor drugs including cisplatin, vinblastin and doxorubicin on non-small-cell lung carcinoma (NSCLC)-derived spheroids and discovered that there were big differences in drug efficacy of the different drugs. More striking, they found that the same drugs had different efficacies depending on the proliferative status of the spheroids [59]. This variability makes it difficult to compare independent drug exposure studies on spheroids. A similar observation was made by Zanoni *et al*., who showed that 3D cell cultures heterogeneous in shape and volume may respond differently to chemical or physical treatments. They developed open-source software capable of automatically analyzing several morphological parameters of spheroids, thereby reducing data variability and enhancing the biological relevance [60]. Mathematical models can also help simulating dynamics of drug distribution within spheroids, as exemplified by Mehta *et al* [33]. These models predict gradients of oxygen, nutrients, lactate and glucose, as well as the extent and location of quiescent cells in spheroids. This enables researchers to predict the effectiveness of drug treatments.

In addition, 3D cell culture models are not being used as a routine tool in preclinical cancer research since the *in vivo* multicellular complexity of tumors cannot yet be fully recapitulated using these models. Tumors do not function as solitary units. Their microenvironment often harbors different types of cells that contribute to tumorigenesis in a specific way. For instance, endothelial cells can vascularize tumors after undergoing an angiogenic switch [61]. Vasculature enhances the tumor's nutrient and oxygen availability and thus influences tumor growth and survival *in vivo* [62]. The

majority of the developed 3D models do not include a vascular component which is very important for tumor growth and survival *in vivo* [62]. Therefore, contemporary 3D models may be adequate to study cell function in an avascular tumor microenvironment, but cannot be used to examine tumor vascularity. Progress in the field of vasculature in combination with the development of improved microfluidic tools can help improve 3D cell culture models and make them increasingly interesting for preclinical cancer research.

To conclude, 3D models have proven to be useful for evaluating adverse side effects and efficacy of antitumor drugs at an early stage in the drug discovery pipeline and can contribute to present-day methodologies used in preclinical studies. Improvements in 3D cell culture models overcome barriers related to reproducibility, costs, and cumbersome procedures. However, the lack of standardization limits their implementation in cell-based drug screening programs. In addition, the majority of the developed 3D models do not include a vascular component. Therefore, these models cannot be used to study tumor vascularity and instead can solely be implemented in avascular tumor research.

6.3 Scaffold and non-scaffold techniques

Tissue engineers and cell biologists have been trying to mimic the highly complex 3D arrangement of cells for many years. In general, there are two methods that can be used for spheroid formation: scaffold techniques and scaffold-free techniques. A schematic overview of the most common 3D culturing techniques applied to grow spheroids is provided in figure 6.2. 3D scaffolds either rely on biological or synthetic polymers. This microarchitecture reflects the native ECM composition and can provide biologically active microenvironment for the cells to interact with each other, to proliferate, and to migrate [23,33]. Biological scaffolds are created from a range of biological components such as agarose, laminin, collagen, vitronectin, fibronectin, and gelatin. Cells can be dispensed in a microwell previously coated with a particular scaffold, or hydrogel-based matrices can be used.

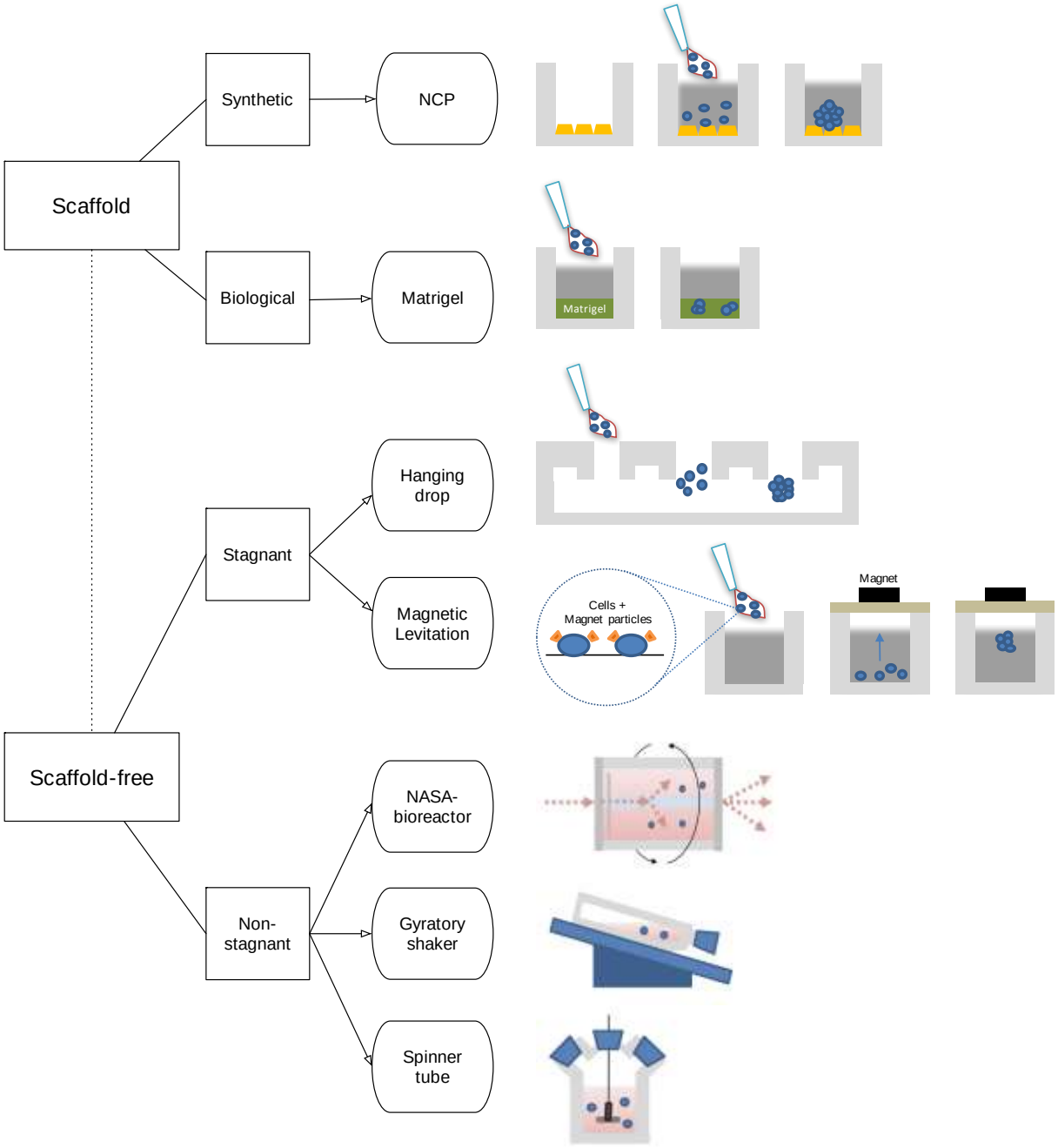

Fig.6.2. Schematic overview of the different 3D cell culturing systems (adapted from Ref [63] as well as Ref [64]).

Hydrogels are natural or synthetic networks of crosslinked polymer chains that possess elevated water content, which facilitate nutrient, oxygen, and waste transport. Hydrogels derived from a natural origin are highly bioactive due to the presence of a wide variety of endogenous molecules, which can be advantageous for many cellular processes including proliferation or differentiation. One of the most commonly used naturally-derived hydrogels is the so-called Matrigel, which is composed of a mixture of ECM proteins secreted by Engelbreth-Holm-Swarm sarcoma cells [65]. However, such scaffolds are often not well characterized making it challenging to identify the endogenous factors that promote a certain cell behavior. Biological hydrogels may also contain unknown or unwanted

components which limits their use for clinical work. On the other hand, hydrogels composed of synthetic polymers such as polyethylene glycol (PEG) are relatively well characterized, highly reproducible, and easily manufactured, but lack the bioactive endogenous molecules that can be beneficial for cell function [51].

Due to recent progress in micro-fabrication, micropatterned surface microplates were developed. These plates can be optimized for spheroid formation and cell networking events by imbedding different possible micro-configurations in the bottom. One of the latest micropatterned 3D cell culture products was engineered by Organogenix, Inc. (Woburn, MA, USA). Seeded cells attach to the nano-scale structure plastic film on the well-bottom surface of the so-called NanoCulture Plates (NCP). On the bottom, a structure is present that mimics the normal ECM [56,66]. Because cells do not adhere strongly to the microstructure on the culture surface, they start migrating and reorganize into 3D structures.

Even though NCPs do not overcome all of the above mentioned disadvantages (*e.g.* lack of vasculature, expensive) inherent to working with 3D cell cultures, they overcome flaws of other scaffold-type 3D culture systems such as lot-to-lot variation, difficulty of imaging, and cumbersome culturing workflows [56]. Growing spheroids using NCPs is also suitable for high-throughput screening and offers great potential for future integration into contemporary drug screening procedures [67].

Scaffold-free methods have also been devised to generate 3D cell cultures. The best known example hereof is the so-called hanging drop method, in which single cells are placed in a hanging drop culture and incubated under physiologically relevant conditions until they form 3D spheroids [68]. This technology is based on the fact that cells self-assemble into 3D structures in the absence of a surface to which they can adhere. This is technically achieved by creating plates with a small opening at the bottom of the well, thereby enabling droplet formation of the culture medium. This droplet enables the cells to form multicellular spheroids. Surface tension prevents the droplets from being displaced during experimental manipulation. Using this method, Messner *et al.* successfully obtained spheroids of hepatocytes that exerted hepatic functions such as glycogen storage and bile canaliculi formation [69]. The hanging drop technique allows easy control of spheroid size, but is relatively low throughput [58].

Liquid overlay spheroid cultures are scaffold-free cultures that use microplates coated with agar/agarose (flat-bottom wells) or poly(2-hydroxyethyl methacrylate) (poly-HEMA) (round-bottom wells) to prevent cell attachment to the surface. This forces cells into a suspended state, enabling the formation of 3D multicellular spheroids [70]. Ivanov *et al*. used these ultra-low attachment (ULA)

spheroid microplates to monitor growth kinetics and drug toxicity of neuronal stem cells [71]. Vinci *et al.* demonstrated that the ULA-approach compares closely with conventionally-generated 3D spheroids, but with the additional advantage that automated analysis is easier [72]. However, according to Katt *et al.*, experiments that require long-term cultivation of the 3D spheroids can be difficult using this approach [58].

In the scaffold-free Magnetic Levitation Method (MLM) cells are bound by a nanoparticle overnight in order to make them magnetic [73]. The cells are then resuspended in medium and a magnetic field is applied in such a way that the cells concentrate at the air-liquid interface and form aggregates. 3D spheroids can be obtained in less than 16 hours, which is faster compared to other scaffold-based cultures. In addition, there is no need for specialized medium or an artificial substrate. Hau *et al*., used this approach to form spheroids of the colon cancer LoVo cells and showed that these 3D cultures were more resilient to anticancer therapy than corresponding monolayer cultures [74].

All scaffold-based culturing systems, as well as the hanging-drop and the liquid overlay system, have one common drawback: the medium is stagnant which can cause problems related to nutrient supply and waste disposal [16,17]. This is especially disadvantageous when growing spheroids over longer periods of time. For the MLM, some magnet based techniques can be used to facilitate medium exchange or spheroid handling, *e.g*. MagPen^{TM} from n3D Biosciences [73].

For long-term cultivation, non-stagnant culture systems such as the spinner flask are often more suitable. Within the spinner flask, cells lack a substrate and as a result they interact with each other and form aggregates. Spheroids can also be preformed using a non-adherent initiation dish, a so called mother dish, which is meant for short term cultivation. After initiation, the spheroids are transferred into the spinner flask. The spinner flasks already exists for over 30 years but remains one of the most efficient scaffold-free systems for obtaining large amounts of spheroids within a particular size range under well controlled nutrient supply. Other commonly used non-stagnant systems are roller tubes and the gyratory shaker [63].

More recently, bioreactor systems were developed that provide efficient mass transfer and automated control of temperature, pH, and other environmental factors [75]. An example is the rotating wall vessel (RWV) or NASA bioreactor that allows for continuous medium perfusion and a well-controlled nutrient flow rate. In this rotary system, cells are kept in suspension under very low sheer stress by microgravity simulation [76]. Since the RWV is more expensive than the spinner flask and since it has a less straightforward setup, the advantages are limited.

The demand for systems that adequately mimic the *in vivo* environment of cells led to the development of 'body-on-a-chip' systems. Their resemblance with functional tissue is achieved by imbedding the latest generation microfluidics in order to enhance perfusion of the microenvironment. These systems are further improved by exposing the cells to matrix proteins such as collagen or Matrigel so that the system meets the spheroid's need for nutrients, oxygen and waste removal. [75,77]. These systems hold great promise for long term cultivation and repeated *in vitro* drug exposure studies.

A serious drawback of all rotating systems and systems with perfusion is that they require high quantities of medium while in drug testing it is often preferred to use low amounts of candidate drugs [77]. Therefore, drug exposure tests might be better of using stationary systems such as the ones described previously. Perfusion-based systems are rather positioned in between high-throughput *in vitro* screening and *in vivo* preclinical models.

In conclusion, many different approaches exist that allow for spheroid formation. Some systems are better for obtaining large amounts of spheroids or large-sized spheroids, others are better in maintaining nutrient supply and waste disposal and yet others are better for culturing spheroids over longer periods of time.

Since the spheroid's size, shape and environment strongly depend on the culturing system, it is pivotal to develop standardized protocols before spheroid systems can be implemented in mainstream drug discovery pipelines [60]. These protocols will limit the variability between different experimental setups and thus will increase the comparability of the results. In-depth studies must be performed to determine which culturing system is best suited for a particular application. To determine which system is best for evaluating antitumor therapeutic efficacy, different factors have to be considered including throughput, cost, spheroid size, size distribution, and shape. When studies employ the same experimental setup, it becomes more meaningful to compare spheroid parameters such as volume growth, viability, survival, migration, and pathophysiological status. Once a standardized 3D system gets widely accepted for therapeutic efficacy determination, it can add significant value to the drug discovery chain as it can give determinative information that is often missed by conventional *in vitro* and *in vivo* drug screening models.

6.4 Conclusion

Scientists have been looking for models to bridge the gap between *in vitro* findings and *in vivo* relevance for a long time. 3D models offer great promise as intermediate models between conventional 2D cultures and animal experimental models *in vivo*. In 3D cell cultures, cells form

multicellular spheroids that re-acquire many features of native tissues or tumors. Their organization limits unnatural cell-synthetic material contacts. 3D spheroids have proven to be useful in many areas of biology, including studies of drug discovery, differentiation, cell proliferation, gene and protein expression, apoptosis, and pharmacology. Currently, one can choose among a variety of 3D culture methods, each characterized by its advantages, but also by a series of limitations. The current culturing systems are improving and will continue to improve due to technological innovations of media supplements, ECM-like materials, microfluidic devices, and nano-scale coatings. However, in order for these models to translate in more effective drug discovery programs, standardized protocols must be developed employing one suitable culturing system. This will improve result comparability, will lower the complexity of working with 3D systems, and will help prevent drawing false conclusions from independent studies.

References

[1] C. Giaccotto, R.E. Santerre, J.A. Vernon, Drug prices and research and development investment behavior in the pharmaceutical industry, Journal of Law and Economics, 48 (2005) 195-214. doi:10.1086/426882.

[2] J. Avorn, The $2.6 billion pill – methodologic and policy considerations, N. Engl. J. Med. 372 (2015) 1877-1879. doi: 10.1056/NEJMp1500848

[3] M.J. Waring, J. Arrowsmith, A.R. Leach, P.D. Leeson, S. Mandrell, R. M. Owen, G. Pairaudeau, W.D. Pennie, S.D. Pickett, J. Wang, O. Wallace, A. Weir, An analysis of the attrition of drug candidates from four major pharmaceutical companies, Nature rev. Drug. Dis. 14 (2015) 476-485. doi:10.1038/nrd4609

[4] J.P. Hughes, S. Rees, S.B. Kalindjian, K.L. Philpott, Principles of early drug discovery, Br. J. Pharmacol. 162 (2011) 1239-1249. doi: 10.1111/j.1476-5381.2010.01127.x

[5] I. Beets, T. Janssen, E. Meelkop, L. Temmerman, N. Suetens, S. Rademakers, G. Jansen, L. Schoofs, Vasopressin/oxytocin-related signaling regulates gustatory associative learning in C. elegans, Science. 338 (2012) 543-545. doi:10.1126/science.1226860.

[6] R.A. Kobet, X. Pan, B. Zhang, S.C. Pak, A.S. Asch, M.H. Lee, Caenorhabditis elegans: A Model System for Anti-Cancer Drug Discovery and Therapeutic Target Identification, Biomol. Ther. (Seoul) 22 (2014) 371-383. doi:10.4062/biomolther.2014.084.

[7] D. Cunningham, Z. You, In vitro and in vivo model systems used in prostate cancer research, J. Biol. Methods. 2 (2015) pii: e17. doi:10.14440/jbm.2015.63.

[8] J.C. Walrath, J.J. Hawes, T. Van Dyke, K.M. Reilly, Genetically engineered mouse models in cancer research, Adv. Cancer Res. 106 (2010) 113-164. doi:10.1016/S0065-230X(10)06004-5.

[9] A. Knight, Systematic reviews of animal experiments demonstrate poor human clinical and toxicological utility, Altern. Lab. Anim. 35 (2007) 641-659. doi:10.12174/157488708784223844.

[10] D. Antoni, H. Burckel, E. Josset, G. Noel, Three-dimensional cell culture: a breakthrough in vivo, Int. J. Mol. Sci. 16 (2015) 5517-5527. doi:10.3390/ijms16035517.

[11] J. Gordon, S. Amini, M.K. White, General overview of neuronal cell culture, Methods Mol. Biol. 1078 (2013) 1-8. doi:10.1007/978-1-62703-640-5_1.

[12] Y. Miki, K. Ono, S. Hata, T. Suzuki, H. Kumamoto, H. Sasano, The advantages of co-culture over mono cell culture in simulating *in vivo* environment, J. Steroid Biochem. Mol. Biol. 131 (2012) 68-75. doi:10.1016/j.jsbmb.2011.12.004.

[13] L. Goers, P. Freemont, K.M. Polizzi, Co-culture systems and technologies: taking synthetic biology to the next level, J. R. Soc. Interface. 11 (2014) 1-13. doi:10.1098/rsif.2014.0065.

[14] N. Gomez-Roman, K. Stevenson, L. Gilmour, G. Hamilton, A.J. Chalmers, A novel 3D human glioblastoma cell culture system for modeling drug and radiation responses, Neuro. Oncol. xx (2016) 1-13. doi:10.1093/neuonc/now164.

[15] O.S. Aljitawi, D. Li, Y. Xiao, D. Zhang, K. Ramachandran, L. Stehno-Bittel, P. Van Veldhuizen, T.L. Lin, S. Kambhampati, R. Garimella, A novel 3 dimensional stromal-based model for in vitro chemotherapy

sensitivity testing of leukemia cells, Leuk. Lymphoma. 55 (2014) 378-391. doi:10.3109/10428194.2013.793323.

[16] R. Edmondson, J.J. Broglie, A.F. Adcock, L. Yang, Three-dimensional cell culture systems and their applications in drug discovery and cell-based biosensors, Assay. Drug Dev. Technol. 12 (2014) 207-218. doi: 10.1089/adt.2014.573.

[17] M. Ravi, V. Paramesh, S.R. Kaviya, E. Anuradha, F.D. Paul Solomon, 3D cell culture systems: advantages and applications, J. Cell. Physiol. 230 (2015) 16-26. doi:10.1002/jcp.24683.

[18] P. Hingorani, W. Zhang, S. Piperdi, L. Pressman, J. Lin, R. Gorlick, E.A. Kolb, Preclinical activity of palifosfamide lysine (ZIO-201) in pediatric sarcomas including oxazaphosphorine-resistant osteosarcoma, Cancer Chemother. Pharmacol. 64 (2009) 733-740. doi: 10.1007/s00280-008-0922-4.

[19] V.M. Weaver, O.W. Petersen, F. Wang, C.A. Larabell, P. Briand, C. Damsky, M.J. Bissell, Reversion of the malignant phenotype of human breast cells in three-dimensional culture and in vivo by integrin blocking antibodies, J. Cell. Biol. 137 (1997) 231-245. doi:10.1083/jcb.137.1.231.

[20] K. Bhadriraju, C.S. Chen, Engineering cellular microenvironments to improve cell-based drug testing, Drug Discov. Today. 7 (2002) 612-620. doi:10.1016/S1359-6446(02)02273-0.

[21] F.P. Guengerich, Cytochrome P450 and chemical toxicology, Chem. Res. Toxicol. 21 (2008) 70-83. doi:10.1021/tx700079z.

[22] S.C. Ramaiahgari, M.W. den Braver, B. Herpers, V. Terpstra, J.N.M. Commandeur, B. van de Water, A 3D in vitro model of differentiated HepG2 cell spheroids with improved liver-like properties for repeated dose high-throughput toxicity studies, Ar. Tox. 88 (2014) 1083-1095. doi:10.1007/s00204-014-1215-9.

[23] L.G. Griffith, M.A. Swartz, Capturing complex 3D tissue physiology in vitro, Nature Rev. Mol. Cell. Biol. 7 (2006) 211-214. doi:10.1038/nrm1858.

[24] K.M. Yamada, E. Cukierman, Modeling tissue morphogenesis and cancer in 3D, Cell 130 (2007) 601-610. doi:10.1016/j.cell.2007.08.006.

[25] W. Fayad, S. Brnjic, D. Berglind, S. Blixt, M.C. Shoshan, M. Berndtsson, M. Hägg Olofsson, S. Linder, Restriction of cisplatin induction of acute apoptosis to a subpopulation of cells in a three-dimensional carcinoma culture model, Int. J. Cancer. 125 (2009) 2450-2455. doi:10.1002/ijc.24627.

[26] M. Wartenberg, F.C. Ling, M. Muschen, F. Klein, H. Acker, M. Gassmann, K. Petrat, V. Putz, J. Hescheler, H. Sauer, Regulation of the multidrug resistance transporter P-glycoprotein in multicellular tumor spheroids by hypoxia-inducible factor (HIF-1) and reactive oxygen species, (FASEB J. 17 (2003) 503-505. doi:10.1096/fj.02-0358fje.

[27] A.I. Minchinton, Drug penetration in solid tumours, Nat. Rev. Cancer, 6 (2006) 583-592. doi: 10.1038/nrc1893.

[28] C.R. Thoma, M. Zimmermann, I. Agarkova, J.M. Kelm, W. Krek, 3D cell culture systems modeling tumor growth determinants in cancer target discovery, Adv. Drug. Deliv. Rev. 69 (2014) 29-41. doi: 10.1016/j.addr.2014.03.001.

[29] V. Härmä, H.-P. Schukov, A. Happonen, I. Ahonen, J. Virtanen, H. Siitari, M. Akerfelt, J. Lotjonen, M. Nees, Quantification of Dynamic Morphological Drug Responses in 3D Organotypic Cell Cultures by Automated Image Analysis, PLoS one, 9 (2014) e96426. doi:10.1371/journal.pone.0096426.

[30] H. Acker, J. Carlsson, W. Mueller-Klieser, R.M. Sutherland, Comparative pO2 measurements in cell spheroids cultured with different techniques, Br. J. Cancer, 56 (1987) 325-327. PMC2002210.

[31] J. Carlsson, H. Acker, Relations between pH, oxygen partial pressure and growth in cultured cell spheroids, Int. J. Cancer, 42 (1988) 715-720.

[32] S. Walenta, J. Dötsch, B. Bourrat- Flöck, W. Mueller-Klieser, Size-Dependent Oxygenation and Energy Status in Multicellular Tumor Spheroids, Adv. Exp. Med. Biol. 277 (1990) 889-893. doi:10.1007/978-1-4684-8181-5_102.

[33] G. Mehta, A.Y. Hsiao, M. Ingram, G.D. Luker, S. Takayama, Opportunities and challenges for use of tumor spheroids as models to test drug delivery and efficacy, J. Control. Release. 164 (2012) 192-204. doi:10.1016/j.jconrel.2012.04.045.

[34] S. Strese, M. Fryknas, R. Larsson, J. Gullbo, Effects of hypoxia on human cancer cell line chemosensitivity, BMC cancer. 13 (2013) 1-11. doi:10.1186/1471-2407-13-331.

[35] R.Z. Lin, H.Y. Chang, Recent advances in three-dimensional multicellular spheroid culture for biomedical research, Biotechnol. J. 3 (2008) 1172-1184. doi:10.1002/biot.200700228.

[36] Y.-C. Tung, A.Y. Hsiao, S.G. Allen, Y. Torisawa, M. Ho, S. Takayama, High-throughput 3D spheroid culture and drug testing using a 384 hanging drop array, Analyst. 136 (2011) 473-478. doi:10.1039/c0an00609b.

[37] D.B. Longley, D.P. Harkin, P.G. Johnston, 5-fluorouracil: mechanisms of action and clinical strategies, Nature reviews cancer, 3 (2003) 330-338. doi:10.1038/nrc1074.

[38] W.A. Denny, W.R. Wilson, Tirapazamine: a bioreductive anticancer drug that exploits tumour hypoxia, Expert. Opin. Investig. Drugs. 9 (2000) 2889-2901. doi:10.1517/13543784.9.12.2889.

[39] D. Loessner, K.S. Stok, M.P. Lutolf, D.W. Humacher, J.A. Clements, S.C. Rizzi, Bioengineered 3D platform to explore cell-ECM interactions and drug resistance of epithelial ovarian cancer cells, Biomaterials. 31 (2010) 8494-8506. doi:10.1016/j.biomaterials.2010.07.064.

[40] H. Gaskell, P. Sharma, H.E. Colley, C. Murdoch, D.P. Williams, S.D. Webb, Characterization of a functional c3A liver spheroid model, Toxicol. Res. 5 (2016) 1053-1065. doi:10.1039/C6TX00101G.

[41] Y. Takahashi, Y. Hori, T. Yamamoto, Y. Ohara, H. Tanaka, Three-dimensional (3D) spheroid cultures improve the metabolic gene expression profiles of HepaRG cells, Biosci. Rep. 35 (2015) e200208. doi:10.1042/BSR20150034.

[42] S. Sakai, S. Ito, K. Kawakami, Calcium alginate microcapsules with spherical liquid cores templated by gelatin microparticles for mass production of multicellular spheroids, Acta. Biomater. 6 (2010) 3132-3 137. doi:10.1016/j.actbio.2010.02.003.

[43] K.M. Olsavsky, J.L. Page, M.C. Johnson, H. Zarbl, S.C. Strom, C.J. Omiecinski, Gene expression profiling and differentiation assessment in primary human hepatocyte cultures, established hepatoma cell lines, and human liver tissues, Toxicol. Appl. Pharmacol. 222 (2007) 42-56. doi:10.1016/j.taap.2007.03.032.

[44] O. Jeon, R. Marks, D. Wolfson, E. Alsberg, Dual-crosslinked hydrogel microwell system for formation and culture of multicellular human adipose tissue-derived stem cell spheroids, J. Mater. Chem. B. 4 (2016) 3526-3533. doi:10.1039/C6TB00064A.

[45] J. R. Wisniewski, A. Vildhede, A. Noren, P. Artursson, In-depth quantitative analysis and comparison of the human hepatocyte and hepatoma cell line HepG2 proteomes, J. Prot. 136 (2016) 234-247. doi:10.1042/BSR20150034.

[46] F. Lakehal, D. Wendum, V. Barbu, L. Becquemont, R. Poupon, P. Balladur, L. Hannoun, F. Ballet, P.H. Beaune, C. Housset, Phase I and Phase II drug-metabolizing enzymes are expressed and heterogeneously distributed in the biliary epithelium, Hepatology. 30 (1999) 1498-1506. doi: 10.1002/hep.510300619.

[47] A.C. Luca, S. Mersch, R. Deenen, S. Schmidt, I. Messner, K.-L. Schäfer, S.E. Baldus, W. Huckenbeck, R.P. Piekorz, W.T. Knoefel, A. Krieg, N.H. Stoecklein, Impact of the 3D microenvironment on phenotype, gene expression, and EGFR inhibition of colorectal cancer cell lines, PLoS One. 8 (2013) 1-11. doi: 10.1371/journal.pone.0059689.

[48] S. Ghosh, G.C. Spagnoli, I. Martin, S. Ploegert, P. Demougin, M. Heberer, A. Reschner, Three-dimensional culture of melanoma cells profoundly affects gene expression profile: a high density oligonucleotide array study, J. Cell. Phys. 204 (2005) 522-531. doi:10.1002/jcp.20320.

[49] O.M. Maria, O. Maria, Y. Liu, S.V. Komarova, S.D. Tran, Matrigel improves functional properties of human submandibular salivary gland cell line, Int. J. Biochem. Cell. Bio. 43 (2011) 622-631. doi:10.1016/j.biocel.2011.01.001.

[50] D. Haouzi, S. Baghdiguian, G. Granier, P. Travo, P. Mangeat, U. Hibner, Three-dimensional polarization sensitizes hepatocytes to Fas/CD95 apoptotic signaling, J. Cell. Sci. 118 (2005) 2763-2773. doi:10.1242/jcs.02403.

[51] M.W. Tibitt, K.S. Anseth, Hydrogels as extracellular matrix mimics for 3D cell culture, Biotechnol. Bioeng. 103 (2009) 655-663. doi:10.1002/bit.22361.

[52] S. Zhang, F. Gelain, X. Zhao, Designer self-assembling peptide nanofiber scaffolds for 3D tissue cell cultures, Sem. Cancer Biol. 15 (2005) 413-420. doi:10.11016/j.semcancer.2005.05.007.

[53] S. MacNeil, Progress and opportunities for tissue-engineered skin, 445 (2007) 874-880. doi: 10.1038/nature05664.

[56] Y. Yoshii, A. Waki, K. Yoshida, A. Kakezuka, M. Kobayashi, H. Namiki, Y. Kuroda, Y. Kiyono, H. Yoshii, T. Furukawa, T. Asai, H. Okazawa, J.G. Gelovani, Y. Fujibayashi, The use of nanoimprinted scaffolds as 3D culture models to facilitate spontaneous tumor cell migration and well-regulated spheroid formation, Biomaterials. 32 (2011) 6052-6058. doi:10.1016/j.biomaterials.2011.04.076.

[57] T. Magdeldin, V. Lopez-Davila, C. Villemant, G. Cameron, R. Drake, U. Cheema, M. Loizidou, The efficacy of cetuximab in a tissue-engineered three-dimensional in vitro model of colorectal cancer, J. Tissue. Eng. 5 (2014) 1-9. doi:10.1177/2041731414544183.

[58] M.E. Katt, A.L. Placone, A.D. Wong, Z.S. Xu, P.C. Searson, In vitro tumor models: advantages, disadvantages, variables, and selecting the right platform. Front. Bioeng. Biotechnol. 4 (2016) 1-14. doi:10.3389/fbioe.2016.00012.

[59] H.R. Mellor, S. Snelling, M.D. Hall, S. Modok, M. Jaffar, T.W. Hambley, R. Callaghan, The influence of tumour microenvironmental factors on the efficacy of cisplatin and novel platinum(IV) complexes. Biochem. Pharm. 70 (2005) 1137-1146. doi:10.1016/j.bcp.2005.07.016.

[60] M. Zanoni, F. Piccinini, C. Arienti, A. Zamagni, S. Santi, R. Polico, A. Bevilacqua, A. Tesei, 3D tumor spheroid models for in vitro therapeutic screening: a systematic approach to enhance the biological relevance of data obtained, Sc. Rep. 6 (2016) 19103. doi:10.1038/srep19103.

[61] L.C. Kimlin, G. Casagrande, V.M. Virador. In vitro three-dimensional (3D) models in cancer research: an update. Mol. Carcin. 52 (2013) 167-182. doi:10.1002/mc.21844.

[62] V. van Duinen, S.J. Trietsch, J. Joore, P. Vulto, T. Hankemeier, Microfluidic 3D cell culture: from tools to tissue models, Curr. Opin. Biotech. 35 (2015) 118-126. doi:10.1016/j.copbio.2015.05.002.

[63] J. Friedrich, R. Ebner, L.A. Kunz-Schughart. Experimental anti-tumor therapy in 3-D: Spheroids – old hat or new challenge? J. Rad. Biol. 83 (2009) 849-871. doi:101080/0955300701727531.

[64] L. Li, Y. Lu, Optimizing a 3D Culture System to Study the Interaction between Epithelial Breast Cancer and Its Surrounding Fibroblasts, J. Cancer, 2 (2011) 458-466.

[65] A. Bachmann, M. Moll, E. Gottwald, C. Nies, R. Zantl, H. Wagner, B. Burkhardt, J.J. Martinez Sanchez, R. Ladurner, W. Thasler, G. Damm, A.K. Nussler, 3D cultivation techniques for primary human hepatocytes, Microarrays. 4 (2015) 64-83. doi:10.3390/microarrays4010064.

[66] K. Aritomi, Y. Ishitsuka, Y. Tomishima, D. Shimizu, N. Abe, T. Shuto, M. Irikura, H. Kai, T. Irie, Evaluation of three-dimensional cultured HepG2 cells in a nano culture plate system: an in vitro human model of acetaminophen hepatotoxicity. J. Pharmacol. Sci. 124 (2014) 218-229. doi:10.1254/jphs.13135FP.

[67] S.R. Horman, C. Hogan, K.D. Reyes, F. Lo, C. Antczak, Challenges and opportunities toward enabling phenotypic screening of complex and 3D cell models, Fut. Med. Chem. 7 (2015) 513-525. doi:10.4155/fmc.14.163.

[68] R. Foty, A simple hanging drop cell culture protocol for generation of 3D spheroids, J. Vis. Exp. 6 (2011) 2720. doi:10.3791/2720.

[69] S. Messner, I. Agarkova, W. Moritz, J.M. Kelm, Multi-cell type human liver microtissues for hepatotoxicity testing, Arch. Toxicol. 87 (2013) 209-213. doi:10.1007/s00204-012-0968-2.

[70] A. Rotem, A. Janzer, B. Izar, Z. Ji, J.G. Doench, L.A. Garraway, K. Struhl, alternative to the soft-agar assay that permits high-throughput drug and genetic screens for cellular transformation, PNAS, 112 (2015) 5708-5713. doi:10.1073/pnas.1505979112.

[71] D.P. Ivanov, T.L. Parker, D.A. Walker, C. Alexander, M.B Ashford, P.R. Gellert, Multiplexing spheroid volume, resazurin and acid phosphatase viability assays for high-throughput screening of tumour spheroids and stem cell neurospheres, PLoS one, 9 (2014) e103817. doi:10.1371/journal.pone.0103817.

[72] M. Vinci, S. Gowan, F. Boxall, L. Patterson, M. Zimmermann, W. Court, C. Lomas, M. Mendiola, D. Hardisson, S.A. Eccles, Advances in establishment and analysis of three-dimensional tumor spheroid-based functional assays for target validation and drug evaluation, BMC Biol. 10 (2012) 1-20. doi:10.1186/1741-7007-10-29.

[73] W.L. Haisler, D.M. Timm, J.A. Gage, H. Tseng, T.C. Killian, G.R. Souza, Three-dimensional cell culturing by magnetic levitation, Nat. Prot. 8 (2013) 194-1949. doi:10.1038/nprot.2013.125.

[74] H. Hau, D. Khanal, L. Rogers, N. Suchowerska, R. Kumar, S. Sridhar, Dose enhancement and cytotoxicity of gold nanoparticles in colon cancer cells when irradiated with kilo- and mega-voltage radiation, Bioeng. Transl. Med. 1 (2B13) 94-102. doi:10.1002/btm2.10007.

[75] J.A. Hickman, R. Graeser, R. de Hoogt, S. Vidic, C. Brito, M. Gutekunst, H. van der kuip, Three-dimensional models of cancer for pharmacology and cancer cell biology: Capturing tumor complexity in vitro/ex vivo, Biotechnology J. 9 (2014) 115-1128. doi:10.1002/biot.201300492.

[76] M. Ingram, G.B. Techy, R. Saroufeem, O. Yazan, K.S. Narayan, T.J. Goodwin, G.F. Spaulding, Three-dimensional growth patterns of various human tumor cell lines in simulated microgravity of a NASA bioreactor, In Vitro Cell. Dev. Biol. 33 (1997) 459–466. doi:10.1007/s11626-997-0064-8.

[77] M. Jang, P. Neuzil, T. Volk, A. Manz, A. Kleber, On-chip three-dimensional cell culture in phaseguides improves hepatocyte functions *in vitro*, Biomicrofluidics, 9 (2015) 034113. doi:10.1063/1.4922863.

Chapter VII

Comprehensive evaluation of differential receptor expression between 2D and 3D cell cultures of HT-29 colorectal adenocarcinoma cells

---

Abstract

The quest to develop more predictive and physiologically relevant cell culture systems has led to the development of several types of 3D cell culture models. Current 3D systems allow researchers to mimic *in vivo* cell behavior more closely compared to cells grown as a monolayer. Despite the recognition of the potential of 3D cell culture models among a growing number of researchers, 3D cell cultures have not yet replaced monolayer cultures on a large scale. One of the reasons that hampers a shift from 2D to 3D cell culture systems is the lack of a detailed biochemical characterization of multicellular 3D spheroids. For example, little easily accessible information exists on differential receptor expression between cells cultured in 2D and 3D. To bridge this gap, we used RNA-sequencing to measure differential receptor expression in the human colon adenocarcinoma cell line HT-29 cultivated in 2D and 3D. We identified 17 differentially expressed genes encoding GPCRs, as well as several clinically relevant RTKs and ion channels. A substantial number of receptors that were significantly upregulated in 3D cell cultures were also upregulated in colorectal tumor samples. In addition, pathway enrichment analysis revealed that a number of pathways were altered among HT-29 spheroids and 2D cell cultures, including pathways associated with cell cycle progression and glucose metabolism. In summary, the present study outlines gene expression differences between 2D and 3D HT-29 cell cultures and lays the foundation for further functional studies of differentially expressed genes potentially involved in colorectal carcinogenesis.

7.1 Introduction

Colorectal cancer (CRC) is a major public health issue, particularly in the United States and other Western countries. The CRC burden is expected to increase to more than 2.2 million new cases and 1.1 million deaths by 2030 [1]. As CRC becomes more common, the demand for new anticancer drugs increases. This has resulted in large investments in the area of oncology drug development during the past few decades. However, according to Hutchinson and Kirk, the return on these investments is often low as preclinical cancer drug research has a lower clinical success rate than other therapeutic areas [2]. In comparison with other drugs, more oncology drug failures seem to reach late-stage clinical trials where the expenses are huge [3]. This is partially due to the fact that the majority of cancer model systems lack efficiency when it comes to identifying molecules that alter the outcome of cancer development and progression [2,4].

Present-day researchers rely on a wide range of *in vitro* cancer models to study different aspects of the biology of CRC. Primary or immortalized cell lines derived from a human or animal tumor are a popular starting point for evaluating the potential anticancer effect of test compounds. In the majority of cases, cells are seeded and grown as monolayers on a glass or polystyrene plastic surface in culture flasks. These two-dimensional (2D) cell cultures offer a variety of advantages, such as easy cell observation, manipulation, and environmental control [5,6]. Even though 2D cell culture models have served a key role in identifying some of the driving forces behind CRC development and progression, it is becoming increasingly apparent that cells cultured under these conditions fail to recapitulate important aspects of *in vivo* tumor biology. One of the major reasons is a reduced ability of 2D cell cultures to form cell-cell and cell-extracellular matrix (ECM) communication networks, as they spread and adhere to artificial substrates. This may have important biological consequences, ranging from differences in sensitivity to pharmacological compounds to aberrant differentiation of cells [5-9]. Moreover, it has economic consequences further down the drug development pipeline, as it at least partially accounts for the high attrition rate of drug candidates in clinical trials [3,10].

In order to overcome these shortcomings, researchers have made progress in developing alternative models that are physiologically and biochemically more similar to the complex *in vivo* microenvironment. This has led to the introduction of three-dimensional (3D) culture systems, in which cells are permitted to attach to one another in a 3D conformation (see chapter 6). These larger 3D cell aggregates, called spheroids, preserve the characteristics of the native tissue more accurately [11]. Accumulating evidence suggests that 3D cell culture systems are often superior to their 2D counterparts as model systems for cell migration, communication, differentiation, and survival. In

addition, growing cells as multicellular 3D spheroids reveals more realistic drug responses, which could lead to more predictive data for *in vivo* tests [5-8,12].

Despite the aforementioned benefits of growing cells as 3D spheroids, a paradigm shift from 2D to 3D cell culture systems has not yet been achieved [13]. This is especially remarkable since a wide range of commercially available culturing tools have emerged that permit cells to grow in three dimensions [6]. However, working with 3D cell cultures is not always convenient due to the variability of spheroid size, reproducibility, cost, and compatibility with conventional assays or high throughput equipment [13,14]. Another major issue that precludes universal standardization of 3D cell culture models for drug development is the lack of a detailed biochemical characterization of multicellular 3D spheroids. Deepening our understanding of complex 3D models can be achieved by imaging techniques or high-throughput technologies such as genomic or transcriptomic profiling.

In this exploratory study, we used RNA-sequencing (RNA-Seq) to compare gene expression profiles between 2D and 3D cell cultures of HT-29 colorectal adenocarcinoma cells. This cell line was chosen because of its widespread use as an *in vitro* model in preclinical cancer research [15-19]. Several reports indicate that 3D cell cultures of HT-29 cells resemble human colorectal tumors more closely than conventional 2D cultures. For instance, Osswald *et al*. report that HT-29 3D cell cultures display several relevant features of solid tumors such as an outer region of proliferating cells and apoptotic and hypoxic regions in the core [17]. Magdeldin *et al*. also suggest that HT-29 3D spheroids are suitable *in vitro* cancer models to bridge the current *in vitro – in vivo* gap [19]. In addition, HT-29 cells are commonly used to assess effects of test compounds on food digestion, mucin secretion, and bioavailability [20,21].

Other research groups have determined gene expression profiles of multicellular HT-29 spheroids [17,18,22]. However, most studies use microarray technology to reveal gene expression signatures in response to a particular test compound, leaving valuable information about untreated control samples in the dark. Expression data from quantitative polymerase chain reaction (qPCR), microarray technology, and RNA-Seq experiments can be retrieved from publicly accessible repositories, but their systematic use has been limited due to the lack of an open vocabulary and open submission structure. Moreover, many publications do not include conventional 2D models, which could facilitate the incorporation of 3D models in the drug discovery process. The outcome of a gene expression profiling experiment can also be influenced by experimental design and environmental conditions. The current lack of standardized protocols to generate multicellular spheroids or analyze gene expression data hampers cross-comparisons between different studies.

To deal with some of these issues, we compared the transcription profiles of 2D and 3D cell cultures of HT-29 cells and provide a comprehensive summary on the subject. 3D cell cultures were grown on nanoculture plates (NCP), which are engineered with a nanoscale-patterned structure on the culture surface. Because cells do not adhere strongly to the imprinted film on the bottom of the well, they start to migrate randomly, which facilitates spontaneous multicellular spheroid formation. Yoshii *et al*. reported that 3D cell cultures grown on NCPs exhibit many features that are also seen when growing tumors *in vivo* [23]. In addition, spheroid formation involves little alterations to 2D cell culture procedures.

Our results indicated that 2D cell cultures of HT-29 cells have distinct variations in their transcriptional profile compared to multicellular HT-29 spheroids. These divergent gene expression patterns could lead to differences in drug transporter or receptor expression which in turn drives an altered response/resistance to anticancer drugs. Because receptors are typically envisaged as drug targets, knowledge about differentially expressed receptors in 2D and 3D cell cultures are of great value to define new therapeutic targets or develop new therapeutics. Therefore, one of our goals is to provide the reader with an easily accessible profile of differential receptor expression among HT-29 cells cultured in 2D and 3D. In addition, we performed Gene Ontology (GO) as well as Kyoto Encyclopedia of Genes and Genomes (KEGG) pathway enrichment analysis to gain further insight into the biological functions of the identified differentially expressed genes (DEGs). We observed changes to a number of signaling pathways associated with cell cycle progression, DNA replication, mismatch repair, and glucose metabolism, which suggest that the proliferative and metabolic capacity of 3D-cultured HT-29 cells was altered in comparison to 2D-cultured cells.

7.2 Material and methods

Reagents

McCoy's 5A, Phosphate Buffered Saline (PBS), Fetal Bovine Serum (FBS), Penicillin/Streptomycin, Trypsin/Ethylenediaminetetraacetatic acid (EDTA), and RNaseZAP were purchased from Sigma-Aldrich (St.-Louis, MO, USA).

2D cell cultures

The human colon adenocarcinoma cell line HT-29 was used in this study (ECACC, Porton Down, Wiltshire, UK). Mycoplasma-free HT-29 cells were freshly thawed from the liquid nitrogen stock and a cell suspension was transferred to polystyrene cell culture flasks from Sigma-Aldrich (St.-Louis, MO, USA). HT-29 cells were cultured in McCoy's 5A medium, complemented with 10% FBS, 100 units penicillin/0.1 mg streptomycin, and incubated at 37 °C with 5% CO_2 surroundings. 70% confluent cell cultures were first washed with PBS and then removed from the cell culture flask with trypsin-EDTA (0.25% trypsin, 0.02% EDTA). HT-29 cells were passaged two times using conventional 2D cell culture techniques. Subsequently, cells were allowed to grow in 2D cell culture flasks for six days.

3D cell cultures

NCPs (Scivax, Kanagawa Prefecture, Kawasaki, Japan) were used for spheroid formation of HT-29 cells. Freshly thawed HT-29 cells were cultured using conventional 2D cell culture techniques and passaged two times. After three culturing cycles, a cell suspension was prepared for plating on NCPs. Heat-inactivation of FBS is required to prevent monolayer cell growth. Cells were seeded in a 24-well NCP (Micro-honeycomb (MH) pattern) and cell density was adjusted to 60000 cells per well. NCPs containing the cells were allowed to incubate at ambient temperature for 20 minutes allowing the cells to spread equally across the micropatterned surface. NCPs were then placed in the 5% CO_2/95% air incubator at 37°C for six days before proceeding with RNA extraction.

RNA-extraction

Cells were grown in 2D on standard tissue culture plastic and in 3D using NCPs for six days. Following this period of growth, the cells were harvested for RNA extraction. RNA isolation of the 2D and 3D cultures was conducted using the RNeasy mini kit from Qiagen (Hilden, Germany) according to the manufacturer's protocol with a few optimizations. For 2D cell cultures, the RNA extraction was performed with one million cells. Cell counting was done using the nucleocounter from Chemometec (Allerod, Denmark). For 3D cell cultures, spheroids were harvested by centrifugation for 4 minutes at 800 rounds per minute (RPM) and subsequently used for RNA extraction.

After dissolving the cell pellets in 700 µL guanidine thiocyanate containing RLT lysis buffer included in the RNeasy mini kit, Qiashredder spin columns were used to homogenize the cells. Next, an equal volume of 70% ethanol was added to the lysate and the mixed solution was transferred to a Qiagen spin column. The final concentration of ethanol in the solution promotes RNA binding. Next, the column was washed using 350 µL washing buffer. The RNA attached to the column was further purified by including an on-column DNase-step as described in the RNeasy protocol. During this step, the DNase solution was incubated for 15 minutes on the column to degrade DNA before washing the column with washing buffer twice at 9000g for 20 seconds. Next, an ethanol-containing RPE solution was added to the membrane to dissolve remaining salts. This was done twice, each time followed by centrifugation for 20 seconds at 9000g. The column was washed one last time with RPE for two minutes at 9000g and the spin columns were then dried by centrifugation at maximum speed for one minute. As an additional optimization step the spin columns were left open on the bench-top for 5 minutes to evaporate ethanol. Next, the columns were transferred to a collection tube and 30 µl of RNase-free water was added. After two minutes of incubation, the columns were centrifuged for one minute at 9000g to collect the purified RNA. The purity of the RNA samples was assessed using the Nanodrop ND-1000 spectrophotometer from Thermo Scientific (Waltham, Massachusetts, USA). Important parameters are the yield of RNA and absorbance ratios at 260nm/280nm and 260nm/230nm, which indicate whether the RNA sample is sufficiently pure for sequencing. Further quality control was performed by the 2100 Bioanalyzer from Agilent Technologies (Santa Clara, CA, USA).

RNA-Seq and statistical analysis

Following RNA extraction, complementary DNA (cDNA) samples were pooled and run on Illumina's HiSeq 2500, 50 base pairs (bp) single-end read mode obtaining approximately 10 million reads per sample (Genomics Core Facility, UZ Leuven). Quality control of FASTQ-files was performed with Picard (v1.118) and FastQC (v0.11.5) and adapters were filtered with ea-utils (v1.2.2). Read-mapping was performed using TopHat (v2.0.13) and Bowtie (v2.2.4) against the *Homo sapiens* genome, assembly 19, Ensembl version 75. The resulting BAM alignment files were then handled with Samtools (v0.1.19) and Bamtools (v2.3.0). Read counts were normalized by library size (table 7.1) and differential expression analysis was performed with the R-based Bioconductor package DESeq. DESeq assumes a negative binomial distribution of gene-read counts. DESeq returned p-values as well as adjusted p-values (Q-value) to correct for multiple testing using the Benjamini-Hochberg procedure to determine the false discovery rate (FDR). Genes with an FDR less than 5% (Q-value < 0.05) are declared differentially expressed.

Sample	Used read counts	Size factor
HT-29 (2D)	10777143	0.975269
HT-29 (2D)	8381744	0.827177
HT-29 (2D)	9321921	0.932161
HT-29 (3D)	10117273	1.058
HT-29 (3D)	11074519	1.164596
HT-29 (3D)	1078220	1.102572

Table 7.1. Normalization method included in DESeq package. DESeq calculates a size factor for each sample which is used to adjust for library size (*i.e.* sequencing depth) and produce read count values in a common scale. If size factors are approximately equal to 1, the libraries have been sequenced to the same depth.

GO and KEGG pathway enrichment analysis

DEGs were mapped to the GO and KEGG pathway databases using the Enrichr platform (developed by the Icahn school of medicine and available at http://amp.pharm.mssm.edu/Enrichr/), a web-based open source application that includes 117 gene-set libraries (August 2017), such as KEGG, Reactome, Wikipathways, and the GO database. Each gene-set library falls into one of the following categories: transcription, pathways, ontologies, diseases, cell types, and miscellaneous. This enables users to view enrichment results across different libraries. Enrichr implements p-values and adjusted p-values (Q-value) to report enrichment results. P-values are computed using the Fisher's exact test and adjusted p-values are obtained using the Benjamini-Hochberg method to correct for multiple hypotheses testing. A Benjamini-Hochberg adjusted p-value < 0.05 was chosen as the cut-off value for enriched GO terms and KEGG pathways. To avoid redundancy of GO terms, we used REVIGO (freely available at http://revigo.irb.hr/) to simplify the interpretation of our list of significant GO terms. This is relevant, as several GO child terms with highly statistically significant enrichment were identified and the parent term also appeared significantly enriched as a consequence of encompassing all the genes from the enriched child term. By relying on semantic similarity measures, REVIGO reduces the number of significant GO terms (for more information about REVIGO, see reference 24).

7.3 Results

7.3.1 Experimental design and data quality assessment

Three vials of HT-29 cells were dispensed into standard plastic cell culture flasks and cultured under 2D cell culture conditions for two passages. For experiments, the cultures were harvested and a part of each cell culture was grown under 2D conditions for 6 days while the other part was seeded in 24-well NCPs at 6x10^4 cells/2 ml, allowing spontaneous spheroid formation to occur (figure 7.1-A). On the sixth day of the culture period, dense and solid HT-29 spheroids were microscopically observed for cells grown in the NCP system (figure 7.1-B). Cells were then harvested before proceeding with RNA extraction. To prevent RNA degradation due to trypsinization, 2D cell cultures were harvested by cell scraping and resuspended in a 5 ml falcon. Cell scraping was not required for 3D cell cultures as they do not adhere strongly to the micropatterned surface and detach easily.

The RNA isolation method allows up to 100 µg of RNA longer than 200 bases to bind to the silica-based membrane, providing an enrichment of messenger RNA (mRNA). Next, the quality of isolated RNA was assessed via two methods, *i.e.* a spectrophotometer and a microfluidics system. RNA has its UV absorption maximum at 260 nm and the ratio of UV absorption at 260 nm and 280 nm is used as an indicator of RNA purity (figure 7.1-C) [25]. A ratio of approximately 2 is generally accepted as high purity RNA. A representative example of the spectral output of a 3D sample is displayed in figure 7.1-C (the 260/280 purity ratio is 2.11). Additionally, the RNA quality of the same sample was assessed by calculating the 28S/18S ribosomal RNA (rRNA) ratio via an RNA analysis method based on electrophoresis (figure 7.1-D). Samples with a 28S/18S rRNA mass ratio of approximately 2:1 indicate high RNA integrity (28/18S rRNA ratio is 2.2) [26].

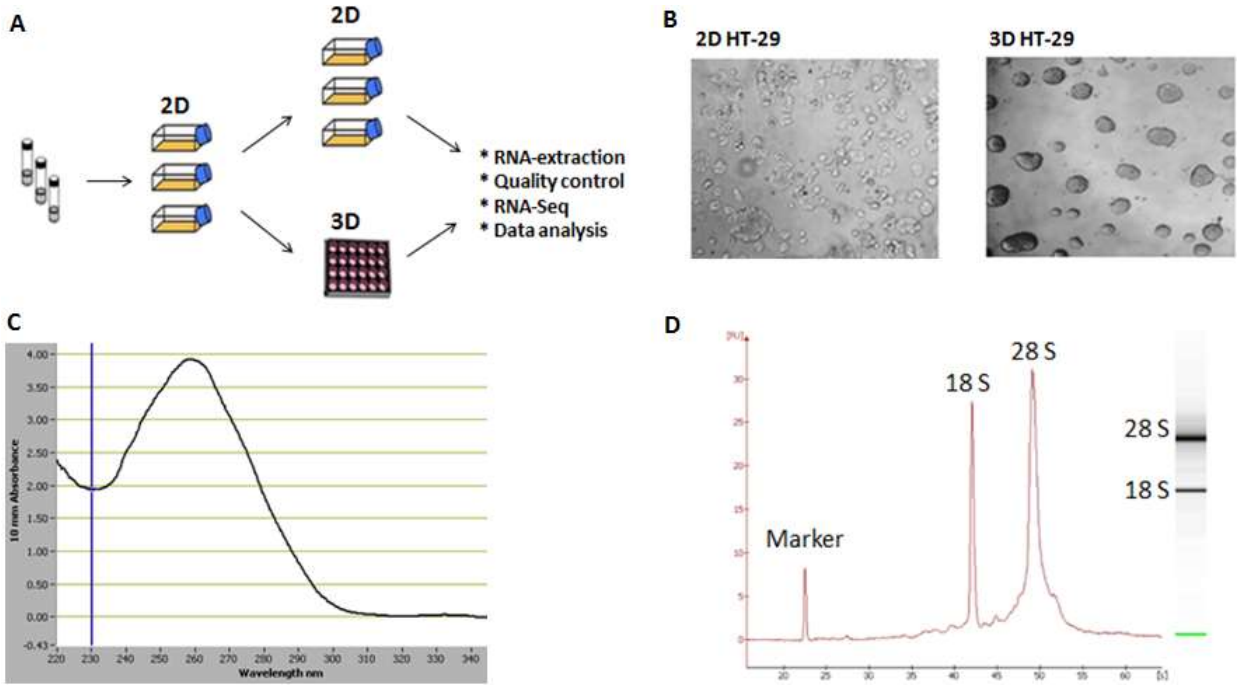

Fig.7.1. Overview of the experimental set-up. Three vials of HT-29 cells were freshly thawed and cultured under 2D conditions for two passages. Cells were either maintained under these conditions or seeded and cultured in NCPs for six days, allowing spontaneous spheroid formation to occur (**A**). 2D and 3D cell cultures (6 days old) as observed under standard inverted microscope (**B**). Representative example of quality analysis of RNA extracted from HT-29 cells under 3D conditions by spectrophotometric measurement (**C**) and Bioanalyzer electropherogram (**D**). Gel images obtained from the 2100 Bioanalyzer are shown at the right with intact 28S and 18S rRNA bands indicated.

A multitude of bioinformatics and statistical tools have been developed to analyze gene expression using RNA-Seq data. A useful starting point in any RNA-Seq analysis is to assess overall similarity between experimental groups. Principal component analysis (PCA) is generally employed to investigate whether two groups can be viewed as different, *e.g.* due to the presence of distinct gene expression patterns. PCA is a descriptive dimensionality reduction approach commonly used to solve the multi-colinearity problem [27]. The first principal component is the linear combination (LC) with maximal sample variance among all LCs of the variables. The second principal component is calculated such that it accounts for the second greatest variance in the data set [27]. Consequently, replicates of a particular cell type grown under exactly the same culture conditions should cluster together, as they should have similar transcription profiles. Figure 7.2 displays the PCA plot for HT-29 cells cultured under 2D and 3D conditions. PCA analysis shows a distinct separation among 2D (green) and 3D (blue) samples, indicating that both groups can be viewed as different due to the presence of DEGs. The x-axis (first principal component) is the direction along which samples show the largest variation and this accounts for 79% of the overall variability, whereas the y-axis (second principal component) explains 12% of the total variance. For practical reasons, the PCA plot was generated by the R-bioconductor package DESeq2 instead of DESeq.

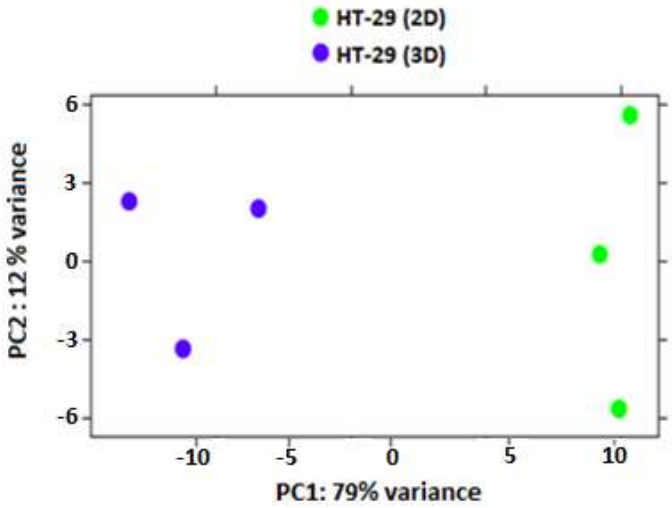

Fig.7.2. A plot of the RNA-seq expression data projected onto the first two principal components, where each spot represents a sample cultured under either 2D (green) or 3D (blue) conditions. Samples that have undergone the same treatment cluster together. The first principal component (PC1) accounts for 79% of the total variance whereas the second principal component (PC2) accounts for 12% of it.

7.3.2 Analysis of differential gene expression

The PCA-plot suggests that HT-29 cells grown in 2D and 3D cell cultures display different gene expression profiles (figure 7.2). 4480 (17,2% of the total) genes were differentially expressed when considering exclusively a significance threshold of p-value less than 0.05. 2185 genes remained significant after correction for multiple testing (FDR ≤ 0.05) (see supplementary material at end of this chapter). Of the 2185 genes, 1173 genes were upregulated and 1012 genes were downregulated in 3D cell cultures relative to 2D cell cultures. We decided on a 5% cut-off *a priori* due to the exploratory nature of this study and we did not want to overlook important differences in gene expression. The value of FDR at which genes are selected is mostly conventional (a FDR between 1% and 10% is commonly used in the literature) and depends on the goal and further analysis options. For example, the use of a more stringent FDR might be more appropriated when expensive or time-consuming work will follow, such as the generation of transgenic mice or designing a drug trial. However, the magnitude of calculated fold changes, and/or (adjusted) p-values does not guarantee biological significance as even small imbalances in a gene expression could initiate a cascade of events which have an impact on cell behavior. On the other hand, large differences in transcript levels do not automatically lead to more protein or metabolite production due to potential PTMs of proteins.

One goal of this study is to identify differentially expressed receptors among 2D and 3D cell cultures of HT-29 cells and highlight receptors with potential relevance in CRC. These differentially expressed transcripts can then be confirmed by complementary methods such as qPCR. Because receptors are major players in cell-cell and cell-ECM communication, changes in receptor gene expression may

drive an altered response to test compounds or environmental stimuli. Therefore, outlining differences between the endogenous receptor repertoire of 2D and 3D cell cultures is of great value. In line with the introductory chapter of this thesis, we will focus on GPCRs, RTKs, and ion channels. We detected differential expression of 38 genes encoding GPCRs, RTKs, and (subunits of) ion channels (figures 7.3-7.5). This number is not too large for subsequent qPCR analysis to validate our RNA-Seq results. Importantly, note that the R package DESeq does not use a default threshold value or strategy to filter low-read counts and we recommend inspecting the results displayed in tables 7.2, 7.3, and 7.4 in a case-by-case manner. This involves checking per sample reads and per condition the average number of read counts for a gene of interest. For example, if all samples show a low number of reads (*e.g.* 5), then there is a case to remove this gene from the list of DEGs since low expression genes can potentially lead to spurious differential expression results. On the other hand, if in one condition the average number of reads is low but in the other one the average number of read counts is high, we would be in favor of keeping this gene. Because we aim to provide a complete overview of our differential expression results, and receptors such as GPCRs are usually expressed at low levels, we opted to display all significantly differentially expressed receptor genes and not to filter genes with low read-counts.

Lynch and Wang suggest that GPCRs play a central role in the development and progression of different types of cancer (including CRC) [28]. Therefore, they are heavily investigated drug targets. Using a 5% FDR ($P_{adj} \leq 0.05$), we extracted 17 differentially expressed GPCRs from the list of 2185 DEGs (figures 7.3 and 7.4). Note that under-expressed genes in 3D cultures have negative $\log_2$ values, whereas over-expressed genes have positive $\log_2$ values.

The list of differentially expressed GPCRs constitutes a combination of well-characterized GPCRs, such as 5-hydroxytryptamine receptor 1D (HTR1D), and so-called orphan GPCRs. Orphan GPCRs are usually named 'GPR' followed by a number, *e.g*. GPR128.

Of class A GPCRs, 3D cultures of HT-29 cells expressed higher levels of mRNA of HTR1D, adrenoceptor α-2A (ADRA2A), G protein-coupled estrogen receptor 1 (GPER1), free fatty acid receptor 2 (FFAR2), opioid related nociception receptor 1 (OPRL1), neuropeptide Y receptor 6 (NPY6R), lysophosphatidic acid receptor 6 (LPAR6), olfactory receptor family 51 subfamily E member 1 (OR51E1), G protein-coupled receptor 137B (GPR137B), GPR146, and GPR160. The gene encoding neurotensin receptor 1 (NTSR1) was expressed to a lower extent when compared to 2D cell cultures.

Of class B GPCRs, differential expression of GPR110, GPR126, and GPR128 was detected. GPR128 was strongly upregulated in 3D cell cultures relative to 2D cell cultures, whereas the opposite is true for genes encoding GPR110 and GPR126.

Two genes encoding class C GPCRs showed differential expression between 2D and 3D culture conditions. In the 2D situation, a significant increase in the expression of G protein-coupled receptor group 5 member A (GPRC5A) was observed, whereas an increased expression level of G protein-coupled receptor group 5 member C (GPRC5C) was detected in 3D spheroids. No genes encoding class F/S GPCRs were identified with statistically significant expression differences. Table 7.2 provides an overview of differentially expressed GPCRs, along with the physiological processes in which they participate.

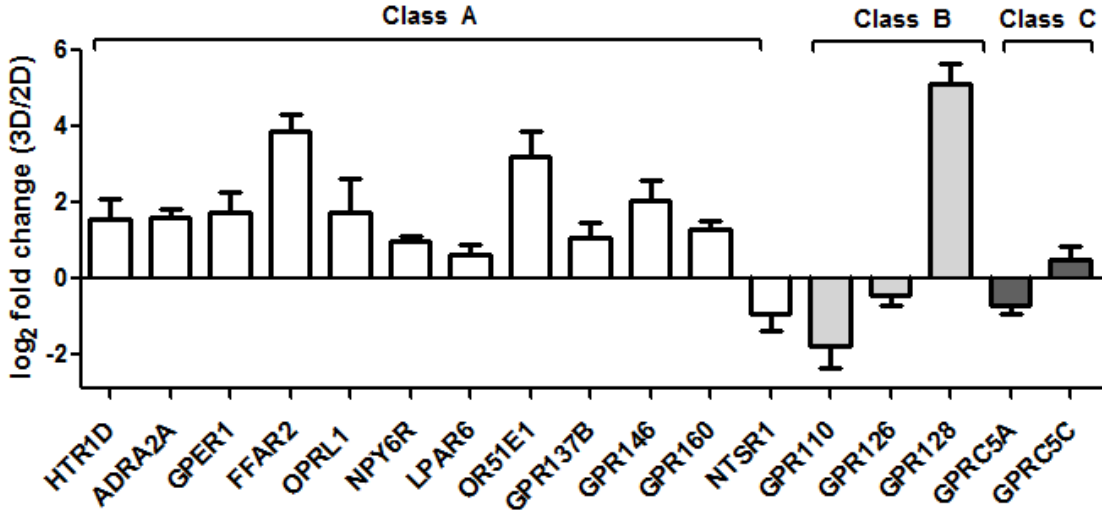

Fig.7.3. DEGs encoding GPCRs in 2D and 3D HT-29 cell cultures as measured by RNA-Seq ($p_{adj} \leq 0.05$). The bar height represents fold changes (log2 based) between groups calculated by DESeq and error bars represent the standard error for the log2 fold change estimate.

Gene symbol	Norm. read counts 2D	Norm. read counts 3D	Log2fc	P_{adj}	Biological relevance
HTR1D	40.2	117.6	1.54	0.004	Stimulation of CRC metastasis by regulating β-catenin/MMP-7 pathway [29].
ADRA2A	269	132	1.61	7.64E-12	Regulation of solute and water transport and cell proliferation. Potential link with inflammatory bowel disease and colon carcinogenesis [30,31].
GPER1	6.2	20.6	1.72	0.02	Mediates estrogenic responses in metabolic and cardiovascular disease. Binding of 17 β-estradiol to estrogen receptors in HT-29 cells induces ERK1/2 activation and increases expression of vitamin D receptor (VDR) gene [32].
FFAR2	1.7	26.4	3.89	8.09E-07	Receptor for short-chain free fatty acids (SCFFA) involved in nutrient sensing [33]. Identified as a functional tumor suppressor in the colon [34].
NPY6R	48.3	95.82	0.98	0.002	Expressed in gastrointestinal tissues. May be the product of a pseudogene.
LPAR6	117.6	181.5	0.62	0.02	LPARs are commonly overexpressed in hepatocellular carcinomas. Mazzocca *et al*. suggest that LPAR6 is an important therapeutic target in HCC tumorigenesis [35].
OR51E1	15.9	146.3	3.2	0.0008	OR51E1 is a potential biomarker for small intestine neuroendocrine carcinomas [36].
NTSR1	895.1	471.9	-0.92	0.045	Neurotensin receptors are expressed in various human colon cancer cell lines, including HT-29 [37].

					Neurotensin, a paracrine/endocrine peptide in the gut, stimulates growth of HT-29 cells *in vitro* [38].
OPRL1	7.4	24.9	1.74	0.038	Nuclear expression of opioid receptors in HT-29 cells reported by Nylund *et al*. Morphine administration may affect invasive properties of tumor cells [39].
GPR137B	45.1	94.7	1.07	0.002	Orphan receptor of unknown function. Gene is upregulated during kidney development [40]. Knockdown of GPR137 inhibits colon cancer cell proliferation [41].
GPR146	7.9	33.4	2.06	0.0003	Orphan receptor of unknown function. GPR146 is crucial for C-peptide signaling in the kidney [42]. Associated with intestinal metabolism during perinatal period of preterm neonates [43].
GPR160	383.5	952.6	1.32	4.25E-14	Orphan receptor of unknown function. GPR160 is highly expressed in the gastrointestinal tract [44].
ADGRF1	671.7	196.2	-1.77	3.71E-18	Orphan receptor (GPR110) of unknown function. Potential marker for lung and prostate cancer [45]. Associated with sensing nutrients and intestinal cancer [46].
ADGRG6	765.6	566.5	-0.43	0.044	Type IV collagen is suggested as the activating ligand for GPR126 [47]. GPR126 mediates Shwann cell myelination and plays a role in breast cell cancer development [48,49].
ADGRG7	0.35	12.5	5.1	0.0005	Orphan receptor of unknown function. Expressed in gastrointestinal tract [50]. Knockout of GPR128 in mice models reduced body weight and enhanced peristaltic contraction frequency [51].
GPRC5A	6837.5	4212.2	-0.7	2.35E-5	Orphan receptor of unknown function. GPRC5A is expressed at high levels in CRC. Potential use as a marker in diagnosis of CRC [52].
GPRC5C	164.5	253.4	0.51	0.0487	Orphan receptor of unknown function. Controls acid-base balance in kidney [53].

Table 7.2. Summary of differentially expressed GPCRs between 2D and 3D cell cultures of HT-29 cells (Benjamini-Hochberg adjusted p-value < 0.05). The mean of normalized read counts from HT-29 cells cultured under 2D (norm. read counts 2D) or 3D (norm. read counts 3D) conditions is provided in columns 2 and 3, respectively. The logarithm (to basis 2) of the fold change from condition 2D to 3D is given in column 4 (log2fc) and p_{adj} is the p-value adjusted for multiple testing with the Benjamini-Hochberg procedure, which controls FDR.

Aside from GPCRs, we studied differential gene expression profiles of various RTKs as they are also rational targets for anticancer therapy. Humans have 58 known RTKs, which can be classified into twenty families. Members of the EGFR family are frequently linked to CRC progression and metastasis [54]. Analysis of differential gene expression revealed lower EGFR expression in 3D cell cultures in comparison to 2D monolayers (figure 7.4). Intriguingly, even though ErbB3 exhibits similar structural characteristics to EGFR, increased mRNA expression was observed in 3D cell cultures relative to 2D cell cultures. Similarly, discoidin domain receptor 1 (DDR1), serine/threonine/tyrosine kinase 1 (STYK1), and several members of the fibroblast growth factor (FGF) and ephrin RTK family were expressed to a higher extent in 3D HT-29 spheroids in comparison to 2D cell cultures, whereas the opposite is true for the insulin growth factor receptor 2 (IGF2R). Table 7.3 includes additional information about each of these differentially expressed RTKs.

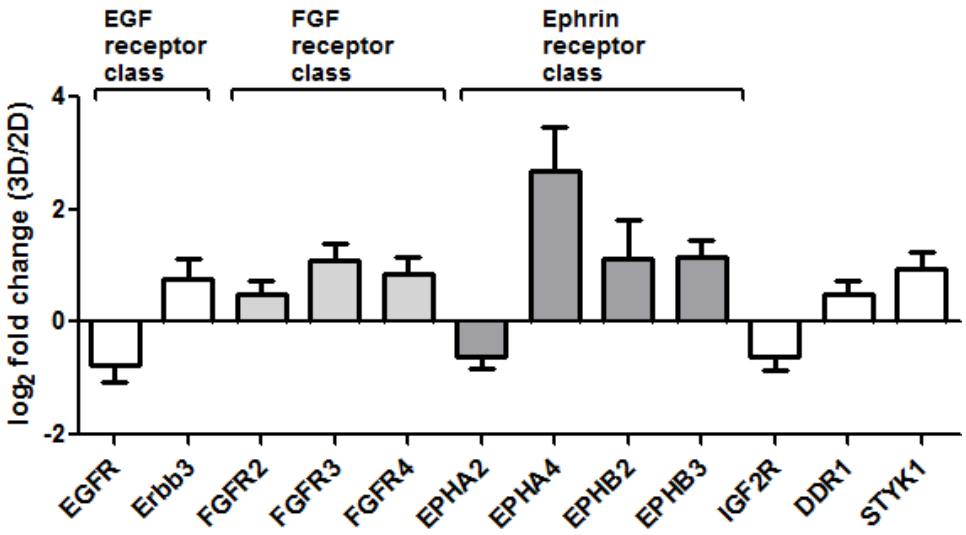

Fig.7.4. DEGs encoding RTKs in 2D and 3D HT-29 cell cultures as measured by RNA-Seq ($p_{adj} \leq 0.05$). The bar height represents fold changes (log2 based) between groups calculated by DESeq and error bars represent the standard error for the log2 fold change estimate.

Gene symbol	Norm. read counts 2D	Norm. read counts 3D	Log2fc	P_{adj}	Biological relevance
EGFR	2321.1	1344.9	-0.78	0.0005	Key target of various therapeutic strategies to treat metastatic CRC. Alterations within EGFR signaling cascade have been reported to contribute to colorectal carcinogenesis [55].
Erbb3	2891.7	4951.7	0.77	0.03	Promising target in cancer drug therapy [56]. ErbB3 is overexpressed in colorectal tumor samples in comparison to normal human colon samples [57].
FGFR2	468.9	667.3	0.5	0.013	FGFR2 is highly expressed in NCI-H716 CRC cells and FGFR2-selective inhibitors inhibit cell viability *in vitro* [58].
FGFR3	289.7	616.2	1.08	1.27 E-05	Involved in several malignancies including CRC [59].
FGFR4	370.6	671.9	0.86	3.66 E-0.6	FGFR4 is highly expressed at both RNA and protein levels in CRC tumor tissue compared with normal colon samples [60].
EPHA2	1578.5	1023.3	-0.63	0.0006	Upregulated in CRC, especially in early stages of CRC [61].
EPHA4	2.5	16	2.68	0.006	EphA4-mediated signaling pathways promote invasion and metastasis in CRC after radiotherapy [62].
EPHB2	38.4	85.1	1.15	0.002	Prognostic factor in CRC [63].
EPHB3	104	232.4	1.16	5.17 E-07	Acts as tumor/invasion suppressor in CRC [64].
IGF2R	2883	1871.3	-0.62	0.002	Increased expression of (genetic variants of) IGF2R are associated with increased colon cancer risk, but the precise role of IGF2R in tumor development is uncertain [65,66].
DDR1	917.5	1308.2	0.51	0.01	Involved in cancer progression by regulating interaction of tumor cells with surrounding collagen matrix [67]. Inhibition of DDR1 reduces colon cancer migration and metastasis [68]
STYK1	109.8	211	0.94	0.002	Upregulated in CRC tissue. May be used a tumor marker [69].

Table 7.3. Summary of differentially expressed RTKs between 2D and 3D cell cultures of HT-29 cells ($p_{adj} \leq 0.05$). The mean of normalized read counts from HT-29 cells cultured under 2D (norm. read counts 2D) or 3D (norm. read counts 3D) conditions is provided in columns 2 and 3, respectively. The logarithm (to basis 2) of the fold change from condition 2D to 3D is given in column 4 (log2fc) and p_{adj} is the p-value adjusted for multiple testing with the Benjamini-Hochberg method, which controls FDR.

Dysregulation of ion channel activity has also been linked to the growth of CRC [70]. Figure 7.5 shows significant changes in gene expression of different types of ion channels. Genes encoding subunits of voltage-dependent calcium channels (*CACNA1A*, *CACNA1H*, and *CACNB3*) as well as potassium channels (*KCNH2*, *KCNK1*, *KCNJ2*, *KCNJ3*) were upregulated in 3D cell cultures of HT-29 cells in comparison to monolayer cell cultures. Two members of the connexin family (Gap junction beta-1 (GJB1, also known as connexin 26), and gap junction beta-3 (GJB3, also known as connexin 31) were downregulated in 3D spheroids. Furthermore, a select group of genes encoding the P2X purinoceptor 4 (P2XR4), transient receptor potential cation channel subfamily M member 4 (TRPM4), and acetylcholine receptor subunit beta (CHRNB1) were expressed to a higher extent in multicellular HT-29 spheroids. A decreased expression of the integral water channel protein aquaporin 5 (AQP5) was observed in 3D cell cultures compared to 2D cell cultures.

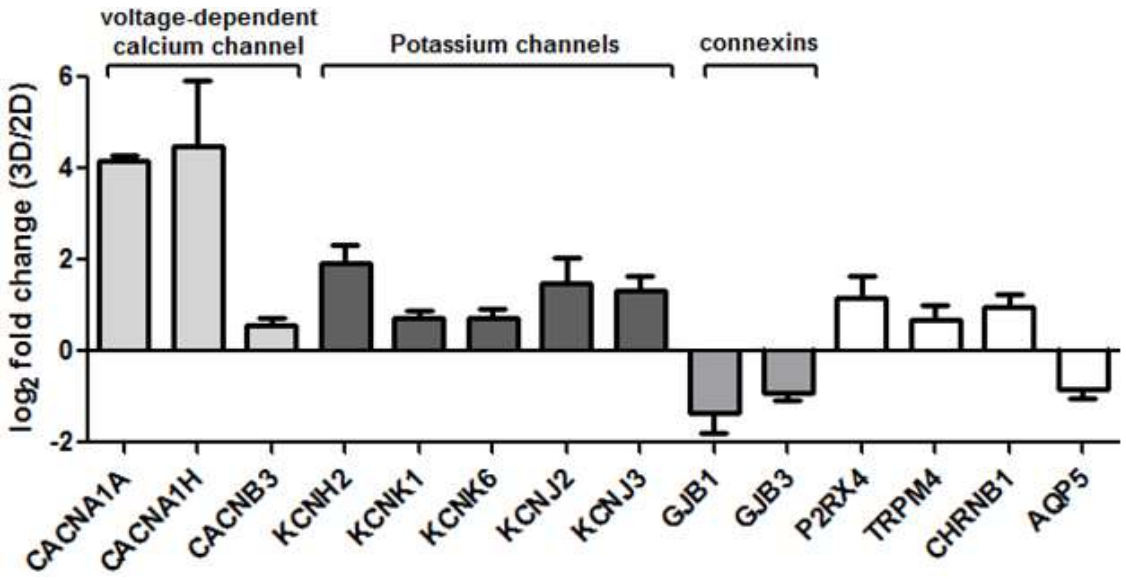

Fig.7.5. DEGs encoding ion channels in 2D and 3D HT-29 cell cultures as measured by RNA-Seq ($p_{adj} \leq 0.05$). The bar height represents fold changes (log2 based) between groups calculated by DESeq and error bars represent the standard error estimate for the log2 fold change estimate.

Gene symbol	Norm. read counts 2D	Norm. read counts 3D	Log2fc	P_{adj}	Biological relevance
CACNA1A	0.7	12.6	4.17	0.001	The remodeling of intracellular calcium homeostasis contributes to CRC, but evidence for a role of CACNA1A in colorectal carcinogenesis is lacking [70].
CACNA1H	1	23.1	4.5	1.11 E-06	The remodeling of intracellular calcium homeostasis contributes to CRC, but evidence for a role of CACNA1H in colorectal carcinogenesis is lacking [70].
CACNB3	196	292.4	0.58	0.02	The remodeling of intracellular calcium homeostasis contributes to CRC, but a role for the regulatory beta subunit CACNB3 in colorectal carcinogenesis has not been demonstrated [70].
KCNH2	19.8	74.6	1.91	0.01	Potassium channel expressed in a variety of cancer types where they regulate several cellular processes including cell proliferation and apoptosis. KCNH2 is overexpressed in colorectal cancer [71].

KCNK1	160.3	262.7	0.71	0.004	KCNK1 is overexpressed in different types of cancer, but not CRC [72].
KCNK6	127.8	210.6	0.72	0.004	KCNK6 showed decreased expression in colorectal adenocarcinoma [72].
KCNJ2	8.2	23.3	1.49	0.04	KCNJ2 modulates cell growth and drug resistance by regulating MRP1/ABCC1 expression in small-cell lung cancer [73].
KCNJ3	61	151.6	1.31	0.017	KCNJ3 is upregulated in tumors of patients with breast cancer [74].
GJB1	528.7	196.9	-1.42	2.92 E-05	CRC development is associated with a loss of connexin expression in comparison to normal colonic epithelial tissue [75].
GJB3	289.3	153.8	-0.91	4.39 E-0.5	GJB3 is downregulated in CRC tumors compared to normal tissue [76]
P2RX4	50.1	111.7	1.16	0.02	P2RX4 primarily participates in immune responses. Its precise role in CRC development and progression is unknown.
TRPM4	250.4	400	0.67	0.02	Decreased expression of TRPM4 in CRC tumor samples as compared to normal colonic tissues has been demonstrated [77].
CHRNB1	45.2	87.3	0.95	0.006	CHRNB1 is a potential predictive prognostic marker in CRC [78].
AQP5	250.2	140.8	-0.82	0.0006	AQP5 is highly expressed in colon cancer tissue with almost no expression in normal colonic epithelium. AQP5 activation may influence colon cancer development by interacting with the Ras/ERK/Rb signaling pathway [79].

Table 7.4. Summary of differentially expressed (subunits of) ion channels between 2D and 3D cell cultures of HT-29 cells ($p_{adj} \leq 0.05$). The mean of normalized read counts from HT-29 cells cultured under 2D (norm. read counts 2D) or 3D (norm. read counts 3D) conditions is provided in columns 2 and 3, respectively. The logarithm (to basis 2) of the fold change from condition 2D to 3D is given in column 4 (log2fc) and p_{adj} is the p-value adjusted for multiple testing with the Benjamini-Hochberg procedure, which controls FDR.

7.3.3 GO and KEGG pathway enrichment analysis

A variety of bioinformatics tools have been developed for gaining insight into high-throughput gene expression experiments. We used the Enrichr platform to perform GO and KEGG pathway enrichment analysis. GO and KEGG enrichment studies identify GO terms (biological process, cellular compartment, or molecular function) and KEGG pathways that are over- or under-represented using annotations for a particular set of genes.

The majority (94%) of DEGs mapped to at least one GO term. Among the identified DEGs, 1173 genes were upregulated in multicellular HT-29 spheroids in comparison to 2D cell cultures. Using a 5% Benjamini-Hochberg adjusted p-value threshold, we found that upregulated DEGs were significantly enriched for 3 GO-terms ('glucose homeostasis', 'brush border', and 'endoplasmic reticulum') and 2 KEGG pathways ('metabolic pathways' and 'glycolysis/gluconeogenesis'). The top 5 enriched GO terms (categorized into 3 groups: biological process, cellular compartment, and molecular function) and KEGG pathways associated with upregulated genes ranked by statistical significance is shown in figure 7.6. Raw data of the Enrichr analysis as well as list of genes belonging to enriched GO terms or KEGG pathways can be found in the supplementary files at the end of this chapter.

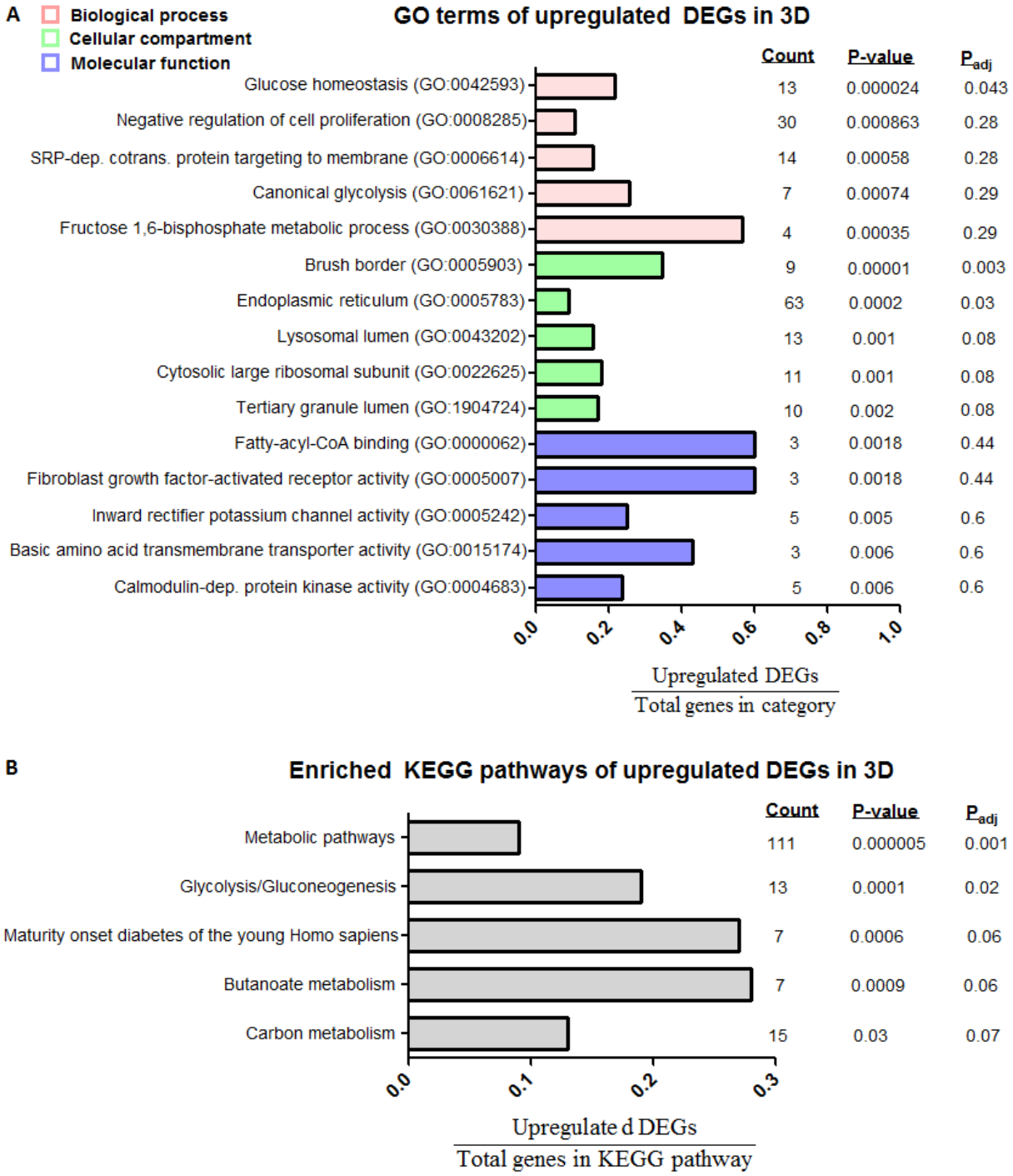

Fig.7.6. Top 5 enriched GO terms (derived from the 'biological process' (pink), 'cellular compartment' (green), and 'molecular function' (blue) categories) of upregulated DEGs (**A**). Graph **B** displays the significantly enriched KEGG pathways among the upregulated DEGs in 3D cell cultures. Bars denote the proportion of upregulated DEGs relative to the total number of genes in the *H. sapiens* genome mapped to each term or KEGG pathway. The last column shows Benjamini-Hochberg adjusted p-values (P_{adj}).

1012 genes were downregulated in HT-29 spheroids in comparison to 2D cell cultures. Significant GO term lists were reduced using REVIGO (see material and methods), which eliminates semantically redundant GO terms [24]. This resulted in 112 semantically-distinct GO terms (59 related to 'biological process', 30 related to 'cellular compartment', and 23 belonging to 'molecular function') associated with downregulated genes in 3D cell cultures. The complete list of enriched GO terms as

well as KEGG pathways can be found in the supplementary files. The top 5 enriched GO terms and KEGG pathways (ranked by Benjamini-Hochberg adjusted p-values) associated with downregulated genes in 3D cell cultures is displayed in figure 7.7. We observed significant enrichment for GO terms from the 'biological process' (including DNA replication, G1/S transition of mitotic cell cycle, DNA repair), 'cellular compartment' (*e.g.* nucleolar part, mitotic spindle pole, polar microtubule), and 'molecular function' (including RNA binding, helicase activity, ATP-dependent microtubule motor activity, and ATPase activity) categories. In addition, the top 5 KEGG pathways enriched among downregulated genes are pathways related to the cell cycle, DNA replication, RNA transport, ribosome biogenesis, and mismatch repair. As mentioned before, additional information regarding the list of genes belonging to enriched GO terms and/or KEGG pathways can be found in the supplementary files at the end of this chapter.

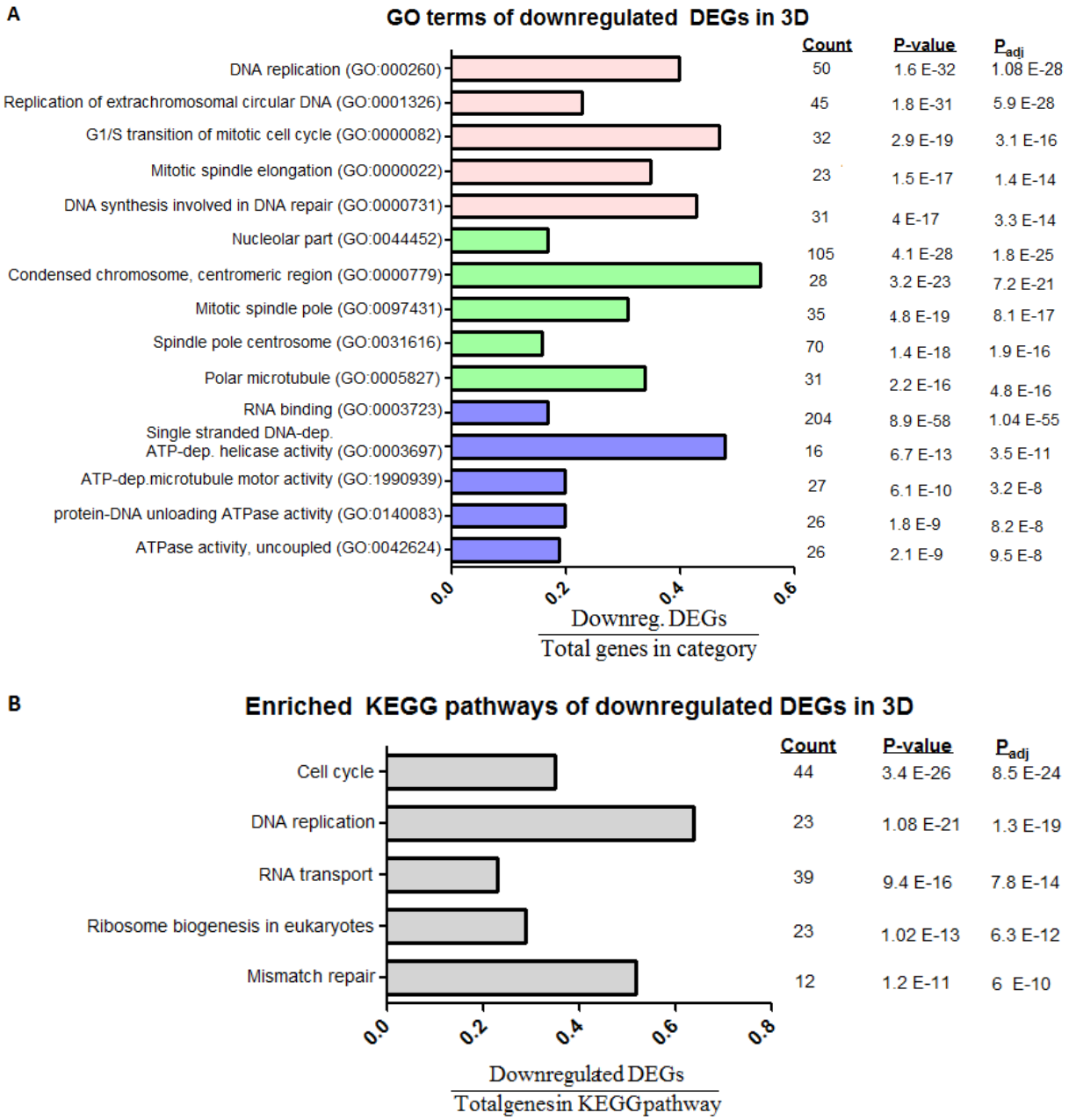

Fig.7.7. Top 5 enriched GO terms (derived from the 'biological process' (pink), 'cellular compartment' (green), and 'molecular function' (blue) categories) of downregulated DEGs (**A**). Graph **B** displays the significantly enriched KEGG pathways among the downregulated DEGs in 3D cell cultures. Bars represent the proportion of upregulated DEGs relative to the total number of genes in the *H. sapiens* genome mapped to each term or KEGG pathway. P-values were adjusted (P_{adj}) using the Benjamini-Hochberg method to correct for multiple hypothesis testing.

Figure 7.8 shows the outcome of a KEGG pathway enrichment analysis for all identified DEGs. This is necessary as results might differ when up- and downregulated genes are considered together or separately. For instance, if a pathway comprises a large number of upregulated genes and a few downregulated genes, the total number of DEGs in the KEGG pathway might appear not to be statistically significant, whereas performing the same analysis with only upregulated genes might identify significantly enriched pathways. KEGG pathway enrichment analysis found DEGs significantly

enriched in 15 pathways related to DNA replication, cell cycle, pyrimidine and purine metabolism, RNA transport, ribosome biogenesis, proteasome, mismatch repair, and several metabolic pathways.

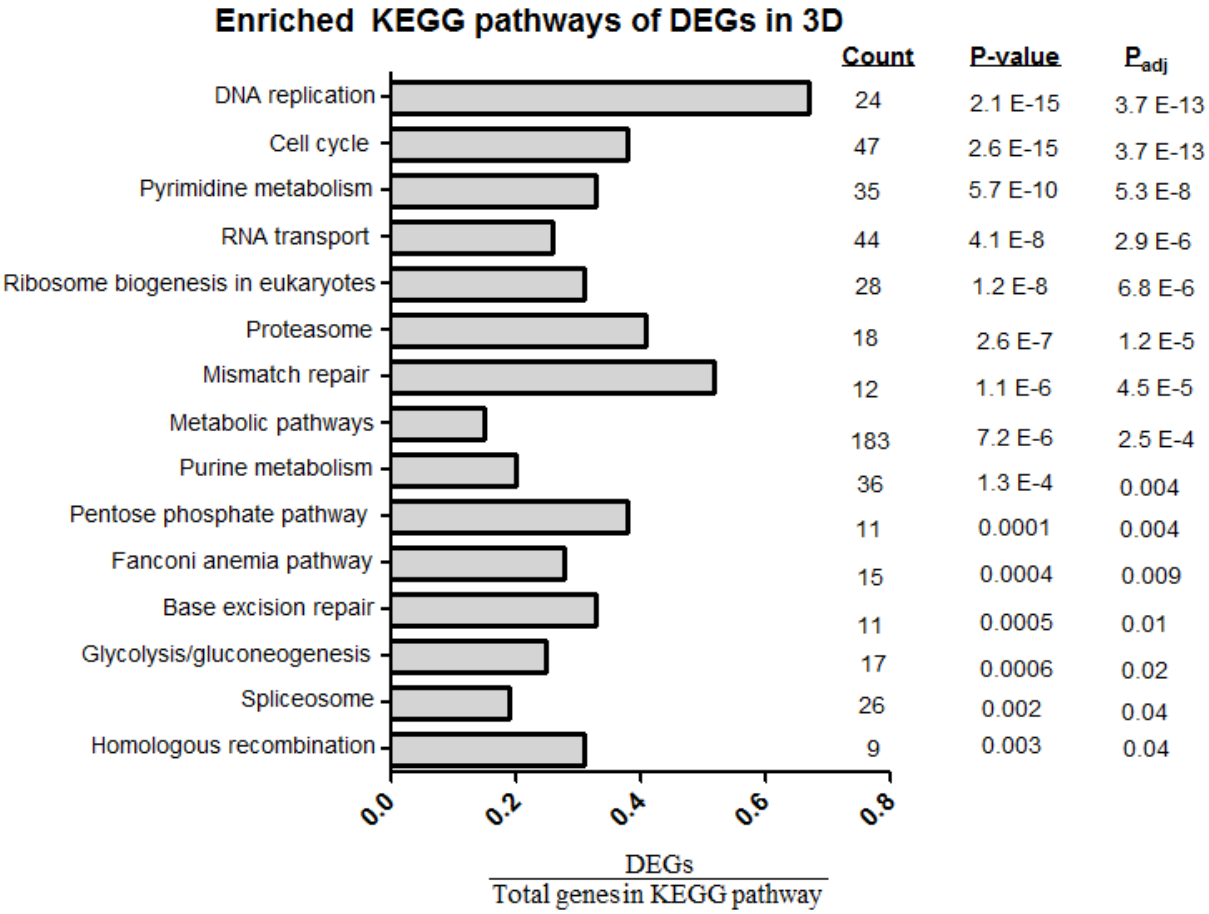

Fig.7.8. KEGG pathway enrichment analysis for identified DEGs ranked by statistical significance ($p_{adj} < 0.05$). The bar chart shows the proportion of DEGs relative to the total number of genes in the *H. sapiens* genome mapped to each KEGG pathway. P-values were adjusted (P_{adj}) using the Benjamini-Hochberg method to correct for multiple hypothesis testing.

7.4 Discussion

The high failure rate (96% in 2012) of anticancer compounds in clinical trials fuels the demand for more accurate preclinical cancer research tools [80]. This has led to the emergence of a plethora of 3D cell culture approaches which mimic more closely natural or tumor tissues than cells cultured as monolayers. Despite the recognition of the potential of 3D cell culture systems among a growing number of scientists, 3D models have not yet replaced 2D cell culture models on a large scale. Even though some of the older obstacles related to cumbersome cell culture procedures are gradually overcome by innovation, there appears to be a deeper underlying cause. For instance, accumulating evidence suggests that 3D and 2D cell cultures exhibit different gene expression profiles which can profoundly influence the outcome of drug toxicity and efficacy studies [5-7,16,18,23]. However, these divergent gene expression signatures often remain buried in repositories of high throughput gene expression data and only a limited amount of easily accessible information is currently available that delineates gene expression differences between 2D and 3D cell cultures.

This exploratory study provides researchers an overview of the differences in receptor (GPCRs, RTKs, and ion channels) gene expression between 2D and 3D HT-29 cell cultures. In addition, pathway enrichment analysis was performed to identify GO terms and KEGG pathways enriched by the significant DEGs. We focused on colon carcinoma, as it is one of the leading causes of cancer-related deaths in the United States and Western countries [1]. Note that this research is not a complete assessment of different types of 3D cell cultures currently available and the outcome of a gene expression profiling experiment can potentially vary depending on the choice of the 3D cell culture method. Therefore, further studies are necessary in order to thoroughly compare gene expression profiles between spheroids obtained by different 3D culturing techniques, but this is beyond the scope of this chapter.

The 3D cell culture model used in this study is relatively simple as it does not incorporate challenging-to-model features such as a vascular component or other components of the tumor microenvironment. Because the complex interplay of tumor cells with their environment increases the difficulty level associated with identifying the source(s) contributing to gene expression variation, we intentionally excluded these features to facilitate interpretation of results. However, the 3D cell culture model used in this study has biological relevance, as CRC spheres have been identified that lacked contact to host structures, thereby closely mimicking *in vitro* generated multicellular spheroids. Riedl *et al*. suggest that detached cancer cell clusters in blood vessels play a putative role in colon cancer metastasis [80]. Similarly, Okuyama *et al*. showed that sphere-like cancer cell

aggregates were involved in liver metastasis in mice [81]. These studies warrant the use of multicellular spheroids as cell culture models for studying some aspects of CRC metastasis.

As a useful first step in a RNA-Seq analysis, the quality of obtained expression data was assessed by PCA analysis. The PCA plot showed that 2D and 3D samples are clustered into 2 distinct groups, suggesting that these samples are different from each other. It appears the DEGs obtained from the analysis differ sufficiently to distinguish experimental groups from each other. 2D and 3D samples group together along PC1 (representing 79% of the variance in gene expression). The 3D group displayed greater intravariance along PC1 than the 2D group. It remains difficult to explain the exact cause of this observation, especially since there are many possible sources of variation that may contribute to this result.

2185 DEGs between 2D and 3D cell cultures of HT-29 cells were identified as significant based on a Benjamini-Hochberg adjusted p-value less than 0.05. It has been postulated that cells, grown in a 3D geometry, respond differently to different types of environmental stimuli and pharmaceutical drugs when compared to cells grown as monolayer cultures [5-7]. This can be explained by the existence of oxygen, nutrients, waste, and proliferation gradients within multicellular spheroids. However, it can also be related to differences in receptor expression among 2D and 3D cell cultures. Since our goal is to improve the biochemical characterization of 3D cell cultures, a comparative analysis of 2D versus 3D receptor transcription profiles is of great value as it can create new testable hypotheses and it can open new avenues of research.

We extracted 17 DEGs encoding GPCRs from the list of 2185 DEGs. Notably, our observations are made in the context of an exploratory study and experimental results must be validated by independent methods such as qPCR analysis or western blot. Furthermore, it remains to be determined whether these differentially expressed receptors are truly functional. However, when comparing our results to relevant scientific sources, many of our findings seem biologically relevant.

For example, Sui *et al*. demonstrated that HTR1D promoted CRC metastasis by regulating β-catenin/matrix metalloproteinase-7 (MMP7) signaling [29]. The authors compared gene expression profiles between normal and CRC tissue and showed that HTR1D is overexpressed in tumor samples. Our RNA-Seq data revealed increased expression of HTR1D in 3D cell cultures of HT-29 cells compared to 2D cell cultures. Because multiple studies suggest that cells grown in 3D more closely resemble *in vivo* cell and tissue biology, HTR1D could be a potential target for patients with CRC. Consequently, 3D cell cultures of HT-29 cells may be preferred over 2D cell cultures to further explore the role of HTR1D in CRC progression and metastasis

Aside from HTR1D, Sui *et al.* identified a select group of genes that were significantly upregulated in colorectal tumor samples, including MMP-7, vascular endothelial growth factor (VEGF), and E-cadherin (CDH1) [29]. The expression of HTR1D correlated positively with matrix metalloproteinase-7 (MMP-7) expression in CRC tissues. In agreement with these results, our data indicated enhanced expression of MMP-7 (log2 fold change=0.69; p_{adj}=0.001) in 3D spheroids relative to HT-29 monolayer cultures. Additionally, genes encoding VEGFB (log2 fold change=0.85; p_{adj}=0.001) and CDH1 (log2 fold change=0.64; p_{adj}=0.0001) were expressed to a higher extent in 3D cell cultures when compared to 2D cell cultures. The gene encoding VEGFA was also upregulated in 3D cell cultures, but this upregulation was not significant (log2 fold change=0.74; p_{adj}=0.4). Worth of note is that CDH1 acts as a tumor suppressor protein and loss of expression of CDH1 is associated with cancer progression. Given its ability to suppress cancer, it is unclear why CDH1 is upregulated in our 3D tumor model as well as in CRC tissues examined by Sui *et al*. However, Riedl *et al.* also report induction of CDH1 expression in 3D spheroid cultures in comparison to 2D cell cultures by using western blot analysis [80]. One possible explanation for these observations is that CDH1 plays alternative roles in tumor progression through stabilization of cell contacts during 'collective cancer cell migration', which refers to a complex process leading to the invasion of tumor cells into surrounding tissues [82]. The activity of CDH1 is also regulated by a complex series of molecular events (*e.g.* phosphorylation, ubiquitination, and proteolysis) that could change the function of CDH1 post-transcriptionally.

ADRA2A, GPER1, FFAR2, OPRL1, NPY6R, LPAR6, and OR51E1 were also significantly upregulated in 3D cell cultures of HT-29 cells in comparison to 2D cell cultures. HT-29 cells express ADRA2As which are involved in various disease processes such as inflammatory bowel disease and colon carcinogenesis [30,31]. Because ADRA2A was upregulated in 3D spheroids, it may have potential as a therapeutic target.

Similarly, it could be of great value to further explore the physiological function of the odorant receptor OR51E1 and FFAR2. Several studies have documented the expression of odorant receptors in different human cell types and tissues, as well as their involvement in different (patho)physiological processes. OR51E1 has been identified as a potential novel tumor biomarker for small intestine neuroendocrine carcinomas [83]. However, the functional role of OR51E1 in CRC is still unclear. FFAR2 (also known as GPR43) is a receptor for SCFFAs, which can exert antitumor activities due to inhibition of histone deacetylase. FFAR2 regulates gut homeostasis by binding to SCFFAs derived from fermentation of dietary fibre. Tang *et al.* examined FFAR2 expression in 9 established human colon cancer cell lines and demonstrated that receptor expression was only detected in HT-29 cells [34]. In agreement with these findings, our RNA-Seq analysis showed mRNA

expression of FFAR2 in both 2D and 3D cultures of HT-29 cells. Notably, our results showed significant mRNA upregulation of FFAR2 in 3D spheroids relative to 2D cultures. Therefore, 3D cell cultures of HT-29 cells may represent an attractive model to study the action of metabolites and their impact on health.

Even though GPCRs account for one of the major drug targets, current GPCRs drugs only target approximately 10% of all GPCRs in the human genome [84]. Therefore, GPCRs whose endogenous ligand has not yet been identified are the subject of considerable research interest. We detected 8 orphan GPCRs whose functions are largely unknown and which were significantly up- or downregulated when comparing 2D and 3D HT-29 cell cultures. Many of these orphan GPCRs belong to the family of adhesion GPCRs, which often play crucial roles in cancer progression and metastasis [48]. For example, GPR128, a member of the adhesion GPCR family, was found to be strongly upregulated in 3D spheroids compared to HT-29 cells grown as a monolayer. GPR128 expression has been detected in intestinal tissues such as the duodenum and colon. Ni *et al*. demonstrated that deletion of *GPR128* in mice models leads to reduced body weight gain and increased peristaltic frequency contractions [51].

GPR128 has not been associated with CRC progression or metastasis so far. However, gene fusion of the trk-fused gene to *GPR128* was identified in approximately 1% of patients with renal cell cancer. Parker *et al.* suggest that fusion genes are promising therapeutic targets due to their inherent expression in tumor tissue alone [85]. GPR137B is another member of adhesion GPCRs upregulated in multicellular HT-29 spheroids. Zhang *et al*. recently showed that downregulation of GPR137B expression inhibits colon cancer cell proliferation [41]. Therefore, GPR137B provides a previously unrecognized target for the development of novel gene therapies of colon cancer. We refer to table 7.2 for a more exhaustive summary of differentially expressed GPCRs along with the physiological processes in which they participate.

Aside from GPCRs, various RTKs have emerged as clinically relevant drug targets for treating several types of cancer. One of the best-studied examples is EGFR, which plays a pivotal role in the development and progression of different malignancies [54,55]. Multiple studies suggest that EGFR is involved in CRC tumorigenesis and various EGFR-directed therapies for the treatment of metastatic CRC are currently in clinical use, such as the monoclonal antibodies cetuximab (Erbitux™; Bristol-Myers Squibb/Im-Clone Systems Incorporated, Montreal, Quebec) and panitumumab (Vectibix™, Amgen, Mississauga, Ontario) [16,55,85]. Cetuximab and panitumumab bind to the extracellular domain of EGFR and block downstream EGFR signaling, ultimately leading to antitumor effects [85].

Remarkably, we observed significant downregulation of EGFR expression in 3D HT-29 cell cultures relative to 2D cell cultures. These results are in conflict with observations made by Magdeldin *et al*., who demonstrated that EGFR expression was significantly upregulated in 3D HT-29 cell cultures in comparison to 2D cell cultures [19]. On the other hand, Luca *et al*. investigated protein expression levels of several components of the EGFR-signaling pathway in 5 established colorectal cancer cell lines, including HT-29, and reported decreased EGFR expression in 3D cell cultures in comparison to 2D cell cultures [16].

Observations concerning variable EGFR expression in 3D cell cultures relative to 2D cell cultures remain difficult to explain. It is possible that the discrepancies are related to the methodology used for growing 3D cell cultures. For instance, Magdeldin *et al*. used RAFT (Real Architecture for 3D Tissue) technology to generate 3D cell cultures, whereas Luca *et al*. used laminin-rich ECM (lrECM) to form multicellular spheroids [19,16]. Furthermore, Magdeldin *et al*. extracted RNA from 3-day-old spheroids, whereas Luca *et al*. used 7-day-old spheroids. This could also affect the outcome of experiments as gene expression profiles may change over time. In order to improve comparability across studies, researchers should consider conducting a large-scale experiment in which EGFR expression is compared among different 3D cell culture approaches at various timepoints. This could help resolve which type of 3D cell culture model - if any - is best suited for studying EGFR signaling. However, it must also be noted that the clinical significance of EGFR overexpression in CRC is uncertain [55]. A wide range of differences in EGFR expression in CRC has been reported and several studies failed to indicate a correlation between EGFR expression in CRC tumors and responsiveness to cetuximab. As a result, CRC patients are currently administered with cetuximab as indicated without the need for EGFR testing. Based on the controversial relationship between EGFR expression and prognosis of patients with CRC, it remains speculative whether the 3D model system used in this work is better suited for studying the impact of EGFR signaling on colon carcinogenesis than 2D cell cultures.

The majority of the identified upregulated genes encoding RTKs in 3D cell cultures have previously been linked to colorectal malignancies. For instance, increased expression of members of the FGFR and ephrin family of RTKs has been detected in spheroids systems. These receptors typically play a role in signaling pathways involved in cancer and both FGFR-targeted as ephrin-targeted therapies represent promising strategies for the treatment of particular types of cancer [86,87]. In addition, enhanced expression of erbB3, DDR1, and STYK1 was observed. ErbB3 belongs to the EGFR family of RTKs and upregulation of erbB3 has been shown to promote CRC cell growth and survival [57]. Hu *et al*. reported that STYK1 could potentially be used as a prognostic tumor marker in CRC [88].

Ion channels have not been studied to the same extent as GPCRs and RTKs, but appear to have important functions in cancer biology as well [71,72]. Increased expression of various genes encoding (subunits of) voltage-operated calcium channels, potassium channels, P2RX4, TRPM4, and CHRNB1 was eminent in 3D cell cultures when compared to 2D cell cultures, whereas decreased expression of 2 members of the connexin family and AQP5 was detected. Some of the identified up- or downregulated genes in 3D cell cultures were also up- or downregulated in CRC. For example, connexins (including connexin 26 and 31) are typically downregulated in various types of cancer, including CRC. Sirnes *et al*. suggest that connexins are important tumor suppressor proteins and downregulation of connexins impairs cell growth, differentiation, and tissue homeostasis [75]. However, for a small number of differentially expressed ion channels (AQP5 and TRPM4), contradictory changes in expression were seen. Koo Kang *et al*. examined colon cancer tissue samples and demonstrated strong expression of AQP5 in cancer cells, whereas we observed decreased expression of AQP5 in 3D cell cultures relative to 2D cell cultures [79]. In addition, Suzocan *et al*. reported lower TRPM4 mRNA expression in CRC tissue as compared to normal colon tissue [77]. Our results showed increased TRPM4 expression in 3D relative to 2D monolayer cultures. Taken together, considerable caution should be exercised when interpreting results of experiments determining the function of identified DEGs as results can potentially vary depending on the choice of the cell culture model.

In the final part of this study, enriched GO terms and KEGG pathways assigned to DEGs were examined. In pathway-based analysis, a group of related genes from a particular GO category or KEGG pathway is assessed rather than investigating a collection of potentially unrelated genes. Pathway-based data usually shows a higher degree of overlap between studies in comparison to overlap between lists of DEGs [89]. KEGG pathway enrichment analysis on DEGs revealed changes to a number of pathways, including DNA replication and cell cycle pathways. This suggests that transcriptional activity is altered in 3D cell cultures in comparison to monolayer cultures. Changes in the DNA mismatch repair pathway indicated that the capacity to repair DNA damage may be affected. In addition, a number of metabolic pathways were revealed to be altered, including the pentose phosphate pathway, glycolysis/gluconeogenesis, and pyrimidine/purine metabolic pathways. Changes in metabolic signaling pathways suggest altered metabolic requirements of 3D cell cultures to fulfill their energetic needs.

Separating DEGs by their direction of expression revealed 3 GO terms (‘glucose homeostasis’, ‘brush border’, and ‘endoplasmic reticulum’) and 2 KEGG pathways (‘Metabolic pathways’ and ‘glycolysis/gluconeogenesis’) significantly enriched in upregulated genes. Since gluconeogenesis is nearly glycolysis in reverse, these two pathways have several enzymes in common. It has long been

known that glucose metabolism is altered in tumor cells in comparison to normal cells. Most research has focused on understanding the metabolic shift to increased aerobic glycolysis in cancer cells, a phenomenon termed “the Warburg effect” [90]. Changes in glucose metabolism and lactate accumulation may also occur in 3D spheroids in comparison to 2D cell cultures. Consistent with this presumption, Longati *et al*. demonstrated that pancreatic 3D cell cultures have increased glycolysis relative to 2D cell cultures [91]. The authors also showed increased mRNA expression of glucose transporter 1 (GLUT1) and lactate dehydrogenase A (LDHA) under 3D culture conditions. Interestingly, LDHA was among the identified upregulated DEGs in 3D HT-29 cell cultures. In addition, various key glycolytic enzymes were found to be upregulated in HT-29 spheroids in comparison to 2D cell cultures, including acyl-coenzyme A synthetase family members 1 and 2 (ACSS1 and ACSS2), alcohol dehydrogenase 1C (ADH1C), aldolase A and C (ALDOA and ALDOC), phosphoglucomutase-1 (PGM1), enolase 2 (ENO2), ATP-dependent 6-phosphofructokinase (PFKL), fructose-1,6-bisphosphatase 1 (FBP1), and aldose-1 epimerase (GALM). However, differential expression of well-established glucose transporter isoforms was not detected. Further experiments may include lactate accumulation measurements to determine whether glycolysis is truly increased in 3D HT-29 cell cultures compared to 2D cell cultures. If the lactate content of the medium increases, it may also induce secretion of hyaluran, which in turn interacts with CD44. In addition, lactate can contribute to increased VEGF expression [91]. Interestingly, both CD44 and VEGF were significantly upregulated in 3D HT-29 spheroids in comparison to 2D cell cultures.

It is also relevant to mention that brush border-associated genes were present among the upregulated DEGs in 3D. The brush border is typically present on the apical surface of enterocytes and plays a role in digestion and nutrient transport [92]. However, it remains questionable whether 3D HT-29 cell cultures are better suited for studying brush border-associated proteins and enzymes than 2D cell cultures. In fact, one can argue that 2D monolayer cultures are better suited for intestinal transport studies as intestinal epithelial cells also grow in a monolayer-like manner *in vivo*.

A large number of GO terms and KEGG pathways were significantly enriched in downregulated genes in 3D spheroids. Most of the downregulated genes in 3D cell cultures belong to cell cycle regulation, DNA replication, and mismatch repair. In addition, the forkhead box O (FoxO) signaling pathway was found to be altered among 3D and 2D cell cultures (see supplementary table in Appendix). FoxO genes are involved in a variety of cellular processes, including the regulation of the cell cycle [93]. Together, these observations suggest that cell cycle progression and proliferation is altered in HT-29 spheroids in comparison to monolayer cultures. This is perhaps not a surprising result as 2D cell cultures are mainly composed of proliferating cells and necrotic cells are typically detached from the surface of tissue culture flasks. Moreover, Riedl *et al*. showed that colon cancer cells grown as

spheroids display reduced cell cycle progression and proliferation in comparison to 2D cell cultures [80]. They observed a strong and significant reduction (more than 50%) of HT-29 cells in the synthesis phase (S-phase) of DNA replication in 3D cell cultures relative to 2D cell cultures. Riedl *et al*. also provide evidence of diminished PI3K-AKT-mammalian target of rapamycin (mTOR) signaling in 3D cell cultures relative to 2D cultures [80]. However, we were unable to confirm these results in our study.

Assigning downregulated DEGs to KEGG pathways revealed that proteasome, RNA transport, and apoptotic KEGG pathways were also significantly enriched. Proteasomes are involved in a variety of cellular processes, including protein catabolism, cell-cycle progression, and apoptosis [94]. Differences in apoptotic activity between 3D and 2D cell cultures could be associated with the existence of oxygen and nutrients gradients within spheroids [95]. Therefore, measuring apoptosis by microscopy or flow cytometry are appropriate follow-up experiments. Interestingly, because non-vascularized spheroids may develop a hypoxic region within the multicellular spheroid, one would expect differential expression of hypoxia-induced genes such as hypoxia-inducible factor 1 (HIF-1). However, the HIF-1 signaling pathway was not among the altered KEGG signaling pathways. This finding is in contrast with a study of Yoshii *et al*., who demonstrated increased HIF-1 transcriptional activity in the core region of HT-29 spheroids relative to 2D cell cultures using an HIF-1 inducible green fluorescent protein (GFP) reporter system [23]. Such contrasting observations are difficult to explain, particularly as Yoshii *et al*. used the same cells and 3D culture method in their study. Variations in spheroid dimensions could possibly play a role as larger spheroids tend to develop central necrosis and zones of hypoxia. Therefore, it is imperative to characterize spheroid features such as size, shape, and density in order to increase comparability among different studies. Interestingly, the authors also compared gene expression profiles between 1-day old and 7-day old HT-29 spheroids and showed that 6 genes related to the glucose metabolism were upregulated in 3D cell cultures on day 7 when compared to the first day of spheroid growth. 4 of these upregulated genes were also identified in this study, *e.g.* ALDOC, ENO2, pyruvate dehydrogenase kinase 1 (PDK1), and LDHA. This suggests that at least some of the observations made by Yoshii *et al*. are in line with the results from this study.

In summary, comparing the transcription profiles between 3D- and 2D-cultured HT-29 cells revealed differences in gene expression. These differences provide many opportunities for follow-up studies in the field of CRC research. Many (but not all) of the genes, found to be up- or downregulated in 3D cell cultures, were also found to be upregulated in tumors. In addition, a number of pathways were altered in 3D cell cultures compared to monolayer cultures, including metabolic and cell cycle-associated pathways. However, our results should be interpreted with considerable caution, as the sample size for this study is fairly small and we only extracted RNA from 2D and 3D cell cultures at

one moment in time. Further research is required in order to validate our results using complementary methods such as qPCR and western blot, especially since a gene's mRNA level cannot be used as a surrogate for corresponding protein levels without verification. Smolders *et al.* propose a promising approach for validating differentially expressed receptors at the protein level [96]. In this approach, biotinylated cell-surface exposed proteins are enriched using streptavidin pull-down and identified by shotgun proteomics. In addition, functional assays for screening GPCR and RTK targets can be conducted to determine whether the receptor of interest is truly functional. The outcome of these analyses will be important in light of adopting 3D-cultured HT-29 cells as routine tool in preclinical CRC research. However, before this can happen, it is necessary to compare gene expression profiles of HT-29 spheroids generated by different 3D cell culture methods.

References

[1] M. Arnold, M.S. Sierra, M. Laversanne, I. Soerjomataram, A. Jemal, F. Bray, Global patterns and trends in colorectal cancer incidence and mortality, GUT 4 (2017) 683-691. doi:10.1136/gutjnl.2015.310912?.

[2] L. Hutchinson, R. Kirk, High drug attrition rates- where are we going wrong? Nat. Rev. Clin. Oncol. 8 (2011) 189-190. doi:10.1038/nrclinonc.2011.34.

[3] J.A. DiMasi, H.G. Grabowski, Economics of new oncology drug development. J. Clin. Oncol. 25 (2007) 209-216. doi: 10.1200/JCO.2006.09.0803.

[4] A. Ocana, A. Pandiella, L.L. Siu, I.F. Tannock, Preclinical development of molecular-targeted agents for cancer, Nat. Rev. Clin. Oncol. 8 (200-209). doi: 10.1038/nrclinonc.2010.194.

[5] E.-T. Verjans, J. Doijen, W. Luyten, B. Landuyt, L. Schoofs, Three-dimensional cell culture models for anticancer drug screening: worth the effort? J. Cell. Phys. (2017). doi:10.1002/jcp.26052

[6] R. Edmondson, J.J. Broglie, A.F. Adcock, L. Yang, Three-dimensional cell culture systems and their applications in drug discovery and cell-based biosensors, Assay. Drug Dev. Technol. 12 (2014) 207-218. doi: 10.1089/adt.2014.573.

[7] M. Ravi, V. Paramesh, S.R. Kaviya, E. Anuradha, F.D. Paul Solomon, 3D cell culture systems: advantages and applications, J. Cell. Physiol. 230 (2015) 16-26. doi:10.1002/jcp.24683.

[8] A.I. Khoruzhenko, 2D- and 3D- cell culture, Biopolymers and Cell. 27 (2011) 17-24. doi:10.7124/bc.00007D.

[9] J.M. Lee, J.P. Mhawech-Fauceglia, N. Lee, L.C. Parsanian, Y.G. Lin, S.A. Gayther, K. Lawrenson, A three-dimensional microenvironment alters protein expression and chemosensitivity of epithelial ovarian cancer cells in vitro, Lab. Invest. 93 (2013) 528-542. doi:10.1038/labinvest.2013.41.

[10] M. Zanoni, F. Piccinini, C. Arienti, A. Zamagni, S. Santi, R. Polico, A. Bevilacqua, A. Tesei, 3D tumor spheroid models for *in vitro* therapeutic screening: a systematic approach to enhance the biological relevance of data obtained, Sc. Rep. 6 (2016) 1-11. doi:10.1038/srep19103.

[11] D. Antoni, H. Burckel, E. Josset, G. Noel, Three-dimensional cell culture: a breakthrough in vivo, Int. J. Mol. Sci. 16 (2015) 5517-5527. doi:10.3390/ijms16035517.

[12] R.Z. Lin, H.Y. Chang, Recent advances in three-dimensional multicellular spheroid culture for biomedical research, Biotechnol. J. 3 (2008) 1172-1184. doi:10.1002/biot.200700228.

[13] M.C. Cox, L.M. Reese, L.R. Bickford, S.S Verbridge, Toward the broad adoption of 3D tumor models in the cancer drug pipeline, ACS Biomater. Sci. Eng. 10 (2015) 877-894. doi: 10.1021/acsbiomaterials.5b00172.

[14] K. Brajsa, M. Trzun, I. Zlatar, D. Jelic, Three-dimensional cell cultures as a new tool in drug discovery, Per. Biolog. 118 (2016) 59-65. doi:10.18054/pb.2016.118.1.3940.

[15] L. Baricault, G. Denariaz, J.J. Houri, C. Bouley, C. Sapin, G. Trugnan, use of HT-29, a cultured human colon cancer cell line, to study the effect of fermented milks on colon cancer growth and differentiation, Carcinogenesis, 2 (1995) 245-252. doi:10.1093/carcin/16.2.245.

[16] A.C. Luca, S. Mersch, R. Deenen, S. Schmidt, I. Messner, K.-L. Schäfer, S.E. Baldus, W. Huckenbeck, R.P. Piekorz, W.T. Knoefel, A. Krieg, N.H. Stoecklein, Impact of the 3D microenvironment on phenotype,

gene expression, and EGFR inhibition of colorectal cancer cell lines, PLoS One. 8 (2013) e59689. doi:10.1371/journal.pone.0059689.

[17] A. Osswald, Z. Sun, V. Grimm, G. Ampem, K. Riegel, A.M. Westendorf, W. Sommergruber, K. Otte, P. Dürre, C.U. Riedel, Three-dimensional tumor spheroids for in vitro analysis of bacteria as gene delivery vectors in tumor therapy, Microb. Cell. Fact. 14 (2015) doi:10.1186/s12934-015-0383-5.

[18] C. Hirt, A. Papadimitropoulos, M.G. Muraro, V. Mele, E. Panopoulos, E. Cremonesi, R. Evanek, E. Schultz-Thater, R.A. Droeser, C. Mengus, M. Heberer, D. Oertli, G. Iezzi, P. Zajac, S. Eppenberger-Castori, L. Tornillo, L. Terracciano, I. Martin, G.C. Spagnoli, Bioreactor-engineered cancer tissue-like structures mimic phenotypes, gene expression profiles and drug resistance patterns observed "*in vivo*", Biomaterials. 62 (2015) 138-146. doi: 10.1016/j.biomaterials.2015.05.037.

[19] T. Magdeldin, V. Lopez-Davila, C. Villemant, G. Cameron, R. Drake, U. Cheema, M. Loizidou, The efficacy of cetuximab in a tissue-engineered three-dimensional in vitro model of colorectal cancer, J. Tissue. Eng. 5 (2014) 1-9. doi:10.1177/2041731414544183.

[20] D. Martinez-Maqueda, B. Miralles, I. Recio, Impact of Food bioactives on Health, *in vitro* and *ex vivo* models. Springer Int. Publishing (2015) 113-124. doi:10.1007/978-3-319-16104-4_11.

[21] Y. Chen, Y. Lin, M. Kimberly, M. Davis, Q. Wang, J. Rnjak-Kovacina, C. Li, R.R. Isberg, C. A. Kumamoto, J. Mecsas, D.L. Kaplan, Robust bioengineered 3D functional human intestinal epithelium, Sc. Rep. 5 (2015) 13708. doi:10.1038/srep13708.

[22] R. Herr, M. Köhler, H. Andrlova, F. Weinberg, Y. Möller, S. Halbach, L. Lutz, J. Mastroianni, M. Klose, N. Bittermann, S. Kowar, R. Zeiser, M.A. Olayioye, S. Lassmann, H. Busch, M. Boerries, T. Brummer, B-Raf inhibitors induce epithelial differentiation in *BRAF*-mutant colorectal cancer cells, Cancer. Res. 75 (2015). doi:10.1177/2041731414544183.

[23] Y. Yoshii, A. Waki, K. Yoshida, A. Kakezuka, M. Kobayashi, H. Namiki, Y. Kuroda, Y. Kiyono, H. Yoshii, T. Furukawa, T. Asai, H. Okazawa, J.G. Gelovani, Y. Fujibayashi, The use of nanoimprinted scaffolds as 3D culture models to facilitate spontaneous tumor cell migration and well-regulated spheroid formation, Biomaterials. 32 (2011) 6052-6058. doi:10.1016/j.biomaterials.2011.04.076.

[24] F. Supek, M. Bosnjak, N. Skunca, T. Smuc, REVIGO summarizes and visualizes long lists of gene ontology terms, PLOS one, 6 (2011) e21800. doi:10.1371/journal.pone.0021800.

[25] P. Desjardins, D. Conklin, Nanodrop microvolume quantitation of nucleic acids, J.Vis.Exp. 45 (2010) 2565. doi:10.3791/2565.

[26] A. Schroeder, O. Mueller, S. Stocker, R. Salowsky, M. Leiber, M. Gassmann, S. Lightfoot, W. Menzel, M. Granzow, T. Ragg, The RIN: an RNA integrity number for assigning integrity values to RNA measurements, BMC. Mol. Biol. 7 (2006) 1-14. doi: 10.1186/1471-2199-7-3.

[27] R. Cangelosi, A. Goriely, Component retention in principal component analysis with application to cDNA microarray data, Biol. Direct. 2 (2007) 1-21. doi:10.1186/1745-6150-2-2.

[28] J.R. Lynch, J.Y. Wang, G protein-coupled receptor signaling in stem cells and cancer, Int. J. Mol. Sci. 17 (2016) 707. doi:10.3390/ijms17050707.

[29] H. Sui, H. Xu, Q. Ji, X. Liu, L. Zhou, H. Song, X. Zhou, Y. Xu, Z. Chen, J. Cai, G. Ji, Q. Li, 5-hydroxytryptamine receptor (5-HT1DR) promotes colorectal cancer metastasis by regulating Axin1/β-catenin/MMP-7 signaling pathway, Oncotarget. 6 (2015) 25975-25987. doi:10.18632/oncotarget.4543.

[30] C. Cayla, S. Schaak, P.A. Crassous, B. Buffin-Meyer, C. Delage, H. Paris, J.M. Senard, C. Denis, Transcriptional down-regulation of human alpha(2A)-adrenoceptors by IFNgamma and TNFalpha in intestinal cells, Eur. J. Pharmacol, 24 (2008) 33-40. doi:10.1016/j.ejphar.2008.04.006.

[31] D.K. Agrawal, D.M. Wildrick, B.M. Boman, Characteristics of alpha-adrenoceptors in two human colorectal cancer cell lines, Biochem. Biophys. Res. Com. 1 (1992) 176-184. doi:10.1016/S0006-291X(05)80972-6.

[32] L.A. Gilad, T. Bresler, J. Gnainsky, P. Smirnoff, B. Schwartz, Regulation of vitamin D receptor expression via estrogen-induced activation of the ERK 1/2 pathway in colon and breast cancer cells, J. Endocrinol. 185 (2005) 577-592. doi:10.1677/joe.1.05770.

[33] M.L. Sleeth, E.L. Thompson, H.E. Ford, S.E. Zac-Varghese, G. Frost, Free fatty acid receptor 2 and nutrient sensing: a proposed role for fibre, fermentable carbohydrates and short-chain fatty acids in appetite regulation, Nutr. Res. Rev. 23 (2010) 135-145. doi:10.1017/S0954422410000089.

[34] Y. Tang, Y. Chen, H. Jiang, G.T. Robbins, G-protein-coupled receptor for short-chain fatty acids suppresses colon cancer, Cancer Cell Biol. 128 (2011) 847-856. doi:10.1002/ijc.25638.

[35] A. Mazzocca, F. Dituri, F. De Santis, A. Filannino, C. Lopane, R.C. Betz, Y.Y. Li, N. Mukaida, P. Winer, C. Tortorella, G. Giannelli, C. Sabba, Lysophosphatidic acid receptor LPAR6 supports the tumorigenicity of hepatocellular carcinoma, Cancer Res. 75 (2015) 532-543. doi:10.1158/0008-5472.

[36] T. Cui, A.V. Tsolais, S.-CH. Li, J.L. Cunningham, T. Lind, K. Oberg, V. Giandomenico, Olfactory receptor 51E1 protein as a potential novel tissue biomarker for small intestine neuroendocrine carcinomas, Eur. J. Endocrinol. 168 (2013) 253-261. doi: 10.1530/EJE-12-0814.

[37] J.J. Maoret, D. Pospaï, C. Rouyer-Fessard, A. Couvineau, C. Laboisse, T. Voisin, M. Laburthe, Neurotensin receptor and its mRNA are expressed in many human colon cancer cell lines but not in normal colonic epithelium: binding studies and RT-PCR experiments, Biochem. Biophys. Res. Commun. 203 (1994) 467-471.doi:10.1006/bbrc.1994.2205.

[38] J.J. Maoret, Y. Anini, C. Rouyer-Fessard, D. Gully, M. Laburthe, Neurotensin and a non-peptide neurotensin receptor antagonist control human colon cancer cell growth in cell culture and in cells xenografted into nude mice, Int. J. Cancer. 80 (1999) 448-454. doi:10.1002/(SICI)1097-0215(19990129)80:3<448::AID-IJC19>3.0.CO;2-N.

[39] G. Nylund, A. Pettersson, C. Bengtsson, A. Khorram-Manesh, S. Nordgren, D.S. Delbro, Functional expression of μ-opioid receptors in the human colon cancer cell line, HT-29, and their localization in human colon, Dig. Dis. Sci. 53 (2007) 461-466. doi:10.1007/s10620-007-9897-y.

[40] C. Spangenberg, A. Winterpacht, B.U. Zabel, R.W. Löbbert, Cloning and characterization of a novel gene (TM7SF1) encoding a putative seven-pass transmembrane protein that is upregulated during kidney development, Genomics 48 (1998) 178-185. doi:10.1006/geno.1997.5170.

[41] K. Zhang, Z. Shen, X. Liang, T. Liu, T. Wang, Y. Jiang, Down-regulation of GPR137 expression inhibits proliferation of colon cancer cells, Acta Biochim Biophys Sin. 46 (2014) 935-941. doi:10.1093/abbs/gmu086.

[42] L. Redlinger, G. Kolar, W. Samson, G. Yosten, Expression of the receptor for proinsulin C-peptide, GPR146, in the kidney (1108.5), FASEB J. 28 (2014) 1108.5.

[43] F. Gao, J. Zhang, P. Jiang, J.W. Wang, Y. Xia, M.V. Ostergaard, J. Wang, P.T. Sangild, Marked methylation changes in intestinal genes during the perinatal period of preterm neonates, BMC Genomics. 15 (2014) 1-14. doi:10.1186/1471-2164-15-716.

[44] V. Marx, Proteomics: an atlas of expression, Nature. 509 (2014) 645-649. doi: 10.1038/509645a.

[45] A.M. Lum, B.B. Wang, G.B. Beck-Engeser, L. Li, N. Channa, M. Wabl, Orphan receptor GPR110, an oncogene overexpressed in lung and prostate cancer, BMC Cancer. 10 (2010). doi:10.1186/1471-2407-10-40.

[46] L. Badiali, J. Cedernaes, P.K. Olszewski, O. Nylander, A.V. Vergoni, H.B. Schiöth, Adhesion GPCRs are widely expressed throughout the subsections of the gastrointestinal tract, BMC Gastroenterol. 12 (2012). doi:10.1186/1471-230X-12-134.

[47] K.J. Paavola, H. Sidik, J.B. Zuchero, M. Eckart, W.S. Talbot, Type IV collagen is an activating ligand for the adhesion G protein-coupled receptor GPR126, Sci. Signal. 7 (2014). doi:10.1126/scisignal.2005347.

[48] X. Tang, Y. Wang, D. Li, J. Luo, M. Liu, Orphan G protein-coupled receptors (GPCRs): biological functions and potential drug targets, Acta. Pharmacol. Sin. 33 (2012) 363-371. doi:10.1038/aps.2011.210.

[49] I. Liebscher, B. Ackley, D. Araç, D.M. Ariestanti, G. Aust, B. Bae, B.R. Bista, J.P. Bridges, J.G. Duman, F.B. Engel, S. Giera, A.M. Goffinet, R.A. Hall, J. Hamann, N. Hartmann, H.-H. lin, M. Liu, R. luo, A. Mogha, K.R. Monk, M.C. Peeters, S. Prömel, S. Ressl, H.B. Schiöth, S.M. Sigoillot, H. Song, W.S. Talbot, G.G. Tall, J.P. White, U. Wolfrum, L. Xu, X. Piao, New functions and signaling mechanisms for the class of adhesion G protein-coupled receptors, Ann. N. Y. Acad. Sci. 1333 (2014) 43-64. doi:10.1111/nyas.12580.

[50] J. Hamann, G. Aust, D. Araç, F.B. Engel, C. Formstone, R. Frederiksson, R. A. Hall, B.L. Harty, C. Kirchoff, B. Knapp, A. Krishnan, I. Liebscher, H.-H. Lin, D.C. Martinelli, K.R. Monk, M.C. Peeters, X. Piao, S. Prömel, T. Schöneberg, T.W. Schwartz, K. Singer, M. Stacey, Y. A. Ushkaryov, M. Vallon, U. Wolfrum, M.W. Wright, L. Xu, T. Langenhan, H.B. Schiöth, International union of basic and clinical pharmacology. XCIV. Adhesion G protein-coupled receptors, Pharmacol. Rev. 67 (2015) 338-367. doi:10.1124/pr.114.009647.

[51] Y.Y. Ni, Y. Chen, S.Y. Chen, B.Y. Sun, F. Wang, X.L. Wu, S.Y. Dang, G.H. Zhang, H.X. Zhang, Y. Kuang, J. Fei, M.M. Gu, W.F. Rong, Z.G. Wang, Deletion of Gpr128 results in weight loss and increased intestinal contraction frequency, World J. Gastroenterol. 20 (2014) 498-508. doi:10.3748/wjg.v20.i2.498.

[52] H. Zhou, I. Rigoutsos, The emerging roles of GPCRC5A in diseases, Oncoscience 12 (2014) 765-776. doi:10.18632/oncoscience.104.

[53] P. Rajkumar, J. Pluznick, Elucidating the physiological role of Gprc5c, a novel orphan GPCR in the kidney, FASEB J. 29 (2015) 809.23.

[54] M.A. Lemmon, J. Schlessinger, Cell signaling by receptor tyrosine kinases, Cell. 141 (7) (2010) 1117–1134. doi:10.1016/j.cell.2010.06.011.

[55] A.M. Krasinskas, EGFR signaling in colorectal carcinoma, Path. Res. Int. 14 (2011) 1-6. doi:10.4061/2011/932932.

[56] C. Desbois-Mouthon, The HER3/ErbB3 receptor: A promising target in cancer drug therapy, Gastroentero. Clin. Biol. 34 (2010) 255-259. doi:10.1016/j.gcb.2010.03.002.

[57] C.A. Maurer, H. Friess, B. Kretschmann, A. Zimmermann, A. Stauffer, H.U. Baer, M. Korc, M.W. Buchler, Increased expression of erbB3 in colorectal cancer is associated with concomitant increase in the level of erbB2, Hum. Pathol. 8 (1998) 771-777.

[58] A. Mathur, C. Ware, L. Davis, A. Gazdar, B.S. Pan, B. Lutterbach, FGFR2 is amplified in the NCI-H716 colorectal cancer cell line and is required for growth and survival, PLoS One, 9 (2014) e98515. doi:10.1371/journal.pone.0098515.

[59] G. Sonvilla, S. Allerstorfer, C. Heinzle, S. Stattner, J. Karner, M. Klimpfinger, F. Wtba, H. Fischer, C. Gauglhofer, S. Spiegl-Kreinecker, B. Grasl-Kraupp, K. Holzmann, M. Grusch, W. Berger, B. Marian, Fibroblast growth factor receptor 3-IIIc mediates colorectal cancer growth and migration, Br. J. Cancer, 102 (2010) 1145-1156. doi:10.1038/sj.bjc.6605596.

[60] R.C. Turkington, D.B. Longley, W.L. Allen, L. Stevenson, K. McLaughlin, P.D. Dunne, J.K. Blayney, M. Salto-Tellez, S. Van Schaeybroeck, P.G. Jonhston, Fibroblast growth factor receptor 4 (FGFR4): a targetable regulator of drug resistance in colorectal cancer, Cell. Death Dis, 5 (2014) e1046. doi: 10.1038/cddis.2014.10.

[61] M.A. Stammes, H.A.J.M. Prevoo, M.C. Ter Horst, S.A. Groot, C.J.H. Van de Velde, A.B. Chan, L.-F. de Geus-Oei, P.J.K. Kuppen, A.L. Vahrmeijer, E.B. Pasquale, C.F.M. Sier, Evaluation of EphA2 and EphB4 as Targets for Image-Guided Colorectal Cancer Surgery, Int. J. Mol. Sci. 18 (2017) 307. doi:10.3390/ijms18020307.

[62] P.G. de Marcondes, L.G. Bastos, J.C. de-Freitas-Junior, M.R. Rocha, J.A. Morgado-Diaz, EphA4-mediated signaling regulates the aggressive phenotype of irradiation survivor colorectal cancer cells, Tumour Biol. 37 (2016) 12411-12422. doi:10.1007/s13277-016-5120-0.

[63] A.M. Jubb, F. Zhong, S. Bheddah, H.I. Grabsch, G.D. Frantz, W. Mueller, V. Kavi, P. Quirke, P. Polakis, H. Koeppen, EphB2 is a prognostic factor in colorectal cancer. Clin. Cancer. Res. 11 (2005) 5181-5187. doi: 10.1158/1078-0432.CCR-05-0143.

[64] S. Jägle, K. Rönsch, S. Timme, H. Andrlova, M. Bertrand, M. Jäger, A. Proske, M. Schrempp, A. Yousaf, T. Michoel, R. Zeiser, M. Werner, S. Lassmann, A. Hecht, Silencing of the EPHB3 tumor-suppressor gene in human colorectal cancer through decommissioning of a transcriptional enhancer. Proc. Natl. Acac. Sci. USA. 111 (2014) 4886-4891. doi:10.1073/pnas.1314523111.

[65] Z. Tian, G. Yao, H. Song, Y. Zhou, J. Geng, IGF2R Expression is Associated with the Chemotherapy Response and Prognosis of Patients with Advanced NSCLC, Cell. Phys. Biochem. 34 (2014) 1578-1588. doi:10.1159/000366361.

[66] C. Hoyo, S.K. Purphy, J.. Schildkratu, A.C. Vidal, D. Skaar, R.C. Milikan, J. Galanko, R.S. Sandler, R. Jirtle, T. Keku, IGF2R genetic variants, circulating IGF2 concentrations and colon cancer risk in African Americans and Whites, Dis Markers. 32 (2012) 133-141. doi: 10.3233/DMA-2011-0865.

[67] R.R. Valiathan, M. Marco, B. Leitinger, C.G. Kleer, R. Fridman, Discoidin domain receptor tyrosine kinases: new players in cancer progression, Cancer Metastasis Rev. 31 (2012) 295-321. doi: 10.1007/s10555-012-9346-z.

[68] R. Yuge, Y. Kitadai, K. Shinagawa, M. Onoyama, S. tanaka, W. Yasui, K. chayam a, Abstract 5070: Inhibition of collagen receptor discoidin domain receptor-1 (DDR1) reduces colon cancer cell migration and metastasis, Tumor Biology 75 (2015) doi:10.1158/1538-7445.AM2015-5070.

[69] A.V. Orang, R. Safaralizadeh, M.A. Hosseinpour Feizi, M.H. Somi, Diagnostic relevance of overexpressed serine threonine tyrosine kinase/novel oncogene with kinase domain (STYK1/ NOK) mRNA in colorectal cancer, Asian Pac. J. Cancer. Rev. 15 (2014) 6685-6689. doi:10..7314/APJCP.2014.15.16.6685.

[70] E. Perez-Riesgo, L.G. Gutierrez, D. Ubierna, A. Acedo, M.P. Moyer, L. Nunez, C. Villalobos, Transcriptomic analysis of calcium remodeling in colorectal cancer, Int. J. Mol. Sci. 18 (2017) 1-23. doi:10.3390/ijms18050922.

[71] E. Lastraioli, T. Lottini, L. Bencini, M. Bernini, A. Arcangeli, hERG1 Potassium Channels: Novel Biomarkers in Human Solid Cancers, BioMed. Res. Int. 201 (2015) 1-9. doi:10.1155/896432.

[72] S. Williams, A. Bateman, I. O'Kelly, Altered Expression of Two-Pore Domain Potassium (K2P) Channels in Cancer, PLoS one, 10 (2013) e74589. doi:10.1371/journal.pone.0074589.

[73] H. Liu, J. Huang, J. Peng, X. Wu, Y. Zhang, W. Zhu, L. Guo, Upregulation of the inwardly rectifying potassium channel Kir2.1 (KCNJ2) modulates multidrug resistance of small-cell lung cancer under the regulation of miR-7 ad the Ras/MAPK pathway, Mol. Cancer, 14 (2015) 1-8. doi: 10.1186/s12943-015-0298-0.

[74] S. Kammerer, A. Sokolowski, H. Hackl, D. Platzer, S.W. Jahn, A. El-Heliebi, D. Scharzenbacher, V.Stiegelbaure, M. Pichler, S. Rezania, H. Fiegl, F. Peintinger, P. Regitnig, G. Hoefler, W. Schreibmayer,T. Bauernhofer, KCNJ3 is a new independent prognostic marker for estrogen receptor positive breast cancer patients, Oncotarget. 7 (2016) 84705-84717. doi:10.18632/oncotarget.13224.

[75] S. Sirnes, G.E. Lind, J. Bruun, T.A. Fykerud, M. Mesnil, R.A. Lothe, E. Rivedal, M. Kolberg, E. Leithe, Connexins in colorectal cancer pathogenesis, Int. J. Cancer. 137 (2015) 1-11. doi:10.1002/ijc.28911.

[76] M. Maes, S.C. Yanguas, J. Willebrords, B. Cogliati, M. Vinken, Connexin and pannexin signaling in gastrointestinal and liver disease, Transl. Res. 166 (2015) 332-343. doi: 10.1016/j.trsl.2015.05.005.

[77] Y. Sozucan, M.E. Kalender, I. Sari, S. oztuzcu, K. Arman, O. Yumrutas, I. Bozgeyik, B. Cengiz, Y.Z. Igci, O. Balakan, C. Camci, TRP genes family expression in colorectal cancer, Exp. Oncol. 37 (2015) 208 -212.

[78] M. Kulendran, J.F. Sebbing, C.G. Marks, T.A. Rockall, Predictive and prognostic factors in colorectal cancers: a personalized approach, Cancers (Basel). 3 (2011) 1622-1638. doi:10.3390/cancers3021622.

[79] S. Koo Kang, YK. Chae, J. Woo, M.S. Kim, J.C. Park, J. Lee, J.C. Soria, S.J. Jang, D. Sidransky, C. Moon, Role of human aquaporin 5 in colorectal carcinogenesis, Am. J. Pathol. 173 (2008) 518-525. doi:10.2353/ajpath.2008.071198.

[80] A. Riedl, M. Schlederer, K. Pudelko, M. Stadler, S. Walter, D. Unterleuthner, C. Unger, N. Kramer, M. Hengstschläger, L. Kenner, D. Pfeiffer, G. Krupitza, H. Dolznig, Comparison of cancer cells cultured in 2D vs 3D reveals differences in AKT/mTOR/S6-kinase signaling and drug response, J. Cell. Sci. (2016). doi: 10.1242/jcs.188102.

[81] H. Okuyama, J. Kondo, Y. Sato, H. Endo, A. Nakajima, J.M. Piulats, Y. Tomita, T Fujiwara, Y. Itoh, A. Mizoguchi, Dynamic change of polarity in primary cultured spheroids of human colorectal adenocarcinoma and its role in metastasis, Am. J. Pathol. 186 (2016) 899-911. doi:10.1016/j.ajpath.2015.12.011.

[82] P. Carneiro, M.S. Fernandes, J. Figueiredo, J. Caldeira, J. Carvalho, H. Pinheiro, M. Leite, S. Meo, P. Oliveira, J. Simoes-Correia, M.J. Oliveira, F. Carneiro, C. Figueiredo, J. Paredes, C. Oliveira, . Seruca, E-cadherin dysfunction in gastric cancer - Cellular consequences, clinical applications and open questions, FEBS Letters, 586 (2012) 2981-2989. doi:10.1016/j.febslet.2012.07.045.

[83] L. Weber, K. Al-Rafae, J. Ebbert, P. Jägers, J. Altmüller, C. Becker, S. Hahn, G. Gisselmann, H. Hatt, Activation of odorant receptor in colorectal cancer cells leads to inhibition of cell proliferation and apoptosis, PLoS One, 12 (2017) e0172491. doi:10.1371/journal.pone.0172491.

[84] Y. Fang, T. Kenakin, C. Liu, Editorial: orphan GPCRs as emerging drug targets, Front. Pharmacol. 6 (2015). doi:10.3389/fphar.2015.00295.

[85] B.C. Parker, W. Zhang, Fusion genes in solid tumors: an emerging target for cancer diagnosis and treatment, Chin. J. Cancer. 32 (2013) 594-603. doi:10.5732/cjc.013.10178.

[85] M. Fakih, R. Wong, Efficacy of the monoclonal antibody EGFR inhibitors for the treatment of metastatic colorectal cancer, Curr. Oncol. 17 (2010) S3-S17.

[86] H.-Q. Xi, X.-S. Wu, B. Wei, L. Chen, Eph receptors and ephrins as targets for cancer therapy, J. Cell. Mol. Med. 16 (2012) 2894-8909. doi: 10.1111/j.1582-4934.2012.01612.x.

[87] M. Katoh, H. Nakagama, FGF receptors: cancer biolgy and therapeutics, Med. Res. Rev. 34 (2014) 280-300. doi:10.1002/med.21288.

[88] L. Hu, H.-Y. Chen, J. Cai, Y. Zhang, C.-Y. Qi, H. Gong, Y.-X. Zhai, H. Fu, G.-Z. Yang, C.-F. Gao, Serine threonine tyrosine kinase 1 is a potential prognostic marker in colorectal cancer, BMC Cancer, 15 (2015) 1-8. doi:10.1186/s12885-015-1285-y.

[89] J.S. Myers, A.K. von Lersner, C.J. Robbins, Q.-X.A. Sang, Differentially expressed genes and signature pathways of human prostate cancer, PLoS one 10 (2015) e0145322. doi: 10.1371/journal.pone.0145322.

[90] S. Fang, X. Fang, Advances in glucose metabolism research in colorectal cancer, Biomed. Rep. 5 (2016) 289-295. doi:10.3892/br.2016.719.

[91] P. Longati, X. Jia, J. eimer, A. Wagman, M.-R. Witt, S. Rehnmark, C. Verbeke, R. Toftgar, M. Löhr, R.L. Heuchel, 3D pancreatic carcinoma spheroids induce a matrix-rich, chemoresistant phenotype offering a better model for drug testing, BMC Cancer. 13 (2013) 1-13. doi: 10.1186/1471-2407-13-95.

[92] R.P. Ferraris, Dietary and developmental regulation of intestinal sugar transport, Biochem. J. 360 (2001) 265-276.

[93] X. Chen, G.A. Muller, M. Quaas M. Fischer, N. Han, B. Stuchbury, A.D. Sharrocks, K. Engeland, The Forkhead Transcription Factor FOXM1 Controls Cell Cycle-Dependent Gene Expression through an Atypical Chromatin Binding Mechanism, Mol. Cell. Biol. 33 (2013) 227-236. doi:10.1128/MCB.00881-12.

[94] K. Tanaka, The proteasome: overview of structure and functions, Proc. Jpn. Acad. Ser. B. Biol. Sci. 85 (2009) 12-36. doi: 10.2183/pjab.85.12.

[95] J. Rak, Y. Mitsuhashi, V. Erdos, S.-N. Huang, J. Filmus, R.S. Kerbel, Massive programmed cell death in intestinal epithelial cells induced by three-dimensional growth conditions: suppression by

mutant c-H-ras oncogene expression, J. Cell. Biol. 131 (1995) 1587-1598. doi:0021/9525/95-12- 1587-12.

[96] K. Smolders, N. Lombaert, D. Valkenborg, G. Baggerman, L. Arckens, An effective plasma membrane proteomics approach for small tissue samples, Sci. Rep. 5 (2015) 10917. doi:10.1038/srep10917.

Chapter VIII

General conclusions and future perspectives

On reading the first part of this dissertation (chapters 1-5), it is hoped that the reader will have gained a better understanding of the complex mechanisms used by peptides to control cellular activities. However, it is also hoped that new questions may have been raised which could open up new avenues for future research. In this final chapter, we will discuss some of the currently unsolved problems and propose follow-up experiments, leading to a look into the future of functional peptidomics research.

The thesis project started with the remark that –from a biological perspective- "*we live in interesting times*". One can say that we have entered the post-genomic era, characterized by the effort to extract useful information from whole-genome sequencing projects [1]. The challenge in the current era is to assign functions to all of the unknown genes, proteins, and peptides. As a reference in the field of invertebrate peptide discovery and characterization, the research group of prof. Schoofs faced this challenge and initiated a large-scale research collaboration, aiming to identify novel biologically active peptides from human and mouse cells, tissues, or body fluids. This work resulted in the creation of a peptide library, harboring more than 700 putative bioactive peptides. Each peptide from our collection contains several hallmarks of biologically active peptides and may exert a signaling function.

Bioactive peptides perform many physiological functions, such as controlling cell division, migration, proliferation, and survival. Because the biological world is currently perceived at an ever-increasing accuracy, several models of cell activation by peptides have been described in great detail [2-7]. The majority of peptides function by binding to their cognate receptor, initiating a cascade of reactions inside the cell [8]. While this dogma has formed the backbone of traditional pharmacology for many decades, more recent data suggest that ligands should be classified based on their individual effects on a cell. More specifically, a certain peptide may differentially modulate different subsets of the receptor signaling repertoire depending on the cell type that is activated [8-10]. This leads to a cell type-specific response, which may include the activation of several secondary messenger systems. To further add to the complexity, peptides can trigger cell activation via receptor-independent mechanisms, *e.g.* by exploiting endocytic pathways or modifying the physicochemical state of the plasma membrane.

This PhD project has primarily focused on the effects induced by the human cathelicidin peptide LL-37 and P318, a C-terminal fragment of CRAMP, on various human and mouse cultured cell lines. The cathelicidin peptide's spectrum of biological activity has a broad range, and includes direct killing of pathogens, chemo-attraction of monocytes, T-cells and neutrophils, promotion of wound healing by stimulating angiogenesis, and re-epithelization. Due to these biological effects, studying the

molecular mechanism of these peptides could have clinical importance. Therefore, the goal was set to identify a cognate receptor(s) for LL-37/P318 and elucidate the signal transduction pathway.

In line with the dogma of a specific receptor mediating the action of particular (set of) ligand(s), we started with the somewhat preconceived idea that LL-37 and P318 were the ligands for one receptor or structurally related receptors. However, a literature survey (chapter 3) revealed that the pleiotropic effects of LL-37 could best be explained by its ability to activate various structurally unrelated cell surface receptors and/or intracellular targets in a wide variety of cultured cell lines. Using EIS and calcium mobilization assays, we confirmed that LL-37 was able to evoke a response in different cell types. The ability of LL-37, as well as P318, to activate a broader set of cell types may be related to its amphipathic nature, which favors the hypothesis that LL-37/P318 initiates a cellular response by residing in the cell membrane.

A membrane-dependent mechanism of LL-37/P318 does not exclude the possibility that LL-37 also interacts with specific membrane-associated proteins and/or transmembrane domains of cell surface receptors. In fact, we did find experimental evidence that at least in some cell types, the activity of LL-37 or P318 could be blocked by an antagonist. For example, the impedance response of A549 lung carcinoma cells to LL-37 was almost completely inhibited by pretreating cells with brefeldin A, an inhibitor of endocytic pathways. Interestingly, this inhibitory effect of brefeldin A was not observed in HEK293T cells, suggestive of a cell type-dependent mechanism of action. In addition, inhibitory effects of PTX on the activity of LL-37 in A549 and RAW264.7 cells suggest the involvement of an as yet unidentified $G_{\alpha i}$-coupled receptor (or possibly, multiple $G_{\alpha i}$-coupled receptors) in the mode of action of LL-37.

On one hand, LL-37 and P318 appear to work via a rather aspecific mechanism of action through interacting with the cell membrane. On the other hand, some actions of LL-37/P318 display selectivity through binding to molecular targets yet to be defined. These observations advocate for a more complex signaling mechanism than the traditional mechanism in which a peptide interacts with one single receptor type. Even though we made progress in elucidating important parts of the mechanisms behind the action of LL-37/P318 on various cultured cell lines, many questions still remain unanswered. For instance, efforts to unambiguously obtain the identity of the molecular target(s) of LL-37/P318 were generally unsuccessful. Notably, other research groups have also struggled to provide conclusive evidence for a conventional ligand-receptor interaction. In my opinion, it is possible that the membrane activity of LL-37/P318 plays a previously unrecognized role through altering membrane homeostasis or specifically interacting with receptor transmembrane domains. These membrane-active properties of LL-37/P318 could also explain why none of the

receptor-selective antagonists used in this study completely inhibited the action of LL-37/P318. Orthosteric inhibitors such as the FPR2-selective inhibitor WRW4 may not work in case LL-37/P318 binds to the membrane interface and allosterically modulates receptor activity. Therefore, our collection of inhibitors should be expanded with antagonists that exert inhibitory effects through mechanisms other than orthosteric inhibition.

Valuable information about the identity of the molecular target(s) of LL-37/P318 can also be obtained through the use of more specialized techniques such as RNAi or conceptually new technologies such as LRC. In addition, we highly recommend conducting experiments with the all-D enantiomer of LL-37 in order to discriminate between a binding of LL-37 to a specific receptor and an association of the peptide with the cell membrane. If the D-enantiomer of LL-37 has identical effects as the L-peptide, a stereoselective interaction of LL-37 with its cognate receptor becomes less likely.

Other studies that can move the field of LL-37 research forward include elucidating the mechanism behind the ability of LL-37 to increase incorporation of receptors in LRs. At present, existing research is limited and it remains unclear how LL-37 promotes the formation of LRs. Furthermore, the priming effect of LL-37 appears to be specific for the SDF-1-CXCR4 axis in HSPCs, but it is not known how such specificity is achieved. Interestingly, other cationic AMPs such as anaphylatoxin C3a and human β-defensin 2 are also able to increase incorporation of CXCR4 in LRs, suggestive of a more general mechanism of action of AMPs. It remains to be determined whether some of the poorly understood effects of LL-37 can be explained by increased LR formation on the surface of target cells.

We anticipate that through ongoing and future research efforts, additional novel applications of LL-37 as well as P318 will emerge. Presently, several cathelicidin-derived peptides are being tested in preclinical trials and companies like HelixBiomedix are committed to developing a range of small, safe, and deliverable peptides using LL-37 as a template, intending to address specific skin conditions and diseases. In addition, Promore Pharma attempts to obtain market authorization for LL-37 in the treatment of small- and mid-sized venous leg ulcers based on experimental data from a phase IIa clinical trial. P318 may also have potential for further development as a lead peptide to coat medical instruments and implants due to its antimicrobial and antibiofilm activity. However, in each aforementioned case, considerable caution must be exercised when evaluating the clinical usability of LL-37/P318, especially since LL-37/P318 may exert (harmful) effects on non-target cells which are not yet fully understood. Some of these effects also appear to be quite subtle and difficult to detect (*e.g.* increasing the incorporation of receptors into LRs), highlighting the need for close monitoring of possible adverse effects of LL-37/P318 in both *in vitro* and *in vivo* models.

One of the techniques that could deliver useful information about the toxicological behavior of peptides at an early stage of the research is EIS. A key advantage of EIS is that both short- and long-term (cytotoxic) effects of peptides can be monitored in a single assay. This is particularly relevant for LL-37/P318 research, as cytotoxic responses of treated cells may occur at a later point in time (*e.g.* the effect of LL-37 on HEK293T cells). Another advantage is that impedance responses generated upon peptide treatment contain complex real-time information on the underlying mechanisms of action. Whether impedance response profiles are truly predictive for a mode of action needs to be clarified in future research efforts. Pattern recognition algorithms can be utilized in order to assign a putative mode of action to a peptide of interest, or to determine that the impedance signature is unique and not similar to the impedance signature of a prototypical compound with a well-defined mechanism of action. Building an extensive database of known cellular impedance responses could also be of interest to the pharmaceutical industry, as information on the mode of action of novel drug candidates is required before proceeding to expensive and long-term preclinical testing. CellSine, a spin-off company from the Schoofs lab, is currently investigating whether impedance responses can be used to differentiate among ligands with distinct signaling profiles. To achieve this goal, they developed a novel dynamic EIS based whole cell assay with an extended spectrum of wavelengths (1 Hz-60 kHz) and efficient data transformation process. Their approach already proved its value in applications designed specifically for cytotoxicity testing. In the near future, CellSine's technology will be expanded to screen for compounds with activity against biofilms or to determine the mechanisms by which viruses enter host cells. Whether or not CellSine becomes a central player in the market remains to be seen. However, it appears the technology behind EIS has still not been exploited to its fullest potential and there is still room for improvement.

In the second part of this dissertation, we took a closer look at 3D cell cultures systems as they are thought to provide more physiologically relevant information and more predictive power for preclinical tests compared to 2D cell culture systems. Driven by the desire of scientists to realistically mimic *in vivo* cell behavior, numerous 3D cell cultures models have been developed over the past two decades. Some of these models are discussed in chapter 6, along with the most prominent advantages and disadvantages of each type of culture.

A growing number of researchers recognize that 3D cell cultures may respond differently to candidate drugs than 2D cell cultures. Differential drug responses among 3D and 2D cell cultures can be related to differences in gene and protein expression that change drug efficacy, metabolism, and cell communication. Using RNA-sequencing, we confirmed that 3D and 2D HT-29 colorectal adenocarcinoma cells exhibit divergent gene expression profiles. Because a large number of druggable targets are receptors, we mainly focused on differential expression of GPCRs, RTKs, and

ion channels. In a next stage of the research, functional tests can be carried out to further explore the putative role of differentially expressed receptors in CRC. Notably, a follow-up study using the methodology of Smolders *et al*. is currently in progress to validate our results at protein level.

Even though 3D cell cultures have not yet replaced 2D cell cultures on a large scale, we believe that the future of 3D cell cultures looks bright. Research on 3D cell culture models has been increasing year after year and this trend is expected to continue. At this moment, a trade-off exists between *in vivo* resemblance and reproducibility as the enhanced complexity of implementing challenging-to-model features such as a vascular component and/or the presence of ECM decreases the reproducibility and limits the comparibility of results obtained with different experimental setups. However, when the right balance is found between usability, cost, and resemblance to *in vivo* tumor behavior, it is expected that 3D cell cultures will claim a permanent place in cell-based research programs.

In my opinion, current 3D models already show great promise for studying basic aspects of cancer biology. However, the sky is not the limit for 3D cell culture systems and it remains to be seen whether observations made in 3D will ever be readily translatable into clinical practice. Recapitulating the complexity and heterogeneity of tumor tissues *in vivo* will remain a daunting task for many years to come, despite the emergence of several sophisticated 3D cell culture approaches and techniques. However, in case we do succeed in developing a 3D model that truly provides an accurate depiction of the *in vivo* situation, the clinical possibilities are vast. For instance, receptors up- or downregulated in 3D cell cultures compared with healthy tissue can be studied in the context of pursuing biomarkers for targeted cancer imaging, which may help the surgeon during surgery. In addition, the emergence of improved patient-specific 3D cell culture platforms aiming to test individual tumor therapy susceptibility is expected to move the field of 3D cell cuture forward.

On a final note, it will be interesting to examine if EIS' technology can be adapted for use with 3D cell cultures. In this way, cellular processes such as receptor pharmacology can be investigated in a more physiologically relevant *in vitro* environment than 2D monolayers can provide. In the author's opinion, it would be very interesting to combine the two major parts of this dissertation, *e.g.* exploring the impedance response of 3D cell cultures to candidate bioactive peptides. Determining whether peptide-induced effects on 3D cell cultures are more pronounced in a particular frequency domain, can be a possible topic for further investigation.

Appendix

Supplementary information chapter 2

Table 1. Results obtained from screening experiments with crude peptides (Chapter 2). Pure (≥ 95% purity) active peptides are indicated by asterisks.

Peptide N°	Cell line	Technique	Remarks
4	B16	EIS	EC_{50} = 4 nM
5	Neuro2A, TE671	EIS	Effect on platelet activation (lab K. Freson)
6	B16	EIS	EC_{50} = 4 nM
8	Mouse embryonic stem cells, B16	EIS, Ca^{2+}	EC_{50} (B16) = 5 µM
14	SK-HEP1	Ca^{2+}	EC_{50} = 1 µM Identical to oxytocin
24*	Neuro2A, TM4	EIS, Ca^{2+}	Truncated variants and alanine scan available
33*	Neuro2A	EIS, Ca^{2+}	Truncated variants and alanine scan available
37	B16	EIS	/
49	CPAE	EIS	EC_{50} = 2 µM
53	B16	EIS	EC_{50} = 5 µM
57	B16	EIS	EC_{50} = 5 µM
62		*In situ* hybridization, behavioral tests	Expression in stomach, intestine, spleen, adrenal gland, thymus, pancreas, hippocampus and bulbi (mouse; lab prof. Arckens). Behavioral tests (Morris water maze, open field tests, passive avoidance learning…) were negative
67	B16	EIS	EC_{50} = 8 nM
71	PHNs	ELISA	Decreased secretion of amyloid-β (40 and 42; lab prof. Dotti)
77	PHNs	ELISA	Decreased secretion of amyloid-β (40 and 42; lab prof. Dotti)
78	B16	EIS	EC_{50} = 10 µM
82	B16	EIS	EC_{50} = 1 µM
98	PHNs	ELISA, organ preparation	Decreased secretion of amyloid-β (40 and 42; lab prof. Dotti) Inhibitory contractile effect on rat duodenal strips at 1 µM (lab prof. Depoortere)

92	B16	EIS	EC_{50} = 2.5 µM
112	Primary hippocampal neurons	ELISA	Decreased secretion of amyloid-β (40 and 42; lab prof. Dotti)
113	PHNs	ELISA	Decreased secretion of amyloid-β (40 and 42; lab prof. Dotti)
116	B16	EIS	/
124	B16	EIS, Ca^{2+}	EC_{50} = 1 µM
125	CTXTNA2	EIS, organ preparation	Fragment of galanin, truncated variants available Previous studies demonstrate that galanin induces contraction of human colonic smooth muscle strips and SAR studies showed that fragments 1-21 remain fully active.
174*	TE671, DOK	EIS, *in situ* hybridization	EC_{50} = 1 µM (TE671) and 5 µM (DOK) Expression in stomach, pancreas, intestine (mouse; lab prof. Arckens) Predicted peptide Truncated peptides and alanine scan available
191	B16	EIS	/
215	B16	EIS, cAMP, organ preparations	EC_{50} = 2.5 µM (B16) Truncated variants available Fragment of 'connecting peptide' Effect on functional-tissue organ bath response (lab prof. De Spiegeleer) due to impurity?
218	Neuro2A, TE671	EIS	/
221*	TM4, OLN-93	EIS, Ca^{2+}	EC_{50} = 5 µM (TM4) and 10 µM (OLN-93)
222	B16	EIS	EC_{50} = 30 nM
223*	B16, primary cortical neurons, U87	EIS, Ca^{2+}, organ preparation	EC_{50} ≥ 10 µM (B16) Variant of hemokinin 1, which is known to be a Sustance P agonist. Induces dose-dependent smooth muscle contractions in rat duodenal strips
235	NMuMG, Kelly	EIS	EC50 = 5µM (Kelly) and 13 µM (NMuMG)
264	NMuMG	EIS	EC_{50} ≥ 40 µM. Fractalkine antagonist?
272*	B16	EIS, Ca^{2+}, membrane potential assay, *in situ* hybridization	EC_{50} = 0.5 µM (B16) expression in cerebellum, hippocampus, cortex, pancreas, thymus and spleen (mouse; lab prof. Arckens).

			Predicted peptide. Truncated variants and alanine scan available
281	HEK293T	EIS	/
282	HEK293T	EIS	/
283		Morris water maze	Improves spatial memory (lab prof. Dedeyn)?
296	CPAE, TM3, Tr6Bc1, PHNs	EIS, in situ hybridization	Expression in bulbi, hippocampus, cortex, hypothalamus, pancreas, spleen, thymus, adrenal gland, lung, stomach and intestines (mouse; lab prof. Arckens)
297	CPAE, NMuMG, SBAC	EIS	EC_{50} = 4 µM (NMuMG)
303	TE671, CXTNA2, HepG2, OLN-93	EIS, Ca^{2+}	/
308	B16	EIS	EC_{50} = 2.5 µM
318*	Many cell types, including B16, HEK293T, HeLa, MRC5, RAW264.7, TE671 and TM3.	EIS, Ca^{2+}, cAMP and membrane potential assay, receptor pull-down experiments	Inhibition fungal and bacterial biofilm formation (lab prof. Thevissen/Cammue). Some of shorter analogues of P318 have increased activity relative to native P318. Activation of neural networks in intestines of guinea pigs (lab prof. Vandenberghe) Activation of neuronal regeneration in mouse pup retina explants (lab prof. Moons) Inhibition of electric field stimulated neuronal responses in rat duodenal strips (lab prof. Depoortere) Truncated variants and alanine scan available
319	B16, MRC5	EIS, membrane potential, cAMP	$EC_{50} \geq 10$ µM
334	PHNs	ELISA	Decreased secretion of amyloid-β (40 and 42)
372	PHNs	ELISA	Decreased secretion of amyloid-β (40 and 42)
384*	TE671, Neuro2A	EIS, Ca^{2+}	$EC_{50} \geq 10$ µM for both cell lines Polycistronic peptide
433	TE671, Neuro2A, CTXTNA2	EIS, Ca^{2+}	Polycistronic peptide
438	B16, TE671, Neuro2A, CTXTNA2, OLN-93	EIS, Ca^{2+}	Polycistronic peptide
444	B16, TE671, Neuro2A, CTXTNA2, OLN-93	EIS, Ca^{2+}	Polycistronic peptide
446	B16	EIS	Antifungal activity (lab prof. Cammue). No shorter analogues with increased activity on *C. albicans* were identified. Alanine scan of P446 not tested.

			Antibacterial activity (lab prof. Lavigne).
456	B16	EIS	$EC_{50} \geq 20$ µM
469	B16	EIS	/
486	Neuro2A	Ca^{2+}	No changes in impedance
493	Tr6Bc1, WI26, 4/4 RM-4	EIS	EC_{50} (Tr6Bc1) < 400 nM, EC_{50} (WI26) < 2.5 µM and EC_{50} (4/4 RM-4) < 400 nM
503	SBAC	EIS	EC_{50}=0.7 µM
571	Neuro2A, RCE	EIS, Ca^{2+}	Truncated variants available
575	B16	EIS	EC_{50} = 2 µM
592	B16	EIS	$EC_{50} \geq 10$ µM
607	B16	EIS	EC_{50} = 10 nM
609	B16	EIS	EC_{50} = 20 nM
614	PHNs	ELISA	Increased secretion of amyloid-β (40 & 42; lab prof. Dotti)
620	B16, NIH3T3	EIS	Identical to lipotropin-γ
629	PC-3	EIS	EC_{50} = 2 µM
646	PHNs	ELISA	Increased secretion of amyloid-β (40 & 42; lab prof. Dotti)
649*	PHNs , SH-SY5Y	ELISA	Increased secretion of amyloid-β (40 &42; lab prof. Dotti)
671	B16	EIS	EC_{50} = 5 µM
677	B16	EIS	EC_{50} = 5 µM

Supplementary information chapter 7

Table 2. Complete list of GO terms and KEGG pathways enriched in downregulated DEGs along with their GO identifier, p-value and Benjamini-Hochberg adjusted p-value.

Index	GO term name (Category: Biological process)	GO id	P-value	P_{adj}
1	anaphase-promoting complex-dependent catabolic process	GO:0031145	1.36E-14	3.6E-12
2	cellular ketone metabolic process	GO:0042180	4.1E-5	1.46E-3
3	CENP-A containing chromatin organization	GO:0061641	2.48E-6	1.2E-4
4	chromatin assembly or disassembly	GO:0006333	2.14E-14	5.46E-12
5	chromatin organization	GO:0006325	1.35E-12	2.37E-10
6	chromatin remodeling at centromere	GO:0031055	1.68E-7	1.03E-5
7	chromosome localization	GO:0050000	9.03E-7	4.91E-5
8	chromosome segregation	GO:0007059	4.96E-16	2.18E-12
9	DNA replication	GO:000260	1.6E-32	1.08E-28
10	DNA strand elongation	GO:0022616	5.62E-11	6.32E-9
11	DNA strand elongation involved in DNA replication	GO:0006271	4.75E-12	7.34E-10
12	DNA synthesis involved in DNA repair	GO:0000731	4 E-17	3.9E-13
13	DNA-templated transcription, termination	GO:0006353	1.57E-4	4.86E-3
14	endonucleolytic cleavage involved in rRNA processing	GO:0000478	2.03E-4	6.15E-3
15	establishment of RNA localization	GO:0051236	1.51E-10	1.52E-8
16	G1/S transition of mitotic cell cycle	GO:00000082	2.9E-19	3.1E-16
17	gene silencing by RNA	GO:0031047	2.84E-10	2.7E-8
18	membrane disassembly	GO:0030397	3.32E-11	4.08E-9
19	microtubule cytoskeleton organization	GO:0000226	4.03E-15	1.12E-12
20	microtubule-based process	GO:0007017	2.29E-12	3.87E-10
21	mitotic nuclear envelope disassembly	GO:0007077	5.17E-12	7.82E-10
22	mRNA metabolic process	GO:0016071	9.96E-9	7.27E-7
23	mRNA processing	GO:0006397	5.48E-9	4.28E-7
24	mitotic spindle elongation	GO:00000022	1.5E-17	1.4E-14

25	ncRNA metabolic process	GO:0034660	1.55E-11	2.1E-9
26	negative regulation of canonical Wnt signaling pathway	GO:0090090	3.22E-4	9.04E-3
27	negative regulation of RNA catabolic process	GO:0006401	2.44E-4	7.1E-3
28	negative regulation of transferase activity	GO:0051348	7.58E-5	2.55E-3
29	nuclear pore complex assembly	GO:0051292	3.74E-12	5.9E-10
30	nucleic acid phosphodiester bond hydrolysis	GO:0090305	1.26E-7	7.9E-6
31	nucleobase-containing compound transport	GO:0015931	7.84E-9	5.77E-7
32	nucleus organization	GO:0006997	1.44E-4	4.47E-3
33	peptidyl-lysine modification	GO:0018205	2.49E-8	1.76E-6
34	positive regulation of chromosome organization	GO:2001252	4.69E-4	1.25E-2
35	posttranscriptional regulation of gene expression	GO:0010608	4.47E-16	1.71E-12
36	protein localization to chromosome	GO:0034502	3.95E-6	1.84E-4
37	protein localization to kinetochore	GO:0034501	4.43E-5	1.58E-3
38	protein modification by small protein conjugation or removal	GO:0070647	2.38E-7	1.39E-5
39	protein sumoylation	GO:0016925	1.26E-10	1.31E-8
40	protein-DNA complex subunit organization	GO:0071824	6.86E-9	5.16E-7
41	regulation of cell cycle checkpoint	GO:1901976	2.74E-9	2.25E-7
42	regulation of cellular amino acid metabolic process	GO:0006521	5.25E-8	3.53E-6
43	regulation of cellular response to heat	GO:1900034	2.45E-12	4.03E-10
44	regulation of cellular response to stress	GO:0080135	1.81E-7	1.09E-5
45	regulation of gene silencing	GO:0016458	9.29E-12	1.31E-9
46	regulation of mRNA stability	GO:0043488	3.09E-11	3.83E-9
47	regulation of phosphorus metabolic process	GO:0051174	7.69E-4	1.9E-2
48	regulation of protein modification by small protein conjugation or removal	GO:1903320	4.71E-6	2.15E-4
49	regulation of protein ubiquitination involved in ubiquitin-dependent protein catabolic process	GO:2000058	7.36E-10	6.32E-8
50	replication of extrachromosomal circular DNA	GO:0001326	1.8E-31	5.9E-28

51	response to abiotic stimulus	GO:0009628	1.14E-8	8.21E-7
52	response to temperature stimulus	GO:0009266	2.15E-4	6.42E-3
53	ribonucleoprotein complex biogenesis	GO:0022613	6.41E-6	2.78E-4
54	ribonucleoprotein complex localization	GO:0071166	4.5E-8	3.06E-6
55	ribosome biogenesis	GO:0042254	4.92E-6	2.23E-4
56	RNA phosphodiester bond hydrolysis	GO:0090501	1.41E-6	7.08E-5
57	rRNA metabolic process	GO:0016072	1.76E-10	1.74E-8
58	tRNA export from nucleus	GO:0006409	1.12E-13	2.47E-11
59	tumor necrosis factor-mediated signaling pathway	GO:0033209	9.25E-5	3.05E-3

Index	**GO term name (Category: Cellular compartment)**	**GO id**	**P-value**	**P_{adj}**
1	90S preribosome	GO:0030686	8.8E-4	1.15E-2
2	cajal body	GO:0015030	5.35E-4	7.32E-3
3	condensed chromosome outer kinetochore	GO:0000940	6.36E-11	2.63E-9
4	condensed chromosome, centromeric region	GO:0000779	3.2E-23	7.2E-21
5	condensed nuclear chromosome	GO:0000794	5.08E-12	2.99E-10
6	envelope	GO:0031975	2.93E-11	1.44E-9
7	heterochromatin	GO:0000792	5.48E-7	1.35E-5
8	intracellular ribonucleoprotein complex	GO:0030529	3.3E-16	2.41E-15
9	MCM complex	GO:0042555	1.13E-11	6.21E-10
10	midbody	GO:0030496	2.76E-7	6.99E-6
11	mitotic spindle pole	GO:0097431	4.8E-19	8.1E-17
12	Ndc80 complex	GO:0031262	9.91E-4	1.25E-2
13	nuclear body	GO:0016604	4.15E-11	1.94E-9
14	nuclear envelope	GO:0005635	2.75E-11	1.39E-9
15	nuclear periphery	GO:0034399	1.11E-7	3.06E-6
16	nuclear pore	GO:0005643	1.77E-11	9.19E-10
17	nuclear pore outer ring	GO:0031080	1.13E-5	2.25E-4
18	nucleolar part	GO:0044452	4.1E-28	1.8 E-25

19	polar microtubule	GO:0005827	2.2E-16	4.8E-16
20	preribosome	GO:0030684	1.87E-10	7.41E-9
21	proteasome regulatory particle	GO:0005838	4.69E-5	8.72E-4
22	replication fork	GO:0005657	2.24E-6	5.24E-5
23	replication fork protection complex	GO:0031298	6.71E-8	1.97E-6
24	ribonucleoprotein complex	GO:1990904	1.27E-16	1.05E-14
25	small nuclear ribonucleoprotein complex	GO:0030532	2.82E-6	6.41E-5
26	SMN-Sm protein complex	GO:0034719	4.69E-5	8.72E-4
27	spindle	GO:0005819	6.29E-11	2.67E-9
28	spindle pole	GO:0000922	2.41E-16	1.57E-14
29	spindle pole centrosome	GO:0031616	1.4E-18	1.9E-16
30	spliceosomal snRNP complex	GO:0097525	3.03E-6	6.81E-5

Index	**GO term name (Category: Molecular function)**	**GO id**	**P-value**	**P_{adj}**
1	adenyl-nucleotide exchange factor activity	GO:0000774	6.77E-4	3.45E-2
2	ATPase activity, uncoupled	GO:0042624	2.1E-9	9.5E-8
3	ATP-dependent microtubule motor activity	GO:1990939	6.1E-10	3.2E-8
4	chromatin binding	GO:0003682	8.91E-8	6.51E-7
5	DNA-dependent ATPase activity	GO:0008094	1.74E-12	3.63E-10
6	enzyme binding	GO:0019899	4.74E-12	9.43E-10
7	histone binding	GO:0042393	1.31E-7	1.69E-5
8	identical protein binding	GO:0042802	1.56E-5	1.27E-3
9	kinase binding	GO:0019900	4.51E-6	4.39E-4
10	lysine-acetylated histone binding	GO:0070577	4.69E-7	2.36E-5
11	nuclear localization sequence binding	GO:0008139	2.17E-7	2.72E-5
12	nucleocytoplasmic transporter activity	GO:0005487	8.14E-7	8.92E-5
13	protein C-terminus binding	GO:0008022	3.99E-4	2.16E-2
14	protein dimerization activity	GO:0046983	1.8E-4	5.4E-2

15	protein homodimerization activity	GO:0042803	9.05E-4	4.18E-2
16	protein-DNA unloading ATPase activity	GO:0140083	1.8E-9	8.2E-8
17	RNA 7-methylguanosine cap binding	GO:0000340	5.02E-5	3.49E-3
18	RNA binding	GO:0003723	8.9E-58	1.04E-55
19	signal sequence binding	GO:0005048	7.44E-5	4.87E-3
20	single-stranded RNA-dependent ATP-dependent helicase activity	GO:0003697	6.7E-13	3.5E-11
21	snoRNA binding	GO:0030515	5.34E-5	3.6E-3
22	structural constituent of nuclear pore	GO:0017056	3.38E-10	5.11E-8
23	ubiquitin conjugating enzyme activity	GO:0061631	6.33E-4	3.26E-2

Index	**KEGG pathway**	**KEGG id**	**P-value**	**P_{adj}**
1	Adherens junction	hsa04520	0.003586	0.03557
2	Apoptosis	hsa04210	0.004269	0.03921
3	Base excision repair	hsa03410	0.0001688	0.002791
4	Cell cycle	hsa04110	3.429e-26	8.504e-24
5	Colorectal cancer	hsa05210	0.003448	0.03557
6	DNA replication	hsa03030	1.082e-21	1.342e-19
7	Fanconi anemia pathway	hsa03460	0.00000142	0.0000352
8	FoxO signaling pathway	hsa04068	0.0009661	0.01261
9	Homologous recombination	hsa03440	0.00000743	0.0001536
10	HTLV-I infection	hsa05166	0.00000196	0.0000442
11	Mismatch repair	hsa03430	1.792e-10	7.408e-9
12	Nucleotide excision repair _	hsa03420	0.00008696	0.001540
13	Oocyte meiosis	hsa04114	0.0004058	0.006291
14	p53 signaling pathway	hsa04115	0.002122	0.02392
15	Pancreatic cancer	hsa05212	0.005272	0.04670
16	Pathogenic Escherichia coli infection	hsa05130	0.001474	0.01740
17	Prostate cancer	hsa05215	0.0004518	0.006590

18	Proteasome	hsa03050	1.216e-11	6.032e-10
19	Purine metabolism	hsa00230	6.640e-7	0.0000183
20	Pyrimidine metabolism	hsa00240	2.660e-10	9.425e-9
21	Ribosome biogenesis in eukaryotes	hsa03008	1.018e-13	6.310e-12
22	RNA degradation	hsa03018	0.001462	0.01740
23	RNA transport	hsa03013	9.430e-16	7.795e-14
24	Spliceosome	hsa03040	1.004e-8	3.112e-7